KU Leuven
Biomedical Sciences Group
Faculty of Medicine
Department of Development and Regeneration

KU LEUVEN

DOCTORAL SCHOOL
BIOMEDICAL SCIENCES

AN IMAGE-BASED MUSCULOSKELETAL MODELING PLATFORM FOR SIMULATION-BASED EVALUATION OF VERTEBRAL MOTION IN ADULT SPINAL DEFORMITY

Thomas OVERBERGH

Jury:

Supervisor:	Prof. Dr. ir. Lennart Scheys
Co-supervisors:	Prof. Dr. Ilse Jonkers
	Prof. Dr. Lieven Moke
Chair examining committee:	Prof. Dr. Kathleen Freson
Chair public defence:	Prof. Dr. Patrick Verschueren
Jury members:	Prof. Dr. Guy Molenaers
	Prof. Dr. ir. Jos Vander Sloten
	Prof. Dr. ir. Friedl De Groote
	Prof. Dr. ir. Dennis Anderson
	Mr. ir. Philippe Maxy

Dissertation presented in partial fulfilment of the requirements for the degree of Doctor in Biomedical Sciences

December 2021

Acknowledgments

Obtaining a PhD may seem like a personal achievement. However, the list of people that motivated, helped, pushed and even dragged me to this final stage is endless.

I am incredibly thankful for Prof. Lennart Scheys, Prof. Ilse Jonkers and Prof. Lieven Moke to have offered me the opportunity to start a PhD. Learning from you has been a tough yet amazing path with a rewarding destination. I thank my doctoral committee, Prof. Jos Vander Sloten, Prof. Guy Molenaers, Prof. Friedl De Groote, Prof. Dennis Anderson and Mr. Philippe Maxy for their critical and constructive feedback. I believe your input over the duration of this project has been indispensable for the quality of this work.

Lennart and Lieven, our story started somewhere in 2015, when my interest for spinal deformity research was ignited in a student project, followed by a master thesis and ultimately this PhD. Thank you for your tireless enthusiasm and for continuously placing your trust in me. Ilse, I have always deeply appreciated the directness of your guidance. Thank you all for your ongoing encouragement and support throughout this project and setting the outlines in which I could grow.

I extended my knowledge in multiple areas, but the most fulfilling was being part of a multi-disciplinary team of inspiring people leveraging me as a person. I am grateful for the people I have had the opportunity to meet throughout the years. First and foremost, I thank Pieter, my clinical counterpart. Co-founding this new research line within the IORT has been challenging, but it makes me proud to look back at what we, two junior researchers, have achieved. Erica and Thijs, you completed the team. Although collaborating has recently been a challenge, according to our collective message history we have messaged more than four times the amount of words in this thesis. Thank you all for writing this thesis with me.

The spine team and in extension my colleagues from the IORT, Dr. Schelfaut, Dr. Moens, Karel, Pierre, Lore, Kristel, Rowie, Charline, Goedele, Gaëtane, Hilde, Alexander, Felix, Orçun, Dalia, Nazanin and Lucas: Thank you for the occasional brainstorm, troubleshooting and rather frequent coffee breaks.

Ten slotte wil ik graag nog mijn familie en vrienden bedanken. Mama, papa, Charlotte, Jan en Kristel, dankzij jullie steun en occasionele catering kon ik dit doctoraat combineren met een hele reeks andere uitdagingen. Mijn lieve Astrid, August en het wondertje dat we binnenkort mogen ontmoeten, woorden schieten tekort om te zeggen hoe dankbaar ik ben jullie in mijn leven te hebben.

On to the next adventure.

Thomas

Table of Contents

List of abbreviations

Δ	Differential
2D	Two-dimensional
3D	Three-dimensional
AIS	Adolescent idiopathic scoliosis
ALARA	As low as reasonably achievable
A-P	Anteroposterior
AR	Axial rotation
ASD	Adult spinal deformity
BMI	Body mass index
C1 to C7	Cervical vertebra 1 to 7
CI	Confidence interval
cm	Centimeter
COM	Center of mass
COMI	Core Outcome Measures Index
CT	Computed tomography
DDF	Directional deviation fraction
DOF	Degree of freedom
DRR	Digitally reconstructed radiograph
EMG	Electromyography
FE	Finite Element
FE	Flexion-extension
FEM	Finite Element Model
FSU	Functional spinal unit
GC	Gait cycle
GSA	Global sagittal axis
HRQoL	Health-related quality of life
Hz	Hertz
IAR	Instantaneous axis of rotation
ICC	Intraclass correlation coefficient
ICP	Iterative closest point
ID	Inverse dynamics
IK	Inverse kinematics
IMU	Inertial measurement unit
I-S	Inferosuperior
ISB	International Society of Biomechanics
IV	Intervertebral
IVD	Intervertebral disc
KPS	Karnofsky Performance Scale
L1 to L5	Lumbar vertebra 1 to 5
LED	light-emitting diode
LF	Lateroflexion

LIV	Lowest instrumented vertebra
LL	Lumbar lordosis
max	Maximal/maximum
MBM	Multi-body model
min	Minimal/minimum
M-L	Mediolateral
mm	Millimeter
MOCAP	Motion capture
MRI	Magnetic resonance imaging
MS (model)	Musculoskeletal (model)
N	Newton
O1 to O3	Operator 1 to 3
ODI	Oswestry disability index
PI	Pelvic incidence
PI-LL	Pelvic incidence minus lumbar lordosis (mismatch)
PROMs	Patient reported outcome measures
PT	Pelvic tilt
QOL	Quality of life
ROM	Range of motion
S1 to S3	Subject 1 to 3
SD	Standard deviation
SDD	Smallest detectable difference
SDEI	Spinal deformity engagement index
SDI	Spinal deformity index
SEM	Standard error of measurement
SKDI	Spinal kinematic deviation index
SO	Static optimization
SoC	Standard of care
SQ	Semi-quantitative
SRS	Scoliosis research society
SRS-22r	Scoliosis Research Society Outcome Questionnaire
SS	Subject-specific
SSM	Statistical shape models
STA	Soft tissue artefact
STS	Sit-to-stance
SVA	Sagittal vertical alignment
T1 to T12	Thoracic vertebra 1 to 12
T1-SPI	T1-spino-pelvic inclination
T9-SPI	T9-spino-pelvic inclination
TGDI	Transverse gravitational deviation index
TLC	Thoracolumbar
UIV	Upper instrumented vertebra
x-ray	Radiographic image

Summary

Adult spinal deformity (ASD) comprises a wide range of three-dimensional (3D) malalignments of the spinal column. Static two-dimensional (2D) radiographic image-based measurements form the basis of current quantitative diagnosis, pre-operative planning and clinical management in ASD. However, as perioperative complications for ASD patients remain common, it is well-recognized that these 2D static assessments alone cannot objectively quantify the full impact of spinal deformities and associated treatment on dynamic spine function during daily life motor tasks. It is therefore mandatory to further investigate if an improved understanding of 3D spinal kinematics in ASD patients has the potential to complement current state-of-the-art diagnostics and clinical decision-making as they provide an improved understanding of the dynamic spine function. Although several studies are analyzing global posture during motion, there is still a need to get more detailed information on the motion of the individual vertebral segments, i.e. spinal kinematics, during activities of daily living in ASD.

To this end, the use of musculoskeletal (MS) computer models and multi-body simulations was proposed to further advance our biomechanical understanding of the functional abilities of ASD patients. While objective dynamic information originating from motion analysis has revolutionized other orthopaedic fields, specific methodological issues are preventing a similar evolution in ASD. Due to the combination of deformed vertebral geometry, spinal malalignment and limited accessibility of sufficient vertebral anatomical landmarks, conventional methods inherently fail to generate a computer model accurately representing a patient-specific spinal deformity. Despite the expected potential of MS simulations in ASD, current models and simulation techniques thus do not allow calculating intervertebral (IV) joint kinematics in ASD, limiting biomechanical research and clinical advances. Therefore, the general objective of this dissertation was to develop a modeling and evaluation platform facilitating the measurement of spinal kinematics, and demonstrate its potential to improve our understanding of pathological spinal kinematics during dynamic activities of ASD patients.

In **chapter 1**, we presented the first validated biplanar radiography-based method to generate subject-specific MS models of ASD subjects. This method allowed the inclusion of subject-specific bone geometries, the personalization of external skin marker locations and the personalization of the 3D weight-bearing spinal alignment. The use of this new modeling method enabled accurate IV kinematic measurements of ASD subjects, previously not possible.

In **chapter 2** we quantified the reliability of spinal kinematics during a forward trunk flexion, in terms of test-retest reliability and operator-dependent reliability. The results indicate that operator-induced uncertainty has a limited impact on kinematic simulations of spine flexion, while test-retest reliability has a much higher variability. Together with the performed

validations of chapter 1, this chapter ensured the validity of the kinematic results, opening perspectives for kinematic evaluation of ASD patients.

In **chapter 3** we applied the developed workflow on a pilot population of fourteen ASD patients and one control subject to measure IV joint kinematics during a maximal voluntary trunk flexion motion. We then introduced novel metrics to comprehensively quantify effects of spinal deformities on spinal kinematics during forward trunk flexion. These metrics were then used to evaluate relations with routinely used, clinical spino-pelvic parameters, vertebral body deformity, and self-reported health related quality of life (HRQoL). Our results indicated the importance of motion strategies associated with static features of ASD as a prerequisite for dynamic kinematic compensation. Furthermore, the complementary nature of the new dynamic metrics to conventional measures was illustrated. Indeed, our pilot results agreed with the growing awareness in literature that static alignment is not the sole driver of kinematic compensation in ASD.

In **chapter 4** we performed model-based evaluations of spinal kinematics during trunk flexion before and after spinal fusion surgery in ASD, to evaluate changes in spinal kinematics. From a methodological perspective, this first exploration of post-operative modeling and kinematic simulations identified pitfalls regarding image-based modeling, skin marker protocols and model assumptions. In addition we estimated, the effect of soft tissue artefact on skin marker-based spinal kinematics. This chapter illustrated limitations and potential opportunities for the use of subject-specific MS models in post-operative ASD patients for quantifying pre- to post-operative spinal kinematic changes.

In conclusion, this doctoral thesis bridged an important methodological gap that previously limited the use of MS models for the measurement of spinal kinematics in ASD. Furthermore, the developments were used in pilot populations of ASD patients before and after spinal surgery demonstrating their potential added value for evaluating dynamic features of the ASD pathology. As such, on the long term, this project contributed to improving insight on pathological spinal motion during activities of daily living and leads the way from the current 2D static patient assessment towards the integrated 3D functional evaluation of spinal deformities.

General introduction

"*How will spine surgery impact my life? Will I still be able to put on my shoes, lift up my grandchildren or work in the garden?*" After explaining the option of corrective spinal surgery to the patient suffering from adult spinal deformity (ASD), orthopaedic spine surgeons are very often confronted with these questions. While it is crucial to meet the patient's concerns and to clearly set their expectations, both the treating physician and patient struggle with the complexity and uncertainty of predicting their post-operative functionality. Today's advances in medical imaging and computer technology have the potential to provide novel insights that could lead to improved clinical assessment and even the prediction of the post-operative, functional state of ASD patients using *in silico* techniques. This work aims to contribute to that evolution.

Anatomy and function of the spine

The spine or spinal column consists of a series of consecutively connected vertebrae. The functional spinal unit (FSU, Figure 1) represents the mechanical unit between two consecutive vertebrae. Articulation is enabled by the intervertebral disc (IVD), bi-lateral facet joints and connective soft tissues (ligaments and muscles). However, to allow pain-free movement, the spine must be balanced in both the sagittal and coronal plane (Kretzer, 2017). Besides the protection of the spinal cord and nerve roots and provision of mobility, the spine also has an important biomechanical role in maintaining postural stability. During normal daily activities, the spine supports loads up to twice the body weight (500-1000N), during which spinal stability must be maintained while transferring these loads to the pelvis. Although translational and rotational movements in individual FSUs are limited, the summation of these movements along the spine allows considerable range of motion (Boos and Aebi, 2008). This mobility is controlled through complex interactions between passive (intervertebral joint stiffness and ligaments) and active (muscles) stabilization of the vertebral segments. In this regard, the term *kinematics* generally refers to the motion of objects. In the specific field of human biomechanics it is typically used to describe a set of relative coordinates of body segments, representing the joint angles, positions and velocities of (a portion of) the human body at a certain time instant. The terms *spinal or intervertebral (IV) joint kinematics* are thus often used as collective nouns to describe this relative motion at the FSUs of the thoracic and lumbar spine. Finally, the spine also has an important role as center of mass balancer during non-spine specific movement, such as stance or gait (Iorio et al., 2016; Schwab et al., 2006).

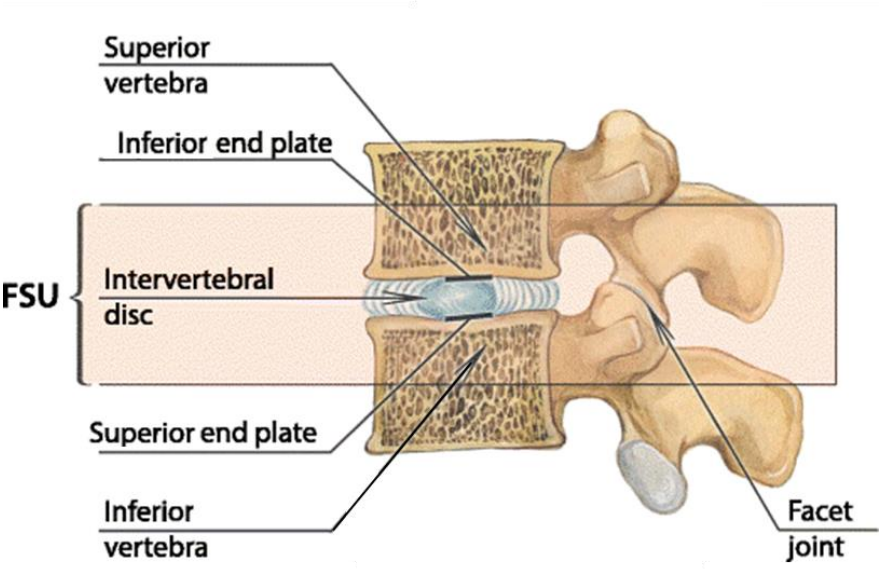

Figure 1: Illustration of a functional spinal unit (FSU). Although none of the vertebrae are geometrically identical, they are grouped according to their location in the spine and show large anatomical similarities within these groups. The upper seven vertebrae are called cervical, followed by twelve thoracic vertebrae to which the ribs attach. The remaining five vertebrae are referred to as the lumbar vertebrae, connecting the sacrum to the thoracic spine. In a FSU, the intervertebral disc (IVD) is positioned between the vertebral body endplates of consecutive vertebrae. Together with the facet joints, formed through the articular processes, the IVD allows and constrains motion in the FSU. (Image modified from Kushchayev et al. (2018) with permission.)

Adult spinal deformity and its etiology

Adult spinal deformity (ASD) comprises a wide range of three-dimensional (3D) malalignments of the spinal column, occurring in at least one anatomical plane or a combination of multiple planes. They are typically associated with changes in both structure and function (Diebo et al., 2019; Smith et al., 2013b).

Based on their etiology (Aebi, 2005), three major types of adult spinal deformities can be defined: Type 1: primary/de-novo degenerative scoliosis (Figure 2), developing after skeletal maturity; Type 2: adolescent idiopathic scoliosis (AIS, a spinal deformity in the coronal plane presenting before the age of eighteen) that progressed in adulthood, Type 3: secondary degenerative scoliosis (originating from other anatomical anomalies such as hip pathology, leg-length discrepancy, metabolic disease or vertebral fractures; or having iatrogenic or neuromuscular causes) (Ailon et al., 2015; Diebo et al., 2019; Kotwal et al., 2011). The majority of the ASD patients suffer from degeneration of IV discs and facet joints (Ailon et al., 2015; Youssef et al., 2013). De-novo scoliosis (Type 1), with a prevalence of 13% in adults aged <60 years and 36% in the >60 year group (McAviney et al., 2020), will be the topic of this dissertation.

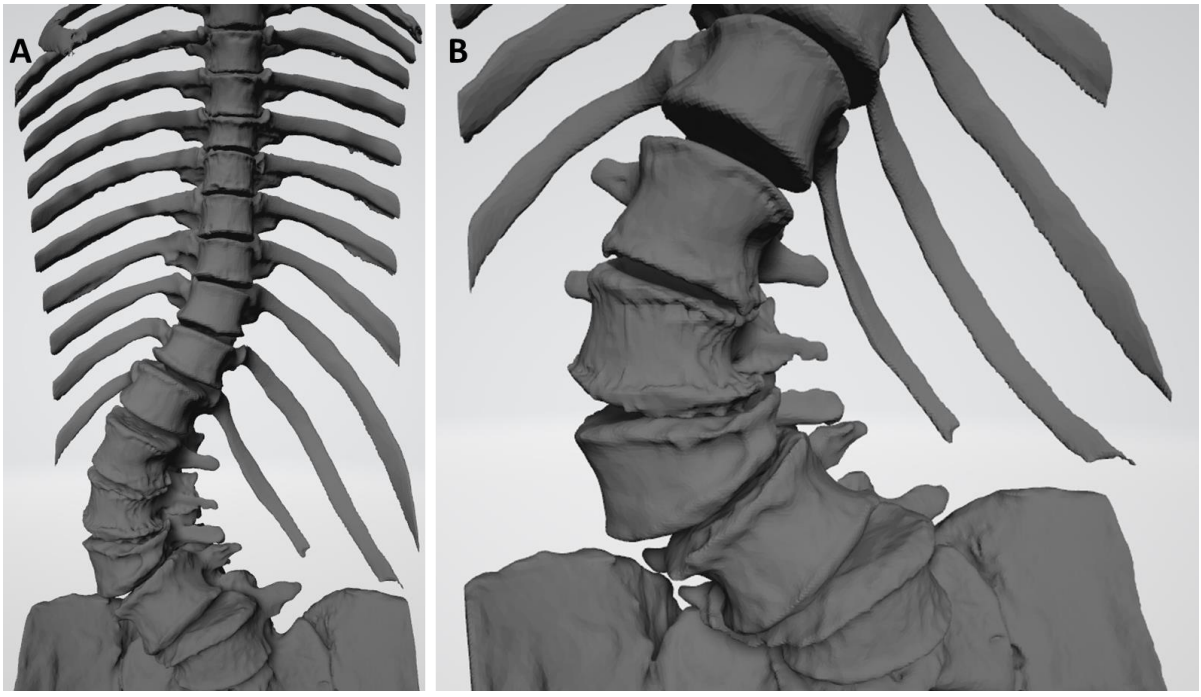

Figure 2: (**A**) Computed tomography (CT) 3D rendering of a female patient (75 years) suffering from a lumbar primary degenerative scoliosis. Over time, asymmetric bone remodeling and vertebral loading, as can be clearly seen in the (**B**) lumbar region, cause the spine to deviate from its normal alignment.

In type 1 ASD, (asymmetric) degeneration typically originates from the facet joints (facet arthrosis) and IVD of one or more FSUs, which eventually leads to (asymmetric) changes in its load-bearing function. These changes result in bone remodeling and instability of the affected FSUs (Mc Donnell et al., 2007), which in turn even further increases the load-bearing changes,

creating a vicious, progressive circle of further accelerated degeneration that also affects spinal ligaments and paraspinal and trunk musculature, eventually inducing spinal instability[1]. This bone remodeling will affect the shape of the vertebral body, which may ultimately lead to an asymmetric collapse of the spine, or spondylolisthesis of the vertebral segments, causing a progressive deviation from the healthy spinal curvature, initially at the level of the affected vertebral segments (i.e. *locally*) but later at the level of the overall spinal curvature (i.e. *globally*). In ASD, the degeneration of the IVD and facet arthrosis can cause a reduction in IVD height, spondylolisthesis, rotatory dislocation, lateral listhesis and therethrough change the global spine alignment resulting in reduced lumbar lordosis, increased thoracic kyphosis or coronal scoliosis (Kotwal et al., 2011).

ASD is usually a progressive condition. It has different clinical presentations and may lead to several impairments, such as axial back and leg pain due to lateral, central or foraminal stenosis (Smith et al., 2009a), problems with maintenance of an upright posture (Barrey et al., 2011), walking abnormalities (Gottipati et al., 2014) and postural compensation (Kretzer, 2017), ultimately leading to decreased participation in daily life (Pellisé et al., 2014). Partly due to this high variability of patient-specific deformities, a more detailed understanding of the impact of ASD on the biomechanical function at a global level or at the local level of individual FSUs, especially during dynamic motor tasks, is currently lacking in the literature. Nevertheless, it is generally appreciated that, besides the anatomical changes in the local FSUs and their effect on the global posture, ASD also considerably affects the spine's dynamic behavior in terms of spinal kinematics, kinetics (forces and moments at the joints) and muscle recruitment. As such, these local changes can induce a secondary chain of compensations in the remainder of the spine as well as in the lower limbs, pelvis or neck.

Pellisé et al. (2014) compared the overall impact of ASD in terms of physical functioning and pain to other chronic disorders, such as osteoarthritis and congestive heart failure, and concluded that the impact on quality of life (QOL) is much higher in the ASD population (Pellisé et al., 2014). Reaching a prevalence of 36% in individuals aged above 60, ASD thus poses a significant burden to healthcare systems globally. Due to an aging population and an increased life expectancy, this prevalence is likely to increase even further (Ailon et al., 2015) which makes ASD a significant health care issue and challenge. Several gaps in the assessment and treatment of ASD, detailed below, are currently limiting an adequate addressing of this health care issue.

Clinical assessment of adult spinal deformity and associated gaps

The diagnostic basis and routine clinical assessments throughout the care pathway for ASD, consist of a physical and mental exam, including the assessment of the neurological system, together with medical imaging; each further detailed below.

[1] When a person's spine loses the ability to maintain its pattern of displacement under normal loading conditions, often associated with neurologic deficit, major deformity, and/or incapacitating pain, this is referred to as clinical instability (Boos and Aebi, 2008; Reeves et al., 2007).

Physical, neurological and mental health assessment

The physical exam typically includes a global deformity and balance assessment where the main manifesting features of ASD, such as shoulder height differences, a rib hump, scoliotic or abnormal lordotic or kyphotic curves, coronal or sagittal shifts in the trunk or pelvis, are visually inspected. Additionally, an evaluation of possible neurological impairment is performed to assess the sensory and motor neuron responses and reflexes. Besides the patient's medical history, their mental wellbeing is evaluated during anamnesis as ASD-induced functional impairment is often associated with limitations in social function, appearance (e.g. hump back), dissatisfactions, anxiety and depression (Verheyden et al., 2007). To better standardize this assessment of physical and mental QOL, patient reported outcome measurements (PROMs) are increasingly being used through standardized questionnaires, such as the Scoliosis Research Society Outcome Questionnaire (SRS-22r) (Asher et al., 2003), Oswestry Disability Index (ODI) (Fairbank and Pynsent, 2000), the Karnofsky Performance Scale (KPS) index (Mor et al., 1984) and the Core Outcome Measures Index (COMI) (Mannion et al., 2016). Their primary aim is to evaluate a range of aspects contributing to the patient's self-reported, and therefore subjective, health-related quality of life (HRQoL). **However, besides these overall subjective and qualitative exams, no objective and quantitative evaluation of the functional abilities of the patient is performed (Clinical gap 1).**

Medical imaging

Following the above-described qualitative functional assessment, the treating physician can use medical imaging to confirm the diagnosis and, more importantly, quantify the type and severity of the pathology. Medical imaging is indeed still considered the cornerstone for quantitative clinical assessment in ASD (Diebo et al., 2019). More specifically, traditional radiographic (x-ray) systems provide sagittal and/or coronal two-dimensional (2D) radiographic images and are used to measure a set of parameters that quantify the spino-pelvic alignment, such as the pelvic incidence (PI), lumbar lordosis (LL), pelvic tilt (PT) and sagittal vertical alignment (SVA) (Figure 3) (Cho et al., 2014; Konieczny et al., 2013; Lafage et al., 2008; Smith et al., 2013a). Today, these spino-pelvic parameters form the basis for ASD classification in terms of the severity and type of structural spinal deformity and, based hereon, provide guidance in clinical decision-making (Bess et al., 2013; Ilharreborde et al., 2008; King et al., 1983; Lawrence G. Lenke et al., 2001). The SRS-Schwab classification (Schwab et al., 2013) is one of the most established classification systems for ASD, providing an overview of the coronal description of the curve in combination with specific sagittal measurements.

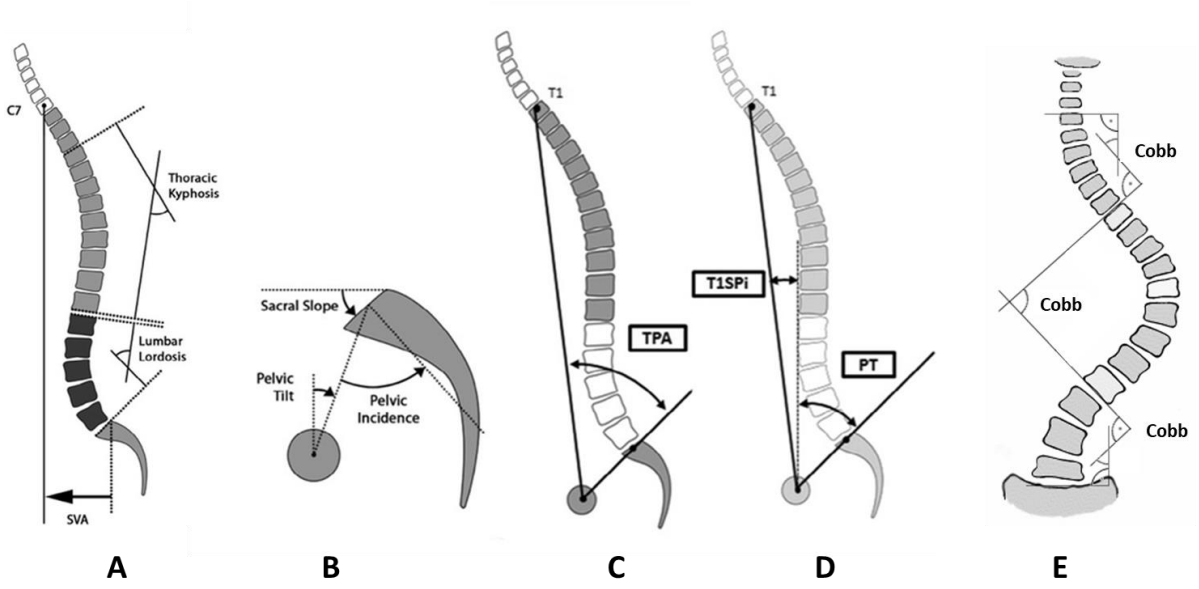

Figure 3: In the sagittal plane (**A-D**) the following spino-pelvic parameters are most often used to quantify the spino-pelvic alignment of a patient: lumbar lordosis (LL), thoracic kyphosis (TK), sagittal vertical alignment (SVA), pelvic incidence (PI), pelvic tilt (PT), sacral slope (SS), total pelvic angle (TPA), T1-spino-pelvic inclination angle (T9-SPI variation also exists). In the coronal plane (**E**) a spinal malalignment is typically measured through Cobb angles. (Images reused with permission. A-D from Buckland et al. (2016) and D from www.physio-pedia.com under the Creative Commons Attribution 3.0 Unported license.)

Complementary to x-ray imaging, computed tomography (CT) can be used to provide more detailed information on the structural deformity as well as a 3D visualization thereof. Besides its use for diagnosis and pre-operative planning, CT can also be used per-operatively to navigate and/or evaluate the placement of surgical instrumentation. Finally, magnetic resonance imaging (MRI) allows analysis of soft tissue structures, including IVD space, adjacent muscles and possible threats to the spinal cord (e.g. spinal stenosis) (M. Y. Wang et al., 2014).

While single-plane medical imaging, such as the traditional x-ray systems, indeed provide a relatively low-cost, fast and often weight-bearing image of the patient, their 2D characteristics inherently limit evaluating the 3D nature of the spinal malalignment in ASD. On the other hand, the highly detailed 3D images from CT and MRI are expensive and subject the patient to a high radiation dosage (CT). Additionally, the -typical- lying position alters the spinal alignment compared to its more functionally relevant upright, weight-bearing, alignment and can be experienced as painful over the duration of the acquisition (Salem et al., 2015; Smith et al., 2017).

Advances in bi-planar[2] radiographic imaging, and more specifically the EOS Imaging System (EOS, Paris, France), however, have recently allowed for the simultaneous acquisition of full-body sagittal and coronal images (Figure 4A-B). Compared to traditional x-ray systems, its slot-scanning collimators eliminate supero-inferior geometric magnification as the x-ray beams

[2] Biplanar imaging is a form of stereoradiography (based on the principles of stereoscopy) where the two images are taken perpendicular to each other (i.e. at an angle of 90°).

move cranially to caudally in tandem with the detectors (Figure 4C). Importantly, the spatially calibrated images allow to generate a 3D reconstruction of the spine (Glaser et al., 2012), thus enabling conceptual extensions to the conventional 2D radiographic parameters (Kadoury et al., 2007; Moke et al., 2020; Pasha et al., 2016; Pasha and Flynn, 2018). Furthermore, these novel systems come with the additional advantage of a significantly reduced radiation dose. This state-of-the-art imaging system is thus particularly useful to assess global spinal alignment in ASD patients in a static, standing position, and to routinely follow-up on the treatment effect of the patient's posture.

Although the static images from these technologies allow to quantify anatomical changes in the spine, they are not fully representative for the impairment an ASD patient may experience during more dynamic activities of daily living. In summary, the anatomical (i.e. static) aspects of ASD can nowadays be adequately objectified in clinical practice, as opposed to the functional (i.e. dynamic) aspects that remain undocumented (Clinical gap 2).

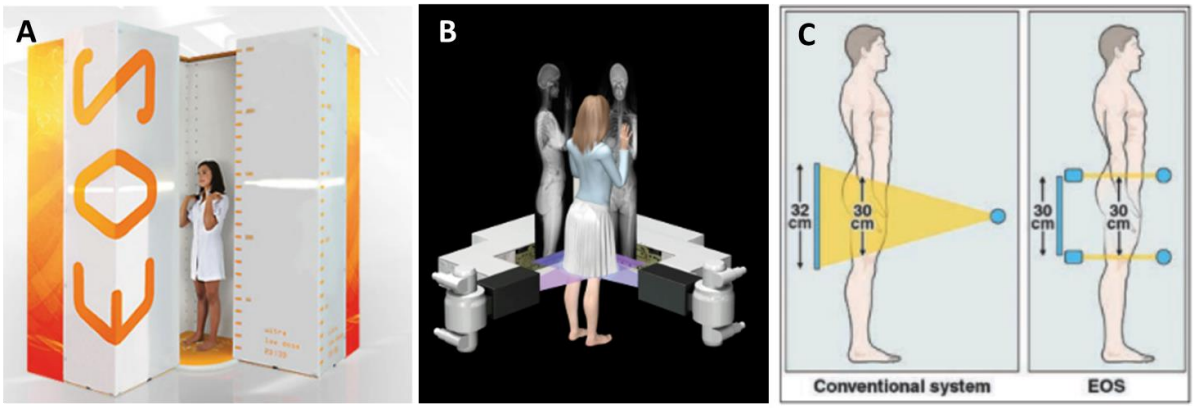

Figure 4: (**A**) The EOS Imaging system (EOS, Paris, France) is a novel biplanar radiographic imaging system. (**B**) Illustration of the imaging acquisition process. The two collimated, beams (purple) simultaneously move down in tandem with the detectors. (**C**) Conventional radiography system (left) with a stationary point source and detector results in geometric magnification, whereas the EOS Imaging System (right) has x-ray sources and detectors that move in tandem, eliminating geometric magnification in the vertical direction. (Images with courtesy of EOS Imaging and reused from Illes et al. (2012) with copyright permission from Elsevier.)

Clinical treatment and associated gaps

Treatment of ASD includes conservative and surgical interventions, both primarily aiming at pain and disability reduction. Conservative treatment typically consists of physiotherapy focusing on physical conditioning programs to reduce pain and improve function and quality of life in ASD patients. While conservative alignment correction using braces is often considered to correct the spinal curve for children and young adolescents (AIS), it is no longer a viable option for adult patients due to skeletal maturity. Once conservative physiotherapy has been exhausted, surgical techniques, such as decompression, spinal osteotomies, alignment correction using instrumentation and fusion, are typically considered. In patients with de-novo degenerative spinal deformity, i.e. the type 1 ASD that this thesis focuses on, surgical treatment usually aims at correcting the sagittal plane deformity, and if possible correcting the scoliotic

curve to prevent curve progression and reduce back pain, induce neural decompression and optimize stabilization (Cho et al., 2014; Kretzer, 2017). Using surgical instrumentation such as screws, rods (Figure 5) or cages, possibly in combination with vertebral osteotomies, bony fusion of the vertebrae in the instrumented region is aimed for. Thus, following spinal fusion surgery in ASD, the surgical fixation and the associated bony fusion, will prevent motion between the fused vertebral segments.

Recently, large discrepancies have been documented between patient expectations and outcomes observed post-operatively. Specifically, the pain reduction and functional improvement after fusion surgery was anticipated to be much higher by the patient than he or she experienced post-operatively (Ryu et al., 2021; Yoo et al., 2019). Although operative treatments were reported to have satisfying effects on pain, disability, spinal alignment and quality of life (Hassanzadeh et al., 2012; Smith et al., 2009b, 2009a; Turner et al., 2015), post-operative complications and revision surgery remain common: 69.8% of surgically treated ASD patients are affected by complications. More than half of these are major complications (55.9%) that can occur either perioperative (<6 weeks: 47.7%) or delayed (>6 weeks: 52.3%) (Smith et al., 2016). Revision rates after surgical correction of spinal deformity are also high, ranging from 9% up to 35.6% (Ha et al., 2013; Pichelmann et al., 2010; Sanchez-Mariscal et al., 2014; Scheer et al., 2013; Soroceanu et al., 2015).

Also, a large variation in surgical treatment planning exists, even between experienced surgeons (Aubin et al., 2007; Majdouline et al., 2007; Robitaille et al., 2007). This is presumably due to the complexity in decision-making for surgical planning. Associated herewith, and even more importantly, also surgical outcomes demonstrate a large variability in terms of functional performance and HRQoL (Faraj et al., 2017; Ryu et al., 2021).

Decision-making for surgical planning is typically based on multiple factors, such as age, type of spinal deformity, risk of progression and the presence of pain, to try to account for the large inter-subject variability in clinical presentation (Boos and Aebi, 2008). An individualized surgical treatment plan is then established by determining the surgical approach, fusion levels (i.e. the upper and lower instrumented vertebra), and choice of instrumentation and technique. However, these decisions as well as the associated patient-specific realignment targets currently rely on the expertise of the surgeon and the interpretation of basic biomechanical algorithms derived from radiograph-based classification systems (Diebo et al., 2019). Strangely, although a multi-level spinal fusion surgery impacts the effective mobility and thus the functionality of the patient, these dynamic aspects are currently not taken into account in the decision-making. **Indeed, there is currently no clear consensus on an objective decision-making tree nor on the treatment associated with optimal outcome (Orina and Berven, 2017). Enhanced metrics for dynamic spine function, complementing current static evaluations, could optimize surgical outcome and thereby decrease the currently high complication and revision rates (Clinical gap 3).**

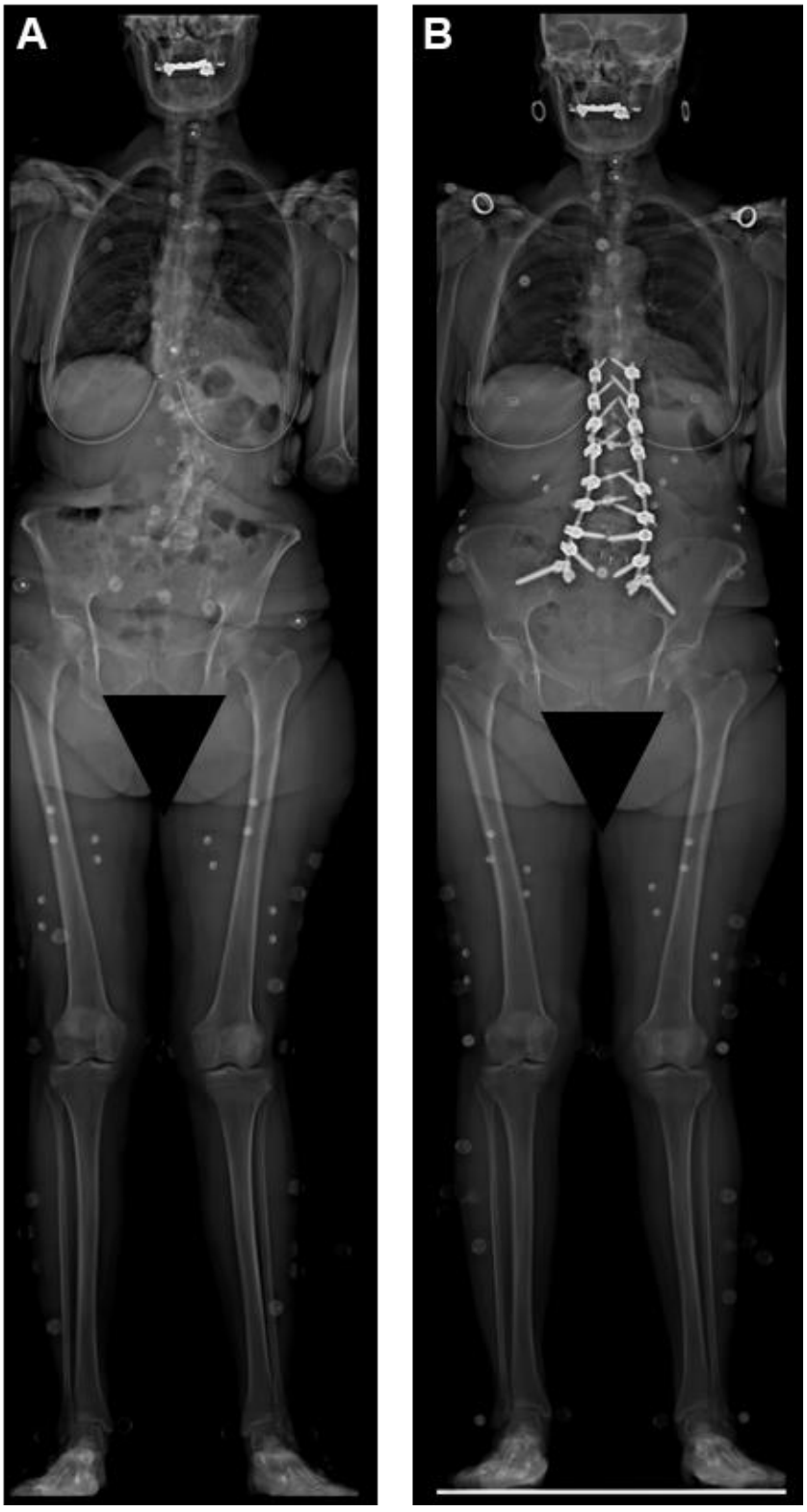

Figure 5: Coronal full-body radiographic images of an ASD patient (**A**) before and (**B**) after spinal fusion surgery.

Conclusion

As described above, current concepts for clinical assessment and treatment of patients with degenerative spinal deformities structurally lack objective assessment of dynamic function. Indeed, they are either based on dynamic but subjective (**Clinical gap 1**), or objective but static assessments (**Clinical gap 2**). Although both are useful, most pain and discomfort for ASD patients does arise during dynamic activities of daily living. This lack of objective dynamic measures is believed to be closely related to the high complication rate of ASD surgery, and more specific the lack of knowledge about how ASD and its treatment impacts the entire locomotor function (Le Huec et al., 2014; L G Lenke et al., 2001; Paul et al., 2015). This creates a large discrepancy between, on one hand, the current mainly static determinants of treatment and outcome assessments used by the treating physician, and on the other hand, the patient's outcome expectations regarding improvement in function and pain. In light of the currently high complication and revision rates (**Clinical gap 3**), objective factors associated with successful and unsuccessful outcomes should be identified to further improve surgical treatment, (Diebo et al., 2014). Indeed, **with regards to the functional aspects of the patient-perceived quality of life, clinicians lack quantitative outcome measures that reflect 3D spine function that could complement insights from subjective PROMs.**

While alterations in gait patterns have been investigating, reporting altered knee, hip an ankle angles compared to healthy subjects and as well as changes before and after spinal surgery (Kawkabani et al., 2021; Severijns et al., 2017; Yagi et al., 2017), these kinematic evaluations are typically not including the affected spine. However, degenerative spinal conditions, such as ASD, are known to be associated with aberrant kinematic behavior compared to healthy spines (Hemming et al., 2018; Quint and Wilke, 2008; Widmer et al., 2019). It is therefore mandatory to further investigate if an improved understanding of 3D spinal kinematics in ASD patients can complement current 2D state-of-the-art diagnostics and clinical decision-making (Diebo et al., 2018; Widmer et al., 2019) as they have the potential to enhance the understanding of dynamic spine function.

In conclusion, quantifying 3D spinal kinematics in ASD during activities of daily living has potential to enhance clinical decision-making and report treatment outcomes objectively (MacWilliams et al., 2013). Advanced quantitative analyses of spinal kinematics in ASD could then be used as a means to complement the quantification of the static spinal radiographic and therefore 2D alignment by reflecting the dynamic impairment during activities of daily living (Diebo et al., 2018). The following section will therefore provide an overview of the most important techniques to measure spinal kinematics available today.

Measuring spinal kinematics

Spinal kinematics are either evaluated *in vivo,* where voluntary movement is generated by the subject's muscle coordination, or *in vitro*, where external forces and conditions are applied to a specimen (Oda et al., 2002; Panjabi et al., 1976). Within the category of *in vivo* spinal research, spinal kinematics have been measured both invasively and non-invasively, as further detailed below.

A first *in vivo* and **invasive technique** studies spinal motion using bone-indwelling pins with markers that are rigidly connected to the vertebrae of interest through their surgical insertion (Figure 6A). Due to the invasiveness, only a limited number of studies have been performed. They primarily focused on lumbar vertebral motion during spine flexion-extension, axial rotation, lateroflexion and gait, and this in both healthy subjects and patients suffering from chronic low-back pain (Dickey et al., 2002; MacWilliams et al., 2013; Steffen et al., 1997). However, no studies to date documented spinal kinematics in ASD patients. Although this approach is considered a gold standard for *in vivo* 3D motion capture of individual spinal segments, the ethical considerations and the risk of neurological complications make it typically a very complex approach, unfeasible for use in larger cohorts.

As a second *in vivo* and less invasive alternative, dynamic radiographic imaging has been used for evaluating spinal motion. Such studies have primarily focused on healthy subjects or patients with low-back pain, while performing for example spinal flexion-extension, axial rotation, lateroflexion or weight-lifting tasks (Figure 6B) (Breen et al., 2019; Li et al., 2009; Wong et al., 2006; Wu et al., 2014; Zanjani-Pour et al., 2018). Although no percutaneous bone pins are required, studies using dynamic (dual) fluoroscopy can also be considered invasive due to the use of (harmful) radiation. Due to the high detail in radiographic imaging, these techniques are also considered as gold standard for *in vivo* 3D motion capture of individual spinal segments. However, due to the limited field of view of fluoroscopic systems, typically only a small region of the (typically lumbar) spine is investigated. Additionally, the exposure to radiation limits the use of (video)fluoroscopy for large study cohorts (MacWilliams et al., 2013).

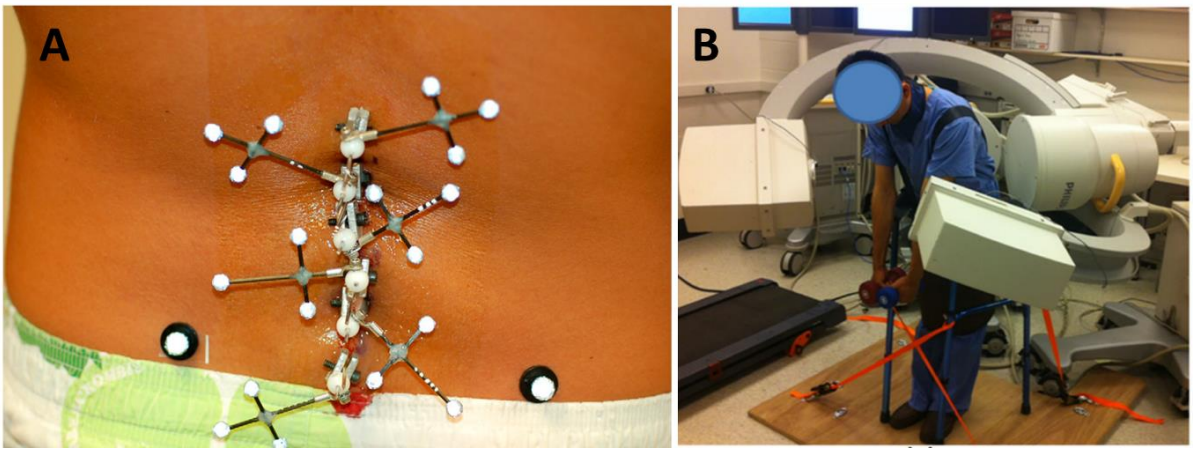

Figure 6: Illustration of in vivo measurements making use of (**A**) indwelling bone pins (MacWilliams et al., 2013) and (**B**) biplanar dynamic fluoroscopy (Wu et al., 2014) to measure accurate lumbar motion during movement. (Images adapted with Copyright permission from Wolters Kluwer Health and Springer Nature, respectively.)

Non-invasive *in vivo* spinal measurements typically rely on skin-mounted sensor systems and have been performed using, for example, inclinometers (Mayer et al., 1984), goniometers (Mannion et al., 2004), surface topography (Degenhardt et al., 2020) and raster stereography (Schroeder et al., 2015). However, they are limited to measuring global spinal alignment and have not been able to measure detailed IV kinematics. Also, non-invasive medical imaging such as MRI has been employed for measuring IV kinematics (Fujii et al., 2007). However, this method is very costly and impractical and only allows for semi-dynamic evaluations (i.e. separate acquisitions at discrete trunk positions).

Alternatively, *in vivo* spinal kinematics can also be measured **non-invasively** using marker-based motion analysis (or optoelectronic motion analysis) (Boos and Aebi, 2008). In research settings, marker-based motion analysis has emerged as a standard and routinely applicable tool to quantitatively describe functional motion with the potential to gain new insights on the dynamic aspects of the human locomotor system. One of its important advantages compared to the invasive techniques is its feasibility to allow routine, non-ionizing, measurements of the human locomotor system. When using marker-based motion analysis, the subject's movement is recorded using an optical motion capture system tracking the 3D trajectories of retro-reflective (passive) or LED (active) markers placed on the skin surface at specific locations overlying specific anatomical bony landmarks of a given body segment (Leardini et al., 2005; Lenke et al., 2001). The collection of the individual 3D marker trajectories throughout the motion task is often referred to as motion capture (MOCAP) data. Several mathematical approaches have been published to extract specific global spino-pelvic parameters (as previously illustrated in Figure 3) from MOCAP data, such as rigid body rotations (Mousavi et al., 2018), circle fitting (Schmid et al., 2016, 2015) or cubic polynomial fitting (Ignasiak et al., 2017), or combinations thereof (Figure 7D). They have been validated for the assessment of global spinal alignment in healthy and AIS subjects.

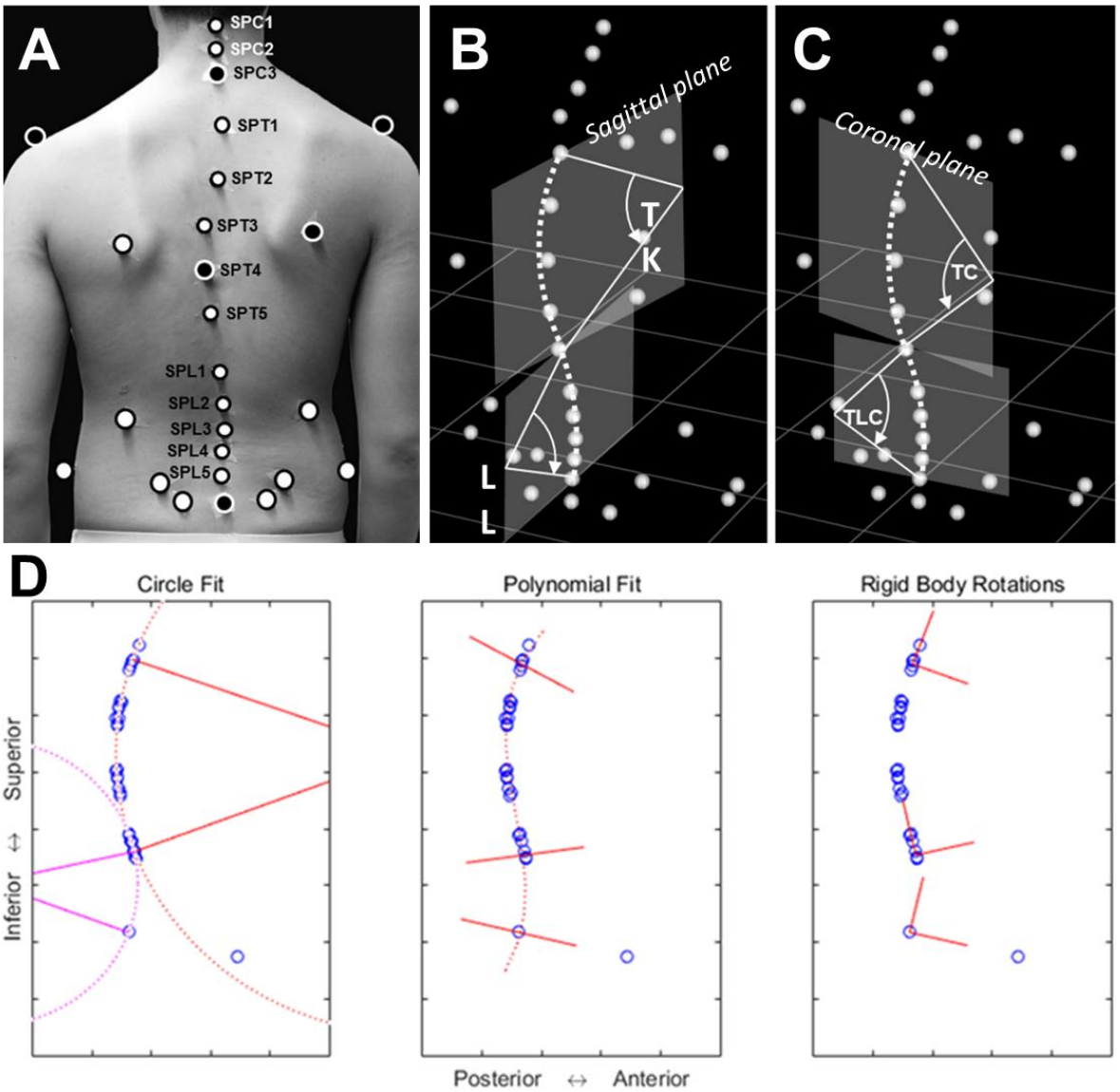

Figure 7: (A) The marker protocol (which is a combination of the plug-in gait full body and an enhanced trunk marker set (marker set from List et al. (2013)) using single markers placed on the spinous process (SP) of the spine. (B, C) MOCAP data from which global spinal alignment changes during gait in AIS patients were estimated in terms of spino-pelvic parameters (as defined in Figure 3), such as the thoracic kyphosis (TK) and lumbar lordosis (LL) in the sagittal plane; and the thoracic (TC) and thoracolumbar (TLC) curvature in the coronal plane. (Figures A-C modified from Schmid et al. (2016)). (D) Illustration of three approaches to process MOCAP data into global spino-pelvic parameters. The circle fitting approach separately fits circles to thoracic and lumbar segments, and then calculates thoracic kyphosis (TK between T1-L1) and lumbar lordosis (LL between L1 – Sacrum) angles. The polynomial fit uses a cubic polynomial curve to fit the markers, after which the angles between the normal to the curve were calculated for TK and LL. Lastly, rigid body rotations consider the T1, T4, T5, T8, T9, T12 and L1 segments as separate objects each having their own reference system. (Images reused with copyright permission of Elsevier. A-C from Schmid et al. (2016) and D from supplementary data of Mousavi et al. (2018).)

Although global spinal alignment can be measured using these methods, the reason they have thus far not been used to measure the 3D IV joint motions in ASD patients (as required in response to **Clinical gap 2**), is twofold.

First, intervertebral movements typically present multi-directional rotations and translations. However, to unambiguously determine the 3D position and orientation of a free-floating object in space (i.e. having six degrees of freedom (DOFs) with a ground reference frame), at least three non-collinear markers are required for the system to be fully determined. Additional (sometimes referred to as 'technical') markers can be placed, to increase the number of markers per segment in case of obscured visibility or generally to improve tracking accuracy. If a system has more DOFs than can be traced, it is underdetermined and marker tracing cannot unambiguously determine the position and orientation of the instrumented object. Unfortunately, marker-based spinal motion analysis suffers from space restrictions on the back as well as limited availability of palpable vertebral landmarks to which markers can be attached on the skin. Typically, only the posterior part of the vertebra's spinous process (*processus spinosus*) can be easily palpated through the skin. Based on this anatomical vertebral landmark, several full spine single-marker configurations or protocols have been developed (Figure 8). In the context of this work, the term '*full-spine*' refers to the sacrum, the five lumbar (L1-L5) and twelve thoracic vertebrae (T1-T12), i.e. excluding the cervical region (C1-C7). For example, the protocol illustrated in Figure 8A was applied in AIS subjects to estimate global spinal curvature in static conditions (Leroux et al., 2000). Good accuracy and reliability with intraclass correlation coefficient between marker-based curvature estimates and radiographic images being 0.94 for kyphosis and 0.91 for lordosis angles were obtained. Alternatively, rigid multi-marker clusters have been used to reduce the amount of undetermined DOFs in the system (Figure 9). Indeed, by placing such clusters on the spinous processes, three markers can be attached to one vertebra thereby defining its orientation and position. Although the use of such marker clusters may seem -at least theoretically- a good solution to track the position of individual vertebrae, its use on multiple adjacent vertebrae is less practical as these clusters may physically contact each other during movement, thereby increasing movement artefacts that interfere with the assumed fixed relation between the marker cluster and the underlying anatomy.

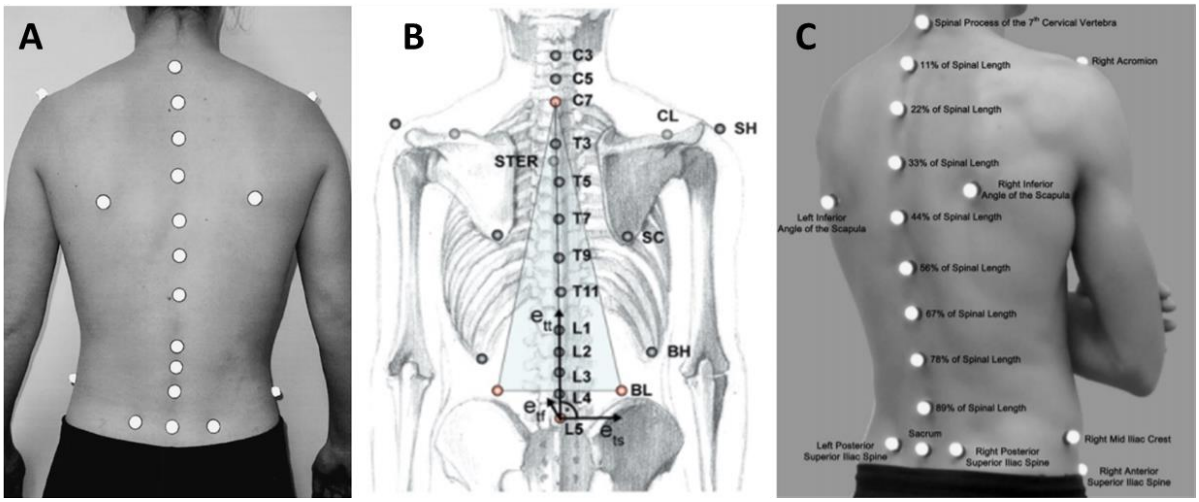

Figure 8: Illustration of previously developed marker protocols only using individual markers. (**A**) This protocol was applied in AIS to estimate spinal curvature in static conditions (Leroux et al., 2000). (**B**) Schmid et al. (2015) selected markers from a previously developed trunk marker set (marker set of List et al. (2013)), placed on the spinous processes of C7, T3, T5, T7, T9, T11 as well as L1-L5. (**C**) Rather than placing markers on specific anatomical landmarks, Rast et al. (2016) placed ten single markers equidistantly (each at 11% of the spinal length between sacrum and C7) in a line connecting all spinal processes. (Images reused with copyright permission of Wolters Kluwer Health and Elsevier. A from Leroux et al. (2000), B from List et al. (2013) and C from Rast et al. (2016).)

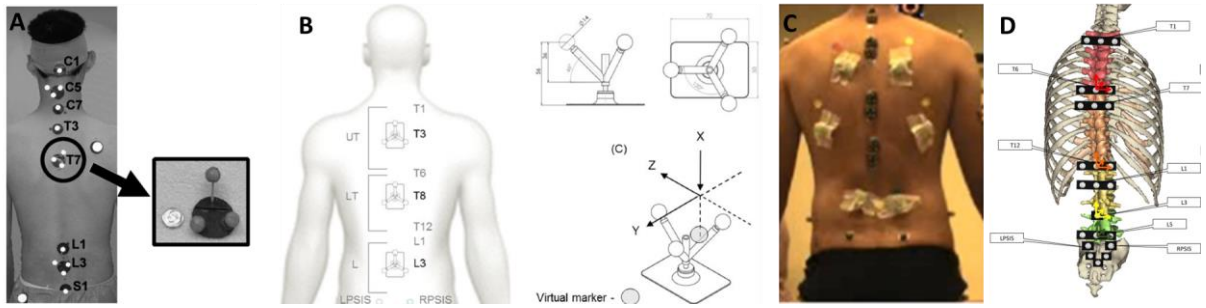

Figure 9: Examples of the use of marker clusters. (**A**,**B**) Three marker triads were used to capture spinal motion during gait in healthy subjects (Konz et al., 2006; Needham et al., 2016). (**C**) Marker protocol used by Mousavi et al. (2018) and Burkhart et al. (2020) consisting of rigid clusters with four markers each, attached over the palpated T1, T4, T5, T8, T9, T12 and L1 spinous processes. (**D**) Papi et al. (2019) defined an upper and lower thoracic as well as upper and lower lumbar region separated by three-marker clusters positioned horizontally over specific landmarks. (Images reused with copyright permission of Wolters Kluwer Health, Open Access of the International Society for Prosthetics and Orthotics 2016 and Elsevier. A from Konz et al. (2006), B from Needham et al. (2016), C from Mousavi et al. (2018) and D from Papi et al. (2019).)

Second, soft tissue presence over palpable spinal landmarks hinders accurate and standardized placement. Single markers -and even more marker clusters- require to be accurately placed - and in case of marker cluster- oriented on the skin overlying the anatomical landmarks according to an agreed marker protocol to obtain accurate kinematic data. However, problematic palpation of anatomical landmarks and consequent marker misplacement has already been reported by Schmid et al. (2015) in AIS subjects. Given the typically more severe alteration in vertebral anatomies, we expect anatomical landmarks to be even more difficult to

palpate in ASD subjects, thereby further amplifying the risk of erroneous marker positioning with respect to the underlying anatomy.

In summary, it is practically infeasible to define an accurate marker protocol in ASD patients that fully and accurately determines the position of each individual vertebra, i.e. having at least three non-collinear markers that can be assumed accurately positioned with respect to the underlying anatomy thereby creating a fully determined system. When this condition is not met, i.e. there are more DOFs than can be traced with the applied set of markers, the system is said to be underdetermined.

In silico

Using only marker-based motion capture, it is thus currently impossible to directly measure 3D spinal kinematics at the IV joint level in ASD subjects. However, as will be explained in this section, *in silico* analyses allow to integrate a priori information of the ASD subject that could enable measuring IV spinal kinematics. *In silico* herein refers to the use of computer models driven by experimentally determined input to measure often difficult to obtain information. A priori information could for example refer to the specification of kinematic constraints that mathematically reduce the DOFs of the system and thus prevent unrealistic intervertebral motions (Alemi et al., 2021). The most frequently used types of *in silico* models in biomechanical research are Finite Element Models (FEMs) and Multi-Body Models (MBMs) (Jalalian et al., 2013).

In spinal research, finite element (FE) studies describe musculoskeletal structures as deformable objects aiming to evaluate stress-displacement and shear distributions of bone and soft tissues with a high spatial and temporal resolution (W. Wang et al., 2014). The typical computationally expensive computer simulations associated with the use of these models require well-defined loading and boundary conditions to calculate spine kinematics and the associated bony deformations. In spinal research, FE models typically study only a limited region of the spine and have for example been used for in-depth analyses of vertebral stresses (Fagan et al., 2002) and vibrational characteristics (Xu et al., 2017). Another important application relates to the assessment of loads on surgical instrumentation that are otherwise difficult to measure. Therethrough, instrumentation failures such as fractures (Wui et al., 2020) or screw loosening (Guvenc et al., 2019) can be investigated in ASD. Additionally, FEMs have also been applied for pre-operative spinal surgery planning (Roth et al., 2021). Nonetheless, they are not preferred for analysis of large musculoskeletal systems (as used in for example lower limb gait analysis or in this case a large amount of consecutive vertebral segments) due to limitations concerning the significant computational burden (Ghezelbash et al., 2017), numerical instabilities (Zhang et al., 2019) and the requirements for well-defined loading and boundary conditions. To *in vivo* evaluate larger regions of or the full-body locomotor system during activities of daily living such as gait, staircase walking, sit-to-stance, etc., MBMs are recommended over FEMs.

MBM or rigid body modeling indeed allows to describe the motion of and load on the non-deformable (i.e. rigid) segments using recorded MOCAP data as input. Belonging to the MBM class, a musculoskeletal (MS) model is a mathematical representation of the skeletal and

muscular anatomy of a person. Herein, each body segment[3] is represented by a mass, a center of mass, inertial and dimensional (scaling) properties and a 3D geometry. In a chain-like structure, each body segment is connected to one or more adjacent segments through a joint that describes the kinematics of the associated DOFs. As suggested by the term *M*S model, these models can also contain a definition of the muscular geometry and force generating capacity, however this is outside the scope of this dissertation. In this dissertation, we will use the term 'model' to refer to computer models representing the anatomy of a person. When a computer model is used to perform an *in vivo* measurement, it is often also referred to as an *in silico* measurement.

It's imperative that the appropriate MS model is selected and that its complexity is in agreement with the demands of a specific research question (Hicks et al., 2015). To that end, a large set of generic MS models have been made available. For example, the SimTK repository (simtk.org) of the OpenSim simulation software (S. L. Delp et al., 2007), an open-source platform for multi-body analyses of biomechanics, and the repository of the AnyBody System (AnyBody Technology A/S, Aalborg, Denmark) (Damsgaard et al., 2006) contain a number of available models. These models are typically build upon previous versions of a model or are based on combinations with other available models (Favier et al., 2021).

The largest portion of available MS models are developed for lower limb research and therefor simplify the spine as one rigid segment without IV joints (e.g. *Gait2392* (Figure 10A) (S. L. Delp et al., 2007)). Hence, they do not allow estimating IV joint motion. Alternatively, the spine has also been represented as a chain of vertebrae (de Zee et al., 2007; Han et al., 2012; Christophy et al., 2012; Bruno et al., 2015, Vasavada et al., 2018), where individual vertebrae are modeled as rigid bodies connected cranially and caudally by a joint (Jalalian et al., 2013), thereby constraining the system and allowing more detailed and physiological analyses of spine motion.

Focusing first on the generic spine models available in OpenSim, the '*constrained lumbar models*' are a set of detailed spine models, developed by Christophy et al. (2012). Three implementations of this model exist (*Lumbar4*, *Lumbar210* and *Lumbar238* model), with the number indicating their increasing number of muscles (Figure 10B). In these three models, the IV joints at the lumbar region are defined as spherical joints thus allowing three rotational DOFs (flexion-extension (FE), lateroflexion (LF) and axial rotation (AR)). A distribution of motion over all lumbar segments is assured through the integration of kinematic constraints that ensure the linear distribution of the overall (or global) lumbar spine motion over the individual five lumbar vertebrae based on ratios previously reported by Christophy et al. (2012). The kinematic constraints thus eliminate the DOFs at each local IV joint, giving the lumbar spine a total of three effective DOFs for global motion. Unfortunately, the thoracic spine and the ribcage are modeled as one rigid body attached to a single vertebra, limiting its

[3] The term 'body segment' is used rather than 'bone' as multiple bones can be grouped together in a rigid 'body segment' to reduce model complexity when motion between the individual bones is not relevant for the research question.

use for full spine motion analysis. The '*enhanced'* model of Senteler et al. (2015) combined the above model with a neck model (Vasavada et al., 1998) and upper extremities (Holzbaur et al., 2005) (Figure 10C). Furthermore, the joint constraints are replaced with linear, 6-DOF bushing elements representing stiffness at the IV joint levels to allow relating forces and moment to displacements and rotations at the IV joint. The '*constrained lumbar models*', more specifically the *Lumbar238* model, was also extended into a fully articulated '*thoracolumbar spine model'* (Bruno et al., 2015), where all IV joints (T1 to sacrum) are also modeled as spherical joints, thus allowing three rotational DOFs: FE, LF and AR between consecutive vertebrae (Figure 10D). The model thus contains 54 DOFs for the pelvis, spine and neck with head. Also, 72 DOFs are included for the ribs, 6 DOFs for the sternum and 14 DOFs for the shoulder and arms. This makes a total of 140 DOFs for the entire model. This model incorporates the cervical spine (C1 to C7) and skull as one rigid object and therefor does not allow motion between the individual cervical vertebrae and the skull. Several additional variations of these models have been introduced in the literature, for example by combining spine models with lower-limb models or modifying joint definitions (Actis et al., 2018; Kim and Zhang, 2017; Raabe and Chaudhari, 2016). Beaucage-Gauvreau et al. (2019) modified the spinal range of motion and the muscle parameters of the latter model, and validated this new model for estimating spinal loading during lifting tasks in patients with low back pain. Very recently, a new full-body MS model including a detailed implementation of the lower limbs and lumbar spine was developed and validated for estimating muscle activations during a range of lifting tasks in healthy individuals (Favier et al., 2021).

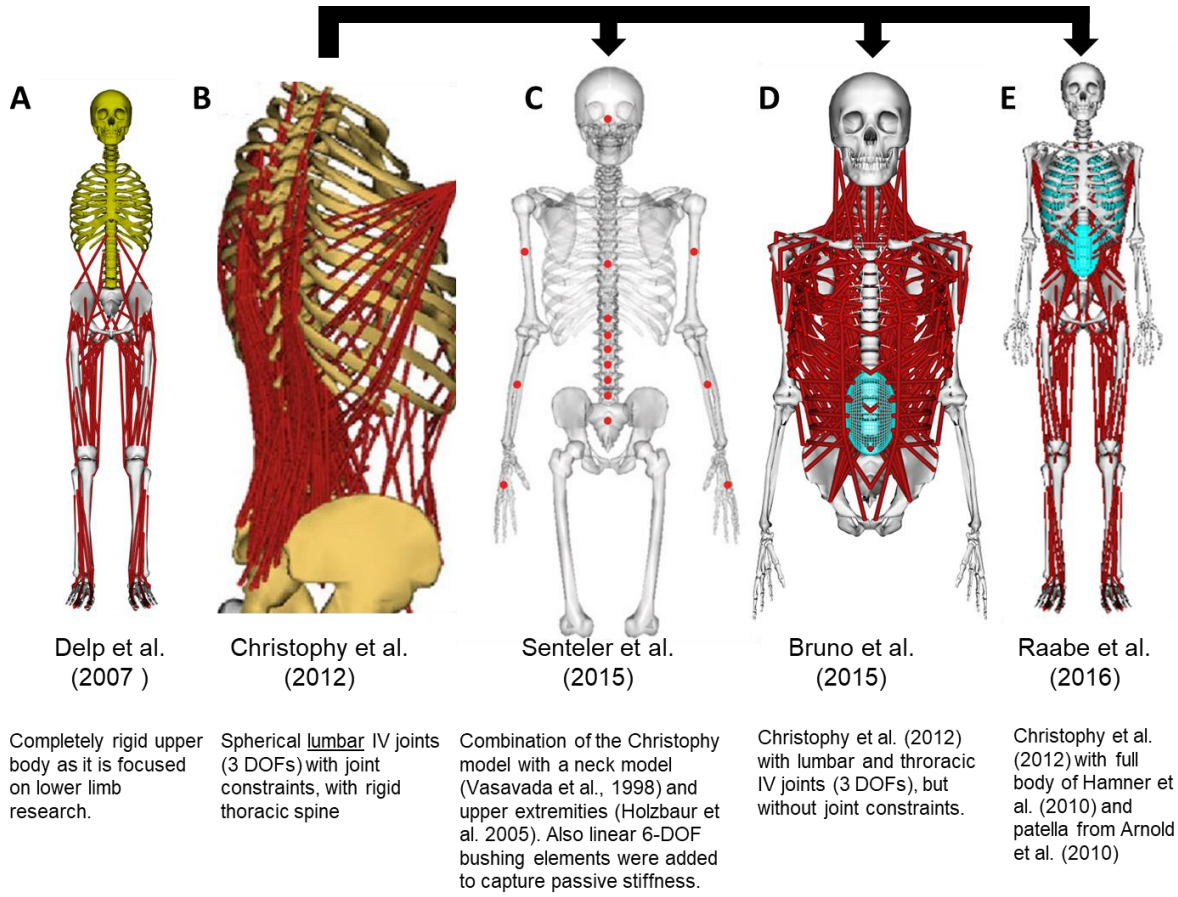

Figure 10: An overview of the most important publicly available generic OpenSim models, relevant in the context of this work. Intermediate developments or small variations on existing models (e.g. changes in muscle parameters or constraint definitions) are not shown here. (Images reused with copyright permission. (A) from S. Delp et al. (2007) through open access of IEEE, (B) from Christophy et al. (2012) through open access of Springer, (C) from Senteler et al. (2015) with permission from Taylor & Francis (D) from Bruno et al. (2015) (image created in OpenSim) and (E) from Raabe and Chaudhari (2016) with permission from Elsevier.)

Also within the AnyBody platform several spine models have been developed. In 2007, de Zee et al. created a lumbar spine model, comprising of a pelvis/sacrum, five lumbar vertebrae and a rigid thorax interconnected using three-DOF spherical joints (Figure 11A). This lumbar spine model was the basis for further developments, such as the *enhanced* spine model of Han et al. (2012). Compared to the model of de Zee et al., this model contains an improved definition of muscles, ligaments, IV disc stiffness and intra-abdominal pressure. The thoracolumbar spine model developed by Ignasiak et al. (2016) was modified to allow articulation in the thoracic region, while the full-body model by Bassani et al. (2017) additionally added the extremities (Figure 11B-D).

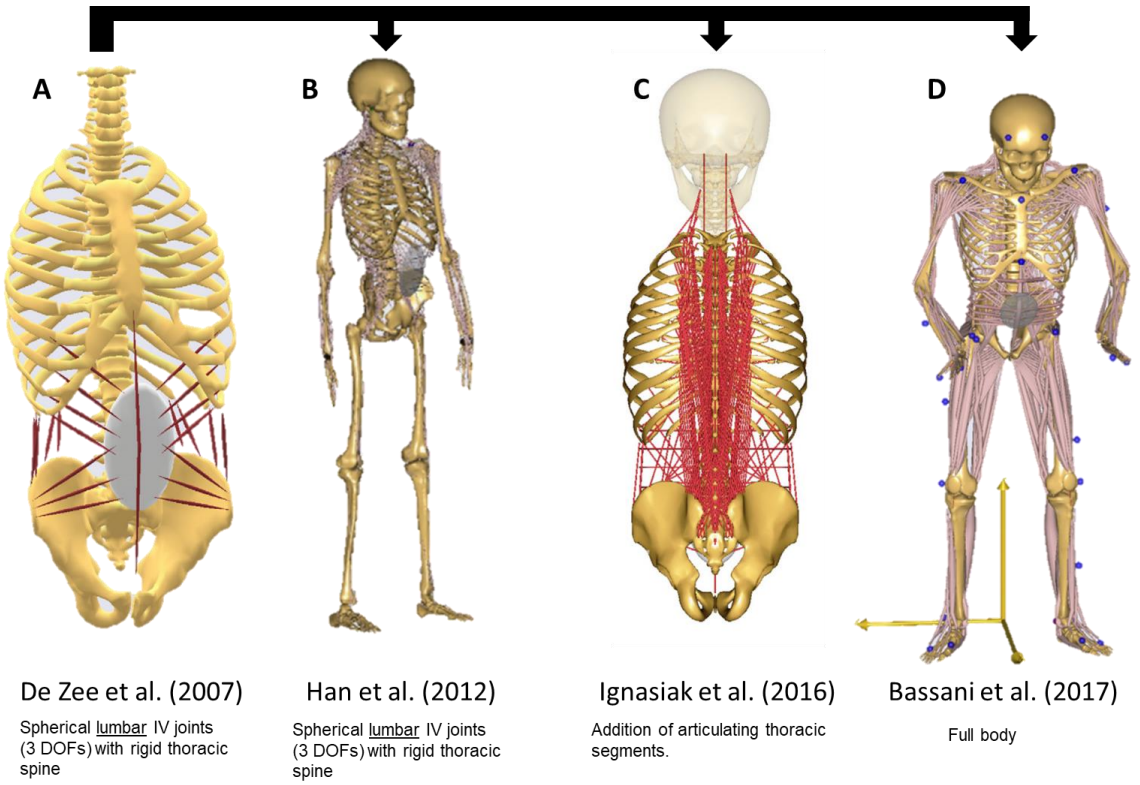

Figure 11: Examples of the spine models in the AnyBody repository. The model by (**A**) de Zee et al. (2007) served as a base model for the development of the models by (**B**) Han et al. (2012), (**C**) Ignasiak et al. (2016) and (**D**) Bassani et al. (2017b). (Images reused with copyright permission from Elsevier.)

Independent of the modeling platform, MS models have been used to assess biomechanical characteristics of the healthy spine up to the level of muscle and contact forces (Actis et al., 2018; Bruno et al., 2017; Burkhart et al., 2017; Connolly et al., 2021; Raabe and Chaudhari, 2016; Rupp et al., 2015; Schmid et al., 2020a). Although such objective dynamic and functional assessments could also provide a wealth of data to investigate locomotor function in ASD, these techniques have, to the best of our knowledge, not yet been used to evaluate dynamic motion in ASD. **The use of dynamic movement analysis based on generic MS models for investigating spinal kinematics in ASD patients is thus still unexplored.**

Challenges for use of musculoskeletal models and simulation in adult spinal deformity

In general, MS models have been frequently used to evaluate (pathological) kinematics of the upper and lower limbs (Anderson and Pandy, 2001; Borbély and Szolgay, 2017; Delp et al., 1990; Kainz et al., 2016). This dissertation will focus on the ASD spine as this, generally unexplored, field within MS modeling and simulation is faced with several new challenges, described hereafter.

MS modeling and simulation have clear potential to provide information on the functional ability of ASD patients (Briggs et al., 2007, 2006; Harrison et al., 2005) and thus may help

responding to the above-defined Clinical gap 2. Indeed, as described before, the use of MS models allows to integrate kinematic constraints interconnecting the articulating segments of the spine. This allows to make estimations on IV joint motion (Alemi et al., 2021), not possible through direct use of MOCAP (as described on p. 28). However, the use of generic MS models in an ASD population poses an additional issue related to the representativeness of the model to the subject.

Indeed, to ensure that estimations of IV joint kinematics are sufficiently accurate, MS models should reflect the subject's anatomy as closely as possible, especially in the case of pathology (Scheys et al., 2008; Wesseling et al., 2016). Applied to ASD, the model should thus be representative of the patient-specific spino-pelvic skeletal deformity. Therefore, the MS model does not require musculature or inertial properties to estimate joint kinematics.

Generic models are commonly first scaled to the subject's anthropometry using marker-based ratios derived from a static pose recorded in the motion lab or *a priori* known scaling factors (for example determined from measurements on medical images). Such marker-based scaling is then achieved by calculating ratios between actual or experimental marker pairs and corresponding virtual or model marker pairs (Figure 12) which are then applied to scale the corresponding bone geometries. The *real* or *experimental* markers are the markers which are attached to the subject's skin, typically at standardized locations above anatomical landmarks. The *virtual* or *model* markers are placed at the corresponding locations on the computer model. During the scaling, the joint angles and positions are also accommodated to the recorded static motion capture data to obtain a scaled model matching the recorded static pose. This step is referred to as *the scaling and initialization of the generic model*.

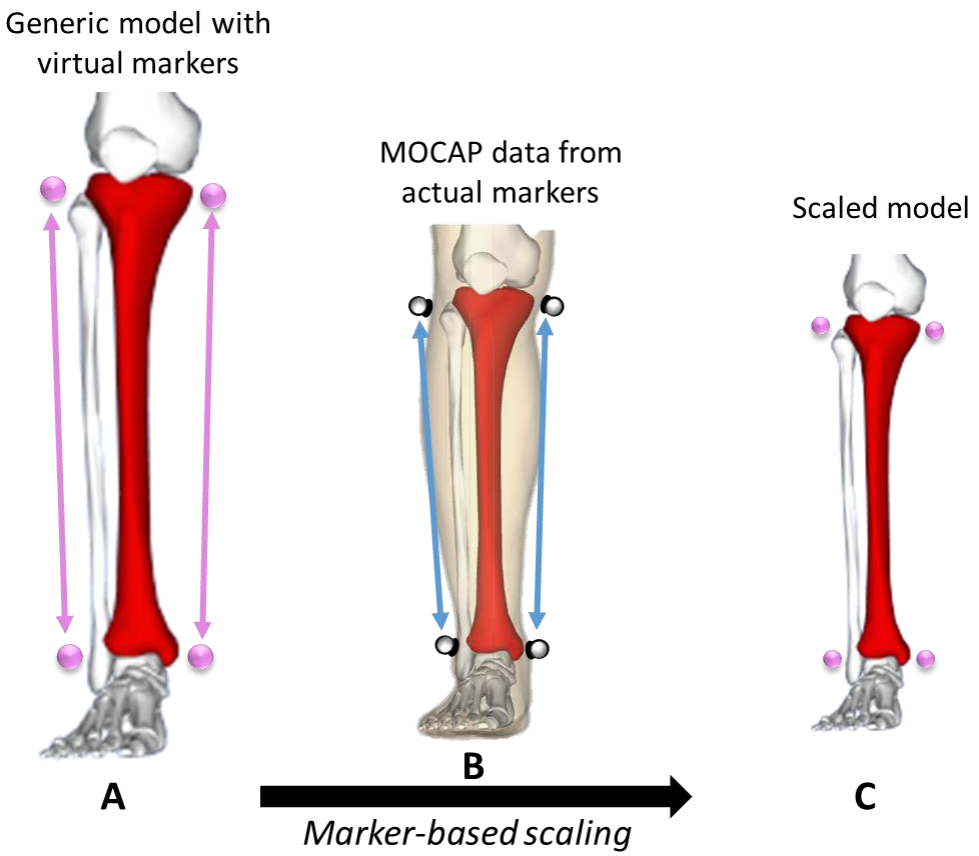

Figure 12: Illustration of the marker-based scaling of a femur. (**A**) A generic model containing virtual markers (pink). (**B**) A subject wearing actual (experimental) markers (white). (**C**) The femur segment is scaled using the ratio of marker-distances determined in A and B. (Open use of images under the CC BY-SA license of Wikipedia.)

Thereafter, inverse kinematics estimates joint kinematics based on this scaled model and the marker trajectories recorded during the motion. For example, in Lu and O'Connor (1999), an optimization algorithm minimizes the difference between the experimental marker positions (recorded as MOCAP data) and corresponding virtual model markers at each time frame. This allows to obtain kinematic information on the relative joint orientations that is generally difficult or not accessible in non-invasive in-vivo research. Although out of the scope of this dissertation, subsequent to inverse kinematics, additional analyses can be performed based on the MS model to obtain estimations of the kinetics and even muscle forces and consequent joint loading underlying the recorded motion.

In healthy subjects, subject-specificity of generic models can indeed be achieved through scaling of the spine and has been demonstrated to provide excellent reliability (Burkhart et al., 2020) and posture estimates (Mousavi et al., 2018). However, as will be explained below, marker-based scaling of generic models fails to correctly represent the spino-pelvic deformities of ASD patients.

As mentioned, marker-based scaling requires the definition of marker pairs between which scaling factors are determined. The markers from which the ratios are defined, should however represent different anatomical landmarks, yet not span multiple joints. However, no marker

model is currently available with multiple anatomical landmarks on each vertebra. This prevents marker pairs to be defined without spanning more than one IV joint and consequently individual vertebrae cannot be scaled. Secondly, the initialization of the ASD model in a semi-static pose, represented by a set of joint angles and positions, cannot be reached unambiguously in an underdetermined system (i.e. having more DOF than constraints). Alternatively, a determined system, through the implementation of kinematic constraints, still fails to reach a representative solution because (1) the generically defined constraints do not allow representing pathological curves and (2) the optimization often suffers from the inaccurate marker placement (described on p. 29) to correctly initiate the model.

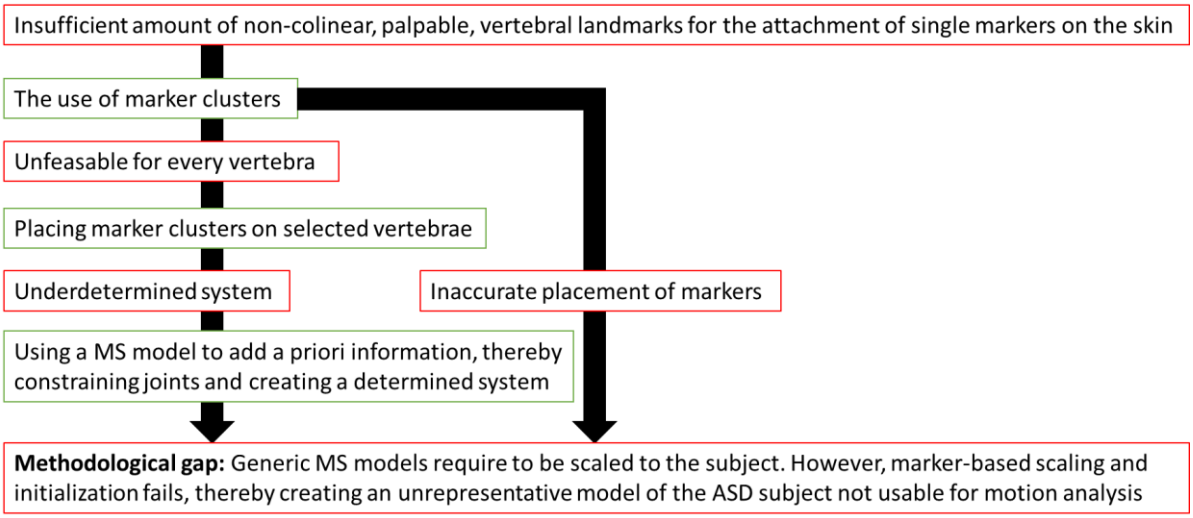

Figure 13: Schematic overview summarizing the different components leading up to the methodologic gap of this dissertation.

In conclusion, the above two reasons invalidate the use of marker-based scaling of generic models to accurately represent an ASD subject's spinopelvic deformity and therefor impede accurate in vivo measurement of IV kinematics (Methodological gap) (Figure 13). Figure 14 illustrates the failing of the marker-based scaling and initialization algorithm to create a representative model for an ASD patient.

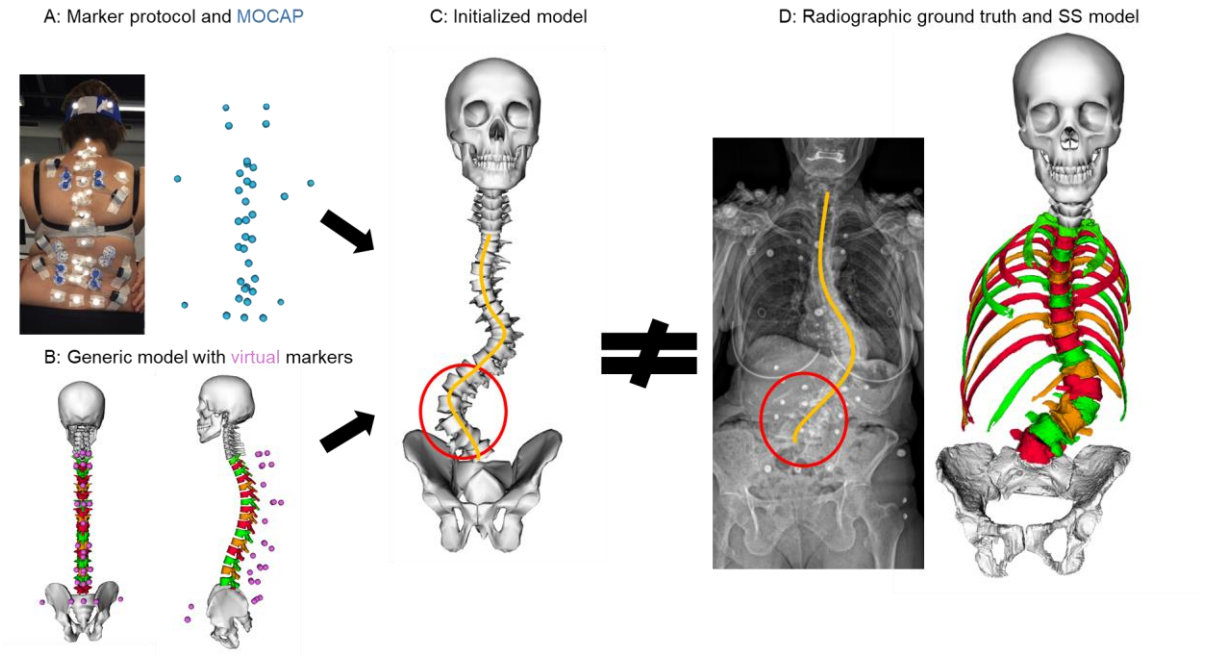

Figure 14: Failing use of a generic model in ASD subjects. (**A**) An ASD subject was instrumented with a representative state-of-the-art spine-specific marker protocol (white dots in the picture) whose 3D position was recorded using motion capture (MOCAP in blue). (**B**) Corresponding virtual markers were attached to the generic spine model of Bruno et al. (2015a) as described in the marker protocol (pink). (**C**) Using OpenSim's initialization algorithm, the determined initial pose strongly diverges from (**D**) the patient's actual spinal alignment in the radiograph and the subject-specific (SS) 3D reconstruction.

Very recent work targeted a similar methodological gap for modeling in the AIS population. Rather than making use of marker-based scaling approaches, radiographic imaging was used to integrate the subject-specific alignment in generic MS models (Barba et al., 2021; Schmid et al., 2020b; Shayestehpour et al., 2021). More specifically, the spinal malalignment of AIS patients was transferred to a model using input parameters such as TK and Cobb angles (Barba et al., 2021; Shayestehpour et al., 2021) or vertebral tilt angles and IV disc distances (Schmid et al., 2020b) measured from biplanar radiographs (Figure 15). These models were then used to evaluate trunk muscle strength and activity, and compressive forces (Barba et al., 2021; Schmid et al., 2020b) or to perform simulations of deformation patterns aiming to evaluate its evolution and pathomechanism (Shayestehpour et al., 2021). Even the effect of surgical interventions on posture and spinal loading in static conditions has been investigated through such models (Ignasiak et al., 2018a; Ignasiak, 2020; Kuai et al., 2019). However, the created models have only been limited to theoretical simulations, referring to the use of prescribed motion to the spine instead of using experimental data collected in the laboratory. To the author's knowledge, no work has been performed where subject-specific modeling was combined with marker-based motion analysis in ASD.

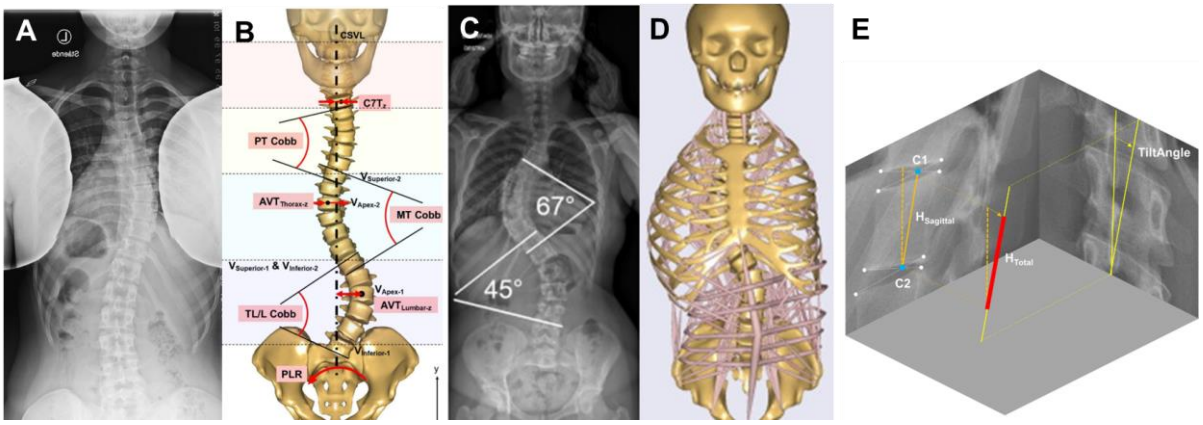

Figure 15: Illustration of recent work in subject-specific modeling in AIS through parameterization of the global alignment of (**A,B**) Shayestehpour et al. (2021) and (**C, D**) Barba et al. (2021). (**E**) Illustration of an anatomical landmark-based measurement of the position and orientation of individual vertebrae in AIS patients (Schmid et al., 2020b), building further on Bassani et al. (2017a). (Images reused with copyright permission from Springer Nature, Elsevier and open access of Frontiers in Bioengineering and Biotechnology.)

Conclusion

Clinical assessment (Clinical gap 1 and Clinical gap 2), surgical decision-making and outcome evaluation (Clinical gap 3) in ASD are currently dominated by their overall subjective and/or static character. While objective dynamic information originating from motion analysis has revolutionized other orthopaedic fields, specific issues (Methodological gap) are preventing a similar evolution in ASD. In summary, due to the combination of deformed vertebral geometry, spinal malalignment and difficult accessibility (Gonnella et al., 1982) of sufficient vertebral anatomical landmarks, marker-based scaling methods inherently fail to generate a model accurately representing a patient-specific spinal deformity. In addition, palpation errors result in inaccurate spinal kinematic simulations (Schmid et al., 2015). These inaccuracies are expected to increase with the more aberrant anatomy associated with ASD causing further complicating palpation of typically-used anatomical landmarks. As a result, generic models combined with marker-based scaling and initialization are likely not representative for the evaluation of spinal motion in ASD patients. **In conclusion, despite the potential of musculoskeletal simulations in ASD, current models and simulation techniques do not allow calculating spinal kinematics in ASD, limiting biomechanical research and clinical advances.**

Objectives

As described previously, the complication and revision rates of surgical treatment in ASD are high. A possible cause is the limited insight in and inclusion of dynamic aspects in the clinical evaluation, decision-making and outcome assessment **(Clinical gap 3**). Although several studies are analyzing global posture during motion, **there is still a need to get more detailed information on the motion of the individual vertebral segments, i.e. spinal kinematics, during activities of daily living.**

To this end, the overarching hypothesis of this work is that MS computer models and multi-body simulations allow to reliably measure spinal kinematics in ASD. Therefore, **the general objective** of this dissertation is to develop a modeling and evaluation platform and illustrate its potential to improve our understanding of pathological spine kinematics during dynamic activities of ASD patients. As such, on the long term, this project aims at improving insight on pathological spinal function during dynamic activities and lead the way from the current 2D static, towards integrated 3D, functional evaluation of spinal deformities.

As described previously, non-invasive, *in silico*, spinal kinematic measurements in ASD patients using generic musculoskeletal models are currently not possible. Therefore, the aim of **Chapter 1** is to (1) develop a patient-specific MS modeling method and associated marker protocol to estimate IV joint kinematics; and, (2) validate the accuracy of this modeling method and the accuracy of marker-based tracking.

Following the developments made in Chapter 1, the aim of **Chapter 2** is to quantify how reliable spinal kinematics can be assessed in ASD patients with the developed modeling method.

Chapter 3 aims to (1) introduce novel methods to comprehensively quantify effects of spinal deformities on spinal kinematics during forward trunk flexion and (2) evaluate relations with routinely used, clinical spino-pelvic parameters, vertebral body deformity, and self-reported HRQoL in a pilot population.

Chapter 4 (Exploratory study) aims to evaluate the modeling and evaluation platform to measure spine kinematics during trunk flexion before and after spinal fusion surgery in ASD, focusing on (1) the changes in *global* spinal motion during maximal voluntary trunk flexion, pre- and post-operatively, as well as (2) the *vertebral (or local)* motion of the unfused vertebrae.

Chapter 1

Development and validation of a modeling workflow for the generation of image-based, subject-specific thoracolumbar models of spinal deformity

Thomas Overbergh[1]
Pieter Severijns[1, 2]
Erica Beaucage-Gauvreau[1]
Ilse Jonkers[3]
Lieven Moke[1,4]
Lennart Scheys[1,4]

Published as:

Overbergh, T., Severijns, P., Beaucage-Gauvreau, E., Jonkers, I., Moke, L., Scheys, L., 2020. Development and validation of a modeling workflow for the generation of image-based, subject-specific thoracolumbar models of spinal deformity. J. Biomech. 110, 109946.

Affiliations:

[1]Institute for Orthopaedic Research and Training (IORT), Department of Development and Regeneration, Faculty of Medicine, KU Leuven, Leuven, Belgium

[2]Department of Rehabilitation Sciences, KU Leuven, Leuven, Belgium

[3]Department of Movement Sciences, KU Leuven, Leuven, Belgium

[4]Division of Orthopaedics, University Hospitals Leuven, Leuven, Belgium

Abstract

Quantitative dynamic evaluation of spino-pelvic motion in subjects with spinal deformity using optical motion analysis is currently lacking. The aim of this study was to develop and validate subject-specific, thoracolumbar spine multi-body skeletal models for evaluating spino-pelvic kinematics in a spinal deformity population.

A new workflow for creating subject-specific spino-pelvic models in a weight-bearing position through computed tomography (CT) and biplanar radiography is described. As part of a two-step validation process the creation of such a model was first validated against a ground truth CT reconstruction of a plastinated cadaver. Secondly, biplanar radiographic images of one healthy and 12 adult spinal deformity subjects were obtained in two standing positions: upright and bent. Two subject-specific models for each of these subjects were then created to represent both standing positions. The result of inverse kinematics solutions, simulating the specific bending motion using the upright models, are compared with the models created in bent position, quantifying the marker-based spino-pelvic tracking accuracy.

The workflow created spinal deformity models with mean accuracies between 0.71-1.59 mm and 1.25-2.27° for vertebral positions and orientations, respectively. In addition, the mean marker-based spino-pelvic tracking accuracies were between 3.1-5.0 mm and 2.9-5.6° for vertebral positions and rotations, respectively.

This study presented the first validated biplanar radiography-based method to generate subject-specific spino-pelvic, MS models that allows the inclusion of subject-specific bone geometries, the personalization of the 3D weight-bearing spinal alignment with accuracy comparable to clinically used software for 3D reconstruction, and the localization of external markers in spinal deformity subjects. This work will allow new concepts of dynamic functionality evaluation of patients with spinal deformity.

Introduction

Static and two dimensional (2D) imaging-based measurements are the basis of current quantitative diagnosis, pre-operative planning and clinical management in adult spinal deformity (ASD) (Terran et al., 2013). Although operative treatments have satisfying effects on pain, disability, spinal alignment, and quality of life (Hassanzadeh et al., 2012; Smith et al., 2009b, 2009a; Turner et al., 2015), post-operative complications and revision surgery remain common: a recent multicenter study indicated that 52.2% of the ASD patients suffered from perioperative complications and 42.6% were affected by post-operative complications (Smith et al., 2016). Revision rates after surgical correction of spinal deformity range from 9% to 35.6% (Ha et al., 2013; Pichelmann et al., 2010; Sanchez-Mariscal et al., 2014; Scheer et al., 2013; Soroceanu et al., 2015).

These high rates are believed to be partly due to the inherent failure of capturing the complete spine functionality using 2D static radiographic evaluation measures (Moke, 2018). Similarly to lower limb research (Scheys et al., 2011a; Wren et al., 2011), instrumented motion analysis can complement current radiographic evaluations of the deformed spine to provide information on functional biomechanical parameters, such as spino-pelvic kinematics and kinetics during functional activities of daily living (Diebo et al., 2018), thus potentially improving its treatment.

When using instrumented motion analysis, the movement of a subject is recorded using optical motion capture systems tracking the three dimensional (3D) trajectories of reflective markers placed on the skin surface overlying specific anatomical bony landmarks of a rigid body (in this case individual vertebrae). A generic model, composed of multiple rigid bone geometries connected by joints (S. L. Delp et al., 2007), is then scaled to the subject's anthropometry using a static pose. Thereafter, inverse kinematics (Lu and O'Connor, 1999), an optimization algorithm minimizing the difference between the experimental marker positions and corresponding virtual model markers at each time frame, provides the joint angles in the scaled model. The trunk is often modeled as one single rigid body by current musculoskeletal models (e.g. *Gait2392_Simbody* (S. L. Delp et al., 2007)), thus limiting analysis of motion of individual spinal segments. Alternatively, the spine has also been represented as a chain of vertebrae (de Zee et al., 2007; Han et al., 2012; Christophy et al., 2012; Bruno et al., 2015), where individual vertebrae are modeled as rigid bodies connected cranially and caudally by a joint (also referred to as a functional spinal unit (FSU)) (Jalalian et al., 2013). Notably, a trunk model with a detailed lumbar spine (Christophy et al., 2012) was developed in OpenSim, an open-source platform for multi-body analyses of biomechanics. That model was further extended into a fully articulated thoracolumbar spine model (Bruno et al., 2015), where the intervertebral (IV) joints (T1 to S1) are modeled as spherical joints, thus allowing three rotational degrees of freedom (DOFs): flexion/extension (FE), lateroflexion (LF) and axial rotation (AR) between adjacent vertebrae. However, to the best of the authors' knowledge, all currently available generic models represent healthy, non-deformed spines and consequently these models have mainly been used to estimate spino-pelvic kinematics, loading and muscle activation of healthy subjects

(Bruno et al., 2015; Rupp et al., 2015; Wada et al., 2014; Xia et al., 2010; Bassani et al., 2019; Ghezelbash et al., 2016).

Musculoskeletal models should be an optimal representation of the subject's anatomy before being used for instrumented motion analysis, especially in the case of pathology (Scheys et al., 2008; Wesseling et al., 2016). Consequently, using generic models in a spinal deformity population is currently problematic. In order to allow marker-based scaling, at least three markers need to be placed accurately on predefined non-collinear anatomical landmarks on each vertebra. However, due to the combination of deformed vertebral geometry, spinal malalignment and difficult accessibility (Gonnella et al., 1982) of at least three vertebral anatomical landmarks, marker-based scaling methods inherently fail to obtain sufficient information to generate a model accurately representing a specific spinal deformity from a healthy generic model. In addition, palpation errors result in inverse kinematics inaccuracies for spinal motion simulations (Schmid et al., 2015) that are expected to increase with the presence of spinal deformities due to the more difficult palpation of typically-used anatomical landmarks in deformed vertebrae.

In contrast to the accepted image-based modeling workflows for lower extremities (Scheys et al., 2008), image-based methods to develop de novo subject-specific models of subjects with spinal deformities have not yet been reported in the literature. The increased use of low-dose biplanar radiography (EOS Imaging System, Paris, France (Luo et al., 2015)) in spinal deformities offers new opportunities to overcome the challenges associated with scaling of generic models. The EOS Imaging System provides detailed three-dimensional (3D) information on (aberrant) weight-bearing spines (Illes et al., 2012; Melhem et al., 2016) of subjects in an upright standing position. As such, the imaged spino-pelvic alignment (i.e. the sacral, lumbar and thoracic vertebrae's relative positions and orientations) is more representative than with the supine imaging modalities commonly used for subject-specific modelling such as magnetic resonance imaging (MRI) or computed tomography (CT) (Brink et al., 2017). Additionally, previous research has indicated the potential of biplanar radiographic imaging for the definition of joints as well as the registration of external optical motion capture markers in relation to the underlying rigid bones (Pillet et al., 2014). Therefore, the objective of this study was to develop and validate a workflow for the construction of subject-specific models of subjects with spinal deformities using biplanar radiography, and to evaluate the spino-pelvic kinematic tracking accuracy of these models.

Materials and methods

The generic thoracolumbar musculoskeletal model with spherical IV joints by Bruno et al. (2015) was used in this study with the simulation software OpenSim 3.3 (Stanford University, USA). To allow the use of a generic model for inverse kinematics analysis in an adult spinal deformity subject, a personalization workflow, schematically represented in Figure 16, was developed to obtain a model with subject-specific spino-pelvic bone geometries (from CT) and alignment (from biplanar radiography).

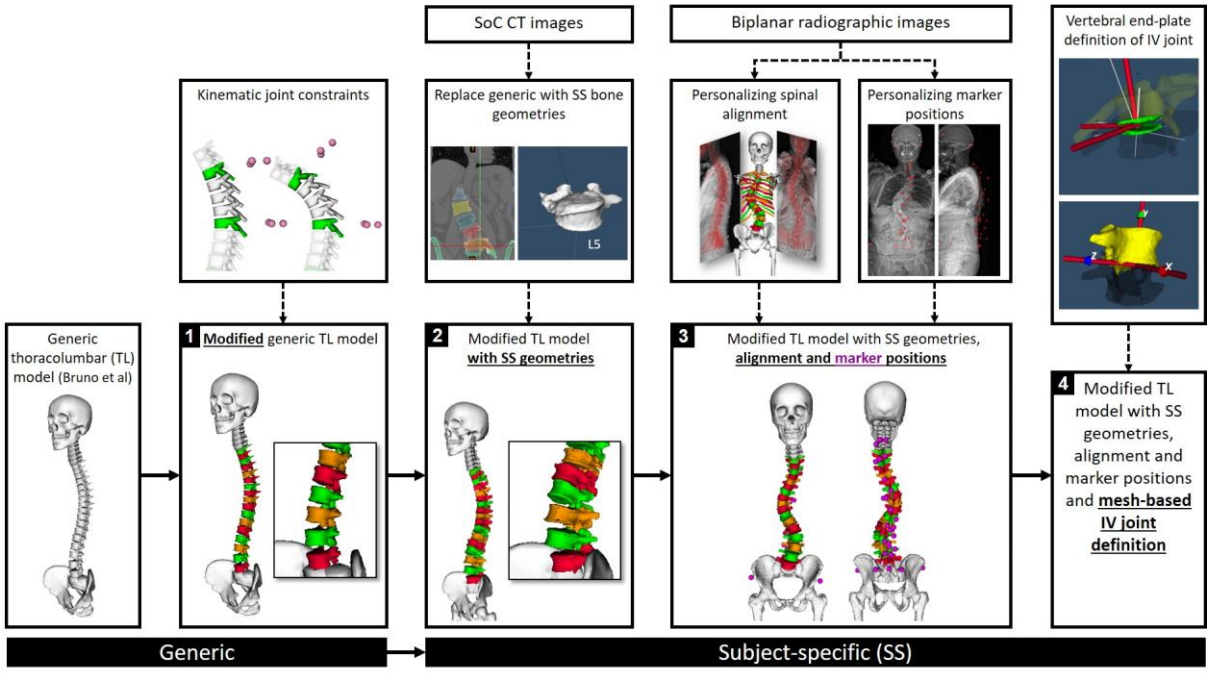

Figure 16: Workflow for creating a subject-specific spino-pelvic model. (**1**) The generic thoracolumbar (TL) model by Bruno et al. (2015) is first modified by adding kinematic coupling constraints to accommodate for the marker placement protocol. (**2**) Standard of care (SoC) CT segmented bone geometries are used to replace the generic bones in the modified TL generic model. (**3**) These subject-specific (SS) bone geometries are manually positioned and rotated, as to obtain the alignment presented in the biplanar radiographic images. From these images, the position of the markers is also extracted. (**4**) The intervertebral (IV) joints are defined using a vertebral endplate mesh-based method (further elaborated in Appendix 2).

Modified generic model

A new spinal marker placement protocol taking into consideration space limitations on the vertebrae and subject comfort during functional task was developed based on a combination of the marker protocols used in Needham et al. (2016) and Leroux et al. (2000). The resulting marker protocol consists of six asymmetrical, 3D-printed marker clusters positioned on the spinous processes of four thoracic (T1, T3, T7, T11) and two lumbar (L2 and L4) vertebrae. In addition, single reflective markers are placed on the left and right, anterior and posterior, superior iliac spine, on the sacrum and on T5, T9, T12 and L3 (Figure 17).

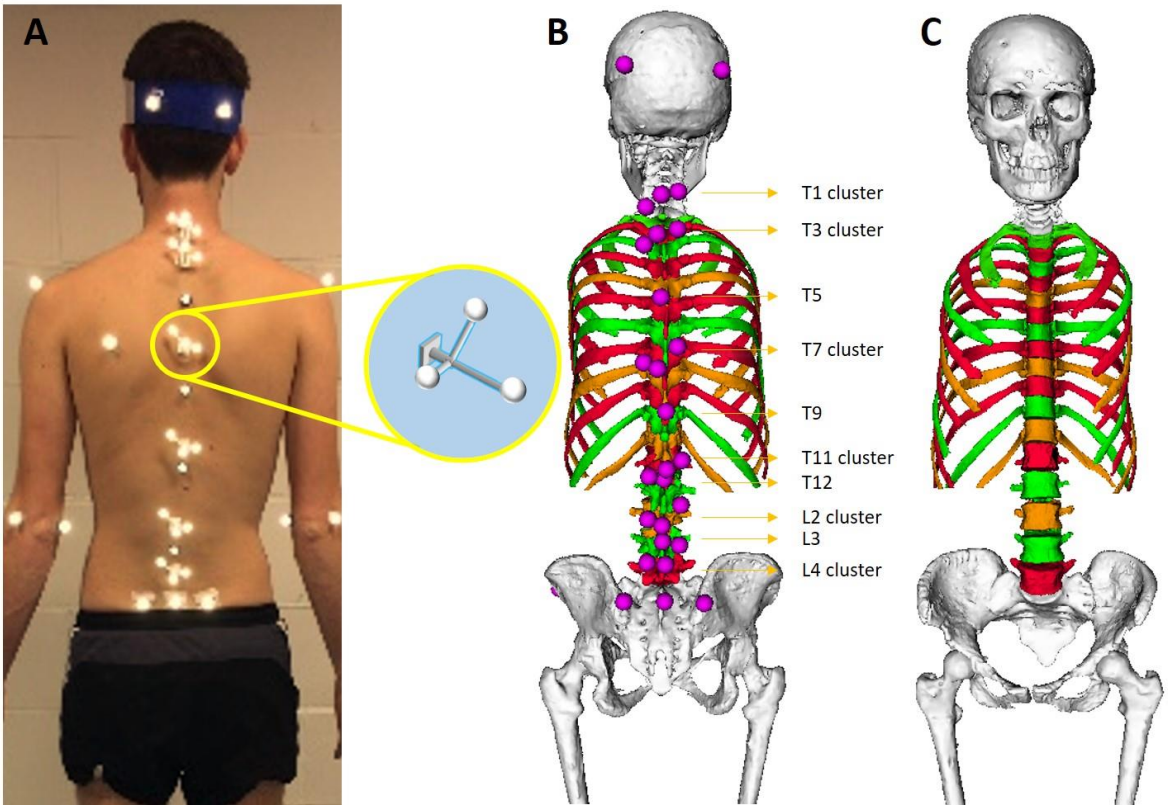

Figure 17: (**A**) Marker placement protocol with zoom on the design of the 3D-printed marker cluster (circle). (**B**) Posterior view of a subject-specific OpenSim-compatible skeletal model with placement of virtual markers (pink). (**C**) Anterior view of the model where green vertebrae have a marker cluster, orange vertebrae have a regular marker linked and red vertebrae are marker-free.

Linear kinematic coupling constraints were added to the generic thoracolumbar model (Bruno et al., 2015) to estimate individual IV joint motion as applied in the lumbar spine models of Christophy et al. (2012) and Beaucage-Gauvreau et al. (2019) and the cervical models of Vasavada et al. (1998) and Cazzola et al. (2017). After 33 kinematic coupling constraints were imposed, spine motion for the model was reduced to 24 DOFs. The kinematic coupling constraint values (Table 1) are described in detail in Appendix 1. The original thoracolumbar model by Bruno et al. (2015) combined with the described linear kinematic coupling constraints is further referred to as the modified generic thoracolumbar model (available on SimTK repository).

Table 1: Parameters for each degree of freedom (DOF) used for the kinematic coupling constraints per functional spinal unit (FSU). The kinematic coupling constraint values for the T1-T3, T3-T7 and T7-T11 groups (separated with double lines) were based on monosegmental ranges of motion (ROM) reported by Wilke et al. (2017), assuming linear relations. Kinematic coupling constraint values for the T11-L2 group were extracted from McDonnell et al. (2016). Values for the L2-L4 and L4-Sacrum groups were based on Christophy et al. (2012) and Fujii et al. (2007). (For more information see Appendix 1.) (Vertebrae in bold green indicate the presence of a marker cluster.)

FSU	Flexion/extension	Lateroflexion	Axial rotation
T1/T2	0.629	0.544	0.553
T2/**T3**	0.372	0.456	0.447
T3/T4	0.257	0.269	0.258
T4/T5	0.225	0.242	0.230
T5/T6	0.260	0.243	0.252
T6/**T7**	0.258	0.246	0.261
T7/T8	0.222	0.231	0.253
T8/T9	0.253	0.240	0.259
T9/T10	0.280	0.279	0.272
T10/**T11**	0.244	0.249	0.215
T11/T12	0.250	0.242	0.299
T12/L1	0.353	0.312	0.281
L1/**L2**	0.397	0.446	0.420
L2/L3	0.531	0.505	0.452
L3/**L4**	0.469	0.495	0.548
L4/L5	0.597	0.572	0.515
L5/Sacrum	0.403	0.428	0.485

Personalization of spino-pelvic bone geometries

Although the biplanar radiographic imaging system comes with proprietary software (sterEOS, EOS Imaging) allowing 3D reconstruction of pelvic and vertebral geometries, those 3D reconstructions were not available for export and could therefore not be integrated in the modified generic model. As alternative, for each subject, the pelvis, sacrum and individual lumbar and thoracic vertebrae are segmented from standard-of-care full spine CT images (BrightSpeed by GE Healthcare, at an inter-slice distance of 1.25 mm and a pixel size of 0.39x0.39 mm) using intensity thresholding, after which a surface wrapping algorithm is applied, filling small defects (Mimics 19.0, Materialise NV, Belgium). Every low-resolution generic body of the generic thoracolumbar model (Bruno et al., 2015) is then replaced with its corresponding higher resolution subject-specific surface mesh through an iterative closest point-based (ICP) registration procedure implemented in Meshlab (Cignoni et al., 2008), allowing to maintain the generic segmental reference frame definitions.

Personalization of spino-pelvic alignment

A custom software tool was developed to determine the subject-specific spino-pelvic alignment of the modified generic model with the inclusion of subject-specific spino-pelvic bone geometry (Figure 18). The spatially calibrated biplanar radiographic images (EOS Imaging) can be loaded into the software's 3D environment. The modified generic model with subject-specific spino-pelvic bone geometries is then placed into the software's 3D environment, automatically

creating contour-based digitally reconstructed radiographs (DRRs) for each bone segment projected onto each 2D radiograph. It hereby takes the radiographic fan-beam effects into account by using the direct linear transform principle (Abdel-Aziz, 2015) combined with the intrinsic calibration parameters of the imaging system.

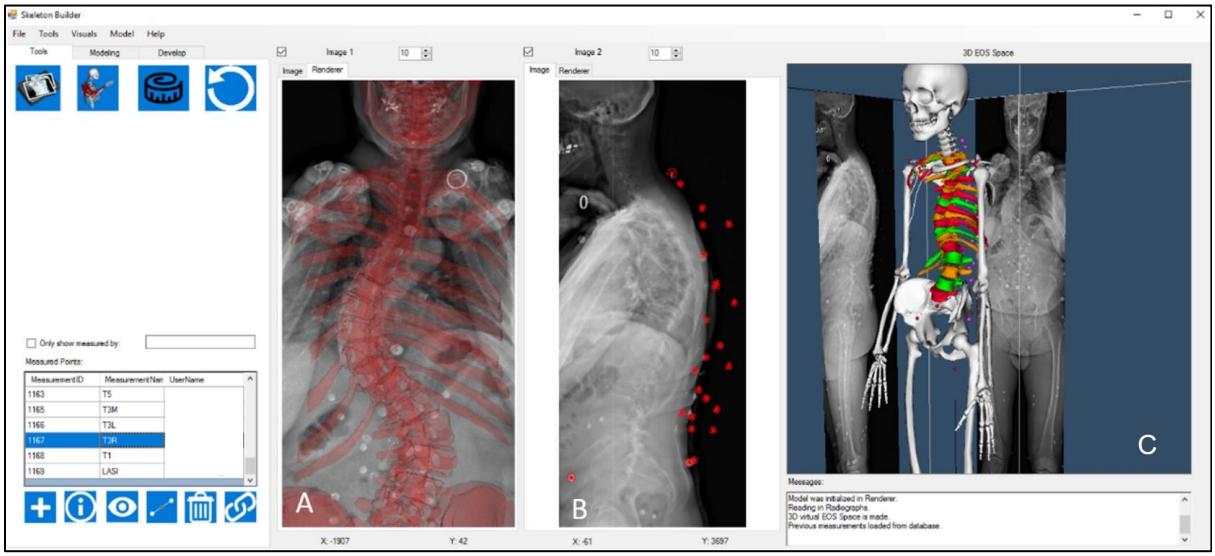

Figure 18: Image of the modeling user interface in the custom modeling software. (**A**) The digitally reconstructed radiograph (DRR)-based projection of the kinematic model onto the 2D radiograph. (**B**) The reflective markers, enhanced with small metal beads, were manually indicated (red points). (**C**) The 3D environment allows interactive manipulations and simultaneous visualization in panels A and B.

Next, the subject-specific 3D position and orientation of each bone segment is manually determined by moving them through the software's 3D environment until visual agreement of the DRRs on both radiographic images. The simultaneous agreement of both 2D projections on their respective radiograph plane, provides the 3D position and orientation of the bony segment in question. Repeating this procedure across all vertebral levels of interest renders a modified generic model with subject-specific spino-pelvic bone geometry and alignment.

Personalization of intervertebral joint definition

The IV joint centre as well as its rotational axes have to be defined in each functional spinal unit (FSU) of the modified generic model with subject-specific spino-pelvic geometry and alignment. Different conventions (Pearcy and Bogduk, 1988; Jalalian et al., 2016) exist but, to the best of the authors knowledge, none of them have been validated for deformed vertebral bodies, as typically present in spinal deformity subjects. Therefore, an extension to the generic definition by Bruno et al. (2015) is adopted, where the centre of rotation is located at the geometric centre of the IV disc and oriented along the axes of symmetry of the IV disc space defined by the inferior and superior enclosing vertebral endplates. This definition was implemented as a semi-automatic mesh-based procedure in the software, further detailed in Appendix 2A.

Subject-specific registration of external optical motion capture markers in relation to the underlying bone geometry

A final level of subject-specificity involves registration of the subject-specific spino-pelvic model, describing the underlying bone geometry and alignment, to the external optical motion capture markers that were modified for this purpose. More specifically, 2 mm diameter iron beads were inserted in the centre of reflective markers of the 3D printed marker clusters to prevent bone and marker superposition or lack of sphericity (Pillet et al., 2014). In case of good marker visibility, the edge of the marker was then delineated using at least five points in both radiograph planes (2D), after which an ellipse fitting algorithm and 3D reconstruction provided the 3D position of the markers. In case of limited visibility of the marker edge, the iron beat was indicated instead. The obtained 3D position was then expressed in the associated bone geometry's reference frame of the personalized model (Figure 18B-C), overcoming the need for a marker calibration procedure prone to palpation errors.

Validation of biplanar radiography-based spino-pelvic personalization

The above described workflow was applied on biplanar radiographic images from a plastinated cadaver (male, age at death 94y, 60kg, 1.60m) with normal spinal alignment. Plastination ensured the spino-pelvic alignment in the upright, weight-bearing position for the biplanar radiography imaging to correspond to the supine position during CT imaging, thereby serving as ground truth. A subject-specific model was developed using the workflow defined above, while being blinded to the ground truth CT reconstruction. Using custom code (C#), the accuracy of the reconstruction method was then evaluated by comparing the resulting 3D position and orientation of each vertebra with the CT-based ground-truth. The position error (mm) was the difference in the position of the origins of the individual vertebral reference frames expressed in the pelvis reference frame, defined according to the ISB convention (Wu, 2002). The orientation error of each individual vertebral body was the difference between XYZ Euler angles describing the difference in orientation between corresponding vertebrae with an identically defined body reference frame.

Validation of the kinematic model

To determine the kinematic tracking accuracy of a subject-specific model created with the described workflow, one healthy and 12 subjects representing varying degrees of spinal deformity were recruited (mean age= 58.88 ± 13.96 years) after having obtained ethical approval and informed consent (S58082). Subjects first underwent CT imaging (BrightSpeed by GE Healthcare, with an inter-slice distance of 1.25 mm and a pixel size of 0.39x0.39 mm) from T1 to pelvis. Thereafter, an experienced physiotherapist instrumented each subject with reflective markers according to the aforementioned marker protocol. With the markers attached to the subject's body, two pairs of full-body images were then acquired in the biplanar radiography system in two standing positions for each subject: 1) in the Scoliosis Research Society free-standing position (fingers-on-clavicle variation) (Horton et al., 2005; M. Y. Wang et al., 2014), referred to as the '*upright*' position (Figure 19A); 2) in one single randomly '*bent*'

position (Figure 19B) (left LF (six subjects), extension (three subjects), flexion (one subject) and left AR (three subjects)), reaching either their maximal range of motion or the field of view limit of the imaging cabin (whichever came first). Using the described spino-pelvic personalization workflow, two skeletal models of the spine were created for each subject, one for the *upright* position and one for the *bent* position (Figure 19C).

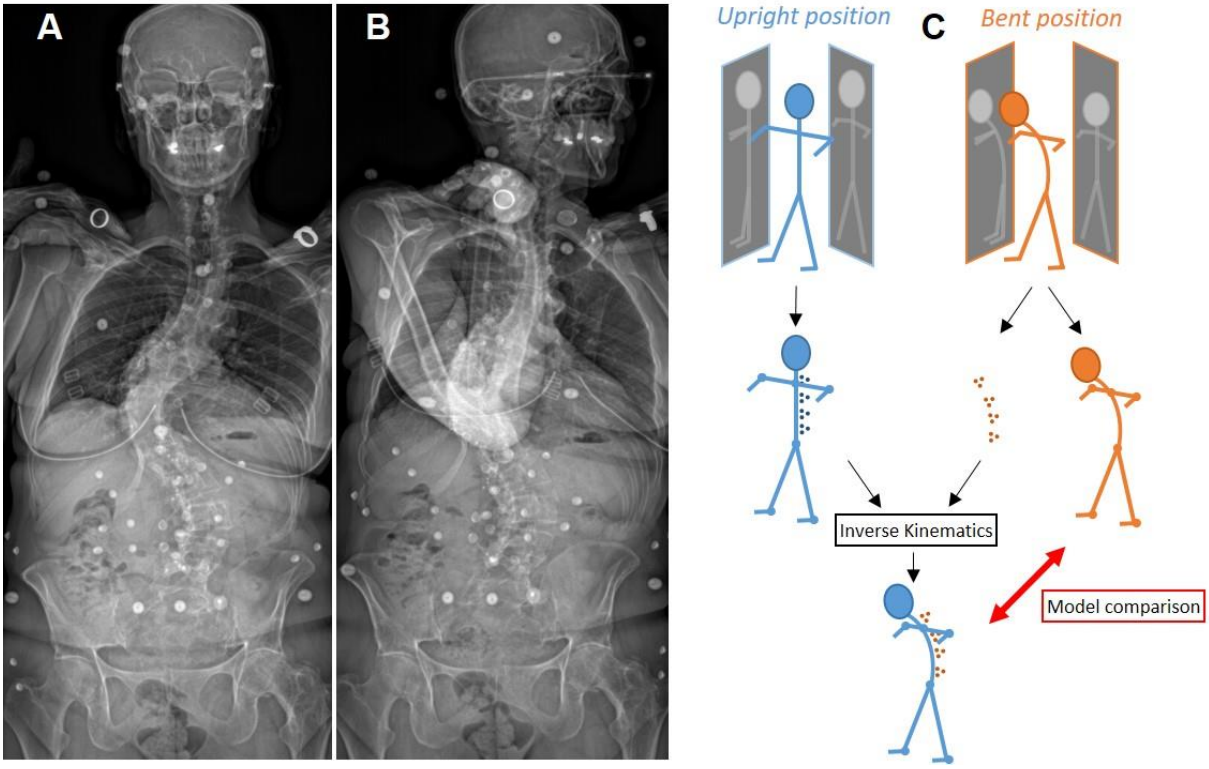

Figure 19: Coronal radiographic image of a spinal deformity subject in (**A**) upright position and (**B**) *bent* position (here: left axial rotation) (**C**) Schematic of the modeling and kinematic error quantification procedure for a forward bent position.

The extracted 3D marker positions from the *bent* position provided the input for an inverse kinematics simulation (Lu and O'Connor, 1999) (OpenSim 3.3) to simulate the static *bent* position using the upright model. The marker weight for the kinematic optimization was equally distributed over the different segments (Appendix 3). The accuracy of this simulated bending motion was evaluated by calculating the difference in position (mm) and orientation (degrees) of each vertebra of the inverse kinematics solution with the model reconstructed for the *bent* position serving as ground truth, identically expressed as above.

Results

Validation of the custom software for spinal alignment reconstruction

The mean (standard deviation, SD) absolute position errors between the plastinated cadaver and its corresponding subject-specific model were 0.83 mm (±0.67), 1.59 mm (±0.83) and 0.71 mm (±0.59), for the anteroposterior, mediolateral and inferosuperior directions, respectively. The mean associated 3D distance error was 2.09 mm (±0.89). The mean (SD) absolute orientation errors were 1.25° (±1.25), 1.63° (±1.44) and 2.27° (±1.63), about the anteroposterior, mediolateral and inferosuperior axis respectively. The largest position error was noted at T5, measuring 3.55 mm in the anteroposterior direction, while the maximal orientation error was 6.03°, at T10 about the inferosuperior axis (Figure 20).

A

Body	Abs. sagittal orientation (°)	Abs. transverse orientation (°)	Abs. coronal orientation (°)	3D distance (mm)	Abs. M-L position (mm)	Abs. I-S position (mm)	Abs. A-P position (mm)
Lumbar 5	0.31	0.92	0.38	0.22	0.07	0.18	0.11
Lumbar 4	1.01	1.11	0.62	2.23	1.15	0.05	1.90
Lumbar 3	1.25	3.93	0.59	3.06	2.78	0.79	1.02
Lumbar 2	1.30	2.20	1.14	1.52	0.96	1.14	0.30
Lumbar 1	1.95	2.66	0.37	2.08	1.80	0.23	1.03
Thoracic 12	2.44	3.26	0.06	2.32	1.69	0.85	1.34
Thoracic 11	1.50	3.05	0.24	2.17	1.71	1.00	0.90
Thoracic 10	4.21	6.03	1.68	3.18	2.41	2.07	0.01
Thoracic 9	0.02	0.86	1.38	1.68	0.88	1.40	0.27
Thoracic 8	0.33	1.03	2.53	0.80	0.56	0.57	0.08
Thoracic 7	0.75	3.87	0.18	2.46	2.19	1.08	0.28
Thoracic 6	4.22	1.12	1.02	1.97	1.45	0.57	1.21
Thoracic 5	4.33	4.27	0.90	3.91	3.55	0.28	1.63
Thoracic 4	2.25	2.44	5.20	2.98	1.43	1.46	2.17
Thoracic 3	0.43	0.04	1.22	1.67	1.60	0.18	0.46
Thoracic 2	1.20	1.37	1.40	1.62	1.24	0.20	1.02
Thoracic 1	0.18	0.39	2.41	1.60	1.57	0.05	0.32
Mean	1.63	2.27	1.25	2.09	1.59	0.71	0.83
SD	1.44	1.63	1.25	0.89	0.83	0.59	0.67
Min	0.02	0.04	0.06	0.22	0.07	0.05	0.01
Max	4.33	6.03	5.20	3.91	3.55	2.07	2.17
RMS	2.14	2.77	1.74	2.26	1.78	0.91	1.05
RMS of Glaser et al. (2012)	1.19	1.91	0.76	1.26	0.51	0.89	0.87

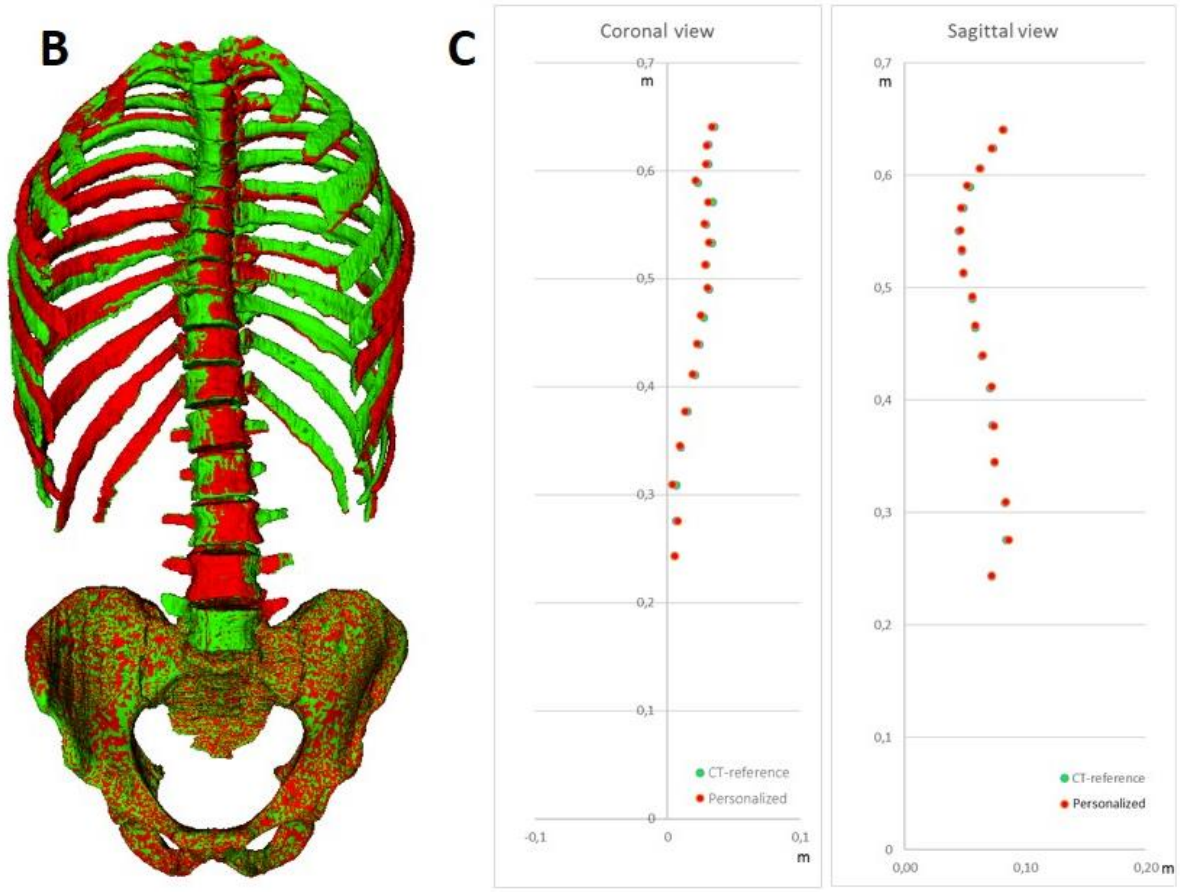

Figure 20: (**A**) The absolute position error values (in mm) for each vertebral level are expressed in the pelvic reference frame. (M-L = mediolateral, I-S = inferosuperior, A-P = anteroposterior). The absolute orientation error values (in degrees) were calculated with an intrinsic X-Y-Z (LF-AR-FE) sequence at segmental level between corresponding vertebrae with an identically defined reference frame (rotation in the sagittal plane is along the mediolateral axis, transverse plane = inferosuperior axis, coronal plane = anteroposterior axis). The last 2 rows were added as comparison of the root mean square (RMS) values of this study and a similar study performed by Glaser et al. (2012). (**B**) Overlay of the model of the plastinated cadaver created using the workflow of this work (red), overlaid with its ground truth CT reference (green). (**C**) Coronal and sagittal point plots, where a green dot is the position of the reference frame of the ground truth and red is the obtained position by using the workflow of this work.

Validation of the kinematic model

In the 13 subjects, the mean (SD) vertebral tracking errors were 3.05 mm (±2.53), 3.66 mm (±3.62) and 4.97 mm (±4.10), in the anteroposterior, inferosuperior and mediolateral directions, respectively. The mean (SD) rotational error was 3.54° (±3.25) along the anteroposterior axis (LF), 5.31° (±3.79) along the inferosuperior axis (AR) and 2.92° (±2.29) along the mediolateral axis (FE) (Table 2). Table 3 and Table 4 present the mean kinematic errors grouped by executed motion and per subject with the addition of their radiographic parameters, age and body mass index (BMI), respectively.

Table 2: For every bone in the spino-pelvic model the mean (standard deviation; maximal) kinematic error in each plane over all subjects was calculated. (M-L = mediolateral, I-S = inferosuperior, A-P = anteroposterior).

	Mean (SD; max) absolute...					
Body	Sagittal orientation error (°)	Transverse orientation error (°)	Coronal orientation error (°)	M-L position error (mm)	I-S position error (mm)	A-P position error (mm)
Sacrum	3.98 (2.37; 8.96)	1.33 (0.92; 2.52)	1.84 (1.46; 4.33)	3.29 (2.69; 9.16)	9.46 (5.36; 21.61)	3.33 (3.13; 9.46)
Lumbar 5	2.55 (1.96; 7.52)	3.11 (1.67; 6.96)	3.13 (3.10; 8.51)	2.39 (1.70; 5.38)	3.06 (2.43; 8.70)	2.90 (2.36; 8.51)
Lumbar 4	3.11 (2.70; 9.18)	4.00 (1.85; 7.52)	4.33 (3.81; 14.20)	3.10 (2.66; 10.22)	3.42 (2.90; 10.76)	2.44 (3.74; 14.20)
Lumbar 3	3.14 (2.42; 8.10)	4.41 (3.04; 11.03)	4.57 (3.89; 14.10)	3.45 (3.55; 13.53)	3.56 (3.82; 13.22)	2.27 (4.14; 14.10)
Lumbar 2	3.19 (2.55; 10.04)	5.82 (4.77; 15.43)	5.32 (3.24; 11.13)	4.62 (4.26; 12.97)	3.46 (3.58; 13.40)	2.93 (4.21; 15.43)
Lumbar 1	2.00 (1.79; 6.42)	3.75 (3.86; 11.97)	3.96 (4.40; 16.94)	6.11 (4.04; 11.44)	3.19 (3.44; 13.19)	3.72 (4.44; 16.94)
Thoracic 12	2.63 (1.90; 6.21)	5.66 (3.76; 13.77)	4.54 (3.60; 15.10)	6.75 (4.86; 16.85)	3.39 (3.49; 11.63)	3.74 (4.96; 16.85)
Thoracic 11	2.36 (3.07; 7.93)	6.60 (3.50; 13.47)	3.07 (3.85; 12.99)	7.22 (5.38; 18.27)	3.47 (3.53; 11.10)	3.38 (4.88; 18.27)
Thoracic 10	1.64 (1.65; 5.61)	7.29 (3.69; 13.29)	1.77 (1.75; 6.40)	7.27 (6.03; 17.85)	3.43 (3.56; 11.21)	2.74 (4.74; 17.85)
Thoracic 9	2.19 (1.58; 5.51)	8.75 (4.44; 17.13)	3.82 (2.58; 10.40)	6.76 (5.69; 16.85)	3.35 (3.68; 10.97)	2.88 (5.07; 17.13)
Thoracic 8	2.41 (1.80; 6.79)	7.62 (3.81; 16.14)	2.56 (2.73; 9.25)	6.05 (4.85; 14.22)	3.76 (3.51; 11.10)	2.74 (4.47; 16.14)
Thoracic 7	2.34 (2.17; 8.19)	4.48 (3.09; 10.51)	2.23 (2.42; 9.35)	6.55 (4.06; 12.15)	3.54 (3.67; 11.65)	2.98 (3.41; 12.15)
Thoracic 6	3.39 (2.61; 8.80)	3.76 (2.42; 8.11)	1.96 (2.28; 8.78)	6.22 (3.26; 11.46)	3.40 (3.47; 11.37)	2.94 (3.16; 11.46)
Thoracic 5	4.03 (1.90; 8.30)	4.76 (2.50; 9.31)	2.81 (2.91; 10.69)	5.37 (3.02; 10.78)	3.31 (3.69; 11.30)	3.05 (3.26; 10.78)
Thoracic 4	4.34 (2.81; 8.22)	5.99 (3.56; 14.72)	4.87 (3.66; 10.89)	4.82 (2.53; 9.86)	3.01 (3.11; 10.77)	3.66 (3.80; 14.72)
Thoracic 3	3.04 (2.16; 6.87)	5.88 (3.55; 12.68)	4.22 (2.64; 8.84)	3.37 (2.31; 9.79)	3.15 (2.82; 8.70)	3.80 (3.35; 12.68)
Thoracic 2	2.84 (2.46; 7.65)	5.38 (3.11; 9.80)	3.51 (3.19; 9.02)	2.25 (2.23; 7.72)	2.66 (1.87; 5.70)	2.62 (2.86; 9.80)
Thoracic 1	3.39 (2.14; 5.73)	7.55 (6.19; 19.64)	5.77 (3.54; 11.75)	3.04 (2.23; 7.23)	2.89 (2.13; 7.15)	2.62 (4.96; 19.64)
Mean (SD)	2.92 (2.29)	5.31 (3.79)	3.54 (3.25)	4.97 (4.10)	3.66 (3.62)	3.05 (2.53)

Table 3: The mean (standard deviation) kinematic error in each plane grouped by executed motion of the subjects. (M-L = mediolateral, I-S = inferosuperior, A-P = anteroposterior, LF = lateroflexion, AR = axial rotation). Error values above the total body average of its respective DOF (from Table 2) are indicated in bold.

Performed motion (number of subjects)	Mean (SD) abs. sagittal orientation error (°)	Mean (SD) abs. transverse orientation error (°)	Mean (SD) abs. coronal orientation error (°)	Mean (SD) abs. M-L position error (mm)	Mean (SD) abs. I-S position error (mm)	Mean (SD) abs. A-P position error (mm)
Flexion (1)	2.05 (2.00)	3.77 (2.34)	**4.27** (3.06)	3.93 (2.01)	3.53 (1.74)	1.51 (1.60)
Extension (3)	2.63 (2.30)	4.51 (3.48)	2.56 (2.52)	2.36 (2.20)	2.84 (3.01)	2.50 (2.07)
LF (6)	2.73 (2.08)	**5.71** (3.77)	3.35 (3.02)	**5.04** (3.56)	2.43 (2.35)	**3.18** (2.67)
AR (3)	**3.91** (2.54)	**5.87** (4.35)	**4.73** (4.02)	**7.97** (5.17)	**7.12** (4.61)	**3.90** (2.64)

Table 4: Mean (SD; max) absolute kinematic error in each plane for every subject, combined with their radiographic evaluation parameterized by the pelvic tilt (PT), sacral slope (SS), lumbar lordosis (LL), thoracic kyphosis (TK), sagittal vertical axis (SVA), pelvic incidence-lumbar lordosis mismatch (PI-LL) and coronal Cobb angle. PT, SS, LL, SVA and PI-LL parameters were compared with normative values from Pratali et al. (2018): values exceeding the normative minimum-maximum range were indicated in bold. TK parameters outside the healthy min-max range for a population of similar age (13° to 66° for ages 19 to 79 years) defined by Fon et al. (1980) were indicated in bold (none). The coronal Cobb angles above 30° were indicated in bold to indicate a moderate to severe scoliosis. Kinematic error values above the total body average of its respective DOF (from Table 2) are indicated in bold.

Subject	1 (healthy)	2	3	4	5	6	7	8	9	10	11	12	13
BMI	14.2	25.6	22.1	26.2	22.9	22.2	16.4	20.8	20.5	19.4	25.8	19.1	28.0
Age	61.5	51.4	69	52.7	71.7	60.3	59.6	65.5	75.3	19.3	46.9	70.2	62
Motion	extension	lateroflexion	lateroflexion	lateroflexion	lateroflexion	extension	axial rotation	axial rotation	axial rotation	lateroflexion	lateroflexion	extension	flexion
Radiographic evaluation													
PT (°)	15.9	21.9	28.8	16.5	**31.8**	18.7	**31.1**	**48.1**	17.1	12.5	10.6	29.4	12.0
SS (°)	43.0	40.9	31.1	44.2	34.5	35.3	22.5	45.2	37.7	32.6	41.1	**10.6**	27.7
LL (°)	69.2	56.7	**25.5**	72.8	47	57.3	**13**	67.1	55	40.5	48.4	**20.6**	44.6
TK (°)	54.8	40.7	21.8	56.1	39.9	48.6	-13	41.5	35.1	33.8	49.3	59.1	51.6
SVA (mm)	1.1	25.1	**91.6**	11.8	38	-14	5.6	34.3	11.5	5.0	**70.5**	39.3	44
PI-LL (°)	-10.3	6.1	**34.4**	-12.1	**19.3**	-3.3	**40.6**	**26.2**	-0.2	4.6	3.3	**19.4**	-4.9
Cobb (°)	0.5	**45.3**	**62.7**	**57.8**	**85.2**	**44.2**	**79.8**	**69.5**	**34.5**	**50.1**	**49.6**	**31.7**	**33.1**
Mean (SD; max) abs. error for each plane													
sagittal orientation (°)	1.78 (1.47; 5.23)	2.41 (2.03; 5.62)	2.87 (1.95; 7.33)	2.05 (1.15; 4.21)	**3.39** (2.26; 8.22)	**3.84** (2.88; 8.96)	**4.01** (2.49; 10.04)	**4.39** (3.01; 8.80)	**3.36** (2.12; 7.93)	**3.19** (2.81; 9.18)	2.37 (1.80; 6.12)	2.28 (1.90; 6.87)	2.05 (2.00; 8.02)
transverse orientation (°)	2.45 (1.65; 5.47)	5.17 (3.25; 12.98)	**6.78** (4.14; 13.77)	3.71 (2.07; 7.44)	4.91 (3.57; 14.85)	**5.41** (4.53; 17.13)	**7.50** (3.95; 15.43)	4.42 (3.59; 9.65)	**5.50** (5.02; 16.14)	5.10 (2.87; 9.05)	**8.39** (4.63; 19.64)	**5.68** (2.81; 10.37)	3.77 (2.34; 8.42)
coronal orientation (°)	1.03 (0.78; 2.77)	3.52 (2.47; 9.02)	**4.28** (4.09; 15.10)	1.64 (1.77; 6.13)	2.91 (3.07; 11.75)	**4.02** (2.99; 10.40)	**6.75** (4.05; 16.94)	**4.40** (4.28; 14.20)	2.89 (2.77; 8.50)	3.49 (2.59; 8.54)	**4.08** (3.20; 11.27)	2.62 (2.35; 9.54)	**4.27** (3.06; 10.89)
M-L position (mm)	1.50 (2.03; 9.16)	2.91 (1.71; 5.37)	**7.12** (4.16; 14.11)	4.05 (1.56; 6.79)	1.88 (1.36; 4.77)	3.62 (2.42; 8.21)	**7.96** (6.60; 18.27)	**8.41** (3.92; 13.35)	**7.56** (5.00; 14.08)	5.98 (2.84; 11.27)	**8.17** (3.74; 13.53)	1.97 (1.62; 6.17)	3.93 (2.07; 7.27)

I-S position (mm)	2.08 (1.49; 7.81)	1.19 (1.51; 6.54)	2.49 (1.10; 4.33)	1.17 (0.80; 3.27)	1.88 (2.13; 9.53)	**4.36** (4.56; 21.61)	**8.26** (2.46; 12.97)	**11.58** (2.06; 17.43)	1.71 (1.81; 7.78)	1.77 (2.78; 12.13)	**5.93** (1.28; 8.15)	2.09 (1.66; 7.48)	3.53 (1.72; 6.38)
A-P position (mm)	2.12 (1.72; 7.52)	**3.23** (2.71; 7.83)	1.81 (1.67; 6.45)	**5.75** (3.39; 9.87)	1.70 (1.44; 5.08)	**3.40** (2.77; 9.46)	**3.87** (1.79; 6.71)	**5.73** (3.23; 9.87)	2.22 (1.38; 5.00)	**5.09** (2.02; 8.44)	1.78 (1.02; 3.54)	1.98 (1.20; 4.93)	1.51 (1.60; 6.19)

Discussion

Instrumented motion analysis through multi-body modeling can complement current radiographic evaluations of the deformed spine to provide information on functional biomechanical parameters, such as spino-pelvic kinematics and kinetics during functional activities of daily living, thus potentially improving its treatment. This study presented the first method to generate subject-specific rigid body models for subjects with spinal deformity, integrating subject-specific spino-pelvic bone geometry and alignment based on a modified generic thoracolumbar model. The inverse kinematics solution of a bending motion (flexion, extension, LF or AR) was evaluated using two static full-body biplanar radiographic image pairs: the initial *upright* position and the randomized *bent* position. We obtained mean kinematic errors between 3.1-5.0 mm and 2.9-5.3°, for the positions and orientations of vertebrae, respectively. We compared our results to Zemp et al. (2014), who quantified the sagittal curvature error associated with soft tissue artefacts of skin markers on the spine of seven healthy subjects during upright sitting and a flexed/extended position. Interestingly, these motions were performed in an open MRI system which, similar to our study, provided both the baseline vertebrae-specific skin marker positions and the ground-truth vertebral orientations for this evaluation. Although our study pertains to spinal deformity subjects, the mean (maximal) sagittal orientation errors of the lumbar and thoracic segments obtained in this study (2.8±2.3° (10.0°) and 2.9±2.3° (8.8°), respectively) were similar as those from Zemp et al. (2014) who reported the following corresponding values: 2.5±2.7° (6.6°) and 1.1±2.9° (9.1°). Given the paucity of the literature on the accuracy of skin marker-driven kinematic evaluations using a spinal rigid body model, a more detailed comparison (i.e. both vertebral position and orientation), also including pathologic subjects, was not possible. However, when presenting the mean kinematic error grouped by executed motion (Table 3), above average errors were noted in each DOF for the AR motion, indicating a lower vertebral tracking capacity for this motion. Except for the overall below average kinematic error of the healthy subject, Table 4 showed no apparent relation between the magnitude of mean kinematic error and their respective severity of the deformity, age or BMI.

Five potential contributors to this spinal kinematic error can be identified. First, the values for the kinematic coupling constraints added to the generic fully articulated thoracolumbar model by Bruno et al. (2015) were based on healthy control subjects (Christophy et al. (2012), Fujii et al. (2007), McDonnell et al. (2016), Wilke et al. (2017)), making them inherently inaccurate in the case of spinal deformity subjects. In addition, these kinematic coupling ratio values are based on experiments involving single-plane motion. Future work should evaluate the effect of multiple plane motion on these kinematic coupling ratios.

Secondly, translational DOFs were not integrated in the IV joints, thus not representing true physiological movement at the joints. Although the unique shape of each vertebra was integrated in the IV joint definition to increase the subject-specificity of the model, the kinematics appeared not to be very sensitive to imposed error in our IV joint definition method in a small pilot study (Appendix 2B). Thirdly, as described by Leardini et al. (2005), all skin marker-based kinematics suffer from soft tissue artefacts. The smaller orientation error in the

sagittal plane is in agreement with Mahallati et al. (2019), who used statistical approaches in healthy subjects to conclude that motions in the coronal and transverse planes are expected to have substantially larger soft tissue artifacts compared to the sagittal plane. A fourth contributor to the reported kinematic error is the manual localization of the reflective markers on the biplanar radiographic images. The localization reliability is expected to be within 0.15 mm (Pillet et al., 2014). However, our newly proposed marker protocol has a modified marker design, i.e. with small iron beats, providing an increased radiographic visibility, which can be expected to further increase the reliability of localization. Lastly, although low, the results of our plastinated cadaver study still show errors in both position (means between 0.71-1.59 mm) and orientation (means between 1.25-2.27°) of the vertebrae. However, as the plastinated cadaver was devoid of internal organs that normally occlude the spinal region, thereby providing clearer images than those typically obtained *in vivo*; these errors may be larger in *in vivo* subjects. Due to the unavailability of a standing CT acquisition system, regular *in vivo* CT validation was precluded as ground truth as the associated supine position would have introduced differences in spinal alignment with the weight-bearing position (Salem et al., 2015) to be reconstructed from the biplanar radiographic images. In future research, the inter-and intra-operator variability of this reconstruction should be further assessed. Glaser et al. (2012) performed a similar 3D reconstruction validation using three phantom spines (a total of 51 vertebrae) which were reconstructed using the 3D spinal reconstruction software that accompanies the biplanar imaging system (sterEOS, EOS Imaging, France) compared to their CT-segmented reference. The corresponding root mean square (RMS) values are shown in Figure 20A. The error values of the current study fall within the same range as those from Glaser et al. (2012). Even if the error values calculated in the current study were based on a reconstruction of 17 vertebrae compared to the 51 vertebrae of Glaser et al. (2012), our study confirmed the larger difficulty to perform accurate reconstructions in the axial plane, based on only coronal and sagittal radiographs.

Future efforts should be made to expand the study population and explore relations between body anthropometry, spinal deformity, and resulting kinematic errors. Additionally, the use of a deformable principal component analysis vertebral model is being investigated as a potential alternative for the CT images with a high radiation dose. Improvements in modeling could be made by automating the residual manual steps in the creation of the subject-specific model (Aubert et al., 2019). In addition, subject-specificity could be expanded beyond reflective marker positions, spinal geometry and alignment to also include subject-specific kinematic coupling constraint values, joint stiffness, or muscle parameters to potentially further increase the accuracy of musculoskeletal simulations. It should be noted that our kinematic accuracy results may represent an overestimation of the accuracy of our subject-specific workflow because of the absence of dynamic motion and the maximum trunk angle in the *bent* position might have been limited due to the physical constraints of the EOS imaging system.

In conclusion, this is the first validated biplanar radiograph-based personalization method that allows the inclusion of subject-specific bone geometries, the personalization of the 3D spinal alignment and the localization of the external markers in spinal deformity subjects.

Comparatively to other available software, such as CT-or MRI-based personalization of lower limbs (Scheys et al., 2008; Valente et al., 2017) where a de novo model is created, our method allows to modify pre-existing generic models to the subject's pathology, thereby avoiding redefining generic definitions or parameters of the model. Furthermore, the developed biplanar radiography-based personalization workflow is not restricted to the creation of spinal deformity models but can be applied to any other anatomical region modeled as a rigid body model. Most importantly, the use of these models in combination with motion capture data enables kinematics analysis of a spinal deformity subject's recorded motion, thus providing opportunities to improve the current static 2D radiographic evaluation with in silico dynamic parameters based on spino-pelvic kinematics. For example information about regional mobility or compensation strategies in the spine could contribute to clinical decision-making and treatment.

Conflict of interest statement

None declared.

Acknowledgement

The authors thank Kristel van de Loock and Rowie De Buysscher for subject inclusion and follow-up, and Thijs Ackermans for his thorough review. We would also like to thank Friedl De Groote, Christopher Dembia and the OpenSim team for their technical expertise during the revision of this manuscript. This study was funded by Internal KU Leuven C2 funds (ASESP-P), Medtronic, internal UZ Leuven Academic research funding (KOOR) and Research Foundation – Flanders (FWO-SB/1S56017N)

Supplementary data of Chapter 1

Appendix 1: The application of joint constraints

1. Intervertebral joint motion

The modified model comprised eighteen bodies (twelve thoracic bodies, five lumbar bodies and a sacral body [rigidly connected to the pelvis, so considered one body for simplicity]) with 108 degrees of freedom (DOFs) (Figure 21A). After the addition of seventeen spherical joints between the vertebral bodies the system still has 57 DOFs (Figure 21B). Thereafter, the remaining DOFs were further reduced by imposing linear kinematic coupling constraints. We grouped the intervertebral joints in six regions: T1-T3, T3-T7, T7-T11, T11-L2, L2-L4, L4-Sacrum. Eleven 3D linear kinematic coupling constraints were added (Figure 21C), thereby removing 33 DOFs and reducing the system to 24 DOFs. As shown in Figure 21C, the inferior IV joint of each region is chosen as the independent coordinate. The calculation of these specific kinematic coupling constraint values is explained below.

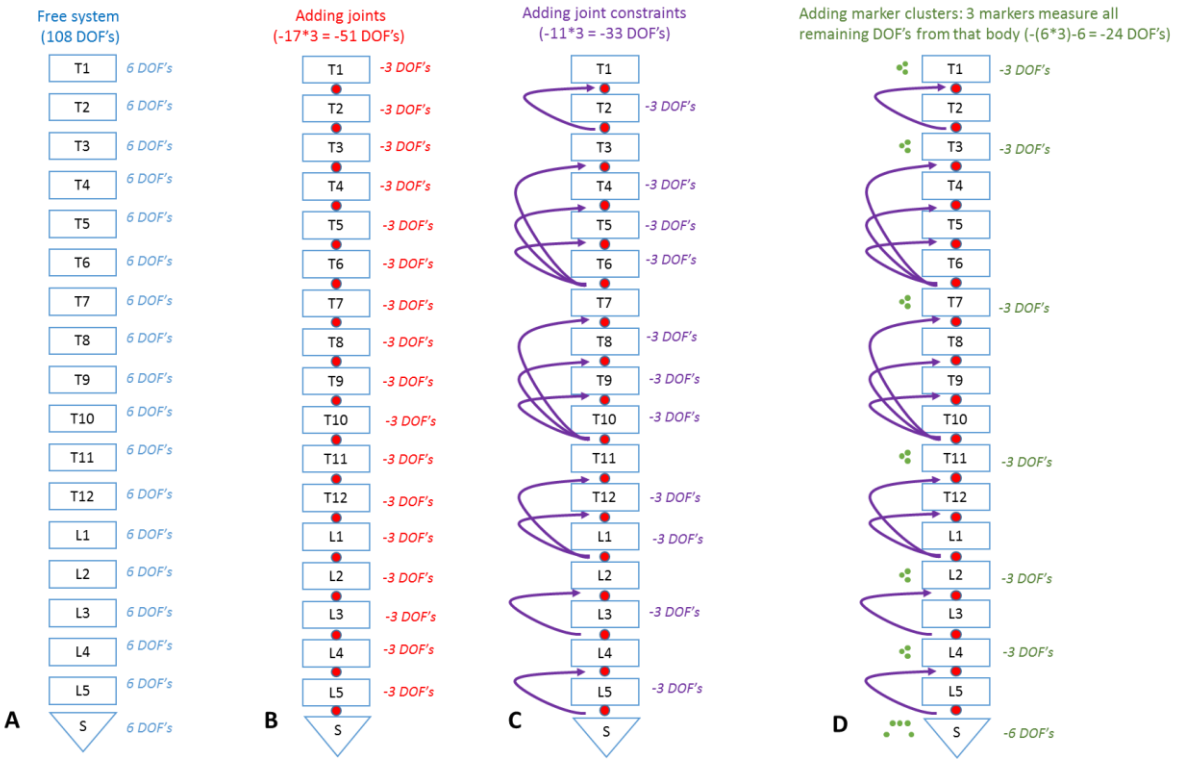

Figure 21: (**A**) The unconstrained system with 18 bodies. (**B**) The addition of 17 spherical joints (red spheres) removes 51 DOFs. (**C**) Adding eleven 3D linear kinematic coupling constraints (purple arrows) between dependent and independent DOFs removes 33 DOFs. (**D**) Motion at the remaining 24 DOFs in the modified model was estimated using the marker set described in this manuscript (indicated with green spheres).

For the L2-L4 and L4-Sacrum groups

Table 5: Table representing the kinematic coupling constraint values for the L2-L4 and L4-Sacrum groups. The groups, bound by a segment containing at least 3 markers (either as a marker cluster or sufficient markers in case of the sacrum rigidly linked to the pelvis, colored in green), are separated using a double line. Grey fields are unused in the calculation of the groups of interest. The values for flexion/extension (FE) and lateroflexion (LF) were copied from the publication of Christophy et al. (2012). The axial rotation (AR) components from Christophy et al. (2012) were altered to better reflect the values of Fujii et al. (2007). Thereto, the original left and right axial rotations, obtained using *in vivo* MRI, were averaged (i.e. the mean AR values Fujii et al. (2007)) and normalized over the total AR ROM. The regional redistributed values are the normalized values relative to the regional intermediate sum.

	Flexion-extension (FE)			Lateroflexion (LF)			Axial rotation (AR)			
FSU	Normalized FE values Christophy et al. (2012)	Regional intermediate sum	Regional redistributed	Normalized LF values Christophy et al. (2012)	Regional intermediate sum	Regional redistributed	Mean AR values Fujii et al. (2007)	Normalized AR values	Regional intermediate sum	Regional redistributed
L1/**L2**	0.2550			0.1880			1.2500	0.16234		
L2/L3	0.2310		0.53103	0.2500		0.50485	1.3500	0.17532		0.44262
L3/**L4**	0.2040	0.4350	0.46897	0.2452	0.49520	0.49515	1.7000	0.22078	0.39610	0.55738
L4/L5	0.1850		0.59677	0.1812		0.57197	1.7500	0.22727		0.51471
L5/**Sacrum**	0.1250	0.3100	0.40323	0.1356	0.31680	0.42803	1.6500	0.21429	0.44156	0.48529
Sum	1.0000			1.0000			7.7000	1.00000		

For the T11-L2 group

Table 6: The values for flexion/extension (FE), lateroflexion (LF) and axial rotation (AR) were copied from the publication of McDonnell et al. (2016). The procedure for the calculations was similar as described in Table 5.

	Flexion-extension (FE)			Lateroflexion (LF)			Axial rotation (AR)		
FSU	Mean FE-values McDonnell et al. (2016)	Regional intermediate sum	Regional redistributed	Mean LF-values McDonnell et al. (2016)	Regional intermediate sum	Regional redistributed	Mean AR-values McDonnell et al. (2016)	Regional intermediate sum	Regional redistributed
T10/T11	4.1912			4.4012			4.7905		
T11/T12	3.7313		0.2497	4.1254		0.2425	1.9921		0.2989
T12/L1	5.2761		0.3531	5.3073		0.3120	1.8735		0.2811
L1/L2	5.9365	14.9439	0.3973	7.5794	17.0121	0.4455	2.7984	6.6640	0.4199

For the T7-T11, T3-T7 and T1-T3 groups

Table 7: The values for flexion/extension (FE), lateroflexion (LF) and axial rotation (AR) were copied from the publication of Wilke et al. (2017). The procedure for the calculations was similar as described in Table 5.

	Flexion-extension (FE)			Lateroflexion (LF)			Axial rotation (AR)		
FSU	Mean FE-values Wilke et al. (2017)	Regional intermediate sum	Regional redistributed	Mean LF-values Wilke et al. (2017)	Regional intermediate sum	Regional redistributed	Mean AR-values Wilke et al. (2017)	Regional intermediate sum	Regional redistributed
T1/T2	6.87672		0.62854	5.87958		0.54408	6.21281		0.55303
T2/**T3**	4.06411	10.94083	0.37146	4.92695	10.80653	0.45592	5.02137	11.23418	0.44697
T3/T4	3.80173		0.25678	5.60588		0.26867	5.82698		0.25752
T4/T5	3.33468		0.22524	5.05751		0.24238	5.19316		0.22951
T5/T6	3.85358		0.26029	5.06479		0.24273	5.70492		0.25213
T6/**T7**	3.81521	14.80520	0.25769	5.13748	20.86566	0.24622	5.90179	22.62684	0.26083
T7/T8	2.80189		0.22247	3.70644		0.23138	4.76969		0.25345
T8/T9	3.19173		0.25343	3.84673		0.24013	4.88063		0.25935
T9/T10	3.52930		0.28023	4.47226		0.27918	5.12559		0.27237
T10/**T11**	3.07144	12.59437	0.24387	3.99373	16.01917	0.24931	4.04282	18.81872	0.21483
T11/T12	3.56807			3.85081			3.32582		

Summary of kinematic coupling constraint values

Table 8: (A) Summary of the values obtained. (B) The lower FSU of each group is considered the independent DOF having kinematic coupling constraint values equal to one (grey), the other FSUs in the group are the dependent DOFs. In the definition of the model a linear relationship between the dependent FSUs and the independent FSU was defined. Therefore, each of the values in A was converted as a fraction of its corresponding DOF of the independent FSU.

A	FE	LF	AR
T1/T2	0.62854	0.54408	0.55303
T2/T3	0.37146	0.45592	0.44697
T3/T4	0.25678	0.26867	0.25752
T4/T5	0.22524	0.24238	0.22951
T5/T6	0.26029	0.24273	0.25213
T6/T7	0.25769	0.24622	0.26083
T7/T8	0.22247	0.23138	0.25345
T8/T9	0.25343	0.24013	0.25935
T9/T10	0.28023	0.27918	0.27237
T10/T11	0.24387	0.24931	0.21483
T11/T12	0.24969	0.24250	0.29893
T12/L1	0.35306	0.31197	0.28114
L1/L2	0.39725	0.44553	0.41993
L2/L3	0.53103	0.50485	0.45161
L3/L4	0.46897	0.49515	0.54839
L4/L5	0.59677	0.57197	0.51515
L5/Sacrum	0.40323	0.42803	0.48485

B	FE	LF	AR
T1/T2	1.692060	1.193350	1.237274
T2/T3	1.000000	1.000000	1.000000
T3/T4	0.996468	1.091173	0.987323
T4/T5	0.874049	0.984436	0.879929
T5/T6	1.010058	0.985852	0.966641
T6/T7	1.000000	1.000000	1.000000
T7/T8	0.912240	0.928065	1.179793
T8/T9	1.039165	0.963192	1.207234
T9/T10	1.149070	1.119819	1.267827
T10/T11	1.000000	1.000000	1.000000
T11/T12	0.628544	0.544285	0.711864
T12/L1	0.888762	0.700233	0.669492
L1/L2	1.000000	1.000000	1.000000
L2/L3	1.132353	1.019576	0.823529
L3/L4	1.000000	1.000000	1.000000
L4/L5	1.480000	1.336283	1.062500
L5/Sacrum	1.000000	1.000000	1.000000

2. Joint constraints during the inverse kinematic optimization

As described in the OpenSim documentation: [Quoted from https://simtk-confluence.stanford.edu/display/OpenSim/How+Inverse+Kinematics+Works] "Inverse kinematics is solved by minimizing the following least squares equation:

$$\min_{\mathbf{q}} \left[\sum_{i \in \text{markers}} w_i \left\| \mathbf{x}_i^{\text{exp}} - \mathbf{x}_i(\mathbf{q}) \right\|^2 + \sum_{j \in \text{unprescribed coords}} \omega_j \left(q_j^{\text{exp}} - q_j \right)^2 \right] \quad (1)$$

$$q_j = q_j^{\text{exp}} \text{ for all prescribed coordinates } j$$

where $\mathbf{q}$ is the vector of generalized coordinates being solved for, $\mathbf{x}_i^{\text{exp}}$ is the experimental position of marker i, $\mathbf{x}_i(\mathbf{q})$ is the position of the corresponding model marker (which depends on the coordinate values), q_j^{exp} is the experimental value for coordinate j. (The marker weights (w_i's) and coordinate weights (ω_j's).)"

In our case, the second part of equation (1) is zero as we have no prescribed coordinates during the motion.

The documentation of OpenSim describes a coordinate coupler as followed [Quoted from https://simtk-confluence.stanford.edu:8443/display/OpenSim24/OpenSim+Models#OpenSimModels-KinematicConstraintsinOpenSim]: "A coordinate coupler relates the generalized coordinate of a given joint (the dependent coordinate) to any other coordinates in the model (independent coordinates). The user must supply a function that returns a dependent value based on independent values."

This means that for every joint kinematic coupling constraint, $q_{dependent}$ is a function of $q_{independent}$ (i.e. $q_{dependent}(q_{independent})$), where $q_{independent}$ is a generalized coordinate relating its value to a dependent coordinate ($q_{dependent}$). Referring to equation (1), $\mathbf{x_i}(\mathbf{q})$ is the position of the corresponding model marker which depends on $\mathbf{q}$, the vector of generalized coordinates. This vector $\mathbf{q}$ could be structured as followed (q_1, q_2, q_3, $q_4(q_1)$, $q_5(q_2)$, $q_6(q_3)$, $q_7(q_1)$, $q_8(q_2)$, $q_9(q_3)$, q_{10}, q_{11}...) if for example the value of the q_4 coordinate was related to the value of q_1, the value of the q_5 coordinate was related to the value of q_2, etc. Therefore, the minimization of the experimental and virtual marker error is performed while respecting the relation between both the independent and the dependent degrees of freedom. The kinematic coupler constraints take precedence over matching the experimental marker positions.

In other words, the kinematic coupling constraints essentially act as gears connecting the vertebra to determine the relative curvature of the spine by relating the motion of the independent coordinate to the dependent coordinates. That is, when trying to match the marker positions during IK, for every degree of rotation at the independent joint – in our example below (Figure 22), this is the L1/L2 joint (as also defined in Table 8) - there is proportional rotation at the dependent joints – T12/L1 and T11/T12 in our example below. Effectively, the back gets more "rounded" as the model leans forward during flexion motion (Figure 22). For every degree of rotation at the independent joint, there will also be rotation at all its dependent joints. As such we would like to stress that the model is not computing a rigid total flexion angle between T11-L2, and then distributing it between the vertebrae, i.e. a kinematic “top-down approach”. Instead, the model is optimizing through a kinematic “bottom-up approach” where the independent coordinate – in our example, the L1/L2 joint angles - solves the inverse kinematics problem while simultaneously enforcing the constraints for the other vertebrae – thus dictating the T12/L1 and T11/T12 joint angles higher up.

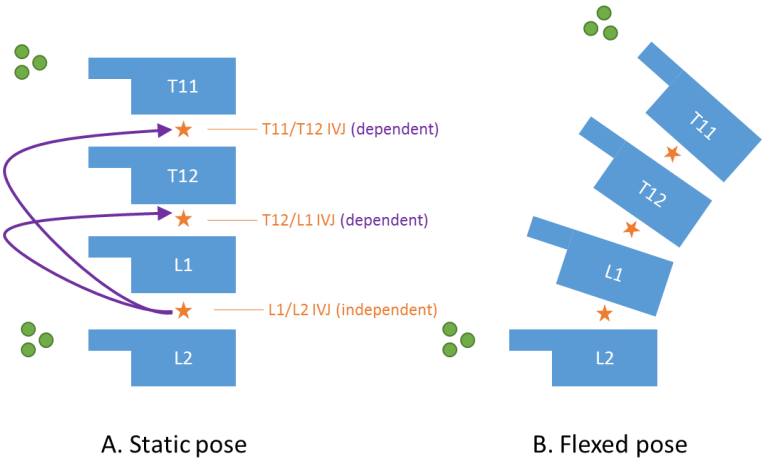

Figure 22: Illustration of the way kinematic coupler constraints are used in the model during flexion for the example region L2 to T11. (L1/L2 is the independent joint.)

Appendix 2

1. A mesh-based IV joint definition for FSUs of spinal deformity subjects

After determining the relative positions and orientations of the vertebrae, the in-between intervertebral (IV) joint has to be positioned and oriented. However, as explained in this work, to the best of the author's knowledge, no guidelines are available on how to do this in case of strongly deformed FSU, as typically present in spinal deformity subjects. Therefore, a subject-specific vertebral mesh-based method to position and orient the IV joint as symmetric as possible to both endplates is proposed. For each FSU, the procedure below was applied.

First, the mesh of each vertebra was virtually cut out to isolate both enclosing vertebral endplates of an FSU, together representing the bounding edges of this virtual IV disc (Figure 23). The geometric centre of this virtual IV disc determined the **location** of the spherical joint. In order to obtain the **orientation** of the IV joint, the shapes of the isolated vertebral endplates were used as follows:

1) Four anatomical landmarks, i.e. the most anterior, posterior, left and right lateral points of the vertebral endplate as visualized in Figure 24, were manually indicated on the inferior endplate, unless a certain landmark was unclear due to artefacts in the CT segmentation*.

2) Using these four landmarks, a fixed endplate reference axis was placed as follows: The most anterior and posterior landmark defined the anteroposterior (X) axis, pointing anteriorly. Following the curvature of the endplate, the line connecting the outer left and right landmark defined the orientation of the mediolateral (Z) axis, pointing to the right. The inferosuperior (Y) axis was perpendicular to the already defined axes, pointing upwards. The origin was placed in the geometric centre of the endplate mesh. This definition was based on the ISB recommendations for defining the vertebral body coordinate system (Wu, 2002).

3) Thereafter, a rigid iterative closest point (ICP) registration was performed fitting both isolated endplates onto each other, thereby obtaining the transformation matrix from the inferior to the superior endplate. The rotational components of this matrix were divided by two and added to the fixed endplate reference axis to define the joint's axes of rotation (Figure 25).

* In case of not clearly visible landmark on the inferior endplate, the superior endplate was used and half of the ICP rotation matrix was subtracted, instead of added, to obtain the orientation of the IV joint.

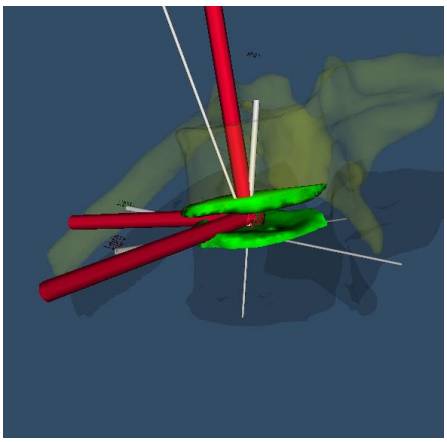

Figure 23: Vertebral endplates (green) enclosing the to-be-defined joint were cut from the vertebrae (translucent), creating surface meshes forming the upper and lower boundary of a virtual disc.

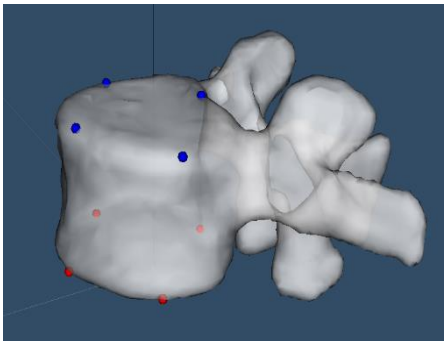

Figure 24: Illustration of the four manually placed anatomical landmarks on the superior (blue) and inferior (red) vertebral endplate, each, of the third lumbar vertebra.

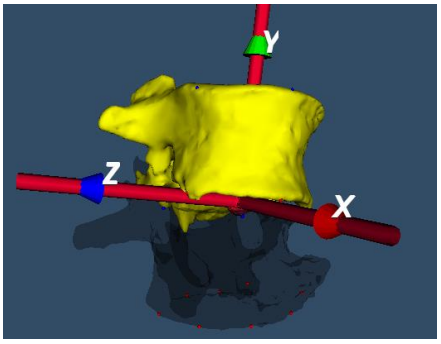

Figure 25: After obtaining the transformation matrix from a rigid iterative closest point (ICP) transformation, fitting one mesh onto the other, the IV joint (red axis) was oriented as symmetric as possible and positioned in the geometric centre of the virtual IV disc.

2. Pilot testing the sensitivity of the IV joint definition on kinematic results

As the 3 DOF spherical IV joints used in our musculoskeletal model are simplifications of the true six DOF IV joint, validation of this mesh-based IV joint definition method is difficult. However to investigate the influence of error during the IV joint definition on the kinematic results, a preliminary sensitivity analysis was performed on one of the subject-specific spino-pelvic models (female, 60 years, 37 kg, 1.50m) in this study. The position of the IV joints, relative to their respective inferior and superior vertebral geometries, was defined as explained in Appendix 2A. The obtained model and the position of the IV joint is referred to as the reference model and position, respectively.

Then, the position of the IV joint at level T10/T11 (arbitrarily selected) was perturbed.

1) We defined a large volume around this reference position, further referred to as the perturbation volume, which was mediolateral and anteroposterior defined by the outer edges of the IV disc, and inferosuperior covering the thickness of the IV disc extending to the mean centre of the superior and inferior vertebrae. The dimensions of the T10/T11 FSU were measured on the CT-segmented vertebrae using Mimics 19.0 (Materialise NV, Leuven, Belgium), shown in Table 9. The dimensions of the perturbation volume were defined as shown in Table 10.

Table 9: Manually determined dimensions of the T11/T10 FSU.

	Mean distance (mm)
Mediolateral width of the IVD	33.62
Anteroposterior depth of the IVD	27.06
Inferosuperior thickness of the IVD	5.073
T10 inferosuperior vertebral thickness	20.89
T11 inferosuperior vertebral thickness	20.39

Table 10: Calculation of the perturbation volume. The outer dimensions of the T10/T11 FSU were divided by two to obtain the single-sided range around the reference centre, and rounded up for ease of use and ensuring the inclusion of the defined perturbation volume.

Axis	**calculation**	**Rounded up single-sided range around the reference centre (mm)**
Anteroposterior (X)	27.06/2	14.00
Inferosuperior (Y)	(5.073 + AVG(20.89; 20.39))/2	13.00
Mediolateral (Z)	33.62/2	17.00

2) The perturbation volume was compartmentalized to four discrete steps on each side of the reference centre (Figure 26), i.e. nine steps along each side of the rectangular perturbation volume. Following the parameters of Table 11, 729 (i.e. 93) models were created, where the IV joint position was perturbed filling the entire defined perturbation volume.

Table 11: Discretization of the perturbation volume.

Axis	**Single-sided range around the reference centre (mm)**	**Number of steps on each side of the reference centre**	**Total steps**	**Step size (mm)**
Anteroposterior (X)	14.00	4	9	3.50
Inferosuperior (Y)	13.00	4	9	3.25
Mediolateral (Z)	17.00	4	9	4.25

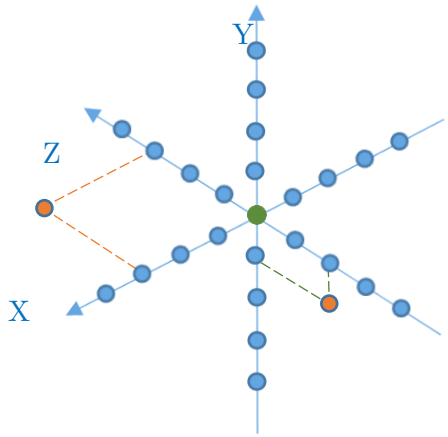

Figure 26: Discretization of the perturbation volume. Along the defined axis and centred around the reference position (green sphere), four steps were equally distributed (blue spheres). The entire perturbation volume was filled, of which two positions (orange) are visualized.

3) Each of the 729 models was used to perform an inverse kinematic simulation (Lu and O'Connor, 1999) of a seated forward flexion motion which the subject performed in the motion lab wearing the markers as defined previously in this work.

Results

A. Absolute data

By means of illustration, the joint angles of the T10/T11 FSU in all three DOF are shown in Figure 27.

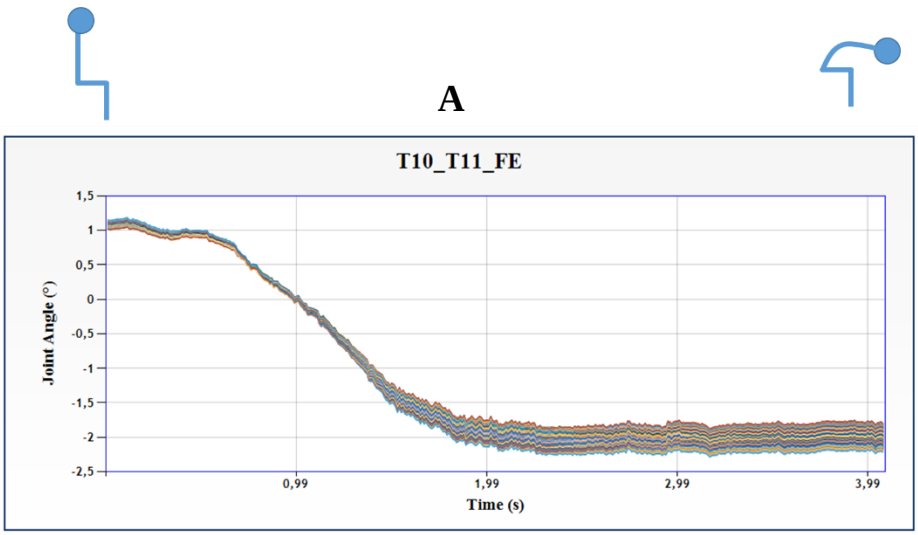

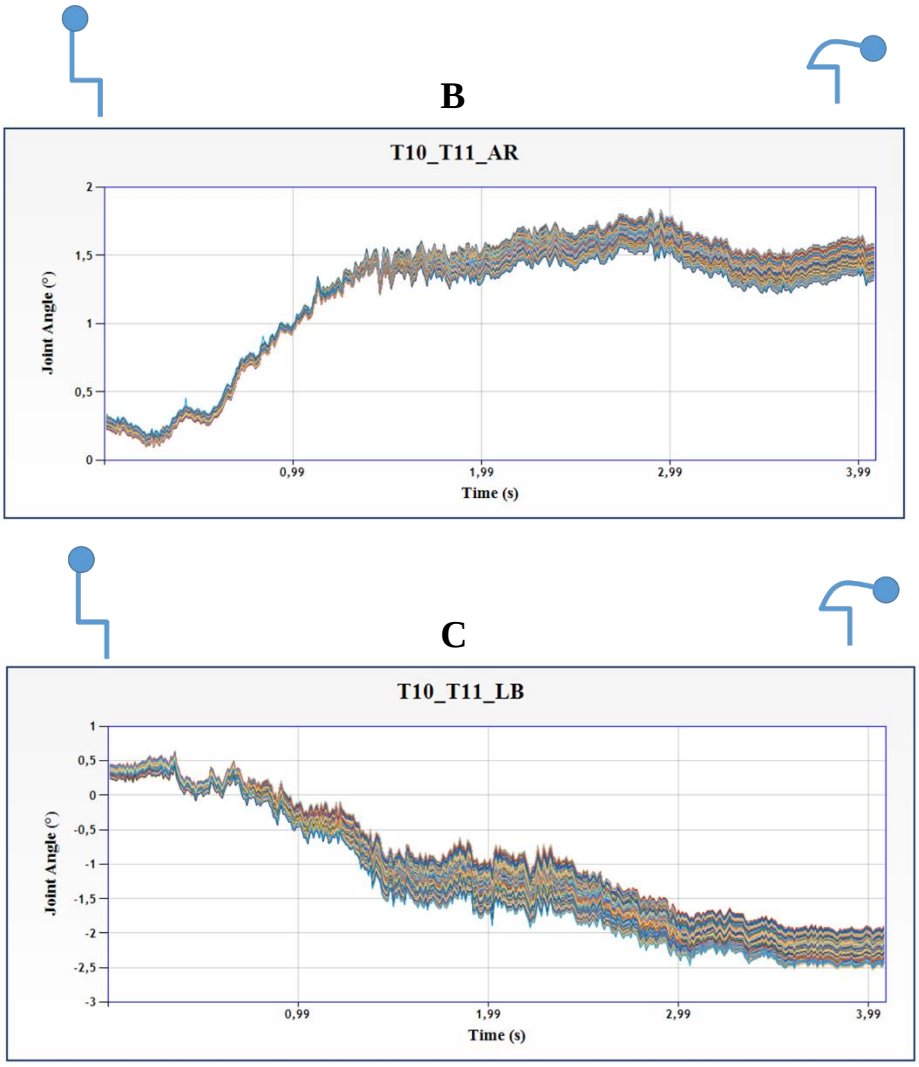

Figure 27: Overlay of 729 inverse kinematic results for the (**A**) flexion/extension (FE), (**B**) axial rotation (AR) and (**C**) lateroflexion (LB) DOF for the duration of the executed forward flexion motion.

B. Relative data

The absolute difference between the inverse kinematic results using the 728 perturbed models and the reference inverse kinematic result was calculated at each time interval. By means of illustration, the maximal error for the flexion/extension DOF of the T10/T11 FSU is visualized over de perturbation volume in Figure 28. The maximal errors for all DOF over the duration of the executed motion is shown in Table 12.

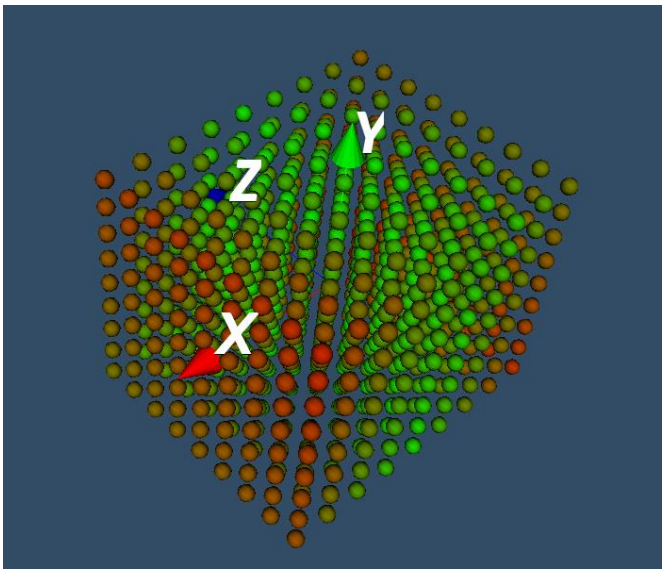

Figure 28: Illustration of the discretized perturbation volume, color-coded according to the maximal error (here: 0,24°) of the DOF in question (here T10/T11 flexion/extension) where green is an absolute mean error of 0° (reference position) and red is the maximal error occurring in this DOF.

Table 12: Overview of the maximal error for each DOF, color-coded according the error range (minimum: 0.09° (white); maximum 0.75° (red)).

	Abs. maximal error (°)		
	Flexion/extension	Lateroflexion	Axial rotation
L5/Sacrum	0.10	0.20	0.12
L4/L5	0.15	0.26	0.13
L3/L4	0.09	0.44	0.16
L2/L3	0.11	0.45	0.13
L1/L2	0.16	0.75	0.23
T12/L1	0.14	0.53	0.15
T11/T12	0.10	0.41	0.16
T10/T11	0.24	0.50	0.17
T9/T10	0.27	0.57	0.16
T8/T9	0.25	0.48	0.21
T7/T8	0.22	0.46	0.20
T6/T7	0.11	0.25	0.26
T5/T6	0.12	0.27	0.25
T4/T5	0.09	0.25	0.23
T3/T2	0.11	0.28	0.25
T2/T3	0.12	0.56	0.14
T1/T2	0.20	0.67	0.17

Discussion and conclusion

We performed a preliminary sensitivity analysis on the IV joint position as a way to estimate the influence of error on the kinematic results, similar to (Zander et al., 2016). The results show an increasing error with increased forward flexion. The error of the kinematics of a perturbation relative to the reference position increased with a further increasing distance from the reference position. However, the obtained maximal error values (Table 12) of this pilot test remained very low. In conclusion, the effect of imposed error on the position of the IV joint was very small/negligible.

This pilot study should be extended with additional subjects and for multiple motions. Additionally, it should be repeated in the form of a Monte-Carlo simulation wherein multiple joints are simultaneously perturbed according to inter- and intra-rater determined uncertainty parameters.

Appendix 3: Marker weights for inverse kinematics

Table 13: During the inverse kinematics optimization the weight of the markers was defined to be equally distributed over the different segments. For example: the individual markers of the cluster on T7, each get a weight of 1/3. The five markers on the pelvis and sacrum each get a weight of 1/5.

Identification of the reflective marker	**Weight**
$T1_1$	0.333
$T1_2$	0.333
$T1_3$	0.333
$T3_1$	0.333
$T3_2$	0.333
$T3_3$	0.333
T5	1.000
$T7_1$	0.333
$T7_2$	0.333
$T7_3$	0.333
T9	1.000
$T11_1$	0.333
$T11_2$	0.333
$T11_3$	0.333
T12	1.000
$L2_1$	0.333
$L2_2$	0.333
$L2_3$	0.333
L3	1.000
$L4_1$	0.333
$L4_2$	0.333
$L4_3$	0.333
SACR (Midpoint of the sacrum)	0.200
LASI (Left Anterior Superior Iliac spine)	0.200
RASI (Right Anterior Superior Iliac spine)	0.200
RPSI (Left Posterior Superior Iliac spine)	0.200
LPSI (Right Posterior Superior Iliac spine)	0.200

Chapter 2

Subject-specific spino-pelvic models reliably measure spinal kinematics during seated forward bending in adult spinal deformity

Thomas Overbergh[1]
Pieter Severijns[1, 2]
Erica Beaucage-Gauvreau[1]
Thijs Ackermans[1]
Ilse Jonkers[3]
Lieven Moke[1,4]
Lennart Scheys[1,4]

Published as:

Overbergh, T., Severijns, P., Beaucage-Gauvreau, E., Ackermans, T., Moke, L., Jonkers, I., Scheys, L., 2021. Subject-Specific Spino-Pelvic Models Reliably Measure Spinal Kinematics During Seated Forward Bending in Adult Spinal Deformity. Front. Bioeng. Biotechnol. 9, 1–11.

Affiliations:

[1]Institute for Orthopaedic Research and Training (IORT), Department of Development and Regeneration, Faculty of Medicine, KU Leuven, Leuven, Belgium

[2]Department of Rehabilitation Sciences, KU Leuven, Leuven, Belgium

[3]Department of Movement Sciences, KU Leuven, Leuven, Belgium

[4]Division of Orthopaedics, University Hospitals Leuven, Leuven, Belgium

Abstract

Image-based subject-specific models and simulations are recently being introduced to complement current mostly static insights of the adult spinal deformity (ASD) pathology and improve the often poor surgical outcomes. Although the accuracy of a recently developed subject-specific modeling and simulation framework has already been quantified, its reliability to perform marker-driven kinematic analyses has not yet been investigated. The aim of this work was to evaluate the reliability of this subject-specific modeling method to measure spine kinematics in ASD patients, in terms of (1) the overall test-retest repeatability; (2) the inter-operator agreement of spine kinematic estimates; and, (3) the uncertainty of those spine kinematics to operator-dependent parameters of the framework.

To evaluate the overall repeatability (1), four ASD subjects and one control subject participated in a test-retest study with a two-week interval. At both time instances, subject-specific spino-pelvic models were created by one operator to simulate a recorded forward trunk flexion motion. Next, to evaluate inter-operator agreement (2), three trained operators each created a model for three ASD subjects to simulate the same forward trunk flexion motion. Intraclass correlation coefficients (ICCs) of the range of motion (ROM) of conventional spino-pelvic parameters [lumbar lordosis (LL), sagittal vertical axis (SVA), thoracic kyphosis (TK), pelvic tilt (PT), T1-and T9-spino-pelvic inclination (T1/T9-SPI)] were used to evaluate kinematic reliability (1) and inter-operator agreement (2). Lastly, a Monte-Carlo probabilistic simulation was used to evaluate the uncertainty of the intervertebral joint kinematics to operator variability in the framework, for three ASD subjects (3).

LL, SVA, and T1/T9-SPI had an excellent test-retest reliability for the ROM, while TK and PT did not. Inter-operator agreement was excellent, with ICC values higher than test-retest reliability. These results indicate that operator-induced uncertainty has a limited impact on kinematic simulations of spine flexion, while test-retest reliability has a much higher variability. The definition of the intervertebral joints in the framework was identified as the most sensitive operator-dependent parameter. Nevertheless, intervertebral joint estimations had small mean 90% confidence intervals (1.04°-1.75°).

This work will contribute to understanding the limitations of kinematic simulations in ASD patients, thus leading to a better evaluation of future hypotheses.

Introduction

Musculoskeletal (MS) models and associated simulations of motion are used to provide a better understanding of the complex biomechanics of, primarily, the healthy spine (Beaucage-Gauvreau et al., 2019; Bruno et al., 2015; Ignasiak et al., 2018). These simulation-based approaches provide parameters that are otherwise difficult, or even impossible, to measure non-invasively *in vivo*, such as intervertebral (IV) joint angles, IV disc loads (Bruno et al., 2017) and spinal muscle forces (Burkhart et al., 2017). Indeed, in healthy subjects these MS models have shown excellent test-retest reliability in terms of spine curvature estimation (expressed as lumbar lordosis and thoracic kyphosis) (Burkhart et al., 2020). More recently, these MS models and simulation-based approaches were introduced in pathological spine populations, such as adult spinal deformity (ASD) (Overbergh et al., 2020) and adolescent idiopathic scoliosis (AIS) (Schmid et al., 2016), to complement the current state-of-the-art mostly static assessments and on the longer term improve the often poor outcomes of surgical treatments (Smith et al., 2016). More specifically, a novel method based on biplanar radiography and computed tomography (CT) was developed to create subject-specific spino-pelvic rigid body models that allows inclusion of personalized spinal alignment, intervertebral joint definitions, and associated virtual skin markers for ASD patients (Overbergh et al., 2020). The resulting subject-specific models from this method can provide innovative, functional biomarkers of pathological spine biomechanics. This novel modeling method circumvents the traditional marker-based scaling step (Burkhart et al., 2020; S. L. Delp et al., 2007), which is applicable to healthy subjects, but not suitable for subjects with a spinal malalignment due to the lack of sufficient a priori information on the specific spinal deformity.

However, to improve the rigor and objectivity of the results prior to clinical interpretation, it is imperative to verify the simulation results of modeling methods both in terms of accuracy and reliability (Hicks et al., 2015; Schwartz et al., 2004). The accuracy of the above-mentioned subject-specific biplanar radiograph-based modeling method, as well as its accuracy in estimating spine kinematics, was validated previously (Overbergh et al., 2020).

Nevertheless, the subject-specific model creation method and the use of these subject-specific models to evaluate spinal kinematics remain susceptible to variability from different sources of errors and the impact thereof has not been investigated yet. Indeed, the creation of image-based subject-specific spino-pelvic models requires operator-dependent manual inputs to define virtual markers, spinal alignment, and IV joints (Overbergh et al., 2020), resulting in an extrinsic variability on the simulation outputs (Schwartz et al., 2004). The reliability of these operator-dependent inputs can be evaluated using an operator agreement analysis quantifying the robustness of the kinematic simulation results to this extrinsic variability (Hicks et al., 2015). In addition, the reliability of the kinematics of a subject is affected by intra-subject differences in performing the motion (i.e. within- or between-session variability), categorized as intrinsic variability (Schwartz et al., 2004). In relation to this intrinsic variability, the test-retest reliability of spino-pelvic parameterization through marker-based polynomial fitting of a sit-to-stance (STS) motion has already been investigated in an ASD population (Severijns et al., 2020). Its performance was reported equally or even more reliable than conventional

radiographic measurements (Severijns et al., 2020). However, the effect of these intra-subject differences in combination with image-based subject-specific models has not yet been investigated in an ASD population.

Specifically for biomechanical modeling and simulation research, the complex non-linear interactions between input and output parameters often require an extension to the conventional operator agreement analyses to obtain a representative range of output variability and identify the aspects of the modeling method that have the highest/lowest impact on the outputs (Hicks et al., 2015). Therefore, uncertainty analyses, such as Monte-Carlo probabilistic simulations, are commonly used to assess the simultaneous impact of uncertainties arising from multiple sources (Hicks et al., 2015; Myers et al., 2015). Monte-Carlo analyses allow computation of sensitivity factors (e.g. correlation coefficients) to determine relations between the input and output distributions (Hicks et al., 2015; Myers et al., 2015) to identify the modeling components with a high impact on the output for future improvements. Thereto, Monte Carlo analyses generate a large number of statistically probable variations of a baseline model, consisting of randomly combined perturbations of the operator-dependent parameters susceptible to uncertainty. These perturbations are sampled from a probability density function representative of the actual variability of the operator-dependent parameters (Hannah et al., 2017; Valero-Cuevas et al., 2003). The impact of these operator-dependent parameters on the simulation outputs can then be translated into confidence bounds on the baseline output (Ackland et al., 2012; Myers et al., 2015; Valente et al., 2014).

The aim of this study was to evaluate the reliability of a previously developed subject-specific spino-pelvic modeling method (Overbergh et al., 2020) to measure spine kinematics in an ASD population, in terms of (1) the overall test-retest repeatability and (2) the inter-operator agreement of spine kinematic estimates; and, (3) the sensitivity of those spine kinematics to operator-dependent aspects of the underlying subject-specific modeling method.

Materials and methods

Participants and data collection

Five participants (2 males (51 and 72 years), 3 females (62, 69 and 70 years)) with varying degrees of spinal malalignment and one control subject (female) participated in this study following ethical approval and informed consent (S58082) (Overbergh et al., 2020). All data collection was performed in at the university hospital of Leuven (UZ Leuven, Belgium). All subjects underwent CT imaging from T1 to pelvis (BrightSpeed by GE Healthcare, with an inter-slice distance of 1.25 mm and a pixel size of 0.39x0.39 mm). Thereafter, an experienced physiotherapist instrumented each subject with reflective markers according to the skin marker protocol described in Overbergh et al. (2020). Full-body radiographic (x-ray) images were then acquired using the biplanar radiography system (EOS Imaging, Paris, France), while the subject was wearing the markers and adopted the Scoliosis Research Society free-standing position (fingers-on-clavicle variation) (Horton et al., 2005; M. Y. Wang et al., 2014). When the subjects arrived at the motion laboratory, they were asked to perform a maximal forward trunk flexion from a normal upright seated position, while the trajectories of the reflective

markers were recorded (100 Hz) using a 10-camera Vicon system (VICON Motion systems, Oxford Metrics, UK). Four of the five ASD patients and the control subject repeated all data collections, apart from the CT imaging, after an average two-week time interval (mean 14.2 ± 9.9 days, 6-33 days). One ASD patient (male) was excluded for the second data collection due to a surgical intervention, but remained part of the study because of a successful first data collection.

Test-retest reliability

To test the repeatability of our workflow for spinal kinematic evaluation, we performed a test-retest reliability analysis between the two repeated data collection sessions available for each of the four ASD subjects (one excluded) and the control subject. Two subject-specific spino-pelvic models were created by one single operator to prevent confounding inter-rater variability; one for the initial data collection and one for the repeated data collection, respectively (Overbergh et al., 2020). The resulting subject-specific spine models each consist of 18 bodies (12 thoracic vertebrae, 5 lumbar vertebrae and a sacrum/pelvis body), interconnected by 17 spherical joints (each with three rotational degrees of freedom (DOFs)) and have a total of 28 virtual model markers each, corresponding to the retroreflective markers placed on the skin of the subject (Overbergh et al., 2020). It should be noted that these aspects of the model (i.e. bodies, joints and markers) all required input from an operator (Overbergh et al., 2020). The maximal forward trunk flexion motion, recorded as three-dimensional (3D) marker trajectories in the motion laboratory, was processed using Vicon Nexus 2.11 (VICON Motion systems, Oxford Metrics, UK) and low-pass Butterworth filtered (6Hz). For each subject and each session, the respective models were used to run an inverse kinematics analysis (Lu and O'Connor, 1999) in OpenSim 3.3 (Stanford University, USA) (S. L. Delp et al., 2007) of the corresponding forward trunk flexion motions. The kinematic outputs (i.e. 51 joint angles ranging from L5/Sacrum to T1/T2) were time-normalized (to 100 frames) and noise reduction was performed using a moving average filter with a three-frame width. The joint kinematics (i.e. relative motion at the joint between two interconnected bodies) were converted to body kinematics (i.e. absolute motion of a body expressed in the ground reference frame) to obtain six common spino-pelvic parameters in the sagittal plane based on a-priori identification of anatomical landmarks on the model: 1) lumbar lordosis (LL), 2) thoracic kyphosis (TK), 3) sagittal vertical axis (SVA), 4) pelvic tilt (PT), and 5) T1 and 6) T9 spino-pelvic inclination (T1-SPI, T9-SPI) (detailed in Appendix 1). The ranges of motion (ROM) of each of these spino-pelvic parameters (defined as the absolute value of the difference between the start and the end of the motion, Appendix 1) were used as an outcome parameter to determine the test-retest reliability. This test-retest reliability was expressed as intraclass correlation coefficients (ICCs) with a two-way random effects model for absolute agreement (ICC(2,1)) (SPSS 25, IBM Corp. Armonk, NY). ICCs were classified as poor (ICC <0.40), fair to good (0.40-0.75) or excellent (>0.75) (Shrout and Fleiss, 1979). Standard error of measurement (SEM) was calculated as:

$$SEM = SD\sqrt{1 - ICC}, \quad (1)$$

with SD the standard deviation of the absolute difference relative to the mean output; and the smallest detectable difference (SDD) (Shrout and Fleiss, 1979) as:

$$SDD = SEM \times 1.96\sqrt{2} \quad (2)$$

Inter-operator reliability

To assess the portion of variability of the modeling method on the kinematic results that can be attributed to operator-dependent inputs (Overbergh et al., 2020), three operator-dependent modeling components (and their associated parameters) were first identified (Figure 29): (A) virtual markers (position parameters): the reconstruction of virtual marker positions requires operators to identify and delineate retro-reflective markers on both biplanar radiographic images; (B) bodies (i.e. vertebrae and pelvis) (position and orientation parameters): the manual reconstruction of the 3D spinal alignment requires operators to match subject-specific vertebrae projections on biplanar radiographic images until visual agreement; (C) joints (position and orientation parameters): the IV joint definition requires operators to manually identify anatomical landmarks on the bodies connected by these joints. This results in a total of 294 operator-dependent parameters [(28 markers x 3 DOFs) + (18 bodies x 6 DOFs) + (17 joints x 6 DOFs)].

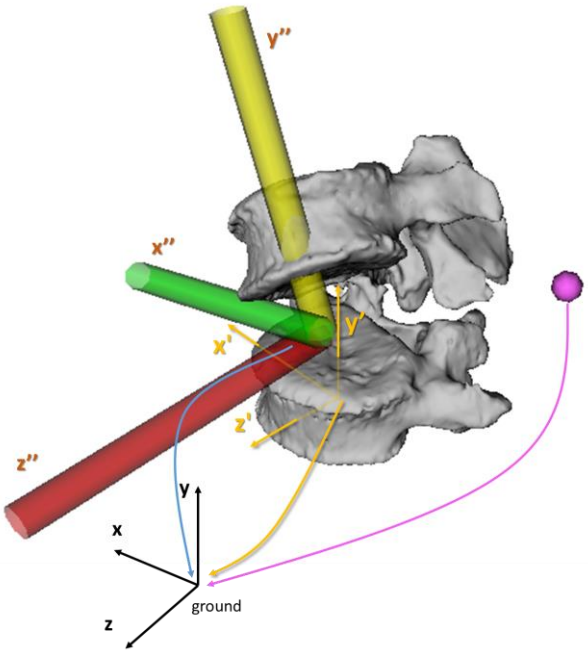

Figure 29: Illustration of the three operator-dependent parameters components. The position of the virtual markers (pink sphere), the position and orientation of the bodies (yellow reference frame, x'y'z') and the position and orientation of the IV joints (yellow, green and red reference frame, x''y''z'') are expressed in the ground reference frame (black, xyz). Within the model, positions of virtual markers, bodies and joints, are expressed in the x (mediolateral), y (inferosuperior) and z (posterior-anterior) directions. The orientations of the joints and bodies are expressed around the x (flexion-extension, FE), y (axial rotation, AR) and z-axis (lateroflexion, LF) using an xyz body-fixed sequence.

Three operators participated in this study. One operator (O1, four years of spine modeling experience and developer of the modeling method), trained two additional operators (O2 and

O3 with six and two years of spinal research experience, respectively) on the required steps of the modeling workflow through a dedicated manual describing optimal use of the custom software. Next, radiographic data of a cadaver with known ground truth spinal alignment due to plastination, was used for acquainting with and training in spinal alignment personalization (Overbergh et al., 2020) (detailed in Appendix 2), followed by a final collective, quantitative feedback session between the operators. Then, each operator created a subject-specific spinal model of three randomly selected subjects (S1, S2 and S3, Figure 30) from the ASD group while being blinded to the other operators. The models were created as described in the modeling workflow of Overbergh et al. (2020), with the exception of segmenting the individual bones from CT which was only performed by O1.

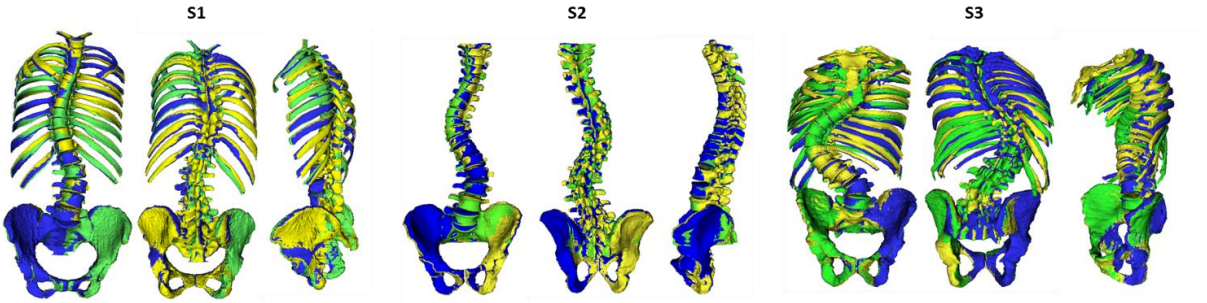

Figure 30: Illustration of the alignment reconstruction for the three subjects (S1 (female), S2 (male) and S3 (male)) by the three operators: O1 (green), O2 (yellow) and O3 (blue).

Inter-operator agreement

Each of the nine created models was used to perform an inverse kinematics simulation of the subject's corresponding maximal forward flexion motion to obtain the ROM values for the six spino-pelvic parameters (LL, TK, SVA, PT, T1-SPI, T9-SPI). ICCs using a two-way random effects model for absolute agreement (ICC(2,1)), SEM (Formula 1) and SDD (Formula 2) on these outcome values were used to assess inter-operator agreement.

Monte-Carlo probabilistic simulation

We performed a Monte-Carlo probabilistic simulation analysis to quantify the distributions of variations on simulated IV joint kinematics caused by operator variability, similar to the work by Valente et al. (2014). First, a baseline model (S-base) was determined for each of the three ASD subjects to avoid operator bias, by averaging the three operator-defined models (Figure 31A). These baseline models were considered as reference models to experimentally estimate the variability of the 294 operator-dependent model parameters. The variations of these operator-dependent components (marker, bodies, and joint) for the three models with respect to its respective baseline model were pooled into histograms over all vertebral levels and subjects, and separated by direction (x, y, z) for each parameter (position and orientation) (Appendix 3). From these experimentally determined variability histograms, continuous probability density functions were estimated (MATLAB, The Mathworks Inc., MA) (Appendix 3), and used as input to sample variations on the 294 operator-dependent model parameters

(Figure 31B). This ensured statistically probable imposed perturbations according to a-priori experimentally determined inter-operator variability. To create a perturbed model, a value was sampled from the probability function for each operator-dependent model parameter and used to vary the value of that parameter in the baseline model. For each subject, every variation of the baseline model was then used to run an inverse kinematics analysis (Lu and O'Connor, 1999) (Figure 31C). The convergence criterion for the Monte-Carlo simulation was defined such that the mean and standard deviation of all output variables (here: joint angles averaged over the duration of the motion) over the last 10% of the simulations were within 2% of each final mean and standard deviation (Appendix 4) (Ackland et al., 2012; Martelli et al., 2015; Valente et al., 2013; Valero-Cuevas et al., 2003).

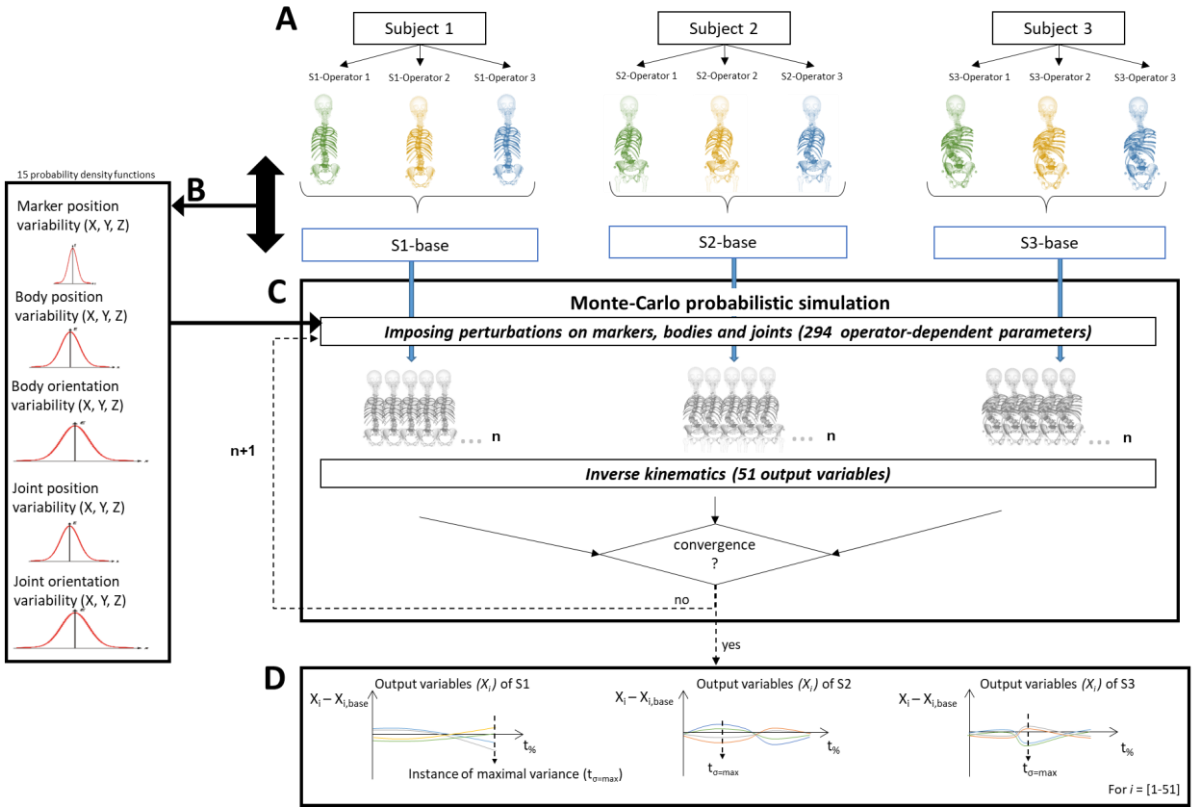

Figure 31: Schematic representation of the determination of the inter-operator reliability of subject-specific modeling. (**A**) For each subject (S) a subject-specific model was created by each of the three operators (O). A baseline model (S-base) was then created for every subject by averaging these three respective models. (**B**) The variability in the operator-dependent parameters was calculated in relation to the respective baseline models, pooled together for all vertebral levels and subjects, and separated by direction. (**C**) In the Monte-Carlo probabilistic simulation, variations on the baseline model were created by imposing statistically probable error combinations on the operator-dependent parameters and then used to perform inverse kinematic simulations until the convergence criterion on the output variables (i.e. the joint angles) was reached. (**D**) The joint angles (X_i with i=1...51) were then expressed relative to the joint angles of the corresponding baseline model ($X_{i,\,base}$) and time normalized ($t_{\%}$). $t_{\sigma=max}$ represents the time instance of maximal variance.

Operator-dependent input parameters

After assessing normality of the parameters of the model components (position and/or orientation of markers, bodies, joints), kernel functions were consistently used to estimate all distribution functions from their respective histograms (Distribution Fitter, MATLAB, The Mathworks Inc., MA) (Appendix 3). To assess the variation of the operator-dependent inputs in the modeling method (markers, bodies and joints), we used the absolute value of the difference between each of the three operator-dependent models and its baseline model to determine the median and maximum values for each individual position and orientation parameter, in each direction.

To assess the robustness of the IV joint kinematics to variations in the operator-dependent model parameters, joint angles of the perturbed models were expressed relative to the joint angles of the baseline model's kinematics. For each subject, we then determined the 5-95% confidence bounds for each of the joint angles (17 joints with three rotational DOFs each), at each time frame of the performed spine flexion motion, which indicates a 90% probability that an estimated joint angle curve is within the confidence intervals with respect to the calculated reference curve (Myers et al., 2015; Navacchia et al., 2016). Thereafter, a box and whiskers plot was created at the time instance of respective maximal variance ($t_{\sigma=max,}$ Figure 31D) for every DOF at every joint (Ackland et al., 2012).

Sensitivity factors

To quantify the sensitivity of simulated kinematics to variability in specific input parameters, sensitivity factors were determined as Pearson correlation coefficients (Myers et al., 2015) between the sampled perturbation values (for each of the 294 model parameter) and the corresponding absolute maximal difference of the IV joint kinematics with respect to the baseline model's IV joint kinematics (for each of the 51 DOFs), pooled for all three subjects (MATLAB).

Results

Test-retest reliability

The test-retest reliability, expressed as ICCs of six spino-pelvic parameters in Table 14, was excellent (ICC>0.75) for the LL, SVA, PT (not significant), T1-SPI and T9-SPI. Nevertheless, high SEM and SDD were noted for TK, which presented with a poor reliability (ICC<0.40).

Table 14: Results of the test-retest reliability analysis. ROM: range of motion, ICC: intraclass correlation coefficient, SD: standard deviation of the absolute differences between both sessions, SEM: standard error of measurement, SDD: smallest detectable difference. Significance level: $p<0.05$ (bold). The confidence intervals for ICCs with a non-significant p value are not applicable.

Spino-pelvic parameter ROM	Test-retest ICC	95% confidence interval	p value	SD	SEM	SDD	Mean ROM (range)
LL (°)	0.86	0.032 - 0.985	**0.028**	5.5	2.1	5.7	20.5 (9.5-42.4)
TK (°)	0.12		0.460	6.2	5.8	16.1	19.8 (1.8-30.9)
SVA (cm)	0.91	0.363 – 0.991	**0.018**	0.9	0.3	0.7	30.0 (25.4-40.6)
PT (°)	0.80		0.095	5.3	2.4	6.6	53.9 (30.4-60.4)
T1-SPI (°)	0.91	0.226 – 0.990	**0.012**	4.7	1.4	4.0	66.7 (46.1-89.7)
T9-SPI (°)	0.91	0.360 – 0.990	**0.015**	4.7	1.4	3.9	60.6 (39.5-81.7)

Inter-operator agreement

Excellent inter-operator agreement (ICCs ≥ 0.875) of the kinematics, expressed as spino-pelvic parameters, was noted for all analyzed parameters (Table 15).

Table 15: Results of the inter-operator reliability analysis. ROM: range of motion, ICC: intraclass correlation coefficient, SD: standard deviation of absolute error relative to mean value, SEM: standard error of measurement, SDD: smallest detectable difference. Significance level: $p<0.05$ (bold).

Spino-pelvic parameter ROM	Inter-operator ICC	95% confidence interval	p value	Mean SD	SEM	SDD
LL (°)	0.970	0.775 - 0.999	**0.002**	1.82	0.3	0.9
TK (°)	0.875	0.189 – 0.997	**0.031**	1.95	0.7	1.9
SVA (cm)	0.964	0.737 – 0.999	**0.005**	0.43	0.1	0.2
PT (°)	0.998	0.981 – 1.000	**<0.001**	0.13	0.0	0.0
T1-SPI (°)	1.000	0.999 – 1.000	**<0.001**	0.06	0.0	0.0
T9-SPI (°)	1.000	0.998 – 1.000	**<0.001**	0.07	0.0	0.0

Monte-Carlo probabilistic simulation

1. Operator-dependent input parameters

The median difference in the virtual marker positions with respect to the baseline models ranged between 0.120-0.122 mm (Table 16). For the 3D distance the median (maximal) difference was 0.262 mm (1.040 mm). The median differences with respect to the body positions and orientations of the baseline models ranged between 0.552-0.739 mm and 0.96°-1.68°, respectively (Table 16). Finally, the median differences with respect to the joint positions and orientations of the baseline models ranged between 0.566-1.058 mm and 1.16°-1.95°, respectively (Table 16). (See also Appendix 3 for the corresponding probability distributions.)

Table 16: Operator-dependent input parameters.

Input parameters	Median (max) X	Median (max) Y	Median (max) Z
Marker position (mm)	0.112 (0.584)	0.120 (0.717)	0.120 (1.039)
Body position (mm)	0.672 (4.71)	0.552 (3.79)	0.739 (14.74)
Body orientation (°)	1.19 (10.4)	1.68 (10.8)	0.96 (6.83)
Joint position (mm)	0.782 (4.44)	0.566 (14.32)	1.058 (12.18)
Joint orientation (°)	1.65 (16.4)	1.95 (9.97)	1.16 (7.09)

2. Kinematic simulation output

Convergence of the Monte-Carlo probabilistic simulations was reached at n= 954, n=814 and n=894 for subject S1, S2 and S3, respectively (detailed in Appendix 4), where n is the number of iterations. For convenience, the minimal number of required iterations for convergence was rounded up to 1000 and set equal for all subjects. Figure 32 illustrates the 90%-confidence intervals (CIs) over the duration of the motion for S1.

The mean (maximum) of the 90%-CIs of the IV joint kinematics at their respective $t_{\sigma=max}$ were 1.04° (3.44° at L2/L3 lateroflexion (LF)), 1.14° (4.79° at L2/L3 LF) and 1.75° (11.72° at L2/L3 LF) for S1, S2 and S3 respectively (Figure 32 and Figure 43-Figure 44 of Appendix 4). The box and whisker plots show a higher variability at the lumbar and low thoracolumbar region compared to the upper thoracic region (Figure 33). Furthermore, S3 presents with larger CIs at the lumbar region than S1 and S2 (Figure 32 and Figure 43-Figure 44 of Appendix 4).

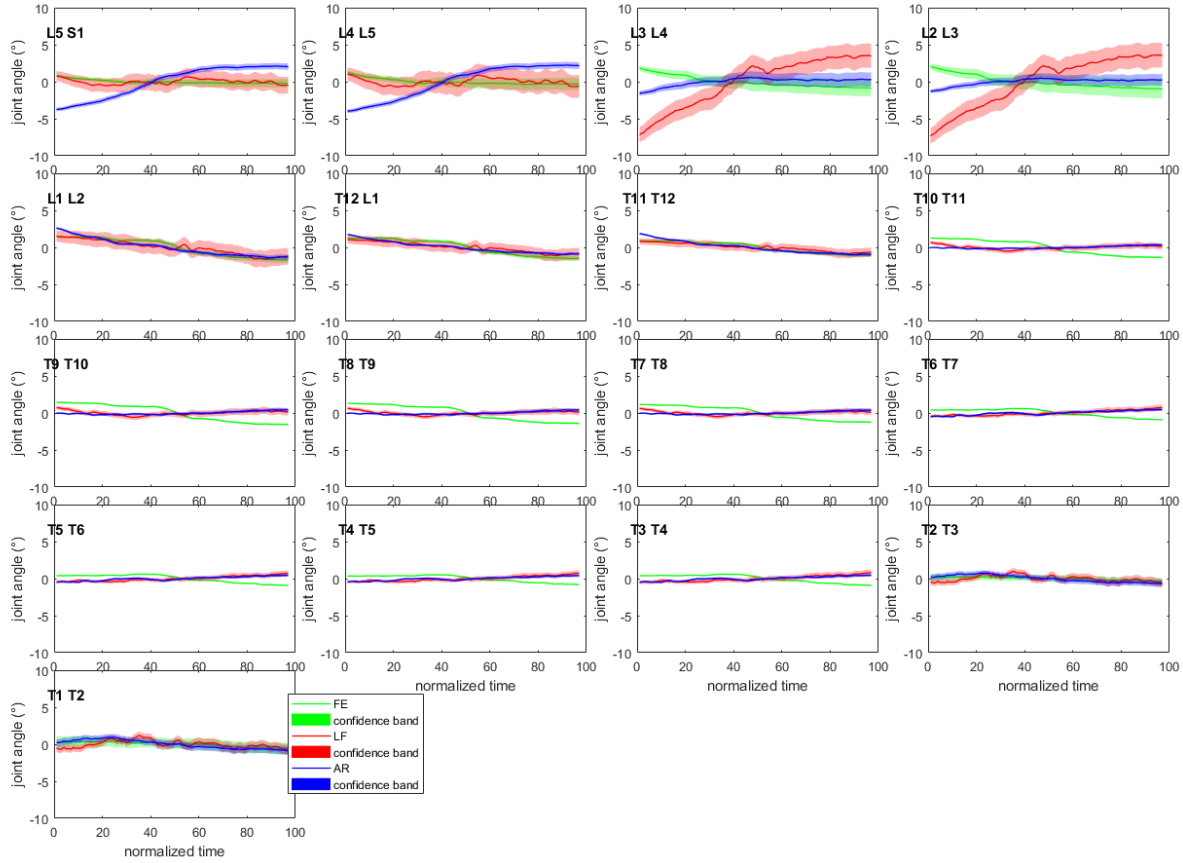

Figure 32: Confidence bands (5-95%) for each of the joint angles of subject 1. All curves have been normalized to their mean value over the length of the motion to allow visualization within the -10° to 10° joint angle range. AR: axial rotation; LF: lateroflexion; FE: flexion-extension. (Graphs for S2 and S3 are available in Figure 43-Figure 44 of Appendix 4)

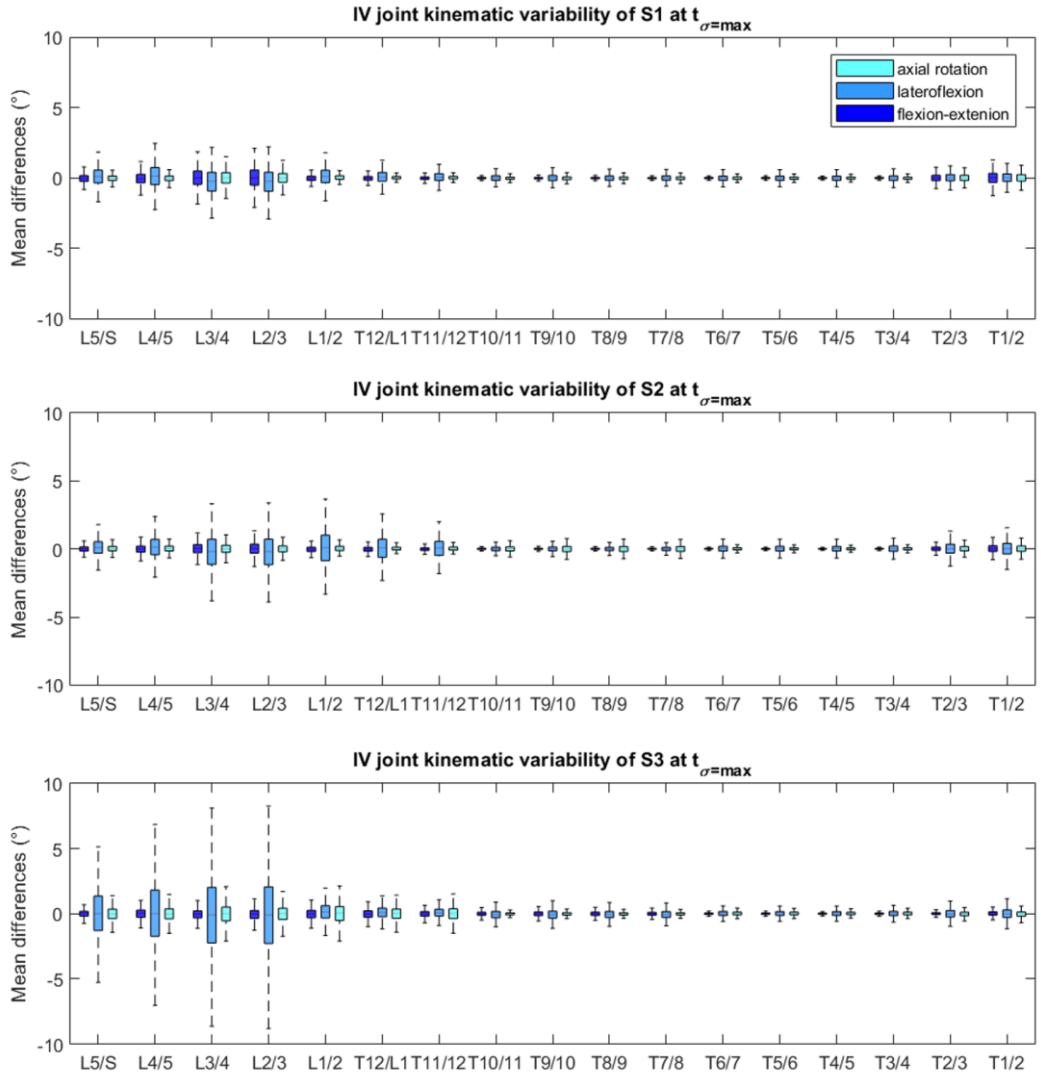

Figure 33: Box and whisker plot of the joint values at $t_{\sigma=max}$ of each DOF, relative to the baseline model's joint angles, for each subject. The upper and lower edges of the box are the 75th and 25th percentiles, the horizontal bar in the box is the median (50th percentile) and the upper and lower bars are maximum and minimum values.

3. Sensitivity factors

Calculating the sensitivity factors for all possible combinations of input (i.e. operator-dependent model parameters) and output (i.e. IV joint kinematics for every DOF) variables, resulted in a 294 by 51 grid of correlations. Mean (maximal) sensitivity factors were 0.015 (0.15) for the marker positions, 0.015 (0.07) and 0.014 (0.06) for the body positions and orientations, respectively; and 0.022 (0.26) and 0.021 (0.47) for the joint positions and orientations, respectively.

Discussion

This study aimed at evaluating the kinematic variability associated with both intrinsic and extrinsic sources of error (Schwartz et al., 2004), of a subject-specific spino-pelvic modeling method previously developed to quantify intervertebral joint motion in ASD subjects (Overbergh et al., 2020).

The test-retest reliability (intrinsic intra-subject and extrinsic intra-operator variability) of the kinematics within individual subjects was evaluated over a two-week time interval. Although our method is capable of measuring spinal kinematics at the level of the IV joint, we gave priority to analyzing spino-pelvic parameters that are more commonly studied and used in clinical practice because of the lack of available literature on IV joint kinematic variability to compare to. Our results were similar to those previously reported in an ASD (Severijns et al., 2020) and healthy (Mousavi et al., 2018) population. Notably, we obtained a similar reliability for LL [ICC: 0.86 vs. 0.84 (Severijns et al., 2020) and 0.79 (Mousavi et al., 2018)] and SVA (ICC: 0.91 and 0.95 (Severijns et al., 2020)), but a lower reliability for TK [ICC: 0.12 vs. 0.95 (Severijns et al., 2020) and 0.78 (Mousavi et al., 2018)]. Although the skin marker set, pathology of the study population (ASD) and amount of subjects (5 and 8, respectively) are comparable to the study by Severijns et al. (2020), differences in the kinematic model (marker-driven subject-specific model vs. polynomial marker fit) along with the difference in motion performed by the subjects (trunk flexion (current work) vs. STS) may explain the notable difference in reliability of the TK parameter. Indeed, a maximal forward flexion is more challenging in terms of standardization compared to a STS movement. Furthermore, the thoracic region is typically more involved during maximal forward flexion compared to STS (mean ROM TK: 19.8° vs. 7.86°(Severijns et al., 2020)). Also, as the modeling method is more reliant on manual operator interaction compared to Severijns et al. (2020), the modeling method may present with a potentially higher intra-operator variability, which is part of the test-retest variability. Lastly, the limited number of subjects (n=5) included in this test-retest reliability analysis should be extended to increase the confidence in the ICC values.

The inter-operator kinematic agreement was assessed to investigate the effects of extrinsic inter-operator variability specifically related to the modeling method. The operator agreement in terms of spino-pelvic parameters, was excellent with ICC values ranging from 0.875 (TK) to (almost) 1 (LL, SVA, PT, T1-SPI, T9-SPI), showing a high to very high agreement amongst the three operators. Compared to Severijns et al. (2020), we report higher ICC values for LL (0.97 vs. 0.92), but slightly lower for SVA (0.964 vs. 1.00) and TK (0.875 vs. 0.91). PT, T1-SPI and T9-SPI were in almost perfect agreement. The comparable, but still slightly higher, inter-operator reliability of Severijns et al. (2020) could possibly be explained by the limited amount of operator-dependent tasks (only marker identification) in their workflow, which can be done with high accuracy (Pillet et al., 2014) compared to the additional operator-dependent tasks (i.e. marker identification, body and joint reconstruction) required to create the fully subject-specific spino-pelvic models in this work. Nevertheless, only the latter allows analysis of individual IV joint angles.

To further quantify the probabilistic effects of subject-specific spino-pelvic modeling uncertainty on intervertebral kinematics in ASD patients, we used a Monte-Carlo probabilistic simulation. The variabilities in the operator-dependent modeling parameters (i.e. the virtual markers, bodies and IV joint definition) were thereto estimated within a small group of trained operators, each creating a model of the same three ASD subjects. The operator variability in segmenting the vertebrae from CT was excluded from this study [similarly to Valente et al. (2014)] due to its previously reported high level of operator precision for lumbar vertebrae (Cook et al., 2012) and the high time cost associated with segmentation. Variability in radiograph-based virtual marker identification was small and of similar magnitude than previously reported values for a similar study (Pillet et al., 2014). Likewise, the variability in spinal alignment reconstruction (i.e. bodies component) (median position and orientation variability between 0.55-0.74 mm and 0.96-1.68°, respectively) was similar to the previously reported accuracy when validated with a plastinated cadaver serving as ground truth (median accuracy between 0.57–1.57 mm and 1.02–2.20° for vertebral positions and orientations, respectively) (Overbergh et al., 2020). The IV joint definition is based on the position and orientation of the caudal vertebral bodies and on additional landmark identification by the operator; therefore resulting in a higher median variability for the positions and orientation of the joint component (0.57-1.06 mm, 1.16-1.95°), compared to the body component. With a mean 90% CI below 2° [1.04° (S1), 1.14° (S2) and 1.75° (S3)], IV joint kinematics were found to be reliable. This is in agreement with the high reliability of the spino-pelvic parameters in our inter-operator agreement analysis. Importantly, this indicates that the modeling method as well as the resulting kinematics during forward flexion are robust towards inter-operator variability. Although, for each subject, the imposed perturbations in the model variations were sampled from the same probability distributions, different IV joint variability can be noted. Interestingly, the largest variation was consistently noted at the lumbar region (especially L2/L3) for each of the three subjects (Figure 33). This could potentially be related to a higher ROM at this region, although preliminary analyses could not confirm this due to the low number of subjects. Notably, one subject (S3) presented with more than twice as large maximal CIs (lumbar region) compared to the other two subjects. Although we need more data to confirm, this may be due to the more severe deformity of S3 (Figure 30) and associated increased sensitivity of the kinematics to modeling error. Furthermore, kinematics demonstrated very low sensitivity to marker variability (maximal sensitivity factor: 0.15). Likely, this is due to the very limited marker variability in reconstruction from x-ray (largest noted variability of 1.04 mm) compared to the traditional error associated with marker-based motion capture systems (errors of 1-5 mm, (Hicks et al., 2015)) and considerably smaller than typical skin motion artefacts (up to 10 mm for human movement, (Hicks et al., 2015)). Very low sensitivity factors were also found for the body positions and rotations (max: 0.07 and 0.06, respectively). This can be explained by the independence of the IV joint kinematics to the alignment, provided that changes to the alignment are isolated from changes to the joint definition and virtual marker positions. Overall, the imposed variability of the IV joint positions and orientations seemed to have the biggest effect on the IV joint kinematics, with maximal sensitivity factors of 0.26 and 0.47, respectively. Consequently, this study identifies modeling

steps contributing to the reliable definition of the IV joints as a primary target for limiting kinematic variability.

There are some limitations associated with this study. Firstly, the input distributions of the probabilistic simulations can vary depending on the operators and subjects, thereby affecting the simulation output. In this study, operator-dependent parameters were grouped as model components (i.e. the marker positions, body and joint positions and orientations) to have a sufficient amount of samples to estimate a representative probability function based on the histograms, disregarding potential variations in variability within different vertebral levels. As part of future work, a larger group of subjects with different complexities of spinal malalignments would allow a more detailed analysis of the subject-, vertebral level- and direction-dependent variability distributions. Secondly, the type of simulated motion is expected to influence the kinematic variability. Besides its clinical relevance as a task of daily living (e.g. putting on shoes), maximal forward spine flexion was used here as a worst-case scenario because of its large spinal ROM. However, one should be careful with direct extrapolation of the results presented in this study to other motions such as gait, presenting with a lower spinal range of motion, or spinal lateroflexion and axial rotation, presenting with spinal coupling, which may provide additional important insights. This uncertainty analysis focused specifically on the operator-dependent components of the modeling method, thereby ignoring additional variability, for example originating from inter-rater variability in skin marker placement. Lastly, our uncertainty analysis was limited to IV joint kinematics as outcome. However additional analyses should be done to assess the uncertainty propagation in possible subsequent simulation steps such as joint reaction forces or muscle activation (Burkhart et al., 2020; Myers et al., 2015).

Our systematic inter-operator approaches identified a limited impact of operator-induced variability on kinematic simulations of spine flexion in an ASD population. This excellent inter-operator agreement, compared to the lower test-retest reliability for the same motion, however, importantly indicates that the dominant portion of overall test-retest variability is only limitedly originating from aspects of the modeling (extrinsic), but rather from intra-subject differences (intrinsic) in motor task execution. Improved standardization of the maximal forward trunk flexion (e.g. pelvic fixation and/or targets) together with multiple acquisitions averaged per session, may thus improve the test-retest reliability.

In conclusion, although the current modeling method is dependent on manual inputs of the operators, causing additional variability in the simulation output, its isolated effect on the kinematics was very limited, indicating the modeling method to be highly reliable for kinematic analysis of spinal motion. In the future, this kinematic variability could likely be even further reduced by eliminating variability in operator-dependent model components through increased automation of the model creation procedures. Furthermore, this would also decrease the currently high time cost of subject-specific modeling (Aubert et al., 2019; Galbusera et al., 2020). Based on this study's results, the primary focus should hereby be on the intervertebral joint definition.

Conflict of interest and funding

This study was funded by KU Leuven C2 funds, Medtronic and a strategic basic research PhD grant (SB/1S56017N) of the Research Foundation – Flanders (FWO).

Author Contributions

TO collected patient data, was one of the operators creating models, conceptualized the study, developed the technical tools necessary for data analysis, processed the data, wrote the initial manuscript and edited the manuscript. PS collected patient data, conceptualized the study and edited the manuscript. EBG was one of the operators creating models, conceptualized the study and edited the manuscript. TA was one of the operators creating models, conceptualized the study and edited the manuscript. LM conceptualized the study and was responsible for subject recruitment. IJ conceptualized the study and edited the manuscript. LS conceptualized the study, edited the manuscript and supervised the project.

Supplementary material of Chapter 2

Appendix 1: Spino-pelvic parameterization of joint kinematics

1. Calculating dynamic spino-pelvic parameters

Joint kinematics (i.e. relative motion at the joint between two interconnected bodies) were converted to body kinematics (i.e. absolute motion of a body expressed in a fixed ground reference frame) using the API of OpenSim 3.3 (Stanford University, USA). Thereafter, anatomical landmarks on the bodies previously indicated during the mesh-based IV joint definition when creating the model are used (Overbergh et al., 2020). As the location of a landmark on a body is fixed during the motion, its transformation matrix was appended to the body kinematics to obtain the 3D trajectory of each anatomical landmark throughout the trunk flexion motion. Thereafter, six common spino-pelvic parameters in the sagittal plane, i.e. lumbar lordosis (LL), thoracic kyphosis (TK), sagittal vertical axis* (SVA, Figure 34), pelvic tilt (PT) and T1 and T9 spino-pelvic inclination (T1-SPI, T9-SPI) were calculated for every time frame (detailed in Table 17). The acetabular cavities of pelvis were used to define the sagittal and coronal plane in which the spino-pelvic parameters are expressed (Figure 34B).

Table 17: Description of the model-based spino-pelvic parameterization.

Spino-pelvic parameter (unit)	**Model-based calculation**
Lumbar lordosis (LL, °)	Calculated from the sagittal plane projection of the four-points angle defined by the line connecting the anterior and posterior landmarks of the T12 superior endplate, and the line connecting the anterior and posterior landmarks of the sacral endplate.
Thoracic kyphosis (TK, °)	Calculated from the sagittal plane projection of the four-points angle defined by the line connecting the anterior and posterior landmarks of the T1 superior endplate, and the line connecting the anterior and posterior landmarks of the inferior T12 endplate.
Sagittal vertical axis (SVA, cm)	The distance between the posterior sacral endplate and the plumb line of the T1 vertebral body, measured in the transverse plane and perpendicular to the line connecting the left and right acetabula (Figure 1.1). *Because our model is limited to the bodies from pelvis up to T1, the T1 vertebral body was used rather than the C7 vertebral body for the calculation of the SVA.
Pelvic tilt (PT, °)	The projection on the sagittal plane of the three-points angle defined by the vertical line on the mid-point of the line connecting the left and right acetabula, and the line then going to the midpoint of the anterior and posterior sacral endpoint.
T1-Spino-pelvic inclination angle (T1-SPI, °)	The projection on the sagittal plane of the three-points angle defined by the line starting on the mid-point of the line connecting the left and right acetabula, to the T1 vertebral body center, with a vertical line from the T1 vertebral body center.
T9-Spino-pelvic inclination angle (T9-SPI, °)	The projection on the sagittal plane of the three-points angle defined by the line starting on the mid-point of the line connecting the left and right acetabula, to the T9 vertebral body center, with a vertical line from the T9 vertebral body center.

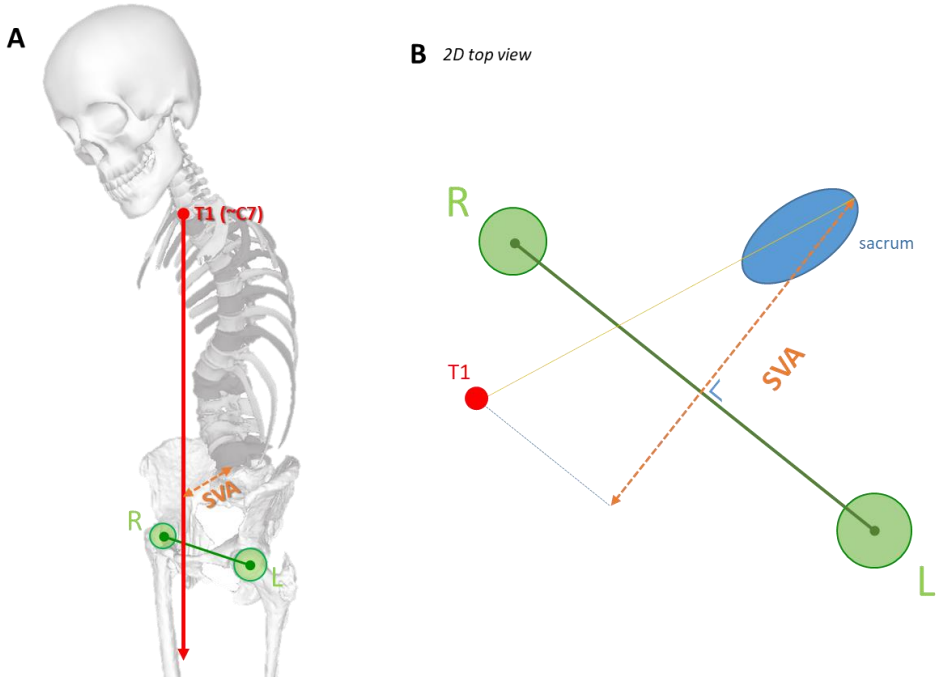

Figure 34**:** (**A**) A visual representation on the model and (**B**) schematic of the sagittal vertical axis (SVA) as described in Table 17.

2. Calculating range of motion

To determine the range of motion (ROM) of these spino-pelvic parameters over the duration of the trunk flexion motion, the absolute difference between the values at the start (mean of the first three frames) and end (mean of the last three frames) of the motion were used. Due to noise on the kinematic simulation output, a different value would have been obtained if ROM would have been calculated based on the minimal and maximal values, whose bounds would not necessarily encloses the complete motion.

Appendix 2: Training the alignment reconstruction

The operators were allowed to familiarize with the modeling software (Overbergh et al., 2020), guided by a written manual, using the images of the control subject, until they felt confident working with the software. The operator training was concluded with the alignment reconstruction of a plastinated cadaver as in (Overbergh et al., 2020). The plastinated cadaver was rigidly fixated, preventing the spinal alignment to change between upright biplanar images, used for alignment reconstruction, and the supine CT, used as ground truth for evaluating the alignment reconstruction accuracy. All operators performed this test, however, the results of the reconstruction accuracy of operator 1 (O1) were previously published (Overbergh et al., 2020). The same randomized start model was provided to the operators (Figure 35A). After reconstruction, the results were compared to the CT-segmented ground truth (Figure 35B, Table 18) for each operator.

The error values for the newly trained operators (O2 and O3) were consistently higher compared to the error value of O1, who developed the method.

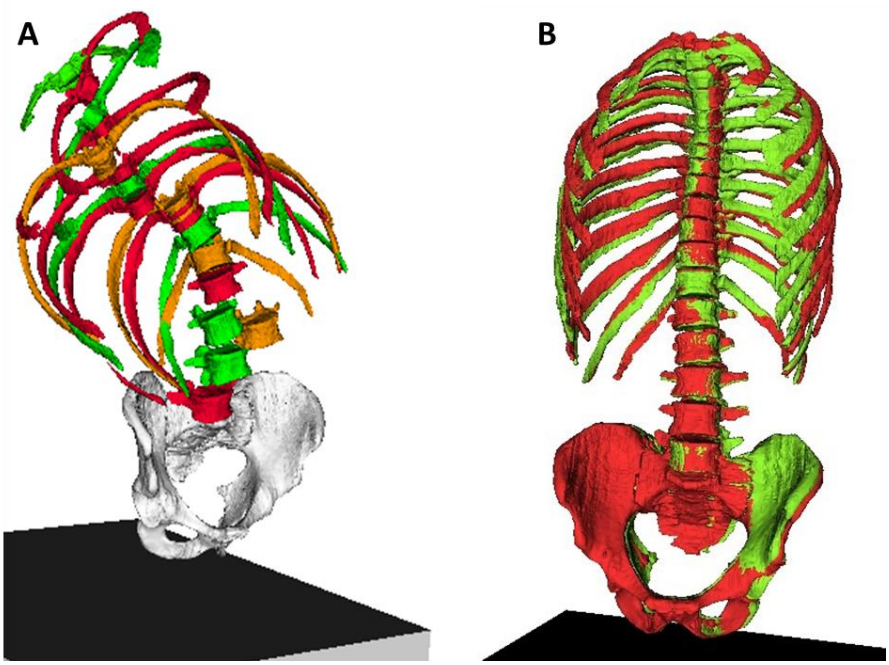

Figure 35: Illustration of (**A**) the randomized initial model of the plastinated cadaver and (**B**) the end result of the model reconstructed by operator 2 (O2, red) superimposed on the CT-segmented ground truth (green).

Table 18: The root mean square (RMS) values of the absolute (abs.) reconstruction error for each of the three operators (O1-3) (M-L = mediolateral, I-S = inferosuperior, A- P = anteroposterior).

	RMS O1 (Overbergh et al., 2020)	**RMS O2**	**RMS O3**
Abs. sagittal orientation (°)	1.19	5.00	4.72
Abs. transverse orientation (°)	1.91	3.87	3.81
Abs. coronal orientation (°)	0.76	2.21	4.47
3D distance (mm)	1.26	6.03	4.33
Abs. M-L position (mm)	0.51	2.82	3.21
Abs. I-S position (mm)	0.89	4.42	1.88
Abs. A-P position (mm)	0.87	2.97	2.23

Appendix 3: Distributions of the variability on the operator-dependent model parameters

The Shapiro-Wilk test was used to test the normality of the parameters (position and orientation) of the model components (markers, bodies, joints), which indicated non-normal distributions of the variability in virtual marker position (Table 19) at the 0.05 significance level (SPSS 26, IBM). Also for the body positions and orientations (Table 20) and the joint positions and orientations (Table 21), the parameters did not all have a normal distribution. Thereafter, kernel functions were consistently used to estimate all distribution functions from the respective error histograms (Figure 36-Figure 38) (Distribution Fitter, MATLAB, The Mathworks Inc., MA).

1. Virtual markers

Table 19: Shapiro-Wilk test for normality on the parameters defining the markers (X: medio-lateral, Y: infero-superior, Z: antero-posterior)

	Statistic	Significance
X position	0.983	0.005
Y position	0.976	0.000
Z position	0.961	0.000

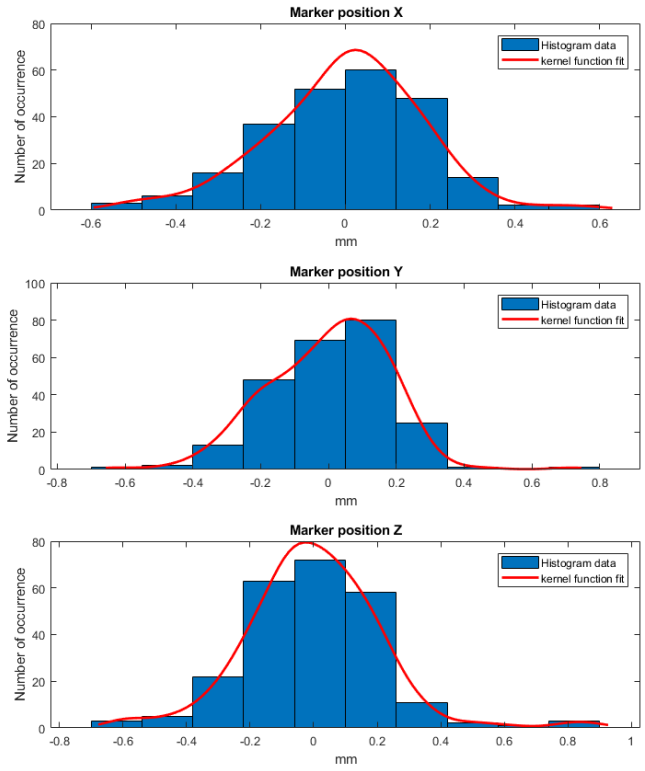

Figure 36: The histograms of the marker position differences relative to the baseline models, for each direction, with fitted kernel functions. (X: medio-lateral, Y: infero-superior, Z: antero-posterior)

2. Bodies

Table 20: Shapiro-Wilk test for normality of the parameters defining the bodies (X: medio-lateral, Y: infero-superior, Z: antero-posterior)

	Statistic	Significance
position X	0.903	0.001
position Y	0.962	0.104
position Z	0.965	0.139
orientation X	0.955	0.054
orientation Y	0.967	0.161
orientation Z	0.981	0.570

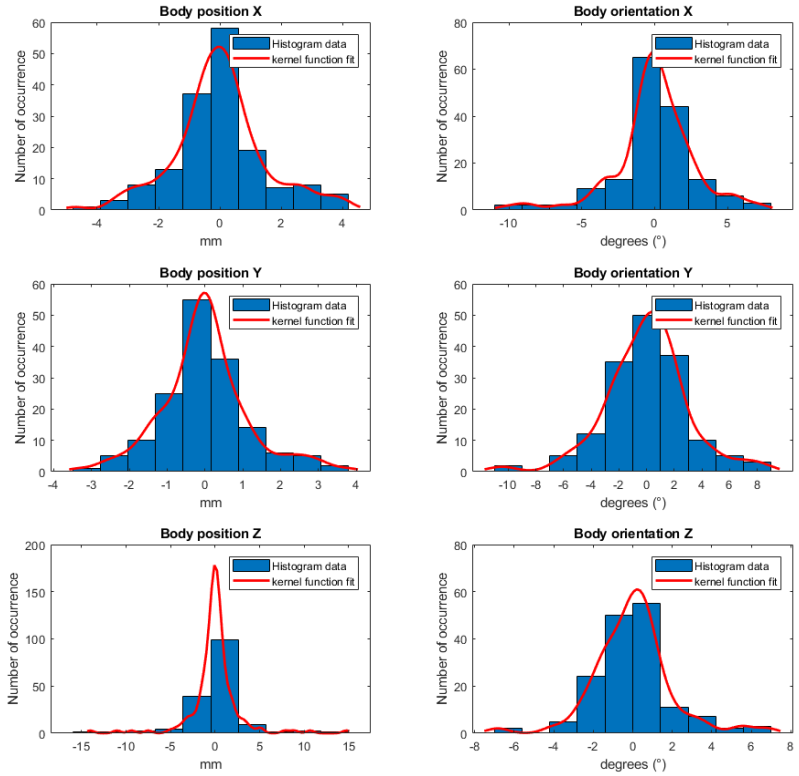

Figure 37: The histograms of the body position and orientation differences relative to the baseline models, for each direction, with fitted kernel functions. (X: medio-lateral, Y: infero-superior, Z: antero-posterior)

3. Joints

Table 21: Shapiro-Wilk test for normality on the parameters defining the joints
(X: medio-lateral, Y: infero-superior, Z: antero-posterior)

	Statistic	Significance
position X	0.977	0.010
position Y	0.736	0.000
position Z	0.834	0.000
orientation X	0.934	0.000
orientation Y	0.983	0.048
orientation Z	0.970	0.002

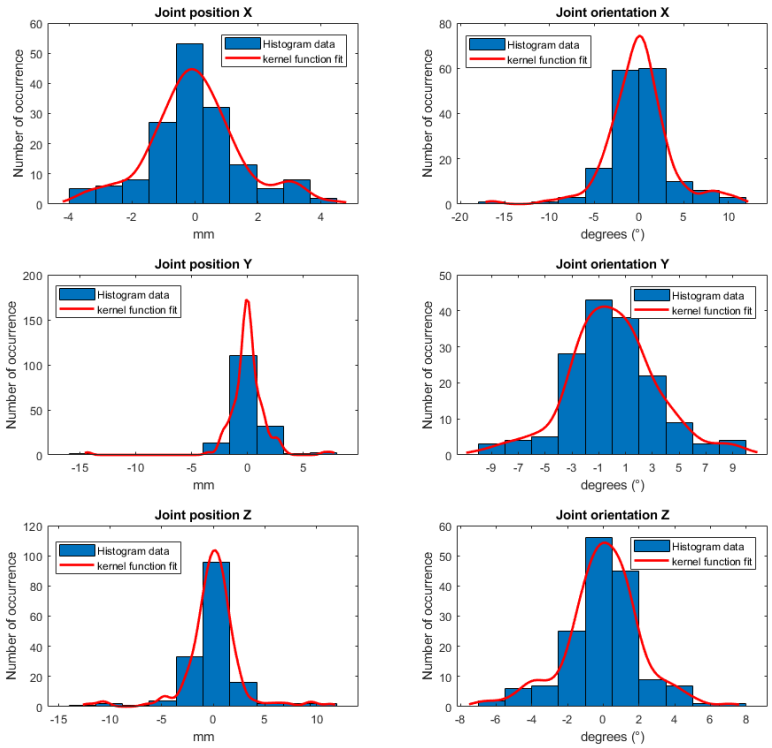

Figure 38: The histograms of the joint position and orientation differences relative to the baseline models, for each direction, with fitted kernel functions. (X: medio-lateral, Y: infero-superior, Z: antero-posterior)

Appendix 4: The Monte-Carlo probabilistic simulation

1. Stop criteria and convergence

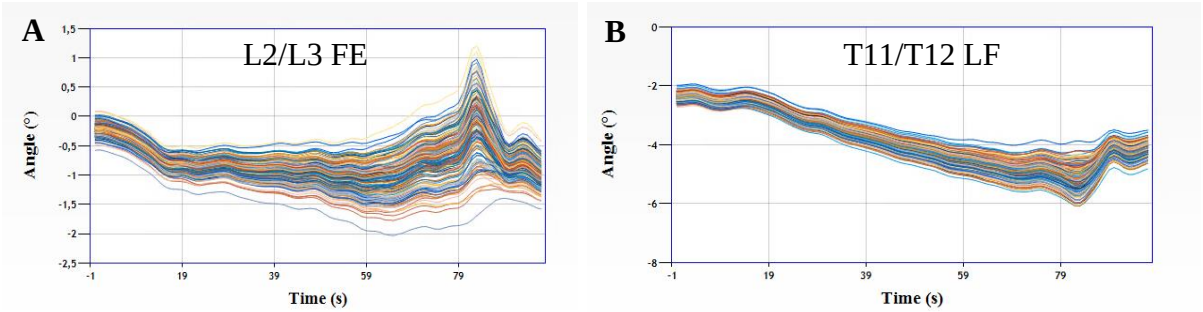

Figure 39: Illustration of 1000 intervertebral (IV) joint kinematics curves for (**A**) the L2/L3 IV joint in the flexion-extension (FE) degree of freedom (DOF) and (**B**) for the T11/T12 IV joint in the lateroflexion (LF) DOF.

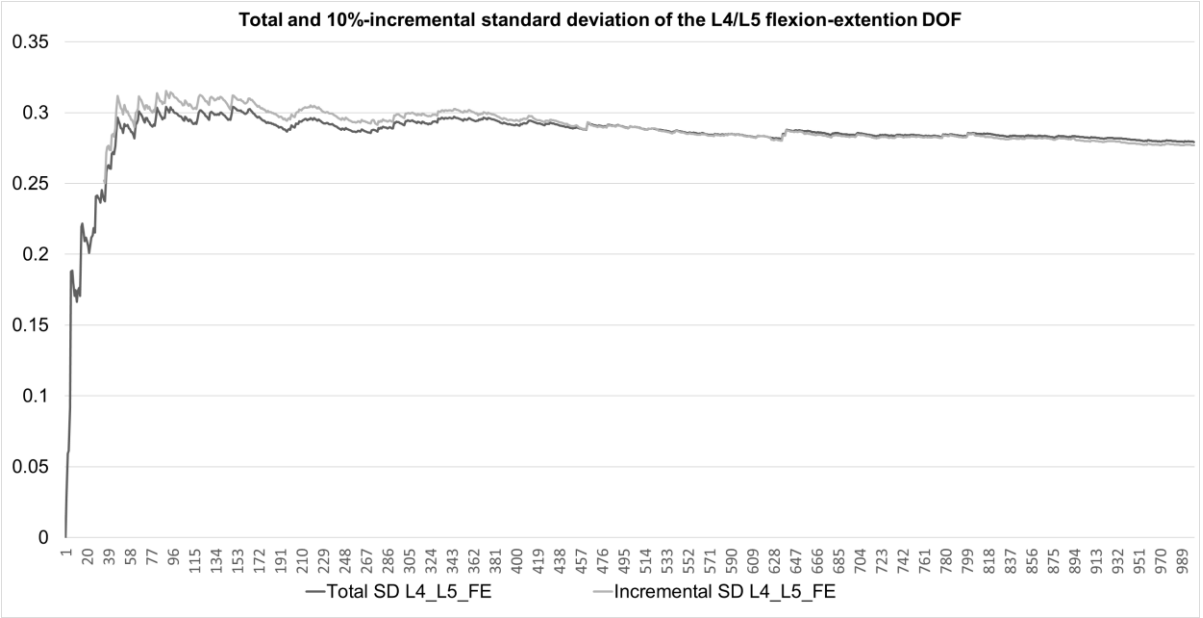

Figure 40: The total standard deviation (SD, black) at each iteration over all samples and the SD computed over the last 10% of samples (grey), up to that iteration index (x-axis). As the amount of iterations increases, the difference between the total SD and the SD over the last 10% of samples becomes smaller (see also Figure 41 for details on the instance of convergence).

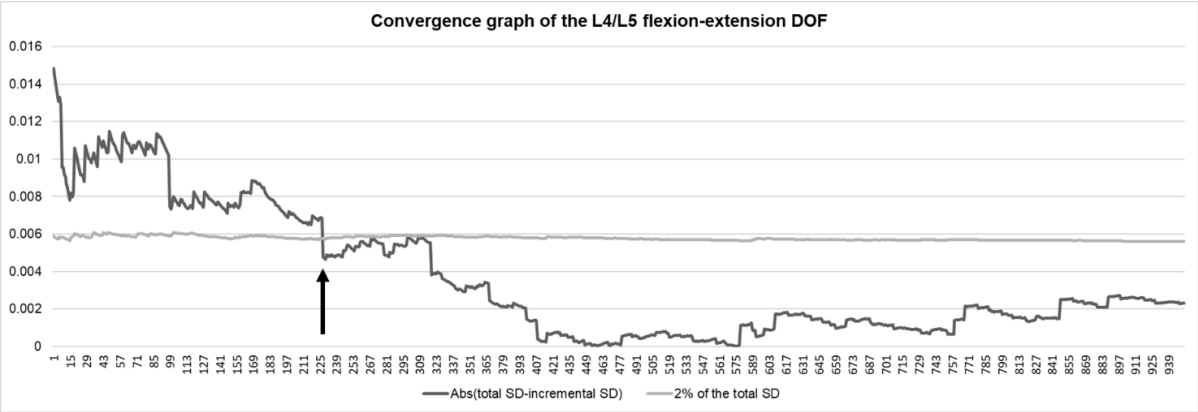

Figure 41: The absolute difference between the total standard deviation (SD) (i.e. over all iterations up to that iteration index) and the SD calculated only over the last 10% of iterations (black). 2% of the total SD calculated (grey). At about 220 iterations the L4/L5 flexion-extension joint angle converges according to the SD stop-criterion.

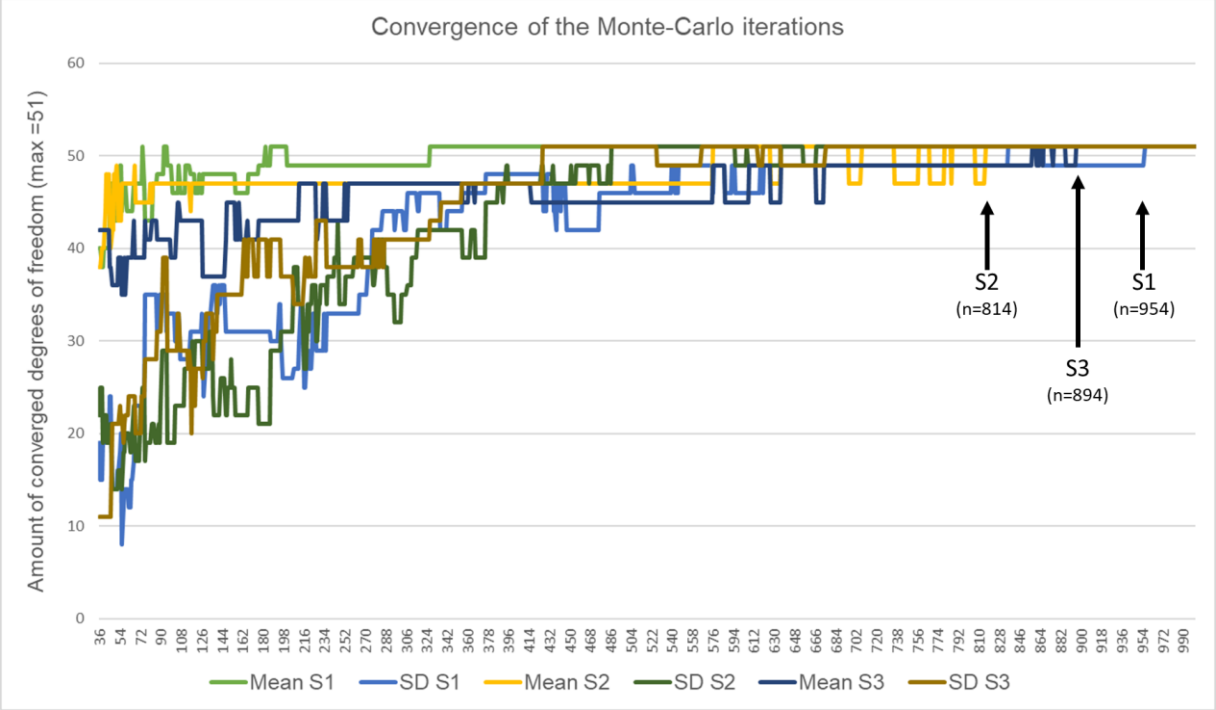

Figure 42: Convergence for Subject 1 (S1), Subject 2 (S2) and Subject 3 (S3) according to the stop criteria on the mean and standard deviation (SD). Convergence is reached at the iteration index (n) (x-axis) where both the stop criteria (i.e. mean and SD) have converged for all of the 51 degrees of freedom (y-axis) and was indicated on the graph for each subject.

Table 22: Iteration indexes at which convergence occurs according to the mean and standard deviation stop criteria. The maximal index (bold) of both criteria determines the convergence index for each subject (S1-S3).

Subject	Iteration index of convergence according to the *mean* criterion	Iteration index of convergence according to the *standard deviation* criterion
S1	325	**954**
S2	**814**	665
S3	**894**	673

2. Intervertebral joint kinematics

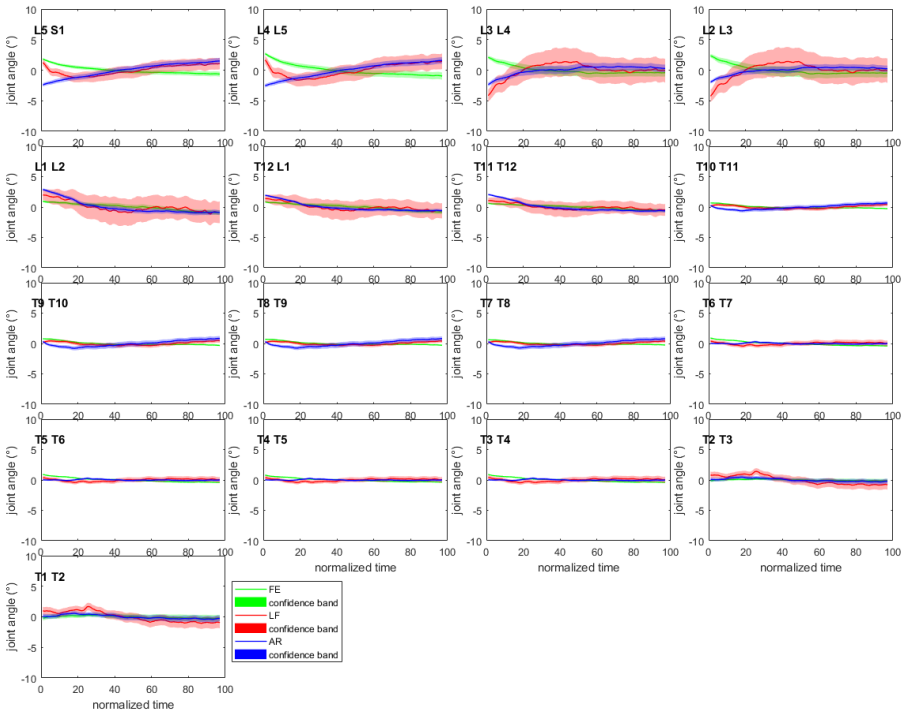

Figure 43: Confidence bands (5-95%) for each of the joint angles for subject 2 (S2). All curves have been normalized to their mean value over the length of the motion to allow visualization within the -10° to 10° joint angle range. AR: axial rotation; LF: lateroflexion; FE: flexion-extension.

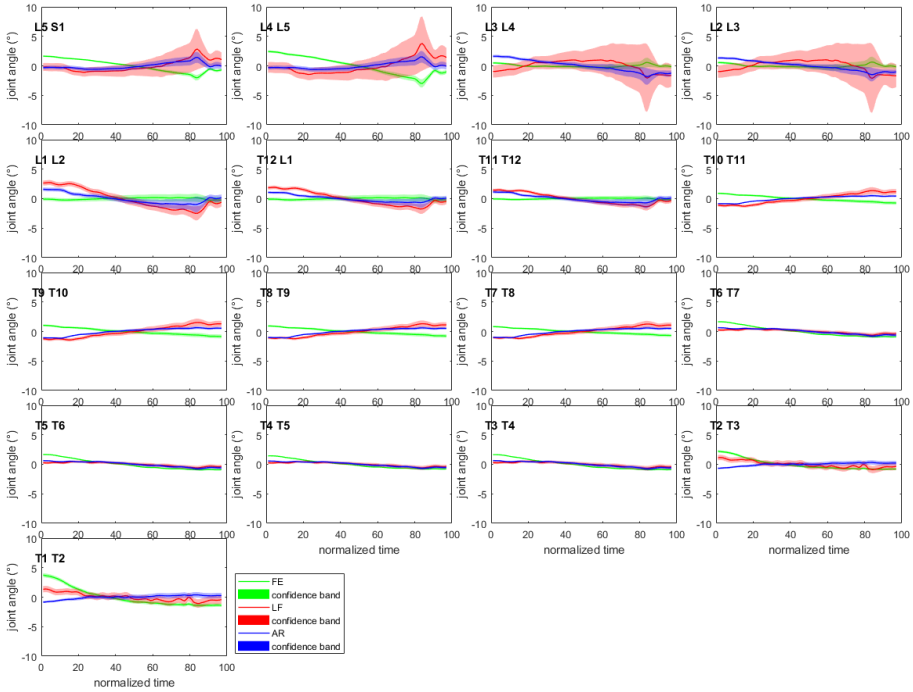

Figure 44: Confidence bands (5-95%) for each of the joint angles of subject 3 (S3). All curves have been normalized to their mean value over the length of the motion to allow visualization within the -10° to 10° joint angle range. AR: axial rotation; LF: lateroflexion; FE: flexion-extension.

Table 23: Time instance (ranging between 1 and 100) of maximal variance ($t_{\sigma=max}$) for the individual joint angles (FE: flexion-extension, LF: lateroflexion, AR: axial rotation) and subjects (S1-S3).

Degrees of freedom	**S1**	**S2**	**S3**
L5_S1_FE	97	100	87
L5_S1_LF	93	59	86
L5_S1_AR	99	100	87
L4_L5_FE	97	100	87
L4_L5_LF	93	59	86
L4_L5_AR	99	100	87
L3_L4_FE	99	51	86
L3_L4_LF	93	40	86
L3_L4_AR	99	45	86
L2_L3_FE	99	51	86
L2_L3_LF	93	40	86
L2_L3_AR	99	45	86
L1_L2_FE	91	53	86
L1_L2_LF	92	44	87
L1_L2_AR	99	84	86
T12_L1_FE	91	53	86
T12_L1_LF	92	44	87
T12_L1_AR	99	84	86
T11_T12_FE	91	53	86
T11_T12_LF	92	44	87
T11_T12_AR	99	84	86
T10_T11_FE	100	19	87
T10_T11_LF	92	44	86
T10_T11_AR	100	44	86
T9_T10_FE	100	19	87
T9_T10_LF	92	44	86
T9_T10_AR	100	44	86
T8_T9_FE	100	19	87
T8_T9_LF	92	44	86
T8_T9_AR	100	44	86
T7_T8_FE	100	19	87
T7_T8_LF	92	44	86
T7_T8_AR	100	44	86
T6_T7_FE	100	96	87
T6_T7_LF	98	97	87
T6_T7_AR	90	83	87
T5_T6_FE	100	96	87
T5_T6_LF	98	97	87
T5_T6_AR	90	83	87
T4_T5_FE	100	96	87
T4_T5_LF	98	97	87
T4_T5_AR	90	83	87
T3_T4_FE	100	96	87
T3_T4_LF	98	97	87
T3_T4_AR	90	83	87
T2_T3_FE	100	90	2
T2_T3_LF	96	98	87
T2_T3_AR	100	97	87
T1_T2_FE	100	90	2
T1_T2_LF	96	98	87
T1_T2_AR	100	97	87

Chapter 3

Relating spinal kinematics to vertebral body deformity in Adult Spinal Deformity

Abstract

An improved understanding of three-dimensional (3D) spinal kinematics can complement the current two-dimensional (2D) and predominant static assessment of adult spinal deformity (ASD) patients. More specifically, the characterization of aberrant spinal kinematics in ASD patients during daily-life motor tasks could integrate spinal kinematics in clinical decision-making to develop more targeted treatment strategies. The aim of the current study is therefore to introduce novel methods to comprehensively quantify effects of spinal deformities on spinal kinematics during forward trunk flexion, using a recently developed and validated subject-specific modeling workflow combined with 3D motion analysis. Furthermore, their relation with routinely used, clinical spino-pelvic parameters, vertebral body deformity, and self-reported health related quality of life (HRQoL) is evaluated in a pilot group of fourteen ASD subjects and one healthy subject.

The treating physician documented the static spinal alignment in fifteen subjects (14 ASD, 1 control) using radiographic spino-pelvic parameters. Thereafter the total vertebral body deformation was rated using the spinal deformity index (SDI). Each subject also completed four HRQoL surveys (Scoliosis Research Society Outcome Questionnaire, Oswestry Disability Index, Karnofsky Performance Scale index and Core Outcome Measures index). Subject-specific spino-pelvic multi-body models were then created for all subjects and related to 3D motion capture data measured during a maximal forward trunk flexion to quantify the dynamic intervertebral joint angles. First, the degree of kinematic compensation, defined as normalized out-of-plane intervertebral motion during a monoplanar motion task, i.e. forward trunk flexion, was quantified, further referred to as the spinal kinematic deviation index (SKDI). Next, the relative contribution of motion of the deformed region to the overall spinal motion was evaluated, further referred to as the spinal deformity engagement index (SDEI). Finally, correlations between the conventional (spino-pelvic parameters, SDI and HRQoL) parameters and these new parameters were investigated.

In the ASD subjects (n = 14) the SKDI during trunk flexion ranged from 0.38 to 3.18, indicating large inter-individual differences. The healthy control subject presented a SKDI of 0.27, the lowest SKDI of all subjects. The SDEI varied from 0.21 to 1.53 in the ASD subjects and was lowest in the control subject (0.10). No correlations between the SDI and SKDI (0.338, p=0.218) or the SKDI and the individual spino-pelvic or HRQoL parameters were found. However, the correlation (0.694, p=0.004) between the SDEI and the SKDI suggests that subjects that use their deformed region more (i.e. a high SDEI) to perform global trunk flexion present with more out-of-plane movement (i.e. high SKDI).

Subject-specific musculoskeletal modeling combined with 3D motion capture data allows to quantify spinal kinematic compensation strategies in ASD subjects. The relation between these spinal kinematic compensation strategies and the static alignment, vertebral deformities and HRQoL can thereafter be investigated. Our pilot results agree with the growing awareness in literature that static alignment is not the sole driver of kinematic compensation in ASD. Indeed, subjects presenting with static features of ASD (vertebral deformity and spinal alignment) do

not necessarily present dynamic kinematic compensation, rather, a motion strategy engaging the deformed region (quantified through the SDEI) seems to be a prerequisite for kinematic compensation (quantified through the SKDI). In the future, insights considering a patient's specific motion strategy based on the newly developed metrics could potentially benefit clinical management and aid in the pre-surgical evaluation towards improved functional outcome in ASD patients. However, future research on a larger number of subjects is needed to investigate the determinants of aberrant spinal motion and confirm their role in patient classification and clinical decision-making.

Introduction

Static two-dimensional (2D) radiographic image-based measurements form the basis of current quantitative diagnosis, pre-operative planning and clinical management in adult spinal deformity (ASD) (Terran et al., 2013). However, as perioperative complications (up to 52.2%) for ASD patients remain common (Smith et al., 2016), it is well recognized that these 2D static assessments alone cannot objectively quantify the full impact of spinal deformities and associated treatment on dynamic spine function during daily-life motor tasks (Diebo et al., 2018; Faraj et al., 2017). Nevertheless, degenerative spinal conditions, such as ASD, are known to be associated with aberrant kinematic behavior compared to healthy spines (Hemming et al., 2018; Quint and Wilke, 2008; Widmer et al., 2019). It is therefore mandatory to further investigate if an improved understanding of three-dimensional (3D) spinal kinematics in ASD patients has the potential to complement current 2D state-of-the-art diagnostics and clinical decision-making (Diebo et al., 2018; Widmer et al., 2019) as they provide an improved understanding of the dynamic spine function. For example, when selecting the upper and lower vertebrae for spinal fusion surgery the surgeon carefully balances achieving maximal alignment correction with mobility loss (Blondel et al., 2013; Ignasiak et al., 2018a). Hence, improved documentation of pre-operative spine kinematics and of spine fusion level thereon is a prerequisite to improve outcome and reduce the high complication rates (Widmer et al., 2019). Eventually, establishing normative, reference ranges of healthy spinal kinematics to which degenerative spinal kinematics can be compared, will be a crucial step to allow a more inclusive health disorder classification for clinical decision-making in ASD (Widmer et al., 2019).

Skin marker-based 3D motion analysis can provide 3D dynamic data (Gracovetsky et al., 1995) to estimate global spino-pelvic parameters (Severijns et al., 2020) or underlying vertebral motion (Zhang and Xiong, 2003). However, technical difficulties associated with reliably measuring full spinal kinematics with sufficient segmental accuracy using marker-based 3D motion capture during clinically-relevant dynamic functional tasks, such as trunk flexion, sit-to-stand, walking, or weight lifting (Zhang et al., 2013) hindered these advancements. This has led to a paucity on *in vivo* spinal joint kinematics in literature, even more in the highly heterogeneous ASD population. We recently developed and validated a workflow for integrating 3D motion analyses with subject-specific musculoskeletal models based on medical images (Overbergh et al., 2020). This method allows marker-driven intervertebral (IV) kinematic measurements with good accuracy (Overbergh et al., 2020) and reliability (Overbergh et al., 2021) in an ASD population.

Nevertheless, analyzing and interpreting 3D spine kinematics during dynamic movements remains complex due to the interdependence of motions across IV joints and planes of movement (Preuss and Popovic, 2010; Widmer et al., 2019). In other words, motion of one IV joint in a given plane can affect motion at adjacent and/or remote IV joints in other planes. Therefore, it is clear that metrics that summarize the complex kinematic spine behavior, while taking into account the coupling of spine motion, are needed to better understand 3D spinal kinematics in ASD patients (Diebo et al., 2018). Furthermore, such method should provide an accurate but comprehensive assessment of 3D spinal kinematics that is easily interpretable by

clinicians to allow functional profiling of ASD patients by complementing associations between health disorder, treatment characteristics with specific spinal kinematic patterns during functional movements. For subjects suffering from gait dysfunction, comprehensive kinematic measures already exist that provide an overall profile of gait quality while allowing successful classification of disease severity (e.g. the Gait Deviation Index (Rosenlund et al., 2016)). However, to the author's knowledge, no such comprehensive measures exist for describing pathologic spine kinematics.

The aim of the current study is to introduce novel comprehensive metrics that provide an overview of spine kinematics during dynamic movements, based on a recently developed and validated multi-body modeling workflow combined with 3D motion analysis (Overbergh et al., 2020). Furthermore, we aim to apply these measures during a forward maximal trunk flexion in a pilot group of ASD subjects and one healthy subject to document the effect of spinal deformities on dynamic spine function. Furthermore, we will explore their added value as functional biomarker for classifying ASD subjects by evaluating their relation to commonly used clinical parameters quantifying spino-pelvic malalignment, vertebral body deformity, and self-reported health related quality of life (HRQoL), thus evaluating the potential complementarity of dynamic and static metrics in ASD.

Materials and methods

Participants and data collection

Fourteen subjects with varying degrees of spinal deformity and one control subject, with non-pathological spinal alignment, were recruited (ASD: mean age= 62.27 ± 7.47 years (10 females, 4 males), control: 61.5 years (female)), after having obtained ethical approval and informed consent (S58082, study conducted in accordance with the declaration of Helsinki). The following exclusion criteria were applied: inability to walk 50 meters independently, lower limb musculoskeletal disorder, neurological disease or a history of spinal instrumentation surgery. HRQoL scores were collected at the start of the measurement using four patient reported outcome measures (PROMs), namely the Scoliosis Research Society Outcome Questionnaire (SRS-22r) (Asher et al., 2003), Oswestry Disability Index (ODI) (Fairbank and Pynsent, 2000), The Karnofsky Performance Scale (KPS) index (Mor et al., 1984) and Core Outcome Measures Index (COMI) (Mannion et al., 2016).

All subjects underwent computed tomography (CT) imaging from T1 to pelvis (BrightSpeed by GE Healthcare, with an inter-slice distance of 1.25 mm and a pixel size of 0.39x0.39 mm). Based hereon, the severity of vertebral body deformity was quantified by combining a previously published semi-quantitative (SQ) grading system for vertebral body deformities (Genant et al., 1993) and the spinal deformity index (SDI), a measure that sums the SQ grades of each vertebra over the thoracic and lumbar spine (Crans et al., 2005). Thereto, an experienced investigator first generated 3D objects of each vertebra of the thoracic and lumbar spine (T1-L5) by segmenting each subject's CT images (Mimics 21, Materialise NV, Belgium). Next, based on (Genant et al., 1993), a score was assigned based on the reduction in the anterior, middle, or posterior vertebral body height: 0 (normal, no height reduction), 0.5

(uncertain or questionable vertebra), 1 (mild, 20-25% height reduction), 2 (moderate, 25-40% height reduction) and 3 (severe, >40% height reduction). Although the SQ grading system is originally defined for sagittal images only, we modified the method as such that vertebral deformation were first individually graded in the sagittal and coronal anatomical planes, whereafter the largest value of both was retained (Figure 45). Finally, the SDI was obtained by summing the SQ grading of all thoracic and lumbar vertebrae, i.e. T1 to L5 (Crans et al., 2005).

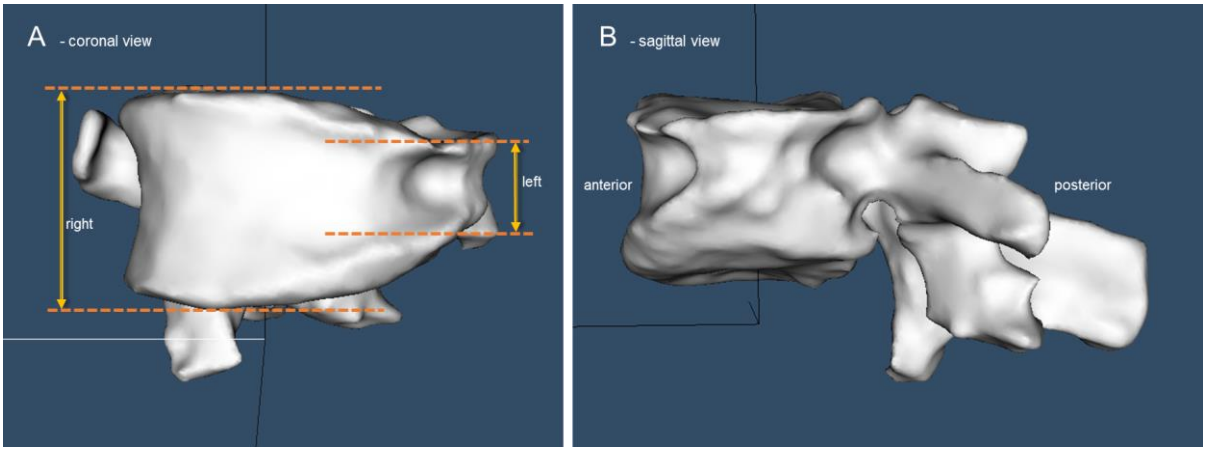

Figure 45: Illustration of the SQ grading of vertebral deformity for the L3 vertebra of a participating ASD subject. After analyzing both the coronal (**A**) and the sagittal (**B**) plane, a score of 3 (i.e. severe) was assigned based on the estimated height reduction (>40%) in the coronal plane.

An experienced physiotherapist then instrumented each subject with 27 reflective skin markers according to the full-spine marker protocol described in (Overbergh et al., 2020). With the markers attached, a pair of full-body x-ray images was acquired using a biplanar radiography system (EOS, EOS Imaging, Paris, France) while the subject adopted the Scoliosis Research Society free-standing position (fingers-on-clavicle position, Figure 46A) (Horton et al., 2005; M. Y. Wang et al., 2014). Based on these biplanar radiographic images, the spinal alignment of each patient was quantified by the treating physician using the following clinically used spino-pelvic parameters: pelvic incidence (PI), pelvic tilt (PT), lumbar lordosis (LL), thoracic kyphosis (TK), sagittal vertical axis (SVA), pelvic incidence minus lumbar lordosis (PI-LL), T1 spino-pelvic inclination (T1-SPI), T1 pelvic angle (TPA) and global sagittal axis (GSA) (Schwab et al., 2012).

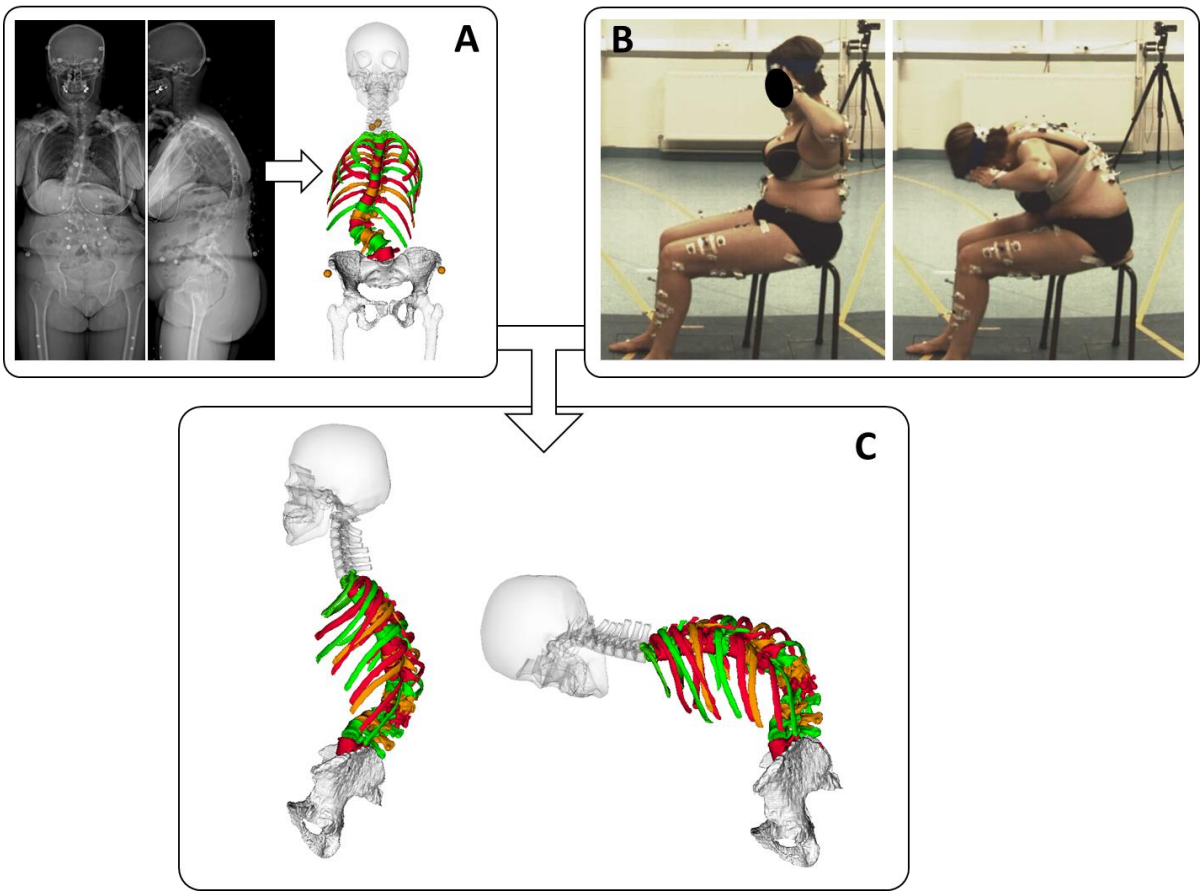

Figure 46: (**A**) Using the modeling workflow of Overbergh et al. (2020) a subject-specific spino-pelvic model was created for each subject. (**B**) Reflective markers were attached to the subject's skin according to the protocol described in Overbergh et al. (2020). Thereafter the trajectories of those markers were recorded during a voluntary maximal forward trunk flexion in a seated position. (**C**) Through combination of the created model and the recorded marker trajectories, IV joint kinematics of the thoracic and lumbar spine were measured using the inverse kinematics algorithm of OpenSim 3.3 (S. L. Delp et al., 2007).

Kinematic evaluation

Thereafter, the trajectories of the reflective markers were recorded (100 Hz) using a 10-camera Vicon system (VICON Motion systems, Oxford Metrics, UK) while the subjects performed a maximal forward trunk flexion from a comfortable upright seated position (Figure 46B). The subjects were instructed to maintain both hands on their head during task execution to avoid obstructing the visibility of the pelvis markers. This trunk flexion motion was chosen as it is representative of functional daily life activities such as putting on shoes or picking up an object from the floor while being seated.

To calculate IV joint kinematics, a subject-specific, marker-driven spino-pelvic kinematic model was created for each subject using a validated workflow (Overbergh, 2020). Based on individually CT-segmented bone geometries combined with full-body biplanar radiographic images (Figure 46A), the relation between the skin markers and the underlying anatomy was defined. These models each comprised of twelve thoracic vertebrae, five lumbar vertebrae and

a sacrum, connected by eighteen spherical joints, thereby only allowing rotational degrees of freedom (DOFs) at the IV joints. The sacrum was rigidly attached to the pelvis; the latter being connected to the ground reference with six DOFs. The 3D marker trajectories were labeled in Vicon Nexus (Version 2.11), cropped to include 0.5 seconds before onset and end of the motion and low-pass Butterworth filtered (6Hz), before being imported in OpenSim 3.3 (OpenSim, Stanford, USA) (S. L. Delp et al., 2007), using a custom MATLAB (The Mathworks Inc., MA) script. IV joint kinematics were then estimated using inverse kinematics (Lu and O'Connor, 1999) (Figure 46C), and time normalized to 100 frames, before being filtered using a three-frame moving average window to further reduce noise.

Spinal kinematic measures

1. Range of motion

As a first kinematic measure, the global trunk range of motion (ROM) during forward flexion was estimated. To this end, the calculation of the T1 spino-pelvic inclination, a 2D sagittal radiographic parameter (T1-SPI, Figure 47A), was modified for use with a 3D model (detailed in Appendix 1): throughout the forward trunk flexion, the sagittal and coronal T1-SPI were calculated at each time instance as the angle between the line connecting the mid-point between both pelvic acetabular centers and the T1 vertebral body center), and the vertical line (i.e. perpendicular to the ground) (Figure 47B). This angle was projected in the subject's sagittal and coronal anatomical planes, defined by the acetabular center axis (Figure 47C). The absolute difference between the initial and final values of the sagittal T1-SPI was calculated, i.e. the sagittal T1-SPI ROM representing the global trunk ROM in the sagittal plane. Similarly, the coronal T1-SPI ROM was calculated, quantifying the out-of-plane motion during the global forward flexion motion. To evaluate if the motion was primarily performed in the sagittal plane, the ratio of the coronal T1-SPI ROM to the sagittal T1-SPI ROM was calculated. It is important to note that these are global measures that do not consider motion of individual (or *local*) spinal segments (Figure 47C), rather they evaluate *global* spinal motion as the relative position of the T1 vertebrae to the pelvis.

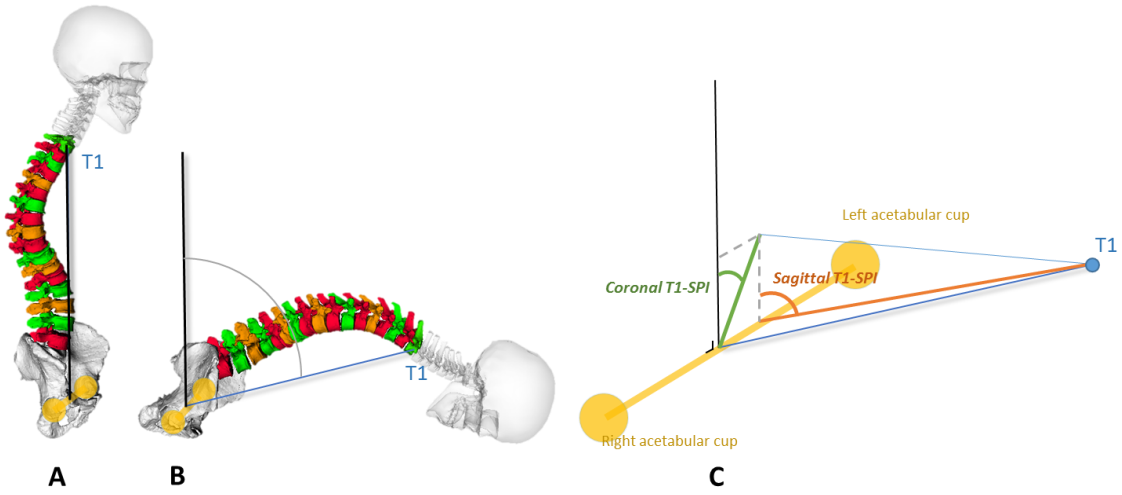

Figure 47: Illustration of the model-based T1 spino-pelvic inclination (T1-SPI) angle as a global measure for the range of motion (ROM) of a forward trunk flexion motion. (**A**) The initial upright position. (**B**) The final position (maximal forward trunk flexion). (**C**) The sagittal and coronal T1 spino-pelvic inclination angle, expressed in the pelvic reference frame.

2. Out-of-plane intervertebral motion

As a second kinematic measure, we quantified the relative out-of-plane range of motion of individual vertebrae, i.e. axial rotation and/or lateroflexion, during the performed monoplanar (or single-plane) motor task, i.e. maximal forward flexion movement. We refer to this measure as the spinal kinematic deviation index (SKDI, Equation (1)):

$$SKDI = \frac{(\mathrm{ROM}_{\mathrm{S1,total}})^2 + (\mathrm{ROM}_{\mathrm{S2,total}})^2}{\mathrm{ROM}_{\mathrm{P,\ total}} \times (\mathrm{ROM}_{\mathrm{S1,\ total}} + \mathrm{ROM}_{\mathrm{S2,\ total}})} \quad (1)$$

where *S1* and *S2* correspond to secondary planes of motion (*S1* and *S2* are interchangeable) and *P* corresponds to the primary plane where motion occurs. $ROM_{X,total}$ represents the total range of motion for a plane *'X'*, summed over all IV joints of the thoracic and lumbar spine (T1-sacrum) (detailed in Appendix 2). This measure thus quantifies the relative amount of kinematic compensation to perform a global single-plane trunk flexion. Herewith, a high SKDI indicates more kinematic coupling, i.e. a large portion of motion in the secondary planes instead of the primary plane, and can be interpreted as a measure of aberrant kinematic motion or compensation in the ASD subject. A theoretical SKDI of 0 indicates a perfectly performed single-plane trunk motion without any coupled motion in the secondary planes.

As an extension to previously published work (Overbergh et al., 2021) where the reliability of spinal kinematics from marker-driven subject-specific ASD models was evaluated, the reliability of the SKDI parameter was similarly assessed. We performed reliability analyses, focusing on in-between session reliability (using four ASD and one control subject over an average time interval of two weeks) and the sensitivity of inter-operator variability in creating subject-

specific models (using three ASD subjects and three trained operators) on the SKDI parameter. For more details the reader is referred to Appendix 3.

3. Deformity-weighted intervertebral mobility

As a third kinematic measure, we evaluated the relative contribution of ROM observed in joints connecting deformed vertebral bodies to the overall spine motion. Vertebral body deformation is quantified using the SQ grading system (Genant et al., 1993). To calculate this third kinematic measure, further referred to as the spinal deformity engagement index (SDEI), the ROM of the IV joint angles is first summed over all three DOFs of individual IV joints:

$$\mathrm{ROM}_{\mathrm{FE,IV\ joint}} + \mathrm{ROM}_{\mathrm{LB,IV\ joint}} + \mathrm{ROM}_{\mathrm{AR,IV\ joint}}. \tag{2}$$

Next, this multi-planar ROM is summed over all IV joints to obtain the overall spinal ROM:

$$\sum_{i=\mathrm{L5/S}}^{T1/T2}(\mathit{ROM}_{\mathrm{FE},i} + \mathit{ROM}_{\mathrm{LF},i} + \mathit{ROM}_{\mathrm{AR},i}). \tag{3}$$

Then we defined the relative contribution of individual IV joints as the ratio of the multi-planar ROM at the individual joint level to the overall multi-planar spinal ROM (detailed in Figure 48). Finally, to account for the severity of the vertebral body deformities on joint mobility at each IV joint, the above relative multi-planar mobility is weighted by the average SQ grading (g in Figure 48) of the vertebrae adjacent to the specific joint. We then sum the *local* index of engaged deformity at each joint, (i.e. the local SDEI) over all joints of the entire thoracic and lumbar spine (Figure 48).

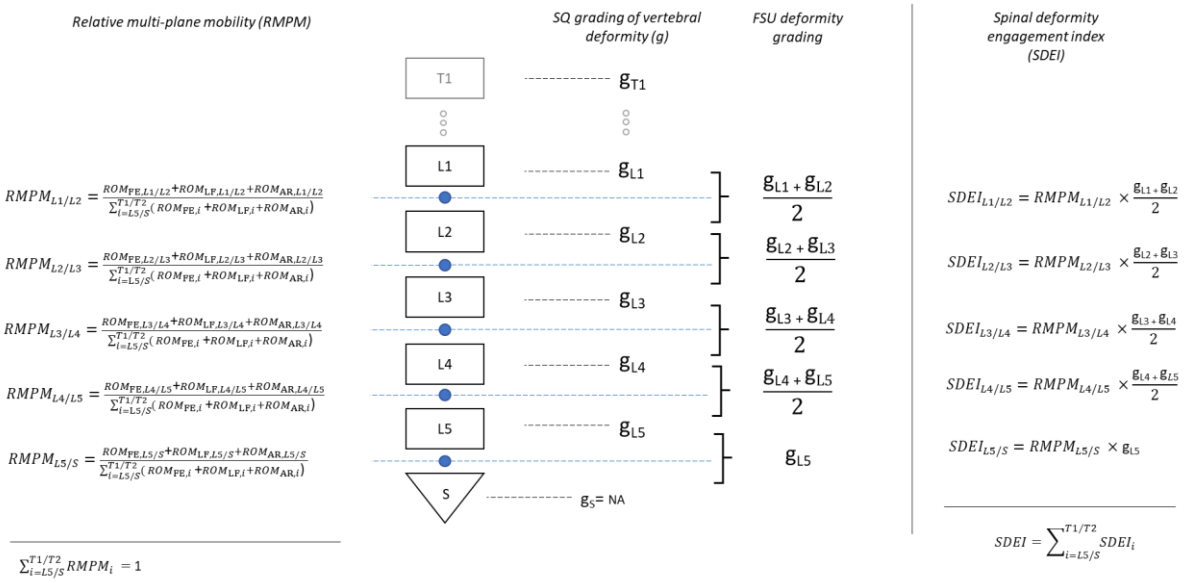

Figure 48: Schematics for the calculation of the spinal deformity engagement index (SDEI). FSU: functional spinal unit; ROM: range of motion; FE: flexion-extension; LF: lateroflexion; AR: axial rotation; g: semi-quantitative (SQ) grading value of vertebral body deformity; S: sacrum.

This measure thus quantifies the relative contribution of joints composed of deformed vertebrae to the overall ROM during a given motor task. Herewith, a high SDEI indicates a high relative amount of motion occurring at joints involving deformed vertebrae, i.e. a high *engagement* of the deformed region in the motions.

Statistical analyses

To investigate the relation between static vertebral body deformity (SDI) and the dynamic engagement of the vertebral body deformity (SDEI) with kinematic compensation (SKDI), we determined Pearson correlation coefficients (two-tailed) between (1) the SDI and the SKDI, and (2) the SDEI and the SKDI, respectively. To investigate if there was a relation between the kinematic compensation and out-of-plane motion or the static spinal malalignment, respectively, we additionally evaluated the correlation between (3) the SKDI and the coronal T1-SPI ROM and (4) the SKDI and the conventional radiographic parameters. Lastly, (5) to investigate a relation between spinal kinematic compensation and self-perceived quality of life, the correlation between the SKDI and the outcome measures of the HRQoL-questionnaires was evaluated. Pearson correlations were determined using SPSS Statistics 26 (IBM Corp. Armonk, NY, USA) and a significance level set at 0.05.

Results

Subject characteristics: HRQoL, radiographic evaluation and SDI

HRQoL scores are displayed in Table 24. The conventional radiographic description of the static spinal alignment can be found in Table 25. The SDI, representing the subject's total vertebral body deformation, ranged between 3 and 15 in the ASD subjects (details are shown in Table 27). The control subject, not presenting with spinal malalignment, had a SDI of 0.5 originating from a – as described by (Genant et al., 1993) - *questionable* height reduction of the L5 vertebra.

Table 24: Summarizing outcome scores of the HRQoL questionnaires: Scoliosis Research Society Outcome Questionnaire (SRS-22r), Oswestry Disability Index (ODI), The Karnofsky Performance Scale (KPS) index and Core Outcome Measures Index (COMI).

Subject	SRS-22r	ODI	KPS	COMI
control	4.05	0.00	0.90	1.50
1	3.32	36.00	0.70	5.15
2	2.73	44.00	0.80	8.10
3	3.14	36.00	0.80	5.35
4	3.73	0.00	0.90	2.00
5	1.55	66.00	0.60	8.50
6	4.46	10.00	0.90	0.20
7	2.18	46.00	0.70	8.60
8	2.68	60.00	0.70	8.10
9	3.36	18.00	0.90	1.30
10	2.64	32.00	0.70	5.00
11	2.59	60.00	0.80	7.60
12	4.46	0.00	0.90	0.00
13	3.18	36.00	0.80	5.80
14	3.59	18.00	0.80	5.20

Table 25: Radiographic parameterization performed by the treating physician on the biplanar radiographic images. PI: pelvic incidence; PT: pelvic tilt; PI-LL: pelvic incidence minus lumbar lordosis; LL: lumbar lordosis; TK: thoracic kyphosis; T1-SPI: T1 spino-pelvic inclination; GSA: global sagittal axis, SVA: sagittal vertical axis; TPA: T1 pelvic angle.

Subject	PI (°)	PT (°)	PI-LL (°)	LL (°)	TK (°)	T1-SPI (°)	GSA (°)	SVA (mm)	TPA (°)	Cobb (°)
control	58.9	15.9	-10.3	69.2	54.8	-5.7	0.2	1.1	10.2	0.0
1	57.5	17.2	6.4	51.1	43.1	-3	2.0	16.1	14.2	35.6
2	47.5	35.3	14.6	32.9	64.5	8.4	3.3	9.0	27.4	39.1
3	40.2	10.5	1.2	39.0	20.9	1.7	1.5	28	11.3	61.9
4	54.0	18.7	-3.3	57.3	48.6	-8.2	0.0	-14	10.5	43.1
5	53.6	31.1	40.6	13.0	-13	-7.2	1.9	5.6	23.9	32.4
6	53.9	16.5	13.1	40.8	48.1	5.6	7.0	97.6	22.1	35.6
7	62.8	21.9	6.1	56.7	40.7	-3.9	4.2	25.1	18	59.3
8	51.7	10.6	3.3	48.4	49.3	4.8	5.5	70.5	15.4	68.4
9	66.3	31.8	19.3	47.0	39.9	-5.1	6.4	38.0	26.7	86.9
10	39.7	12.0	-4.9	44.6	51.6	0.2	2.5	44.0	12.2	29.5
11	40.0	29.4	19.4	20.6	59.1	-7.1	3.5	39.3	22.3	23.3
12	93.3	48.1	26.2	67.1	41.5	-6.5	3.6	34.3	41.6	68.5
13	59.9	28.8	34.4	25.5	21.8	1.3	10.6	91.6	30.1	65.2
14	60.7	16.5	-12.1	72.8	56.1	-4.2	1.2	11.8	12.3	66.8

Kinematic measures

The sagittal and coronal T1-SPI ROMs for all subjects are listed in Table 26. The global trunk range of motion expressed as the sagittal T1-SPI ROM was 79.62° for the control subject, while it ranged from 43.52° to 79.00° for the ASD subjects, with a mean value (standard deviation, SD) of 64.94° (8.75°). The coronal T1-SPI ROM was 5.84° for the control subject and ranged from 0.13° to 21.61° for the ASD subjects, with a mean value (SD) of 8.53° (6.07°). The mean ratio of the coronal to the sagittal T1-SPI ROM was 13.2%, ranging from 0.2% to 31%.

Table 26: Global trunk flexion range of motion (ROM) expressed using the T1-SPI angle in the sagittal and coronal plane. The Shapiro-Wilk tests indicated normal distributions for both parameters.

Subject	Sagittal T1-SPI ROM (°)	Coronal T1-SPI ROM (°)
control	79.62	5.84
1	54.60	17.39
2	67.07	3.20
3	67.48	9.79
4	73.07	14.86
5	79.00	7.55
6	63.30	5.44
7	69.61	3.51
8	43.52	6.39
9	63.93	7.68
10	59.87	0.13
11	76.10	0.23
12	65.13	9.25
13	68.24	12.34
14	58.18	21.61
Mean ASD (SD)	64.94 (8.75)	8.53 (6.07)
Min ASD	43.52	0.13
Max ASD	79.00	21.61

The SKDI and the SDEI values for each subject are shown in Figure 49 and Table 27. The lowest SKDI and SDEI (0.27 and 0.10, respectively) were noted for the control subject.

Table 27: The spinal deformity index (SDI), the spinal kinematic deviation index (SKDI) and the spinal deformity engagement index (SDEI).

Subject	SDI	SKDI	SDEI
control	0.5	0.27	0.10
1	3.0	0.51	0.21
2	4.0	1.01	0.28
3	6.0	1.19	0.48
4	6.5	0.38	0.95
5	7.5	0.54	0.67
6	8.0	0.60	0.51
7	8.5	0.83	0.50
8	9.0	1.12	1.01
9	10.5	0.80	0.61
10	11.0	0.39	0.53
11	11.0	3.18	1.53
12	13.5	0.99	0.93
13	14.0	0.98	0.99
14	15.0	1.03	1.01
Mean ASD (SD)	9.11 (3.50)	0.97 (0.67)	0.73 (0.34)
Min ASD	3.0	0.38	0.21
Max ASD	15.0	3.18	1.53

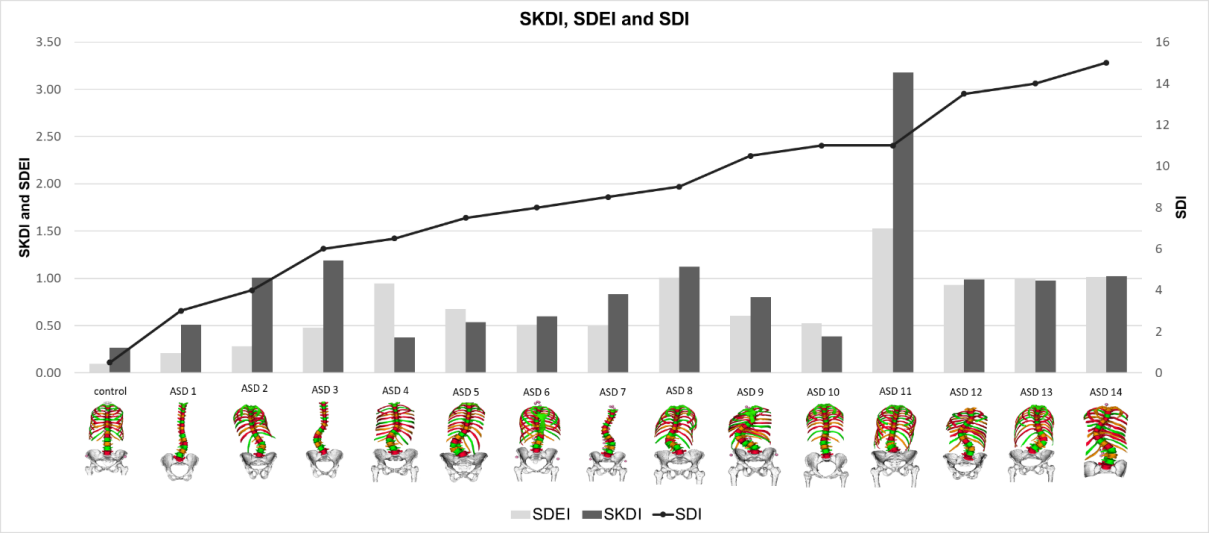

Figure 49: Illustration of the spinal deformity engagement index (SDEI), spinal kinematic deviation index (SKDI), and spinal deformity index (SDI) of all subjects sorted by increasing SDI with their corresponding 3D subject-specific model used for the marker-driven simulation of motion.

Correlations

No significant correlations were found between the SDI and SKDI (0.338, p=0.218) (Table 28). A significant correlation was found between the SDEI and the SKDI (0.694, p=0.004). No significant correlations were found between the sagittal and coronal T1-SPI ROM and the SKDI (Table 28). Finally, the correlations between the SKDI and each of the conventional radiographic and HRQoL outcome parameters are shown in Table 29 and Table 30, respectively. At the 0.05 significance level, no significant correlations were found.

Table 28: Table of the Pearson correlation coefficients (significance) for the spinal kinematic deviation index (SKDI), spinal deformity engagement index (SDEI), spinal deformity index (SDI) and sagittal and coronal components of the range of motion of the T1-spino-pelvic inclination (T1-SPI ROM) angle. (significance level: 0.05)

	Spinal deformity index (SDI)	Spinal deformity engagement index (SDEI)	Sagittal T1-SPI ROM (°)	Coronal T1-SPI ROM (°)
Spinal kinematic deviation index (SKDI)	0.338 (0.218)	0.694 (**0.004**)	0.099 (0.727)	-0.281 (0.310)
Spinal deformity engagement index (SDEI)			-0.029 (0.918)	-0.055 (0.847)

Table 29: Pearson correlation (significance) of the SKDI with each of the spino-pelvic radiographic parameters. (significance level: 0.05) SKDI: spinal kinematic deviation index; PI: pelvic incidence; PT: pelvic tilt; PI-LL: pelvic incidence minus lumbar lordosis; LL: lumbar lordosis; TK: thoracic kyphosis; T1-SPI: T1 spino-pelvic inclination; GSA: global sagittal axis, SVA: sagittal vertical axis; TPA: T1 pelvic angle.

	(°)	PT (°)	PI-LL (°)	LL (°)	TK (°)	T1-SPI (°)	GSA (°)	SVA (mm)	TPA (°)	Cobb (°)
SKDI	-0.247 (0.374)	0.233 (0.403)	0.228 (0.415)	-0.387 (0.154)	0.205 (0.454)	-0.068 (0.809)	0.156 (0.578)	0.182 (0.516)	0.219 (0.432)	0.041 (0.886)

Table 30: Pearson correlation (significance) of the SKDI with each of the outcome parameters of the HRQoL-questionnaires.

	SRS-22r	ODI	KPS	COMI
SKDI	-0.215 (0.441)	0.454 (0.089)	0.003 (0.990)	0.359 (0.217)

Discussion

The primary aim of this study was to introduce novel comprehensive methods that allow to quantify the effect of spinal deformities on spinal kinematics of dynamic motor tasks.

To evaluate global spine ROM, the model-based T1-SPI was introduced. This first parameter was defined as a 3D equivalent to the routine clinically used radiographic 2D version to facilitate clinical interpretation (Appendix 1). The trunk flexion ROM, expressed using the sagittal component of the T1-SPI, indicated that all subjects were able to reach a global trunk flexion of at least 43.52° (mean ASD subjects: 64.94°, control subject: 79.62°). The mean coronal T1-SPI ROM for the ASD subjects was 8.53° (control: 5.84°) and their mean coronal to sagittal T1-SPI ROM ratio was approximately 13% (control: 7.3%). On average the subjects thus performed the forward trunk flexion primarily in the sagittal plane, satisfying the single-plane assumption of the forward flexion motion and prerequisite for the further analyses (specifically for the SKDI).

Indeed, as a second parameter the SKDI evaluates the local IV joint kinematic compensation mechanisms (both lateroflexion and axial rotation) specifically during a monoplanar trunk flexion. In the ASD subjects the SKDI during trunk flexion ranged from 0.38 to 3.18 (Table 27), indicating large inter-individual differences. The healthy control subject had a SKDI of 0.27 (Figure 49), being -as expected- the lowest SKDI of all subjects. This gives a first indication of its construct validity. Furthermore, these calculations of the SKDI demonstrated a high between-session and inter-operator reliability (ICC= 0.862 and 95%CI= 0.0053 as described in Appendix 3 on page 130), respectively. No significant correlations were found between the SKDI and each of the static radiographic parameters of spinal alignment (Table 29), suggesting that current clinical static radiographic quantification methods are not representative of the dynamic IV joint kinematics during functional movements. However, this finding needs to be interpreted with the small and very heterogeneous population of the current study. Furthermore, the large set of radiographic parameters each quantify isolated features (e.g. lumbar/thoracic region, sagittal/coronal plane, spinal/pelvic angles) of the spinal malalignment. Therefore, future research is needed to confirm this statement. Secondly, no relation was found between the SKDI parameter and HRQoL in this pilot cohort, although abnormal coupling patterns have already been suggested to be a clinical indicator for low-back problems (Panjabi et al., 1989). Thirdly, no correlations were found between the overall deformation of the vertebral bodies, i.e. the SDI, and the SKDI. Contrary to the radiographic spino-pelvic parameters quantifying spinal *malalignment*, the SDI rather quantifies the *deformation* of the individual vertebral bodies composing the spine. As such, the absence of any correlation indicates that subjects with a higher (lower) total vertebral body deformation (severity and/or amount of vertebral body deformities), are not necessarily presenting with more (less) kinematic compensation. In conclusion, the overall low correlations with the SKDI indicate that static spinal malalignment nor vertebral deformation are the sole determinants of the amount of spinal kinematic compensation. This illustrates the complementarity of dynamic and static metrics in ASD and further supports the need for future research on the added value

of the dynamic, model-based parameters in the clinical evaluation and decision-making of ASD patients.

The SDEI was introduced as a third kinematic measure in this study, with the specific aim of quantifying the relative amount of motion present at IV joints composed of deformed vertebrae. Indeed, during surgical planning, information regarding the involvement of specific, to-be-fused regions seems to be highly relevant as it potentially may lead to insights reducing fusion instrumentation lengths in favor of the patient's global spine mobility, or alternatively increasing the fusion length to avoid complications and inevitable revision surgery to extend the fusion (Blondel et al., 2013; Diebo et al., 2018; Ignasiak et al., 2018a). Because the SDEI by definition sums IV motions over all planes of motion, its calculation does not strictly require a single-plane trunk motion. Contrary to the SKDI where IV motions are separated by plane, the SDEI could thus conceptually be applied to any motion task. The SDEI varied from 0.21 to 1.53 in the ASD subjects and was lowest in the control subject (0.10), again giving a first indication of its construct validity. Interestingly, further analysis indicated that subjects utilizing (or *engaging*) their deformed region (i.e. a high SDEI) are more likely to use more kinematic compensation (i.e. high SKDI) to maximize their global trunk flexion as indicated by the significant correlation between both parameters (0.694, p=0.004). Alternatively, subjects that only limitedly engaged deformed regions (i.e. low SDEI) during the motion, due to the lesser engagement of the deformed regions, use less kinematic compensation (i.e. low SKDI).

The indicated potential of this work needs to be evaluated within the constraints of the limitations described below.

First, upon interpreting the SKDI and SDEI, attention should be paid to possible flooring effects. Kinematic spine coupling is indeed a natural phenomenon that is present even in healthy subjects (Cook, 2003; Panjabi et al., 1994) and explains why the SKDI is not zero in the control subject. Nevertheless, such flooring effect is not to be expected in the SDEI of healthy subjects. Given the deformity-based weighting, motion at joints composed of non-deformed vertebral bodies -by definition- does not contribute to the overall SDEI. In contrast, a low but larger than zero SDEI indicates either a limited engagement of joints adjacent to deformed vertebrae, or that overall vertebral deformation is not severe (i.e. low number and/or severity of deformed vertebrae). As a second limitation, IV joint kinematic measurements and derived parameters could be affected by different modelling and simulation inaccuracies. These include the presence of noise on the recorded motion capture data, soft tissue artefacts on the skin-mounted markers, optimization assumptions of the inverse kinematics simulation, or error in creating the subject-specific model (Appendix 3) and the assumptions of the IV joint definition (Overbergh et al., 2020; Widmer et al., 2019). Additionally, the SKDI relies on single-plane movement. Any deviation from the single-plane trunk motion (quantified through the coronal T1-SPI ROM) could – at least in theory - affect the SKDI, although no significant relation between the SKDI and coronal T1-SPI ROM was found in the current study. This monoplanar prerequisite is thus not expected to be a hindering factor for further use. However, adequate instructions or the use of targets to standardize the motion thus remain important. A case example wherein we demonstrate how an altered motion strategy, possibly due to

insufficient standardization, was detected and also quantified by the SKDI parameter is therefore provided in Appendix 4. As a third limitation, the SDEI is subject to additional errors originating from the inter- and intrarater variability of the SQ grading system assessing vertebral body deformities (Genant et al., 1993). However, in the future these could be avoided through the use of more reliable and automated assessment methods (Štern et al., 2013). Finally, although the spino-pelvic parameters (Table 25) indicated a high subject heterogeneity, we acknowledge that the developed methods were only evaluated in a limited number of subjects. This heterogeneity in spinal malalignments is also notable in the set of created models (Figure 49).

Nevertheless, future research should evaluate the use of the developed parameters in a larger ASD population to thus provide more insights in the relation between kinematic compensation and spinal deformity. Similarly, their application in a larger number of control subjects could provide a more reliable normative dataset, offering the opportunity to compare normal spinal alignment to spinal malalignment. Additionally, the performed analyses should be extended to other motions to better represent the range of motion strategies that ASD patients apply in everyday life potentially aiding in a more dynamic classification of the spinal deformity population. In the future, the insights considering a patient's specific motion strategy could potentially benefit clinical management and aid in the pre-surgical evaluation towards lower complication rates. This could for example impact surgical decision-making regarding the selection of the upper and lower vertebrae in spinal fusion surgery where the surgeon carefully balances achieving maximal alignment correction with mobility loss (Blondel et al., 2013; Ignasiak et al., 2018a).

Indeed optimized spinal instrumentation to restore healthy kinematics, can benefit from precise knowledge on the complex relation between static deformity and local spine dynamics (Widmer et al., 2019), in particular in conditions relevant for activities of daily living.

In conclusion, this work indicated that, contrary to the conventional radiographic evaluation of ASD patients, kinematic measures derived from a rigid-body modeling based workflow combined with 3D motion capture have clear potential to provide novel insights in kinematic characteristics. Such insights can fulfill the need to complement the static radiographic assessments of adult spinal deformities, currently used in clinical practice, with dynamic information.

Supplementary data of Chapter 3

Appendix 1: Model-based T1-SPI

To determine the T1-SPI parameter on a rigid-body model, 1) anatomical landmarks for the T1 vertebral body center and both pelvic acetabular centers were identified with respect to their respective body reference frames in the model; 2) the estimated IV joint kinematics obtained from inverse kinematics were transformed to express the absolute position and orientation of each individual body reference frame in the ground reference frame using the body kinematics tool in OpenSim 3.3; 3) the positions of the three anatomical landmarks (both pelvic acetabular centers and T1), expressed in their respective body reference frames, created landmark trajectories over the duration of the motion, expressed in the ground reference frame; 4) the angle between a vertical line (i.e. perpendicular to the ground) located at the mid-point between the pelvic acetabular centers and the line connecting the mid-point between the pelvic acetabular centers with the T1 vertebral body landmark was calculated for every recorded time frame of the motion. This angle was projected onto the subject's sagittal and coronal anatomical plane, defined by the acetabular center axis in the transverse plane.

Appendix 2: Definition of the SKDI

Equation (1), defining the SKDI, was obtained in this stepwise procedure.

In a first step, the total range of motion ($ROM_{X,total}$) is calculated for each plane (X= P, X =S1, X=S2) by summing the $ROM_{X,i}$ at each joint level (i) for that plane (i.e. L5/sacrum-joint to the T1/T2 joint), which is calculated as the absolute difference of the joint angle at frame 1 and 100.

$$ROM_{P,total} = \sum_{i=L5/sacrum}^{T1/T2} ROM_{P,i} \qquad (2.1)$$

$$ROM_{S1,total} = \sum_{i=L5/sacrum}^{T1/T2} ROM_{S1,i} \qquad (2.2)$$

$$ROM_{S2,total} = \sum_{i=L5/sacrum}^{T1/T2} ROM_{S2,i} \qquad (2.3)$$

Next, as an intermediate calculation, we introduce the directional deviation fractions (DDFs) which are the ratio of each secondary total ROM ($ROM_{\text{S1, total}}$, $ROM_{\text{S2, total}}$) to the primary total ROM ($ROM_{\text{P, total}}$):

$$DDF_{S1} = \frac{ROM_{\text{S1, total}}}{ROM_{\text{P, total}}} \qquad (2.4)$$

$$DDF_{S2} = \frac{ROM_{\text{S2, total}}}{ROM_{\text{P, total}}} \qquad (2.5)$$

Finally, we obtain the SKDI as the average of DDF_{S1} and DDF_{S2}, weighted by their relative contribution to the total secondary range of motion (i.e. $ROM_{\text{S1, total}} + ROM_{\text{S2, total}}$).

$$SKDI = DDF_{S1} \times \frac{ROM_{\text{S1, total}}}{ROM_{\text{S1, total}} + ROM_{\text{S2, total}}} + DDF_{S2} \times \frac{ROM_{\text{S2, total}}}{ROM_{\text{S1, total}} + ROM_{\text{S2, total}}} \qquad (2.6)$$

After substitution of Equations (2.4) and (2.5) in Equation (2.6), the equation for the SKDI can be reduced to Equation (1).

Appendix 3: Reliability of the SKDI

1. Between-session reliability

In previous work (Overbergh et al., 2021), five subjects (4 ASD, 1 control subject) performed the maximal trunk flexion twice over a time period of, on average, two weeks. Building further on this work, the SKDI was now determined for both sessions and compared for reliability by calculating the interclass correlation coefficient (ICC(2,1)) with a two-way random effects model for absolute agreement (SPSS Statistics 26, IBM Corp. Armonk, NY, USA).

Results

The intraclass correlation coefficient (ICC) for the between-session reliability of the SKDI was 0.862 (Table 31).

Table 31: SKDI values of a maximal forward trunk flexion for five subjects, measured twice in a two-week time interval.

Subject	SKDI session 1	SKDI session 2	Difference
control	0.269	0.368	0.100
1	0.975	0.668	0.307
2	0.808	0.695	0.113
3	0.601	0.517	0.085
4	0.389	0.442	0.053

2. Uncertainty due to inter-operator-induced variability in modeling

As previously described (Overbergh et al., 2021), the manual aspects of creating a subject-specific spino-pelvic model cause unavoidable inter-operator-dependent model variability. This model variability causes variability on the simulation output, and consequently on the parameters derived from it. The results of a Monte-Carlo probabilistic simulation, based on experimentally obtained inter-operator-variability, on three randomly selected ASD subjects and from three trained operators were reused to quantify this variability. More specifically, the SKDI was determined for 1000 inverse kinematic simulations in which a statistically probable model variation was used every time. A boxplot of the SKDI distribution for each of the three subjects was created (Figure 50). Thereafter, the difference with the SKDI of the unperturbed model was determined and pooled over all three subjects, to obtain the 95% confidence intervals (CIs) on the respective SKDIs (Figure 51).

Results

The 95% confidence interval (CI) of the inter-operator variability on the SKDI was 0.0053 with the minimal and maximal relative error: -0.37 and 0.33 (Figure 50-Figure 51).

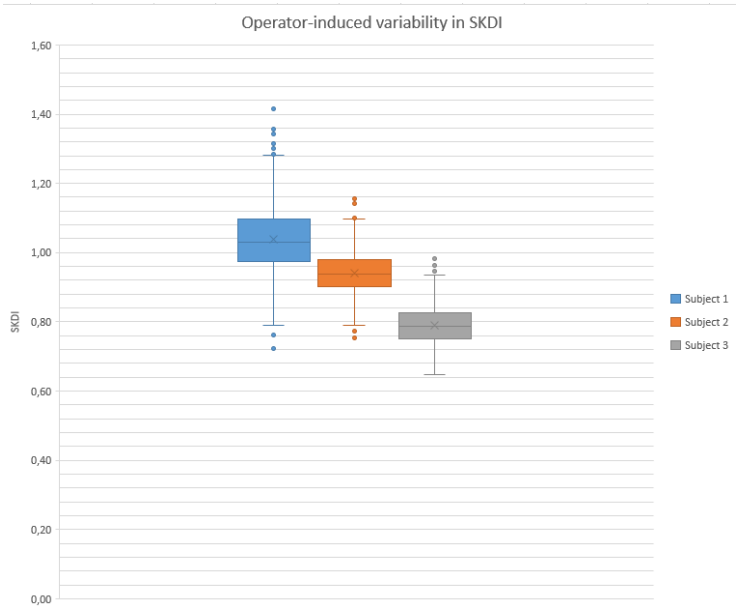

Figure 50: Boxplot of the SKDI variability for each of the three ASD subjects.

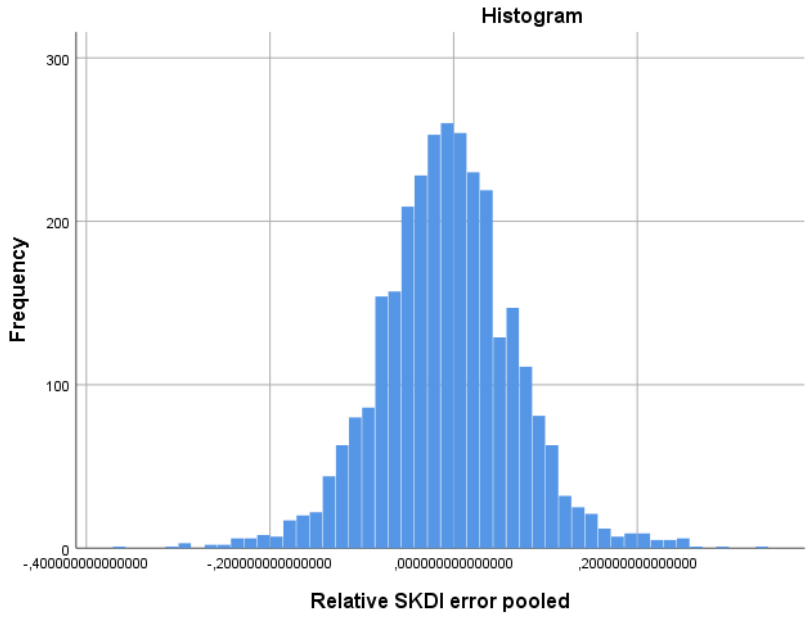

Figure 51: Histogram of the pooled error on the SKDIs of the three subjects, relative to the respective unperturbed (reference) models.

Appendix 4: Remark on the importance of adequate standardization in the motion lab: case example

As an example of the importance of adequate standardization of the motion, we highlight one incidence wherein we believe the instructions given to a specific ASD subject were insufficiently consistent or unclear. This subject, suffering from a predominantly lumbar located spinal deformity (Figure 52A), initially performed a maximal trunk flexion mainly making use of her lumbar region and limitedly engaging her thoracic region (Figure 52B). However, in the second session seven days later, her motion strategy changed, a rigid lumbar region with primarily engagement of her thoracic region (Figure 52C), despite that there were no interventions, injury or illness during this seven day period. Figure 53 shows the range of motion (ROM) of each degree of freedom (DOF) at every intervertebral joint, confirming the different strategy of both sessions. This altered motion strategy is evidently translated in a change of the SKDI: 3.18 (session 1) vs. 0.51 (session 2). The cause of this change in strategy could not objectively be determined. However, it is possible that the subject received or interpreted the instructions differently during one of the sessions, which would indicate the importance of adequate standardization.

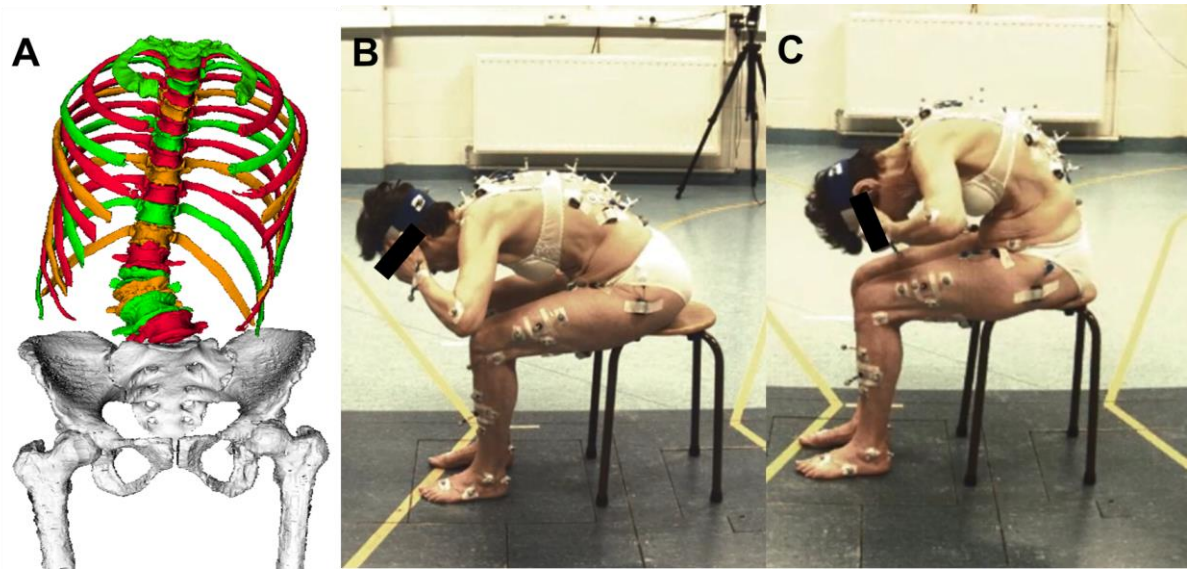

Figure 52: (A) 3D subject-specific model of the subject. Images at the end stage of the maximal forward trunk flexion motion in (B) session 1 and (C) in session 2.

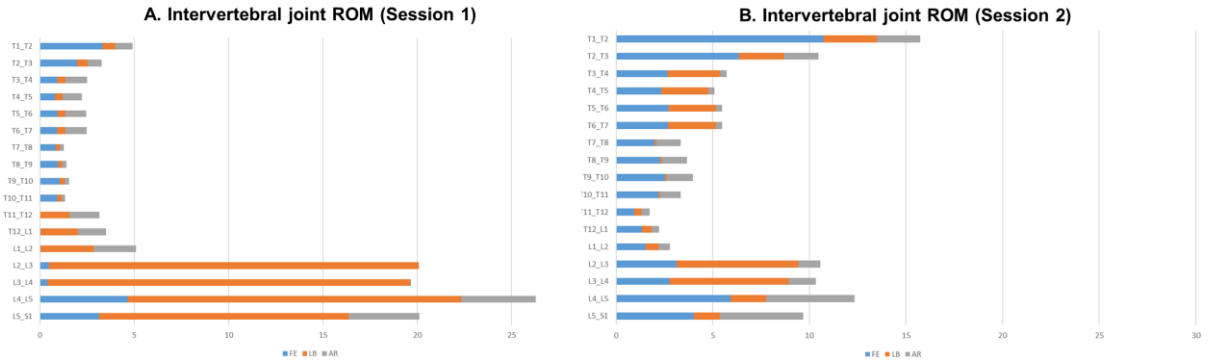

Figure 53: Intervertebral (IV) joint range of motion (ROM) for each degree of freedom at each IV joint in (**A**) session 1 and (**B**) session 2. (FE: flexion-extension (blue), LB: lateral bending (orange), AR: axial rotation (grey).)

Chapter 4

Model-based evaluation of intervertebral kinematics during trunk flexion before and after spinal fusion surgery in Adult Spinal Deformity: an exploratory study.

Abstract

The currently high complication and revision rates of surgery in adult spinal deformity (ASD) have been suggested to be linked to a lack of dynamic information to support surgical decision-making. Additionally, the patients' expectations in terms of post-operative functional improvements is often much higher than typically experienced post-operatively. Besides the evaluation of intervertebral (IV) kinematics before surgery, there thus also seems to be a need for post-operative evaluations to more objectively document outcome. Motion analysis has clear potential to provide quantitative data about functional effects of spinal surgery in ASD.

The aim of this work was to evaluate a previously developed modeling and evaluation platform to measure spine kinematics during maximal voluntary trunk flexion before and after spinal fusion surgery in ASD, focusing on (1) the changes in *global* spinal motion, pre- and post-operatively, as well as (2) the *vertebral (or local)* motion of the unfused vertebrae. Secondary to these aims, this study provided an opportunity to evaluate the impact of soft tissue artefacts (STAs) on the accuracy of marker-based spinal kinematics as the erroneously measured motion at the instrumented, and therefore immobile, IV joints.

All subjects of our pilot population (n=5) presented with (1) a reduced global spinal and pelvic range of motion (ROM) during trunk flexion after surgery compared to their pre-operative motion. On a local level, (2) remaining (i.e. unfused) vertebrae also demonstrated reduced ROM after surgery although they were not part of the fused region. In addition, assuming that physical motion is mechanically prevented in the fused vertebrae, the average effect of STA on the measured IV joint kinematics was estimated to be 0.99°.

From a methodological perspective, we explored post-operative modeling and identified three pitfalls in modeling and simulation of post-operative subjects. Firstly, modeling was complicated due to hindered visibility caused by the surgical instrumentation. Second, the marker protocol requires modifications in post-operative situations. Lastly, the model requires modification to the definition of its joint constraints to accurately account for the mobility reduction due to the fusion.

This study presented the first *in vivo* spinal deformity-specific STA analysis evaluated in terms of error on the measured IV joint kinematics using subject-specific models. Although investigation using larger study cohorts is needed, this work illustrated limitations and potential opportunities for the use of subject-specific musculoskeletal model in post-operative ASD patients to quantify changes is global spino-pelvic and local unfused vertebral motion.

Introduction

The complication rate of surgical treatment in adult spinal deformity (ASD) remains substantial (up to 52.2%) (Smith et al., 2016). Additionally, large discrepancies have been documented between patient expectations and observed outcomes following corrective surgery in ASD. Specifically, the anticipated pain reduction and functional improvement aspects of self-reported health related quality of life (HRQoL) after spinal fusion surgery were much higher than experienced by the patient post-operatively (Ryu et al., 2021; Yoo et al., 2019). When defining the surgical plan, the surgeon will decide on fusion length and types of osteotomies and implants (taking into account the needs for posture correction, progression risk and bone quality) carefully balancing with mobility (Blondel et al., 2013; Kim et al., 2016). However, objective fusion level selection in ASD is currently still a heavily debated topic (Blondel et al., 2013). The lowest instrumented vertebra (LIV) in ASD is most often the sacrum (with or without inclusion of the pelvis), and to a lesser extent L5 or L4 (Taneichi et al., 2020; Yao et al., 2021). Consequently, the fusion length is typically more dependent on the surgeon's selection of the upper instrumented vertebra (UIV). This choice requires careful balancing of risks and benefits as an increase of the fusion length reduces global spinal mobility (Blondel et al., 2013). Although it has been widely accepted that the selection of the UIV in ASD has implications for the functional outcome of corrective spinal fusion surgery (Ignasiak et al., 2018a), it remains unclear to what extent fusion length selection is affecting spinal mobility and should be balanced against the above needs.

Motion analysis has clear potential to provide quantitative data about functional effects of spinal surgery in ASD. Indeed, motion analysis is gaining more and more interest as a tool to non-invasively measure spinal kinematics in ASD (Diebo et al., 2018). Recent work from our group combining image-based subject-specific modeling with marker-based motion analysis has offered new possibilities to non-invasively measure intervertebral (IV) joint angles in pre-operative ASD patients (Overbergh et al., 2020). Nevertheless, the method has thus far not been used to measure *in vivo* spinal kinematics in a post-operative population.

To adequately and objectively evaluate functional outcome after spinal fusion surgery in ASD, analysis of IV joint kinematics requires differentiation between the (1) unfused and (2) fused vertebral segments. Indeed, although spinal fusion instrumentation only directly prevents motion of the fused segments, it can indirectly affect the dynamic behavior of the unfused segments as well as the remainder of the locomotor system through compensatory mechanisms. Cadaveric analysis of IV joint kinematics demonstrated a post-operative reduction in global spinal mobility but an increase in the mobility of unfused segments (Bastian et al., 2001; Chow et al., 1996). Recently, this was confirmed through computer simulations where a range of fusion lengths was applied on a healthy virtual subject (Ignasiak et al., 2018a) and the effect on IV joint kinematics was tested. During a simulated forward trunk flexion, an increased maximal segmental flexion was reported for increased fusion lengths, related to an increase in maximum moment at the unfused segments. However, in these cadaver and computer prediction studies, externally controlled and identical boundary conditions in terms of loads

and/or moments are applied to the spine pre- and post-operatively, which are only limitedly representative for *in vivo* voluntary motion in ASD subjects.

Furthermore, prior to using marker-based IV joint kinematics for evaluating functional effects of spinal surgery in ASD, the accuracy of these measurements, should be known (Zemp et al., 2014). Indeed, all skin marker-based motion measurements are subject to error originating from soft tissue artefacts (STAs) (Leardini et al., 2005). These are caused by the relative motion of the skin (and consequently the marker attached to it) to the underlying anatomical structure due to for example muscle contraction or inertial effects (Mahallati et al., 2016; Zemp et al., 2014). STAs have already been described to negatively impact the accuracy of kinematic measurements of the lower limbs (knee, feet, shank and thigh) (Mahallati et al., 2016). However, studies investigating STA on the entire back are rare. Making use of open magnetic resonance imaging (MRI) as ground truth, Zemp et al. (2014) evaluated the effect of STAs on the marker-based estimation of conventional spino-pelvic radiographic measurements such as lumbar lordosis (LL) and thoracic kyphosis (TK). They concluded that while the absolute values suffer from uncertainty, the use of markers during semi-dynamic forward trunk flexion was suitable for quantifying spinal postural changes. Studies specifically quantifying STA during axial trunk rotations in healthy subjects, reported artefacts up to 9.86 mm at the lumbar levels (L3 and L4) and up to 16 mm at the thoracic levels (T1, T6, T12), making use of open MRI and ultrasound imaging respectively (Heneghan and Balanos, 2010; Mörl and Blickhan, 2006). In healthy subjects performing a 30° trunk flexion and extension, STAs on the entire lumbar and thoracic spine ranged up to 27.4 mm. These studies report STA as a distance or as a 3D vector describing the erroneous motion of the skin marker relative to the anatomical landmark. To quantify the effect of STAs on the spine kinematics, Mahallati et al. (2016) modeled the trunk as a seven-segment system and determined the spinal segment angles based on skin markers (see Appendix 1). They imposed statistically probable perturbations on the markers to simulate STA and concluded that STA minimally affected the segment angles in the sagittal plane (<16% of the full range of motion), but had a larger effect on the transverse (up to 161%) and coronal plane (ranging between 59% and 551%). Contrary to Mahallati et al. (2016) where the segment angles were directly estimated from the marker trajectories, more complex and non-linear optimization algorithm are typically used in musculoskeletal models to estimate IV joint kinematics (e.g. Lu and O'Connor (1999)). Furthermore, the effect of STAs is dependent on the specific marker protocol and on the underlying model used to process the recorded motion capture data. Currently, no such analyses have been performed in ASD.

The aim of this work is to evaluate the modeling and evaluation platform to measure spine kinematics during trunk flexion before and after spinal fusion surgery in ASD. More specifically, we aim to evaluate **(1)** the changes in *global* spinal motion during maximal voluntary trunk flexion, pre- and post-operatively, as well as the *vertebral (or local)* motion of the **(2)** unfused vertebrae (Figure 54). Secondary to these aims, this study provided an opportunity to evaluate **(3)** STA as the erroneously measured motion of fused vertebrae, which limits kinematic accuracy of spinal kinematics.

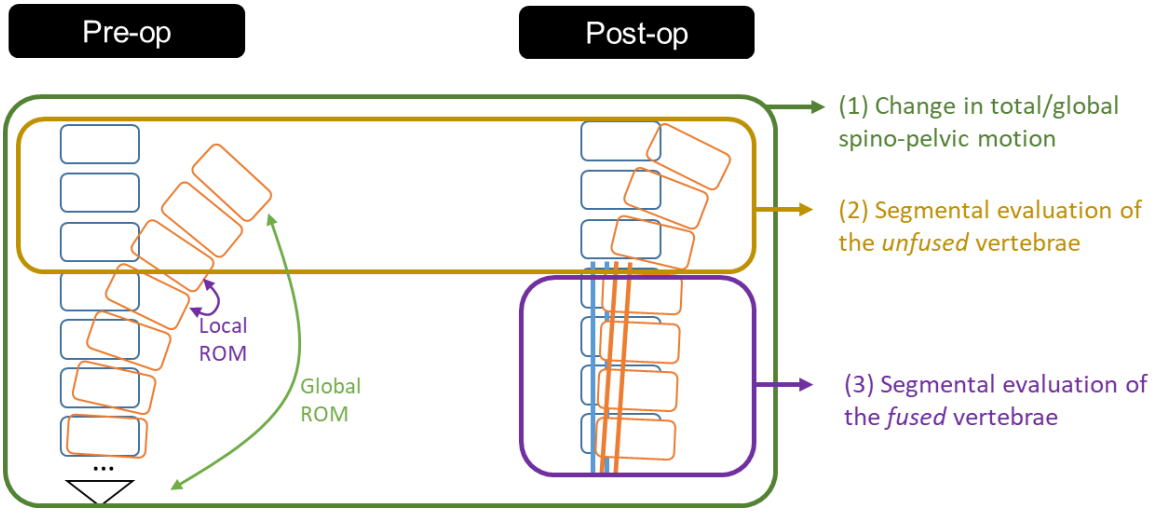

Figure 54: Schematic layout of the aims in this work.

Materials and methods

Participants and data collection

Five participants (2 males (51 and 66 years), 3 females (59, 60 and 67 years)) with varying degrees of spinal malalignment participated in this study, following ethical approval and informed consent (S58082). These subjects were selected from the ASD subjects of Chapter 3 (for which a pre-operative model was already available) if they also participated in the study after surgical correction. All subjects underwent computed tomography (CT) imaging from T1 to pelvis (BrightSpeed by GE Healthcare, with an inter-slice distance of 1.25 mm and a pixel size of 0.39x0.39 mm). Thereafter, an experienced physiotherapist instrumented each subject with reflective markers according to the skin marker placement protocol described in Overbergh et al. (2020). Then, full-body radiographic (x-ray) images were acquired using a biplanar radiography system (EOS Imaging, Paris, France), while the subject was wearing the markers and adopted the Scoliosis Research Society free-standing position (fingers-on-clavicle position) (Horton et al., 2005; M. Y. Wang et al., 2014) (Figure 55). Thereafter, in the motion laboratory, the subjects were asked to perform a maximal voluntary forward trunk flexion from a comfortable upright seated position (Figure 57A-B), while the trajectories of the reflective markers were recorded (100 Hz) using a 10-camera Vicon system (VICON Motion systems, Oxford Metrics, UK). Shortly thereafter, all subjects underwent spinal fusion surgery with fusion lengths ranging from seven to fifteen segments. All subjects were re-evaluated six months after surgery based on biplanar radiographic images (Figure 56) and their execution of a maximal voluntary forward trunk flexion motion (Figure 57C-D).

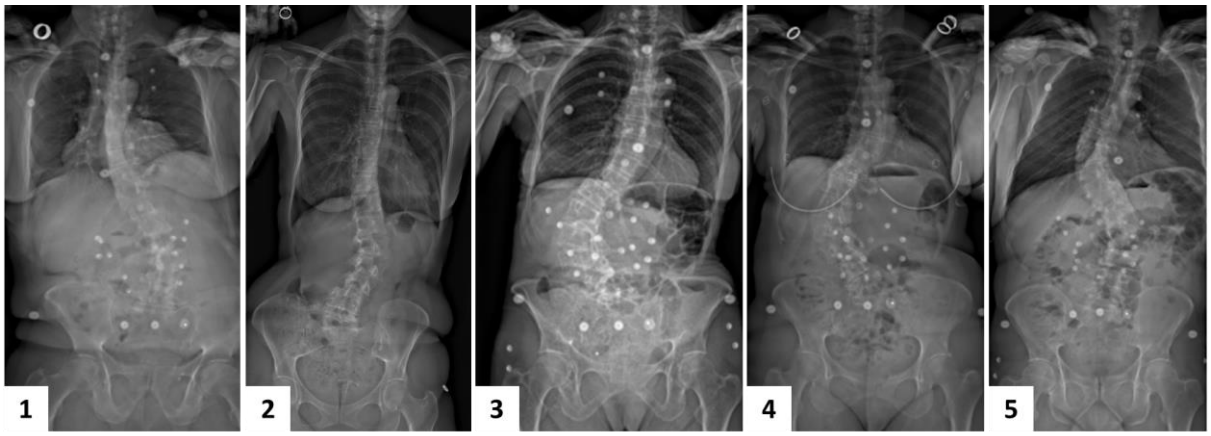

Figure 55: Pre-operative coronal radiographic images of ASD subjects 1 to 5.

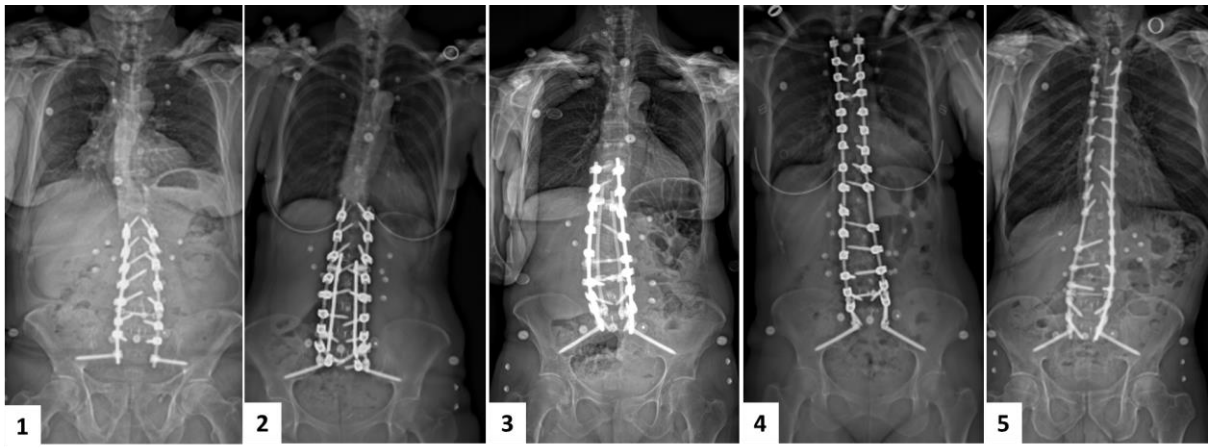

Figure 56: Coronal radiographic image of the six-month post-operative state of the five ASD subjects corresponding to the images of Figure 55.

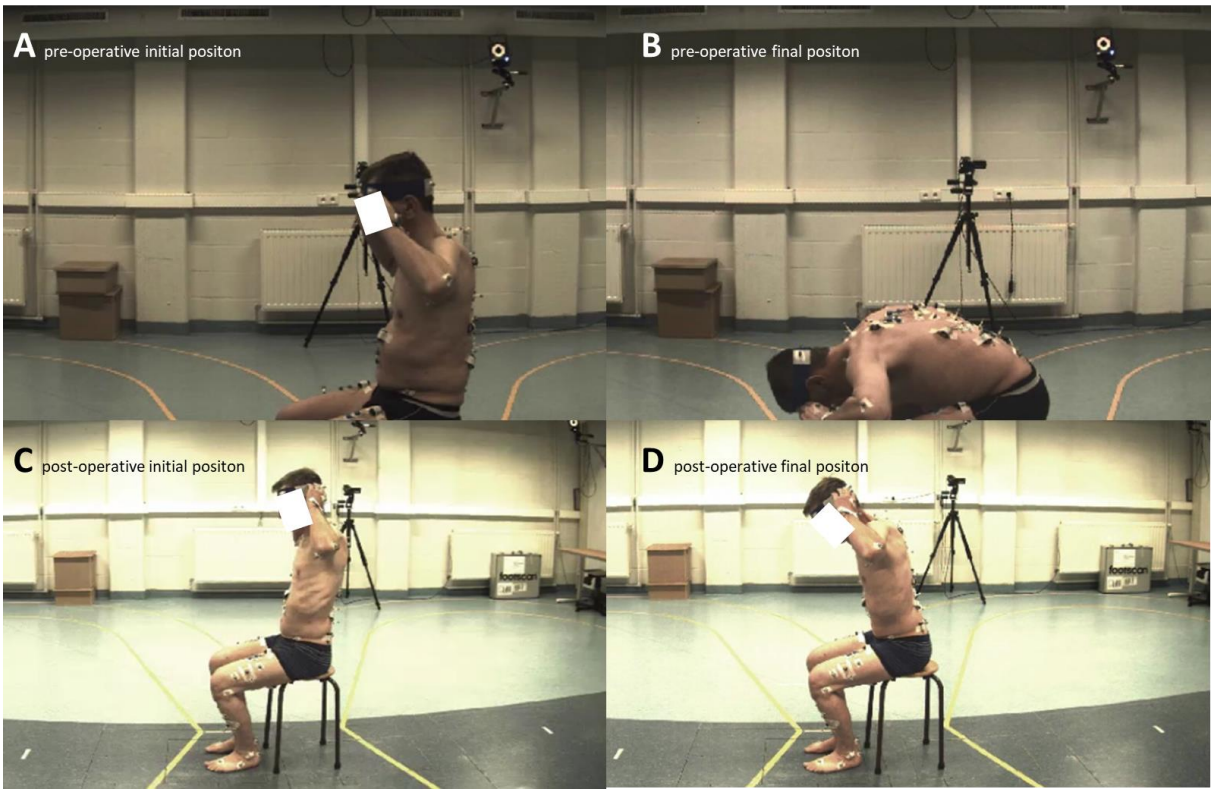

Figure 57: Example of an ASD patient performing the maximal voluntary forward trunk flexion in the motion lab (Subject 1; male, 66.1 years on the pre-operative measurement). The images show the (**A**) initial and (**B**) final position of the motion, pre-operatively and six months post-operatively (**C** and **D**, respectively). The subjects were instructed to place their hands on their head to prevent the obstruction of pelvic marker visibility during the motion.

Pre- and post-operative modeling and simulation

One operator created a subject-specific spino-pelvic model for each of the five ASD subjects in their pre-operative condition (Figure 58) (Overbergh et al., 2020). To create the corresponding six-month post-operative subject-specific models (Figure 59), the pre-operative CT-segmented bone geometries were re-used to reconstruct the post-operative alignment as available in the post-operative biplanar radiographic images.

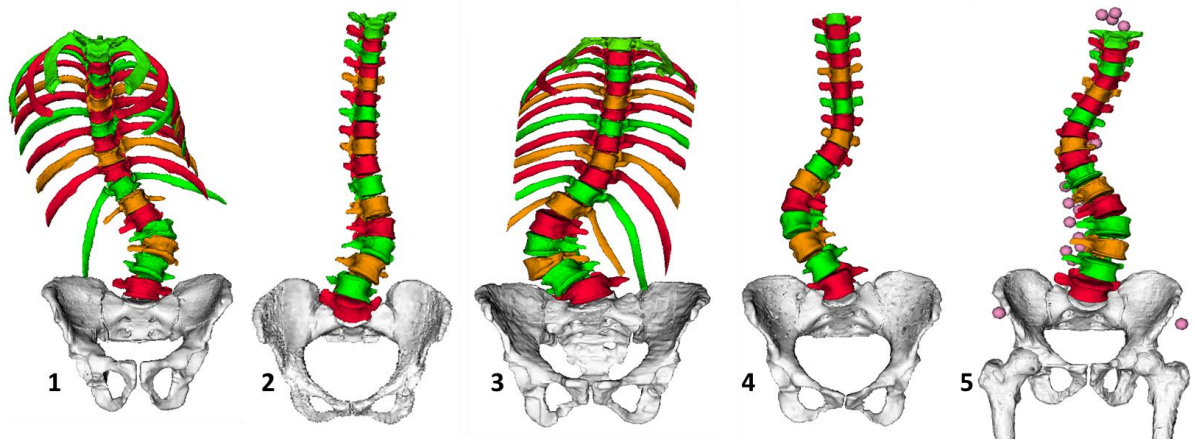

Figure 58: Pre-operative subject-specific models of subjects 1 to 5.

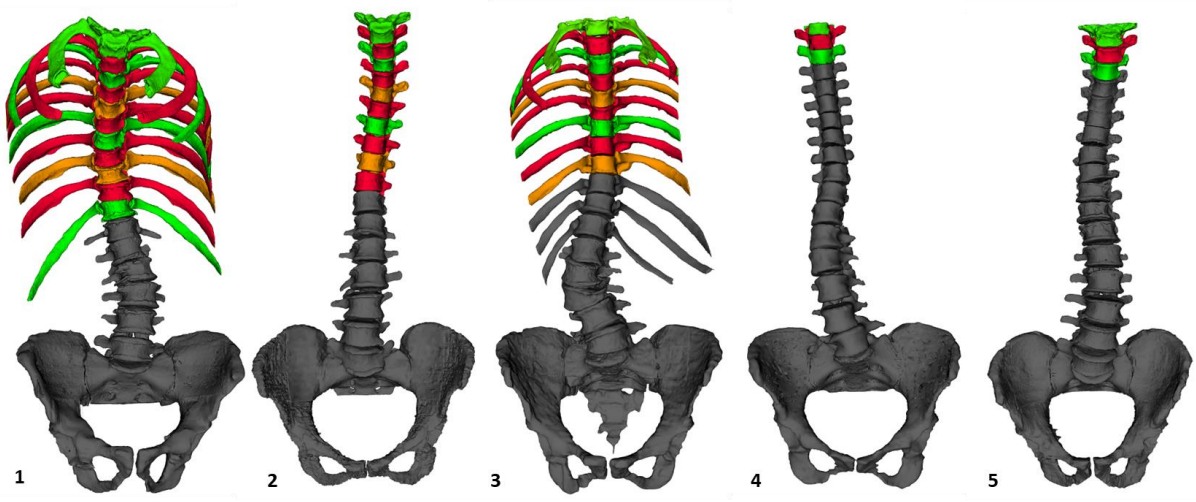

Figure 59: Post-operative subject-specific models of the five ASD subjects, created from their respective biplanar images in Figure 58. Dark grey segments are fused.

As space restrictions on the back for marker placement prevent tracking each individual vertebra, the applied marker protocol impedes tracking of all vertebrae. Therefore, interpolation principles have previously been integrated as joint constraints in the definition of each IV joint (Overbergh et al., 2020). This allows motion, recorded between marker clusters and thus spanning a certain *region*, to be distributed within that region based on experimental data (illustrated for each subject in Figure 60) (Overbergh et al., 2020). It is important to note that in the post-operative condition of subject 1, 3 4 and 5, one *region* thus spans vertebrae both with and without instrumentation. In such regions the recorded regional motion will thus be incorrectly distributed over all joints contained within that region as they include IV joints that can be reasonable expected to no longer have any mobility due to the fusion. As an example, subject 3 has a fused T10/T11 IV joint in the tracked region from T7 to T11 (Figure 60). The kinematic optimization algorithm will distribute motion in this region linearly (according to experimentally determined ratios described in (Overbergh et al., 2020)) over its four containing joints, although only three have actual mobility. As will be described further, this limitation will have implications on the further analyses in this work. In relation to Figure 60, Table 32 summarizes the subject's fusion lengths and regions effectively containing *only* fused or *only* unfused vertebrae.

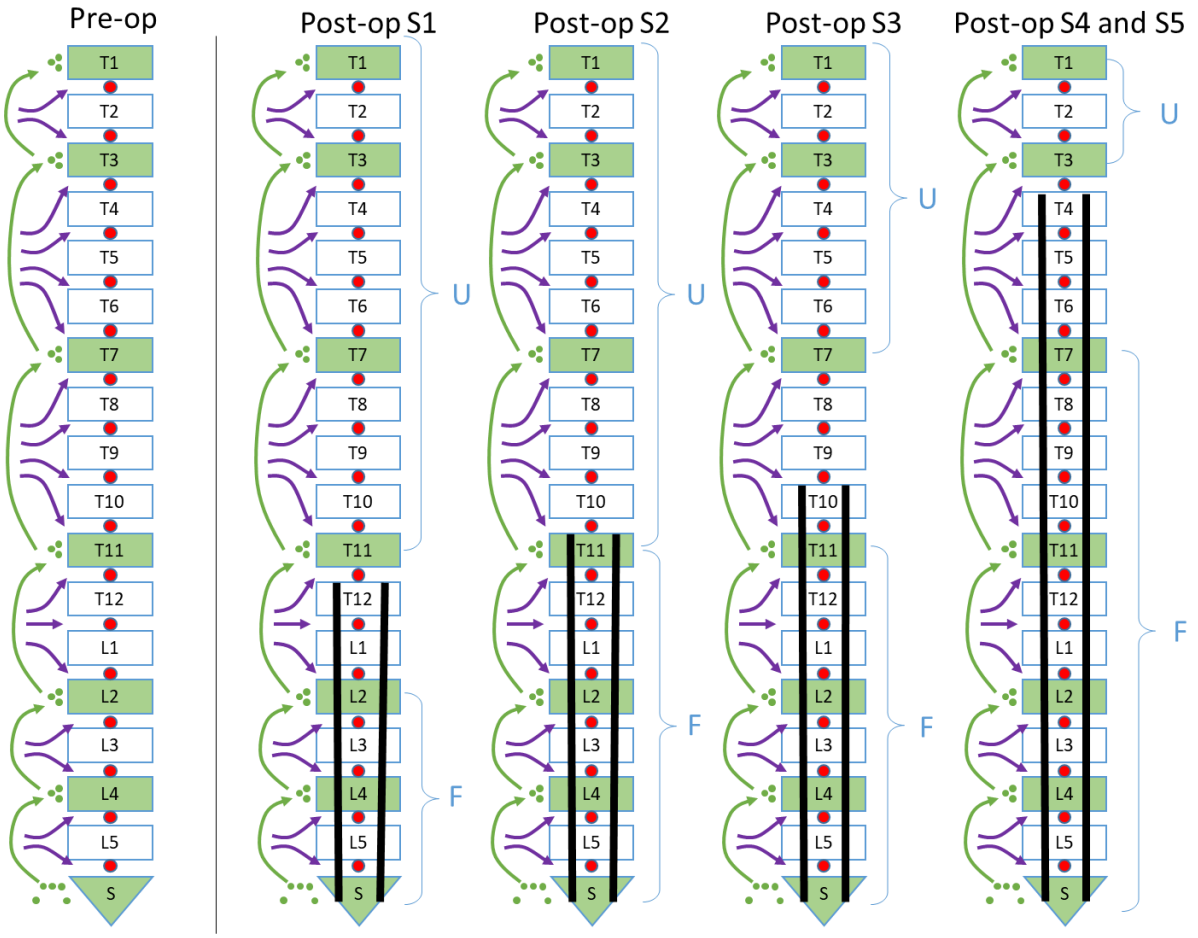

Figure 60: Illustration of the kinematic joint constraints in the model without surgical instrumentation (left). Regional motion (green arrows) is distributed over its containing joints. In the post-operative models (right), regions containing only unfused or fused segments are indicated with U and F, respectively.

Within the fused region of the spine, an opportunity occurs to evaluate STA associated with our specific marker protocol and subject-specific model and, more specifically, their impact on the IV joint angles during forward flexion. In post-operative conditions, actual motion is indeed prevented at IV joints spanned by the surgical instrumentation. Nevertheless, as these joints remained unlocked in the model for all kinematic degrees of freedom (DOFs), any resulting *virtual* motion measured can be considered to result from STA (Figure 61). The term virtual motion is used to indicate motion that was simulated/measured in the model, but is physically not possible in the subject due to the surgical fixation.

Table 32: Summary of the individual subjects, with their fusion lengths and the fused or unfused regions for which our model-based evaluation can be used in further analysis. Subjects are ordered in terms of increasing fusion length comprising the region bound by and including the lower instrumented vertebra (LIV) to the upper instrumented vertebra (UIV).

Subject	Fused region (LIV-UIV)	Only fused joints	Only unfused joints
1	S1 – T12	S1/L5 → L2/L3	T1/T2 → T10/T11
2	S1 – T11	S1/L5 → T11/T12	T1/T2 → T10/T11
3	S1 – T10	S1/L5 → T11/T12	T1/T2 → T6/T7
4	S1 – T4	S1/L5 → T7/T8	T1/T2 → T2/T3
5	S1 – T4	S1/L5 → T7/T8	T1/T2 → T2/T3

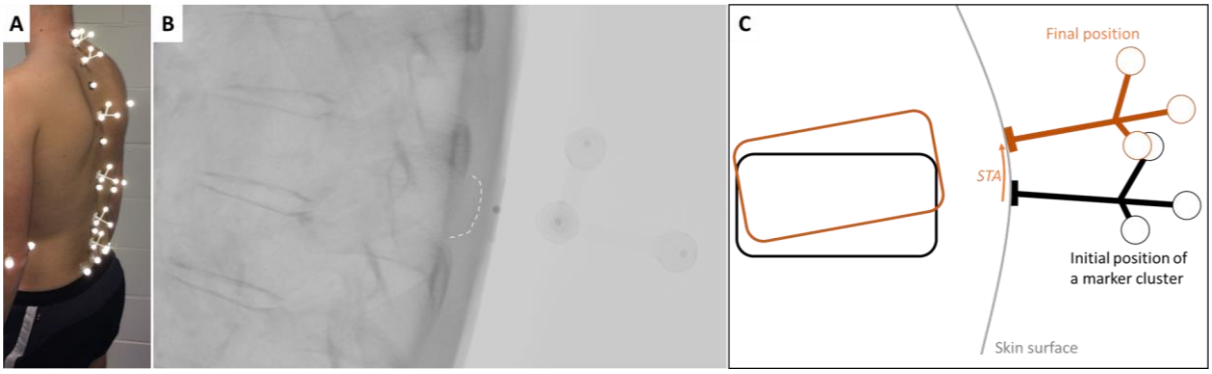

Figure 61: (**A**) Illustration of the marker protocol as defined in Overbergh et al. (2020) and (**B**) the sagittal radiographic image thereof at the thoracic region (posterior part of the spinal process indicated with a dashed line). (**C**) In relation to the assumptions made for the measurement soft tissue artefact (STA), this schematic illustrates how STA on a skin marker cluster (tracking a fused vertebrae) leads to erroneously measured intervertebral joint motion given the fact that any motion would physically be prevented by the surgical instrumentation and subsequent bony fusion.

After processing the recorded motion capture data using Vicon Nexus 2.12, inverse kinematics simulations (Lu and O'Connor, 1999) in OpenSim 3.3 (Stanford University, USA) (S. L. Delp et al., 2007) were performed for the pre- and post-operative motion. As in Chapter 3 the kinematic movements were time normalized to 100 frames and filtered using a three-frame moving average to reduce noise.

Kinematic data processing

Change in global spino-pelvic motion

The global spinal range of motion (ROM) was evaluated pre- and post-operatively based on the ROM of the T1-spino-pelvic inclination angle and the pelvic tilt (PT) angle between the start and the end of the flexion motion (Chapter 3).

Kinematics of the unfused vertebrae

The voluntary mobility[4] at each IV joint was calculated as the ROM summed over all three DOFs (FE: flexion-extension, LF: lateroflexion, AR: axial rotation) (defined in Chapter 3):

$$\mathrm{ROM}_{\mathrm{FE,IV\ joint}} + \mathrm{ROM}_{\mathrm{LF,IV\ joint}} + \mathrm{ROM}_{\mathrm{AR,IV\ joint}}\,. \quad (1)$$

Subsequently, the mean voluntary mobility of the post-operatively unfused IV joints (as defined in Table 32 for each subject) was calculated both before and six months after surgery.

Kinematics of the fused vertebrae

The ROM of each DOF of each IV joint angle was determined as the absolute value of the difference between its initial and final angle. For each subject, the mean and maximal ROM was determined per DOF, i.e. FE, LF and AR, and this for the joints as defined in Table 32 ('only fused joints').

[4] In biomechanics, mobility typically refers to the maximal physical extent of a joint, as sometimes reached during in-vitro testing right before the breaking point (e.g. fracture of the bone or rupture of a ligament or muscle). However, this boundary is rarely reached during daily in-vivo motion. Therefore, in this work, we refer to voluntary mobility as the range of motion (global or local) that a subject actually uses during a recorded voluntary motion.

Results

Global evaluation of the performed motion

The pre- and post-operative global ROM of a maximal voluntary trunk flexion is expressed using the T1-SPI and PT in Figure 62 (detailed data in Table 35 of Appendix 2).

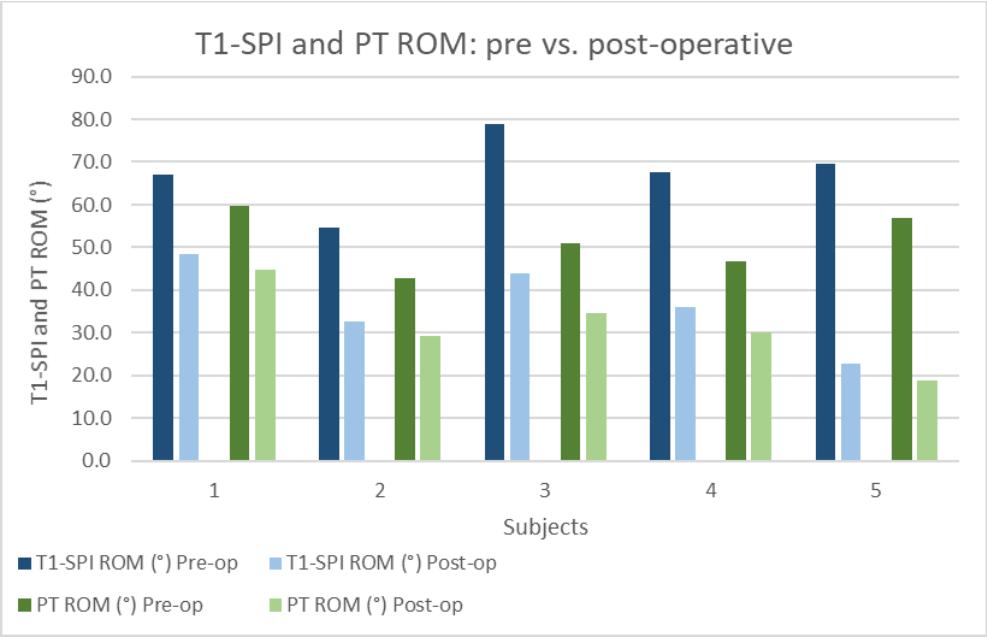

Figure 62: The range of motion (ROM) of the T1-spino-pelvic inclination (T1-SPI, blue) angle and pelvic tilt (PT, green) angle, during a maximal voluntary trunk flexion motion, both before (dark colored) and after surgery (light colored). Subjects are sorted by increasing fusion length as described in Table 32.

Kinematics of the unfused vertebrae: changes in mobility

Small reductions (0.3° – 5.4°) in the mean voluntary mobility (Formula 1) were noted after surgery for those IV joints that were not instrumented (Table 33). No notable relation between mean mobility reduction and fusion length was noted.

Table 33: The mean pre- and post-operative multi-plane ROM during the maximal voluntary trunk flexion motion was determined for the joints that were not part of the post-operative fusion. Subjects are sorted by increasing fusion length as described in Table 32.

	Mean unfused mobility (°)		
Subject	Pre-op	Post-op	Mobility reduction
1	2.1	1.8	0.3
2	4.3	1.9	2.4
3	6.2	4.6	1.6
4	7.3	1.8	5.4
5	2.0	1.6	0.5

Kinematics of the fused vertebrae: soft tissue artefacts

Table 34 expresses the effect of the STA as the mean (maximum) ROM over each IV joint and DOF within the instrumented spinal regions. The mean IV joint motion of the five subjects was 0.64°, 1.62° and 0.70° for FE, LF and AR, respectively. The largest mean ROM (2.96°) was noted for subject 4 in the LF direction. Over all subjects and directions, the mean ROM due to STA was 0.99°.

Table 34: STAs during maximal forward trunk flexion expressed as the erroneously measured IV joint motion in the fused regions of the ASD patients, separated by degree of freedom. (FE: flexion-extension, LF: lateroflexion, AR: axial rotation). Subjects are sorted by increasing fusion length as described in Table 32.

Subject	Mean (max) ROM motion artefact during trunk flexion		
	FE (°)	LF (°)	AR (°)
1	0.89 (1.31)	2.07 (4.17)	0.41 (0.47)
2	0.53 (0.68)	0.66 (0.84)	0.70 (1.08)
3	0.79 (1.70)	1.47 (2.56)	0.73 (0.97)
4	0.56 (2.25)	**2.96** (8.08)	1.32 (3.00)
5	0.44 (1.70)	0.94 (1.44)	0.35 (0.96)

Discussion

The aim of this work was to apply a novel ASD-specific modeling and simulation method to patients both before and after surgery and based hereon document subject-specific changes in post-operative spine kinematics.

First, in agreement with the literature, a pre- to post-surgical decrease in global spino-pelvic mobility was observed for all patients as quantified by the T1-SPI ROM demonstrating a mean decrease of 30.8° (max decrease: 46.7°) during the voluntary trunk flexion. This reduction was associated with a reduction in pelvic motion, as indicated by a reduced PT ROM after surgery (mean decrease: 19.9°, max decrease: 38.0°).

Secondly, a decrease in joint mobility was also noted at the IV joint level of unfused vertebrae (mean decrease: 2.0°, max decrease: 4.4°). Interestingly, this finding contrasts with the *in vitro* literature reporting increased mobility of the unfused segments. However, carefully controlled experimental conditions allow applying identical loading conditions before and after spinal fusion surgery. This suggests that imposing identical pre- and post-operative loading conditions in *in vitro* research is likely not representative for *in vivo* situations. A possible explanation is the voluntary nature of the maximal motion which is affected by fear, caution or even pain in *in vivo* testing, not present in *in vitro* research.

Thirdly, the analysis of the IV joint kinematics at the fused vertebrae presented an opportunity to evaluate STA and its effect on IV joint measurements when using subject-specific kinematic models and the associated marker protocol (Overbergh et al., 2020). Thereto, our main assumption was that any measured IV joint motion in the fused regions was caused by STAs. During the maximal voluntary trunk flexion motion, on average, an erroneous IV joint motion of 0.99° was noted. As in Mahallati et al. (2016), we noted the largest STA during trunk flexion in the coronal plane (i.e. the LF DOF). Although caution is recommended in future analyses of IV joint kinematics when ROM values are in the same order of magnitude, the analyses generally still allow use in research.

This study has some noteworthy limitations. First, this study relied on a relatively small subject group and must be interpreted as a first proof of concept and therefor does not allow far-reaching clinical interpretation or conclusions. Secondly, the accuracy and reliability of the subject-specific modeling platform has only been quantified in pre-operative ASD subjects (Overbergh et al., 2021, 2020). As the post-operative spinal alignment appeared to be slightly more difficult to reconstruct -especially in regions with metallic surgical instrumentation obscuring anatomical landmarks- the accuracy and reliability of post-operative modeling could be lower than reported previously in (Overbergh et al., 2020). A third, technical limitation applies to both the analysis of STA and the mobility of the unfused vertebrae. As previously described in section *"Pre- and post-operative modeling and simulation"*, in four subjects a number of vertebrae could not be included in the analysis of IV kinematics due to erroneous kinematic interpolation in regions containing a combination of instrumented, immobile and non-instrumented, mobile vertebrae. For future measurements in post-operative subjects, it would be advised to redistribute the kinematic interpolation in the model over the remaining

non-instrumented IV joints while locking the kinematic DOFs of instrumented joints. Additionally, kinematic STA quantification using post-operative patients is likely not entirely representative for the pre-operative population. First, as presented earlier, all subjects demonstrated a reduced global trunk flexion post-operatively. As STAs are expected to increase with larger movement (Leardini et al., 2005), our results probably underestimate the effect of STA in unfused regions as well as in a pre-operative population. Secondly, the reported STAs include effects from contracting muscles, skin stretching and inertial effects, but exclude the effects of IV joint motion as a complete fusion was assumed. Lastly, the presence of scar tissue on the back alters normal soft tissue structure and behavior (Corr and Hart, 2013).

In summary, all subjects of our pilot population (n=5) presented with a reduced global spinal and pelvic ROM during voluntary trunk flexion after surgery compared to their pre-operative motion. On a local level, the unfused vertebrae behaved more rigidly after surgery although they were not part of the fused region. The assumption that no physical motion is possible in the fused vertebrae, was exploited as an opportunity to investigate the effect of STA on spinal measurement. On average, STA induced errors in measured IV joint kinematics of 0.99°.

This study presented the first *in vivo* spinal deformity-specific STA analysis evaluated in terms of error on the measured IV joint kinematics using subject-specific models. Furthermore, this work illustrated limitations and potential opportunities for the use of subject-specific MS models in ASD patients and quantified changes is global spino-pelvic and local unfused vertebral motion.

Supplementary data of Chapter 4

Appendix 1: Illustration of the marker protocol of Mahallati et al (2016) and the marker protocol in this dissertation.

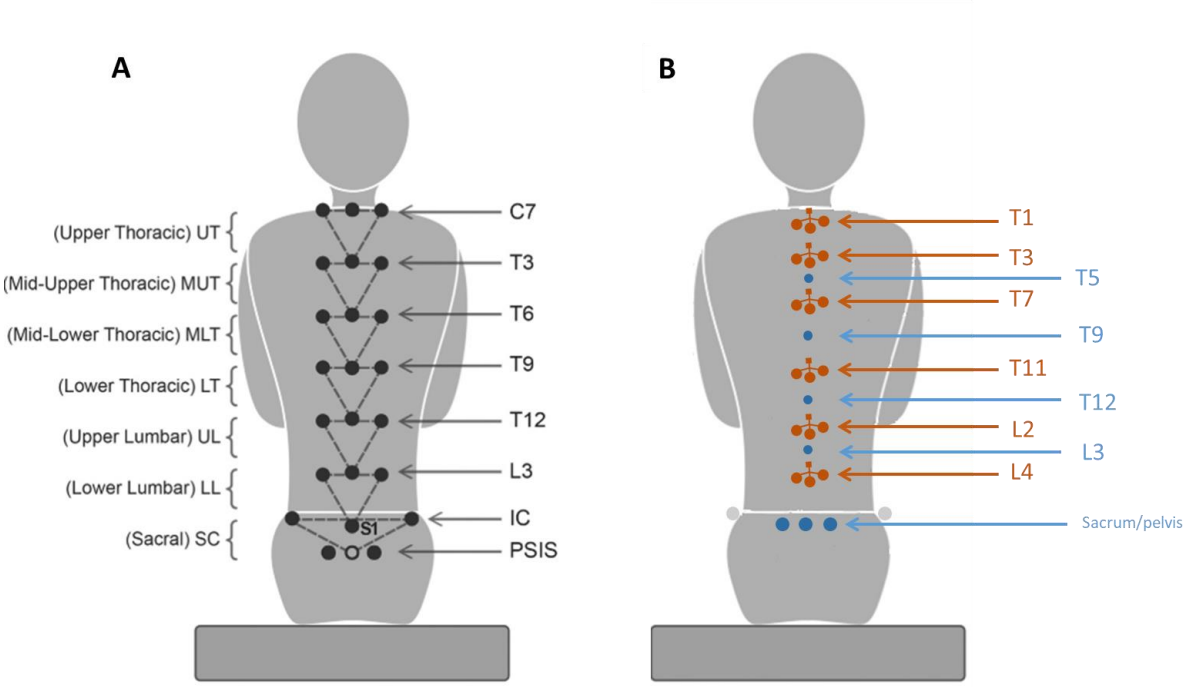

Figure 63: (**A**) Skin marker protocol of Mahallati et al (2016) which was used to estimate the kinematic effects of probabilistic imposed STAs. (reprinted and modified at the courtesy of the author.) (**B**) Skin marker protocol of Overbergh et al. (2020) (Modified image from Mahallati et al. (2016)) (orange: marker cluster, blue: single marker, grey: two anterior pelvis markers).

Appendix 2: Pre-vs. post-operative difference in ROM during maximal forward flexion.

Table 35: Pre-vs. post-operative difference in ROM during maximal forward flexion. A negative differential value indicates a post-operative ROM reduction compared to the pre-operative ROM. Subjects are sorted by increasing fusion length as described in Table 32.

Subject	T1-SPI ROM (°)			PT ROM (°)		
	Pre-op	Post-op	Difference	Pre-op	Post-op	Difference
1	67.1	48.3	-18.8	59.6	44.6	-14.9
2	54.6	32.6	-22.0	42.9	29.3	-13.6
3	79.0	43.9	-35.1	50.9	34.8	-16.1
4	67.5	36.1	-31.3	46.7	30.0	-16.7
5	69.6	22.9	-46.7	57.0	19.0	-38.0

General Discussion

The general objective of this dissertation was to develop a modeling and evaluation platform and illustrate its potential to improve our understanding of pathological spine kinematics during dynamic activities of ASD patients. Therefore, **the first objective** (Chapter 1) was to develop and validate a new image-based, subject-specific modeling method that allows to integrate the geometry of spinal deformity in generic musculoskeletal (MS) models and thus enable the use of MS modeling and associated kinematic analyses of IV joint motion in ASD. **The second objective** (Chapter 2) was to quantify the reliability of such kinematic analyses based on the newly developed subject-specific modeling method. **The third objective** (Chapter 3) was to (A) introduce novel methods to comprehensively quantify effects of spinal deformities on spinal kinematics during forward trunk flexion and (B) to evaluate relations with routinely used, clinical spino-pelvic parameters, vertebral body deformity, and self-reported health related quality of life (HRQoL) in a pilot population. Lastly, **the fourth objective** (Chapter 4) was to evaluate the modeling and evaluation platform, to measure pre- to post-operative changes in spine kinematics, focusing on (1) the changes in *global* spinal motion during maximal voluntary trunk flexion, pre- and post-operatively, as well as (2) the *vertebral (or local)* motion of the unfused vertebrae.

This general discussion section will discuss (1 - Specific conclusions) the specific objectives in the light of the conclusions from the associated individual chapter, followed by (2 - General discussion and critical reflections) further considerations in the light of the overall work and associated suggestions for future research.

Specific conclusions

Objective 1: Develop and validate a new subject-specific modeling method that allows to integrate spinal deformity in generic musculoskeletal (MS) models and thus enable the use of MS modeling and simulation in ASD

Musculoskeletal modeling in ASD is hindered by the combination of deformed vertebral geometry, spinal malalignment and difficult accessibility (Gonnella et al., 1982) of sufficient vertebral anatomical landmarks. As a result, conventional marker-based scaling inherently fails to provide sufficient information to accurately accommodate a generic model to a specific spinal deformity (Methodological gap). In addition, palpation errors are known to result in inaccurate spinal kinematic simulations (Schmid et al., 2015). With the presence of spinal deformities, a further increase of palpation errors of typically-used anatomical landmarks can be expected. Severijns and Overbergh et al. (2021) reported that on average 37% of the placed markers were incorrectly palpated in ASD patients. As a result, generic models combined with marker-based scaling cannot be used for the evaluation of dynamic motion in ASD patients. These specific limitations need to be overcome to unlock the potential of non-invasive, *in vivo*, musculoskeletal simulations for further advancing our biomechanical understanding of the dynamic functional abilities of ASD subjects.

In this work, we presented the first validated biplanar radiography-based method to generate subject-specific spino-pelvic, MS models in ASD subjects that allow the inclusion of subject-specific bone geometries, the personalization of external skin marker locations and the personalization of the 3D weight-bearing spinal alignment. The accuracy of the latter is comparable to clinically used software for 3D reconstruction. In addition, marker-based kinematic accuracies were quantified semi-dynamically based on biplanar radiographs in an upright and bent pose of a patient. This resulted in average errors ranging between 0.9-1.8 mm and 2.9-5.6° for vertebral positions and rotations, respectively.

In conclusion, the use of this new modeling method enables accurate IV kinematic analysis of spinal deformity subjects, previously not possible.

Objective 2: Quantify the reliability of MS simulations for measuring IV joint motion in ASD based on the newly developed modeling method.

Although accurate, the modeling platform and the use of resulting subject-specific models to evaluate IV kinematics remains susceptible to variability from different sources of errors and user-dependent inputs. To improve the rigor and objectivity of the measured kinematics prior to interpretation, we therefore performed a complimentary analysis of the reliability of the modeling method and associated kinematic simulation results (Hicks et al., 2015; Schwartz et al., 2004). More specifically, we evaluated reliability in terms of **(1)** the overall test-retest repeatability; **(2)** the inter-operator agreement of spine kinematic estimates; and **(3)** the uncertainty of the calculated spine kinematics to operator-dependent parameters of the framework.

To evaluate **(1)** the overall repeatability, four ASD subjects and one control subject were included in a test-retest study with a two-week interval. At both time instances, subject-specific spino-pelvic models were created by a single operator and applied to evaluate IV kinematics in each subject during a forward trunk flexion motion. Next, **(2)** inter-operator agreement was evaluated by having three a-priori trained operators each create models of three ASD subjects and evaluate kinematics of the same forward trunk flexion motion.

The reliability of (1) and (2) was quantified using intraclass correlation coefficients (ICCs) of the range of motion (ROM) of conventional spino-pelvic parameters [lumbar lordosis (LL), sagittal vertical axis (SVA), thoracic kyphosis (TK), pelvic tilt (PT), T1-and T9-spino-pelvic inclination (T1/T9-SPI)]. LL, SVA, and T1/T9-SPI had an excellent test-retest reliability for the ROM, while TK and PT did not. Inter-operator agreement was excellent, with higher ICC values than test-retest reliability. These results indicate that operator-induced uncertainty has a limited impact on kinematic simulations of intervertebral kinematics during spine flexion, while test-retest reliability presented a much higher variability.

Lastly, **(3)** a Monte-Carlo probabilistic simulation evaluated the uncertainty of the intervertebral (IV) joint kinematics to operator variability for three ASD subjects. The definition of the IV joints was identified as the most sensitive operator-dependent parameter for the IV joint kinematics. Nevertheless, IV joint estimations still had small mean 90% confidence intervals (1.04°-1.75°). Although the current modeling and simulation method thus remains dependent on manual inputs of the operators and the associated variability, their effect on the kinematics was very limited.

As a result, it can be concluded that the modeling platform and its use for evaluating IV kinematics are both accurate and reliable.

Objective 3: Pilot novel methods to quantify effects of spinal deformities on spinal kinematics and investigate their relation with the currently available (clinical) parameterization of ASD patients.

Objectives 1 and 2, respectively, documented the accuracy and reliability of measuring IV joint kinematics in ASD patients with the novel modeling and evaluation platform. The resulting output data consists of a joint angle throughout time for each three DOFs of each of the seventeen IV joints in the thoracic and lumbar spine.

Because of the large between-subject variability of the spinal deformity and the large amount of data of 3D IV joint angles, interpretation as well as between-subject comparison of these spinal kinematics while taking into account the regional deformity of the spine is challenging and time-consuming. Therefore, we developed two novel parameters that quantitatively relate spinal kinematics to the local deformity: The spinal kinematic deviation index (SKDI) and spinal deformity engagement index (SDEI). Both parameters summarize the amount of *kinematic compensation*. Whereas the SKDI quantifies the out-of-plane joint motion during a monoplanar motor task; the SDEI quantifies the relative contribution of joints associated with deformed vertebral bodies to the overall spinal motion. These parameters were piloted in fifteen subjects (14 ASD, 1 control) during a maximal voluntary forward trunk flexion. Furthermore, the correlation of both parameters with current clinically-used, radiography-based parameters of adult spinal deformity was analyzed.

The pilot application of these novel parameters suggests that subjects engaging their deformed region, i.e. a high SDEI, are also more likely to have a higher kinematic compensation, i.e. high SKDI. Furthermore, the poor correlation of these novel, dynamic parameters with the currently used radiography-based parameters, suggests that the latter, i.e. static parameters, are not the sole determinant for the amount of spinal kinematic compensation (i.e. SKDI) during forward trunk flexion. Indeed, the presence of a deformity does not necessarily elicited kinematic compensation in our pilot cohort. Rather, a motion strategy engaging the deformed region seems to be a prerequisite for kinematic compensation.

In extension to **Clinical gap 1**, the subjective nature of the currently performed functional evaluation, **Clinical gap 2** focused on the limited representativeness of quantitative radiographic evaluations for dynamic spine function in ASD. In summary, this work confirmed that, contrary to the conventional, static radiographic evaluation of ASD patients, the newly developed modeling platform and hereon-based novel parameters such as the SKDI and the SDEI could have potential to provide unique insights in the kinematic characteristics and functional impact of this pathology and its treatment. As such, they can complement the predominantly static radiographic assessment of ASD as currently performed in clinical practice.

Objective 4: Evaluate the modeling and evaluation platform to measure spinal kinematics during trunk flexion before and after spinal fusion surgery in ASD: an exploratory study.

Clinical gap 3 introduced the currently high complication and revision rates of ASD surgery. The literature has suggested this to be related to a lack of functional information in the current surgical decision-making. Additionally, patients' expectations in terms of post-operative functional improvements often importantly exceed the ones subjectively experienced post-operatively (Ryu et al., 2021; Yoo et al., 2019). Besides the evaluation of IV kinematics before surgery (Objective 3), there thus also seems to be a need for post-operative evaluations.

The aim of this work was to evaluate the modeling and evaluation platform to measure pre- to post-operative changes in spine kinematics. More specifically, we aimed to evaluate (1) the changes in *global* spinal motion during maximal voluntary trunk flexion, pre- and post-operatively, as well as (2) the *vertebral (or local)* motion of the unfused vertebrae. Secondary to these aims, this study provided an opportunity to evaluate the impact of soft tissue artefacts (STAs) on the accuracy of marker-based spinal kinematics as the erroneously measured motion at the instrumented, and therefore immobile, IV joints.

All subjects of our pilot population (n=5) presented with (1) a reduced global spinal and pelvic ROM during trunk flexion after surgery compared to their pre-operative motion. At a local level, (2) remaining unfused IV joints also demonstrated reduced ROM after surgery.

In addition, the average effect of STA on the measured IV joint kinematics was estimated to be 0.99°, assuming that physical motion is mechanically prevented in the fused vertebrae.

From a methodological perspective, this first exploration of post-operative modeling and kinematic simulations identified three pitfalls. Firstly, modeling was complicated due to hindered visibility caused by the surgical instrumentation. Second, the marker protocol requires modifications in post-operative situations. Lastly, the model requires modification to the definition of its joint constraints to accurately account for the mobility reduction due to the spinal fusion.

This study presented the first *in vivo* spinal STA analysis, evaluated using subject-specific models. This work illustrated limitations and potential opportunities for the use of subject-specific MS models in post-operative ASD patients by quantifying pre- to post-operative changes at the level of global spino-pelvic kinematics as well as at the local IV level of joints without instrumentation. Although investigations using larger study cohorts are clearly needed, these pilot results suggest that spinal fusion surgery reduces the global spinopelvic ROM as well as at the ROM at the level of non-instrumented IV joints.

General discussion and critical reflections

This general discussion will cover four main topics. First, this section will discuss the crucial role of biplanar imaging for bridging the Methodological gap that limited modeling and simulation approaches in ASD. Secondly, this section will provide a systematic overview of the remaining sources of error and uncertainty associated with the newly developed workflow and their effect on the spinal kinematic measurements. Third, we will suggest possible pathways for clinical translation of the workflow and spinal kinematics in the clinical decision-making process. Lastly, we will provide perspectives for future research as well as more generic applications of the technical developments in this work.

Topic 1: Biplanar radiographic imaging is key for subject-specific modeling in ASD patients

Motion analysis has recently gained increasing interest to provide unique access to previously unobtainable functional data in spinal deformity (Diebo et al., 2018). However, to understand the complex interaction of spinal deformity and motion, advanced analyses that include detailed assessment of IV joint motion are needed. While invasive bone-pin and continuous irradiation studies have been performed on a small number of healthy subjects (section *'Measuring spinal kinematics'* on p. 25), these techniques are ethically not applicable in larger clinical studies or routine clinical practice. However, as demonstrated in this work, 3D segmental IV motion can also be obtained by combining 3D motion analysis data with image-based, MS modeling. Motion analysis offers great potential due to its non-invasiveness and its potential for routine use, as demonstrated by the integration of the technique in routine assessment of cerebral palsy gait dysfunction and its consequent impact on clinical decision-making. **However, technical limitations have thus far prevented the use of MS models to measure in vivo spinal kinematics in the presence of a spinal deformity.** As described in the introduction (Methodological gap), the use of conventional marker-based scaling of generic models fails to create a representative model for a spinal deformity subject. Therefore, other techniques should be introduced for personalizing MS models in ASD. In particular, the spinal malalignment and skin markers position need to be integrated in the model, before combining it with 3D MOCAP to accurately measure in vivo IV kinematics. This section will (A) motivate the use of biplanar radiographic imaging to create subject-specific models in ASD but also (B) discuss the limitations thereof on the modeling workflow.

A. Unique contributions of biplanar imaging to the subject-specific modeling workflow

Biplanar radiographic imaging played a key role throughout this work because of its opportunities to provide the required subject-specific information for the creation of accurate spino-pelvic MS models in ASD. More specifically, the EOS Imaging system (EOS Imaging, Paris, France) was used in this work (section *'Medical imaging'* on p. 19). Interesting features of this imaging technique include its ability to simultaneously obtain a coronal and sagittal, full body, weight-bearing radiographic image of a patient, while only using about 50-80% of the radiation of classic x-ray imaging (Figure 4 on p. 21) (Melhem et al., 2016). To put this reduction in radiation in perspective, a low-dose, full-body, EOS acquisition has been shown to require 800-1000 times less absorbed radiation compared to a typical CT scan used for volumetric 3D reconstruction (Illes et al., 2012). However, in the context of this work it is more important to note that the synchronous, spatially calibrated acquisition of such a pair of 2D images allows 3D reconstructions to be generated of a subject's spinal alignment (Souza and Alves, 2014). To further motivate the use of biplanar radiographic imaging, we will (1) briefly summarize the specific reconstruction principles and (2) discuss how we exploited the practical advantages of the imaging system towards subject-specific MS modeling and simulation in ASD.

1) The imaging system has proprietary software (sterEOS, EOS Imaging, Paris, France) to perform 3D reconstructions of skeletal geometries for clinical measurements making use of statistically deformable models (Illes et al., 2012). Also alternative tools have been published that use biplanar radiography reconstruction of the spine (Barba et al., 2021; Bassani et al., 2017a). However, to the best of our knowledge none of these are suitable for subject-specific musculoskeletal modeling in ASD patients as they fail to adequately incorporate existing bony deformities and subject-specific malalignments. Therefore, a generic biplanar image processing platform was developed as described in Chapter 1. As a first underlying principle, it allows reconstruction of the 3D landmark position based on their identified location in both 2D images, i.e. **2D to 3D reconstruction** (Figure 64A-C). Additionally, 3D anatomical shapes (e.g. vertebrae or pelvis) can be projected onto the 2D x-ray images (using a digitally reconstructed radiograph principle) allowing their projection to be simultaneously registered with the actual images, i.e. **3D to 2D registration**, thereby obtaining their 3D position and orientation (Figure 64D). Both reconstruction principles were exploited in the current work to create a total of fifteen subject-specific spino-pelvic models: First, the CT-segmented 3D bone geometry of each vertebra was simultaneously registered onto both radiographs acquired in the EOS Imaging system, thereby reconstructing the spinal alignment in its weight-bearing upright position. Secondly, because the patients were imaged while already wearing the skin markers for the motion analysis, the spatial relation could be determined between individual *actual* skin marker and the underlying bony anatomy as reconstructed in the first step. This spatial relation then determined the corresponding *virtual* marker definition in the model. In effect, this allows for virtual subject-specific marker-definition, thereby correcting for the error between the ideal marker placement as described in the marker protocol and the effective marker placement as performed by the physiotherapist. When combined, both these steps solved the failing marker-based scaling and initiation step (as described in section *'Challenges for use of musculoskeletal models and simulation in adult spinal* deformity*'* on p. 34) previously limiting the use of generic models in ASD.

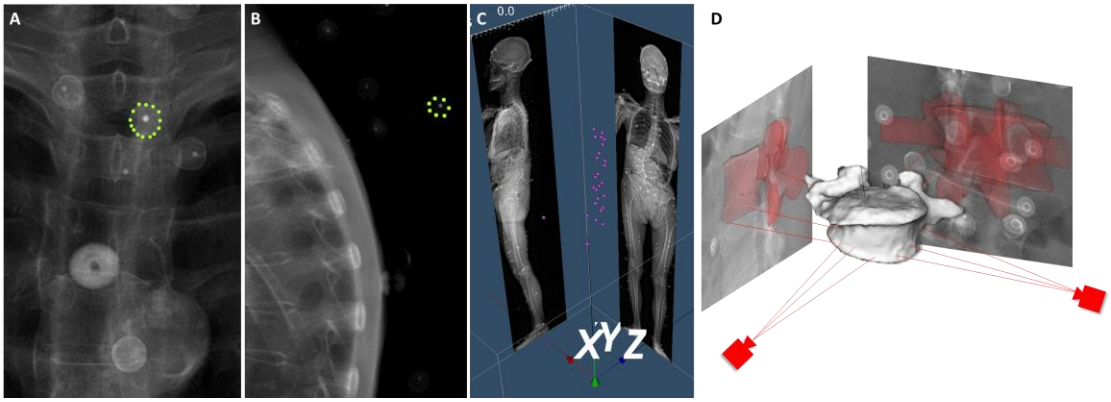

Figure 64: (**A-C**) Illustration of the **2D to 3D reconstruction** principle applied to the reconstruction of a skin marker to the 3D biplanar imaging space. The manual delineation (green points) of the marker in the (A) coronal and (B) sagittal image, followed by an ellipse fit, determines the positon of that marker (pink spheres) in the (C) 3D biplanar imaging space. Small metal spheres were inserted in the center of the skin markers to enhance their visibility on the radiographic images. The same procedure can be used to reconstruct the 3D location of an anatomical landmark, provided it can be unambiguously identified in both images. (**D**) Illustration of the **3D to 2D registration** principle. The mesh of a bone geometry (L3 in this example) is projected back onto the radiographic images, taking into account the intrinsic fan-beam characteristics of acquisition. Upon repositioning the geometry in the 3D space, the 2D projections are updated so a visually pleasing match can be achieved.

2) The specific design and acquisition aspects of the EOS biplanar imaging system allowed weight bearing and free positioning of the subject, which as will be explained below, allowed its use in combination with motion analysis. This biplanar imaging system has a half-open cabin space, making images of the subject in an upright, weight-bearing, position, with maximal dimensions of 170 cm high and 45 cm wide (Figure 4 on p. 21) (Illes et al., 2012). Compared to conventional x-ray imaging, the patient is not required to be positioned against a flat-panel detector (both lying and upright standing systems exist) but can be positioned freely and upright in the cabin space. This allowed us to include the skin markers in the images, as the back is not touching the flat-panel detector. Furthermore, the ability to obtain images with the subject in an upright standing, weight-bearing position is advantageous because of the large discrepancy between supine spinal alignment and spinal alignment during functionally and clinically relevant activities of daily living (Figure 65). Moreover, alternative subject-specific MS modeling tools using for example MRI for lower limb modeling (Scheys et al., 2011b), require the markers to be outlined with ink on the subject's skin, and to be replaced with radio opaque indicators, because of the lying position of MRI. This approach would be unfeasible to also capture the orientation of marker clusters, thereby limiting the definition of subject-specific markers in the model to the individual markers only.

Figure 65: Illustration of the difference in spinal alignment between an upright and lying position. Here, a patient's 3D spinal alignment as recorded in a lying position through CT (white) superimposed on the patient's alignment in an upright, load-bearing, position during biplanar radiographic imaging (multi-colored) (the pelvis of both models were matched). Salem et al. (2015) reported significant changes in the spinal alignment between a standing and lying position in asymptomatic subjects.

Exploiting 1) and 2), we could take advantage of the 3D approaches as the images were taken in free patient-positioning conditions. Indeed, the simultaneous assessment of the coronal and sagittal image eliminates an important patient-positioning prerequisite for conventional radiography used for clinical assessment, where the coronal and sagittal images are evaluated separately. We illustrate this patient-positioning prerequisite as follows: The biplanar radiography system has a half-open cabin allowing free positioning. However, the lack of guidance from a flat-panel detector introduces the disadvantage that patient-positioning needs to be adequately aligned with the patient's anatomical planes, i.e. *in-plane* acquisition (Figure 66A). Alternatively, as illustrated in Figure 66B, *out-of-plane* acquisitions can cause large errors on single-plane radiographic spino-pelvic parameterization. While patient-positioning thus causes variability in 2D radiographic parameterization, it does not affect modeling because the 3D reconstruction uses the sagittal and coronal image simultaneously. This free patient-positioning was further exploited when taking images with the subject in a bent position (for the validation of marker-based kinematics in Chapter 1) as this required the patient to be imaged *out-of-plane*, due to the dimensional constraints of the half-open imaging cabin.

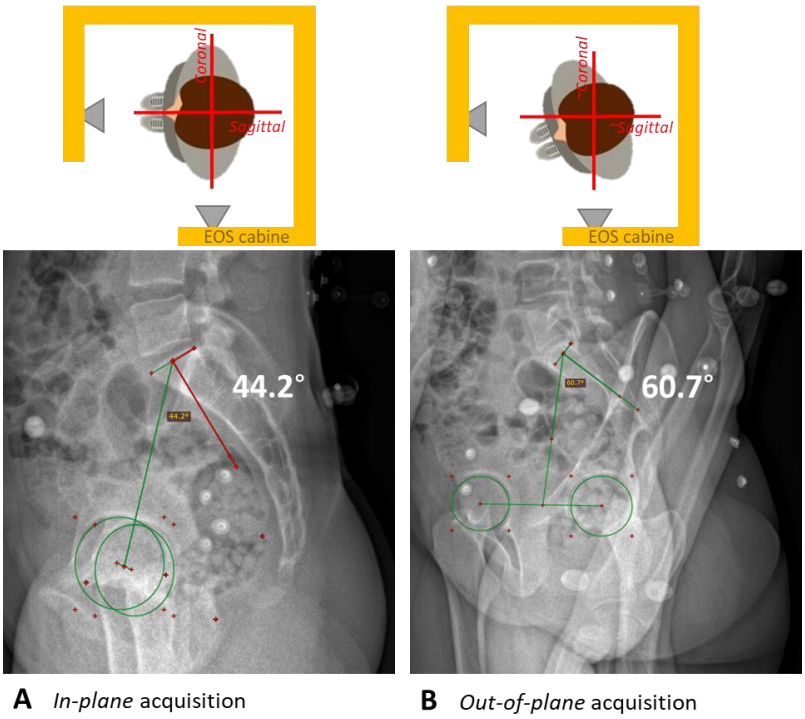

Figure 66: Measurement of the pelvic incidence angle on sagittal radiographic images suffers from inaccurate patient positioning. In (**A**) the patient's anatomical planes were aligned with the imaging planes, while in (**B**) the patient was rotated out-of-plane, causing the 2D pelvic incidence measurement to be more than 15° larger compared to (A).

B. Remaining limitations of the biplanar imaging modeling method

It is important to note that the two image reconstruction principles that underlie our modeling method (i.e. 2D to 3D reconstruction and 3D to 2D registration) are both affected by the **quality** of the images and the **ability to identify** anatomical landmarks and markers in the image itself. As will be outlined hereunder, these closely related aspects influence both the reconstruction accuracy (Chapter 1) and operator variability (Chapter 2) of the presented modeling workflow.

First, radiographic image **quality** can be affected by the presence of 1) soft tissue and 2) motion artefacts (Figure 67), as further discussed below. Indeed, image quality, and more specifically, blurring of the cortical edges primarily complicates the 3D to 2D registration (Figure 64D) as it relies on matching the outer, cortical edges of the vertebral bodies and/or anatomical landmarks located in cortical bone regions (e.g. spinal processes or pedicles), thereby limiting the modeling accuracy. This effect can be illustrated by comparing the radiograph of a healthy subject (Figure 67A) with a plastinated cadaver (Figure 67D) which was devoid of internal organs. The latter demonstrates clearly pronounced edges of outer cortical shell of the vertebrae.

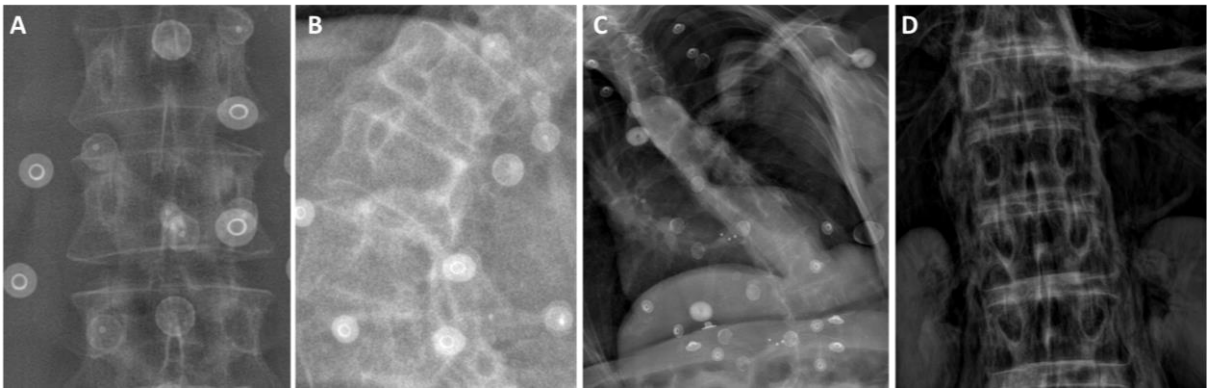

Figure 67: Inferior quality of radiographic imaging can complicate the reconstruction due to the (partial) obstruction of identifiable anatomical landmarks. Coronal radiographic image of (**A**) a healthy control subject and (**B**) an ASD patient. (**C**) Image of an ASD patient (female, 77 years old) with severe balance problems which prevented her to maintain a static pose for the duration of the acquisition (about 10-15 seconds) resulting in motion artefacts presenting as a blurring on the thoracic region. (**D**) Coronal image of the plastinated cadaver with clear visibility of the vertebral anatomical landmarks such as the spinous and transverse processes and vertebral endplates. (The image quality may have been reduced in the printed version of this dissertation)

1) Effect of soft tissues on radiographic images

Radiographic imaging is very suitable to image cortical bone, such as the outer layer of a vertebra. Briefly, this type of dense bone absorbs[5], and thereby blocks, more of the radiation being transmitted from the source to the detectors compared to trabecular bone or soft tissue, allowing easy differentiation due to sharp gradients in their respective grey values in the x-ray image. However, superposition of soft tissues (e.g. skin, fatty tissue and muscles) along an x-ray beam, reduces the amount of collected radiation at the detector, making the grey value gradients and tissue differentiation less clear. In such cases of poor bone visibility, the visibility can be improved, however, at the cost of increased radiation dosages. Indeed, because the dosage is constant over the full body area being imaged, certain areas with less problematic visibility will be irradiated more than minimally required. Currently, the radiology operator determines the radiation dosage based on body dimensions, but also minimizing radiation to sensitive areas such as the reproductive system or the thyroid according to the ALARA concept (as low as reasonably achievable) (Hui et al., 2016). In practice, the radiation dose is therefore kept low, causing a decrease in image quality for some areas. Alternatively, a recent update of the biplanar imaging system (FlexDose of the EOSedge system) allows to determine a modular radiation protocol, with reduced radiation safeguarding sensitive areas, and adequately imaging areas covered by a lot of soft tissue.

[5] The is expressed through the attenuation coefficient, describing the fraction of rays absorbed per unit thickness. This coefficient depends on the material of the absorber and the radiation energy.

2) Effect of motion artefact on radiographic images

A full-body acquisition using the EOS Imaging System takes about 10-25 seconds, during which the x-ray sources and detectors move in tandem from cranial to caudal (Illes et al., 2012). The exact duration of the image acquisition depends on the height of the patient and the radiation dose. Due to body sway or large subject movement during the image acquisition procedure, biplanar imaging can also be associated with so-called motion artefacts blurring the cortical bone edges of the image (Figure 67C) or, in more severe cases, create anatomical inconsistencies wherein a straight bone will appear curved (Simon et al., 2018). Likewise, such image distortions can complicate full-spine reconstructions or, in severe cases, make it impossible. In case the radiology operator observes significant motion artefacts, image acquisition is typically repeated while urging the patient again to stand still. For cases where patient characteristics complicate a stable posture, a handle bar is available in the cabin to provide more stability. However, this was not preferred as it is visible in the image.

Second, the **identification** of the anatomical landmarks or markers affects the accuracy of subject-specific model of an ASD patient. Indeed, to reconstruct the spinal alignment of an ASD patient from the biplanar radiographic images, an operator will extensively rely on the visual identification of specific anatomical landmarks. For example, the delineation of the superior and inferior vertebral endplate enables the operator to obtain an initial estimate on the position and orientation of a vertebra. Thereafter, more detailed landmarks, such as the pedicles on the coronal image or the spinal process on the sagittal image, can be used to fine-tune the reconstruction. Besides the previously discussed causes of reduced image quality, identification of anatomical landmarks or markers can be further reduced because of 1) complex spinal deformities, 2) obstructing anatomical structures, 3) a limited field of view and 4) the presence of metallic objects (e.g., surgical instrumentation, pacemakers or jewelry).

1) Complex spinal deformity

The complexity and variability of vertebral anatomy in ASD complicates anatomical landmark identification for the operator. To this end, subject-specific bone geometries (e.g. segmented from CT) are favorable to generic geometries as they facilitate 3D to 2D registration (Figure 68). More specifically, thanks to detailed CT imaging, theoretically a perfect match exists between the radiographic images and the identifiable anatomical landmarks of the projected CT-segmented anatomy (Figure 68). Currently, the modeling software does allow to non-uniformly scale generic vertebrae. However, in an ASD population the vertebrae are often affected by severe degeneration and deformation. Consequently, generic geometries (based on healthy subjects) may no longer be representative. In effect, the use of subject-specific, CT-segmented anatomies is currently a prerequisite for accurate modeling in ASD (Implications thereof are further elaborated in "*Topic 3: Suggestions for clinical translation*" on p. 191). Furthermore, the complexity of the spinal deformity itself can impact the performance

of 3D to 2D registration of the spinal alignment reconstruction. Here, due to the vertebral body deformations, the operator may have difficulties to interpret the 2D projection of the vertebrae on radiographic images.

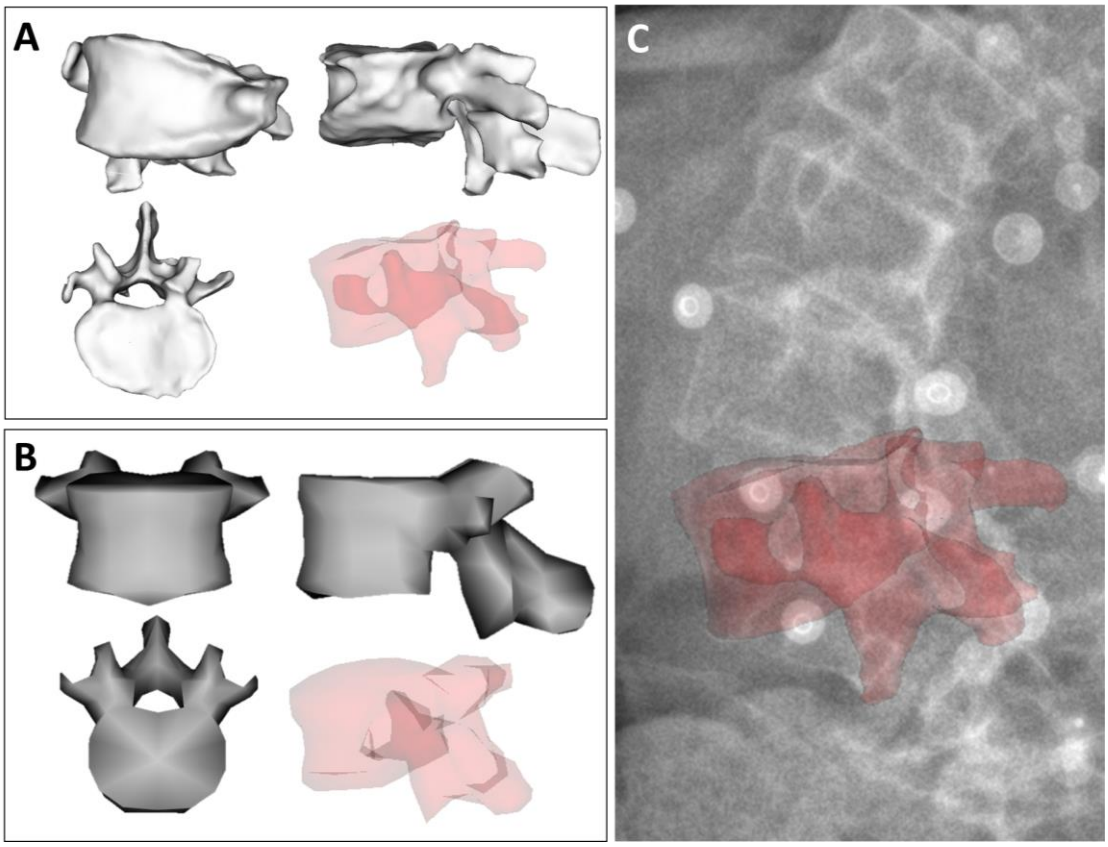

Figure 68: (**A**) Example of a CT-segmented 3D vertebral geometry of an ASD patient (L3 vertebra) in the coronal, sagittal and transverse plane. (**B**) The generic version of the L3 vertebra used in original model of (Bruno et al., 2015a). Notably, the generic vertebrae suffer from a much lower resolution (expressed through the amount of triangles in the mesh) compared to the subject-specific vertebrae. However, making use of higher resolution geometries still requires them to be deformable. (**C**) The projection of the CT-segmented L3 vertebra onto the coronal radiograph.

Indeed, compared to the undeformed regions, the operators (Chapter 2) (subjectively) reported a higher difficulty to reconstruct the spinal alignment of strongly deformed regions in terms of the 3D positions and orientations of the individual vertebrae. A comparison of the operator variability, calculated for each of the three ASD subjects and the plastinated cadaver, partly confirms the increased difficulty the operators experienced when modeling the severe deformity of S3 in comparison to S1 and S2 (Figure 69). Contra-intuitively, the plastinated cadaver (P in Figure 69) also appears to have a relatively high operator variability when compared to S1 and S2. However, as explained in Chapter 2, this created model was the result of a training phase for two of the three of the operators who previously had no experience in spine modeling. Consequently, given this lack of experience, these created models are not fully

representative to assess an increased modeling difficulty due to the complexity of the deformity.

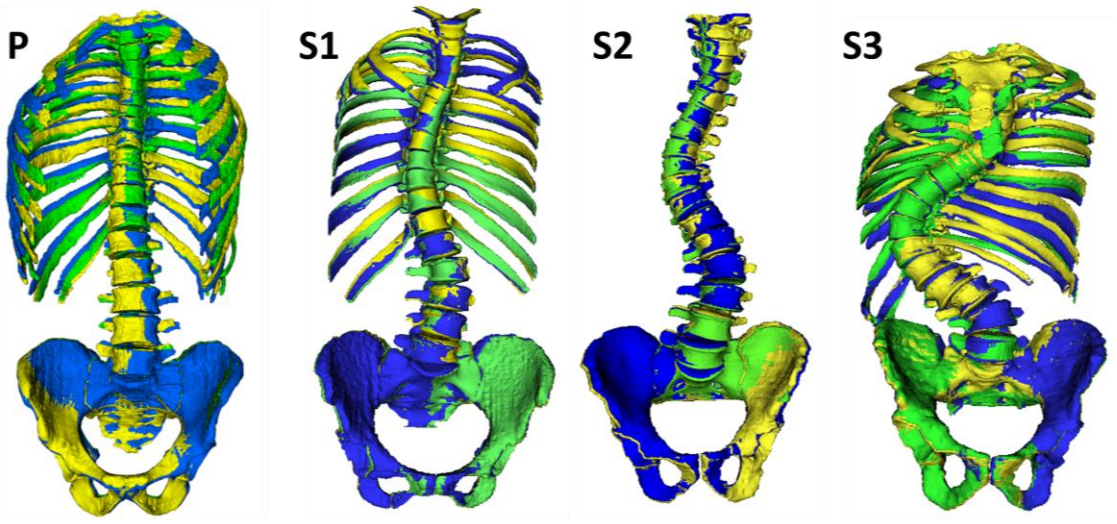

Mean (SD) abs. operator variability	Plastinated cadaver (P)	ASD subject 1 (S1)	ASD subject 2 (S2)	ASD subject 3 (S3)
Orientation X (°)	2.08 (2.07)	0.90 (0.81)	1.80 (2.12)	2.83 (2.20)
Orientation Y (°)	2.20 (1.83)	1.01 (0.77)	2.84 (2.36)	2.53 (2.02)
Orientation Z (°)	2.05 (1.48)	0.85 (0.69)	1.53 (1.50)	1.68 (1.65)
Position X (mm)	1.74 (1.39)	0.51 (0.55)	1.42 (1.12)	1.28 (1.04)
Position Y (mm)	1.21 (1.49)	0.28 (0.26)	0.86 (0.67)	1.27 (0.95)
Position Z (mm)	0.98 (1.03)	0.38 (0.37)	0.98 (0.78)	3.26 (3.45)

Figure 69: Superimposed alignment reconstruction from three operators (represented by a different color: yellow, blue and green). We noted an increased variability in alignment reconstruction with increased complexity of the deformity of the ASD subjects (S1 to S3). Contra-intuitively, the plastinated cadaver (P) which does not present with a spinal deformity also has relatively high variabilities. However, this reconstruction was part of the operator training where operators had no prior experience (Data from Chapter 1 and Chapter 2).

2) Obstructing anatomical structures

The superimposition of other structures such as the rib cage or upper extremities can reduce the visibility of, or even completely obscure, skin-mounted markers or anatomical bony landmarks required for the reconstruction. Firstly, the ribs will unavoidably affect the visibility of the thoracic vertebrae. Secondly, with regards to the upper extremities, patients were instructed to stand in the modified SRS position with their fingers on the clavicle and arms in 45° angle, which specifically aims at avoiding the arms superimposing the vertebrae, while minimally effecting the natural spinal alignment (Horton et al., 2005). Thirdly, specifically in the coronal image, skin-mounted markers tend to suffer from a reduced visibility due to the superimposition of cortical bones and soft tissue. To ensure accurate identification on the images, small metal marbles were inserted in the markers (Figure 70). We recommend this modification as the inserts have higher radiation attenuation coefficients compared to the plastic markers or bone and soft tissue, which allows easier recognition in the images.

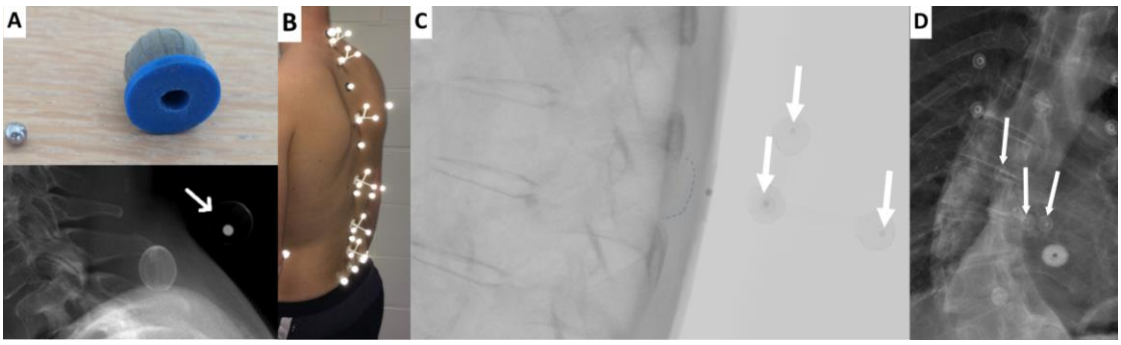

Figure 70: (**A**) Small metal marbles have been inserted into the retroreflective skin markers. (**B**) Their high attenuation coefficient effectively blocks the radiation, increasing its visibility on the radiographs. Although the spherical outline of the skin marker is most often visible in (**C**) the sagittal radiographic image, the metal sphere helps the identification in regions where markers are visually obscured, often the case in (**D**) the coronal radiographic image.

3) Limited field of view

Disadvantages of the narrow cabin design of the EOS Imaging System include the need for adequate patient-positioning (previously discussed on p. 168) by the radiology operator and the occasionally insufficiently wide field of view (FOV) (45 cm wide x 170 cm high). Especially taller subjects or subjects with a high body mass index (BMI) may not be fully captured in the image. Typically, a very low dose pre-scan allows the radiology operator to verify correct patient positioning as well as proper visibility of all skin markers on the back before taking the actual image. Prioritizing markers on the back, sometimes, unavoidably caused an anterior pelvis marker to fall outside the FOV. During an anteroposterior (AP) and left-right (LR) acquisition (referring to the path the x-ray beams follow though the body) the left anterior pelvis marker can fall outside the field of view in the coronal image due to the fan-beam method used in the EOS imaging system. However, in case the subject was rotated out-of-plane, the right anterior pelvis marker will be outside the field of view. Loss of a pelvis marker occurred in eight subjects included in this dissertation. In such cases, only four instead of five markers were visible on the pelvis. Nevertheless, this is still sufficient for accurate marker-based tracking. Additionally, a recently released update of the EOS Imaging System, the EOS edge, has an open cabin and allows a wider field which will likely eliminate this issue (the exact image dimensions were not publicly available at the time of this dissertation).

4) Metallic objects

Finally, metallic objects in the image block almost all radiation from the detector and thereby visually obstruct important bone edges or the identification of landmarks. Therefore, subjects were asked to remove any jewelry potentially blocking the view of the spine. Often however, this cannot be avoided. For example, when creating post-operative models (Chapter 4) the presence of metallic surgical instrumentation (Figure 71) causes visual obstructions and metal artefacts (e.g. scattering) in the images.

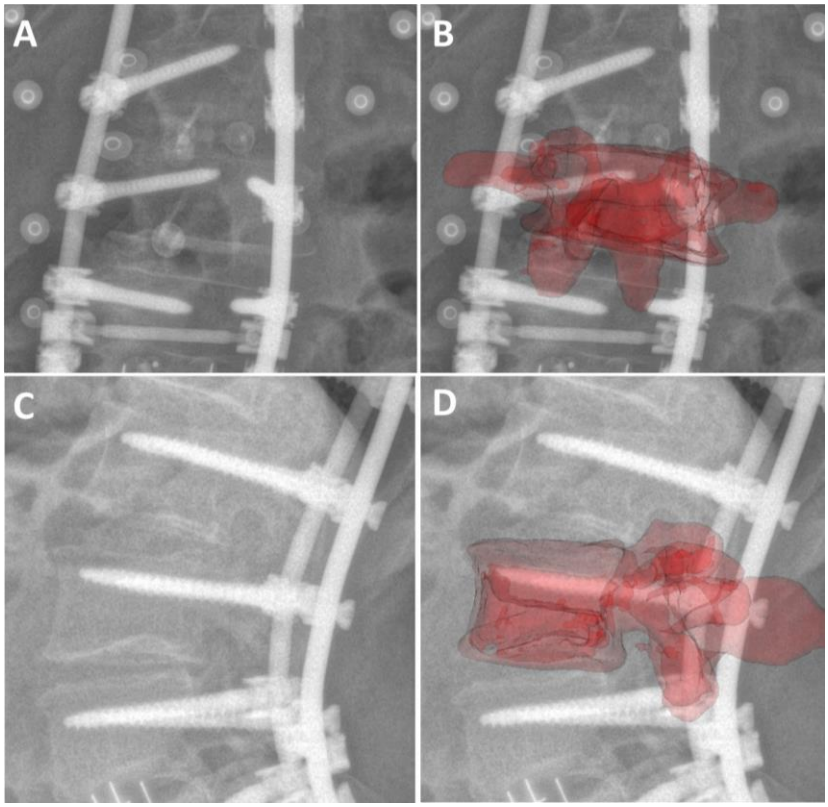

Figure 71: Although the quality of radiographic imaging is only limitedly compromised by metal artefacts due to the surgical instrumentation, they can obscure anatomical landmarks that normally aid in the reconstruction of the alignment. This image shows the (A) coronal and (C) sagittal radiographs of a patient six months after spinal fusion surgery and again with their superimposed vertebral geometries (B and D, respectively). (Image quality may be lower in the printed version of this dissertation.)

In summary, the unique characteristics of the biplanar radiographic imaging technology allowed, for the first time, to create subject-specific MS models for ASD patients, integrating both subject-specific spinal deformity and skin marker placement. Although the use of biplanar imaging for modeling is associated with some specific limitations, it was key to enable detailed motion analysis of spinal kinematics in ASD patients.

Topic 2: Error and variability in the workflow affect the accuracy and reliability of the spinal kinematics

Associated with the introduction of the novel workflow, developed in this work, it is imperative to verify the output results both in terms of accuracy and reliability to improve their objectivity and rigor, prior to clinical interpretation (Hicks et al., 2015; Schwartz et al., 2004). In support thereof, Figure 72 provides an integrated overview of the entire workflow developed from patient data collection, over data processing (mainly the subject-specific modeling method) to the analysis of the spinal kinematics.

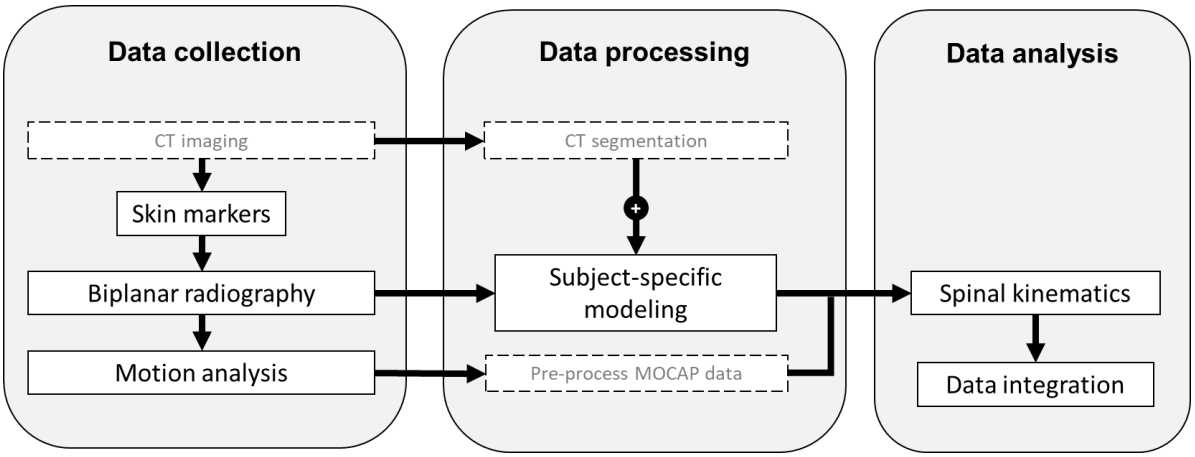

Figure 72: This overview summarizes the step-wise workflow developed in this dissertation. In the first panel, data on the subject is collected: After CT imaging, skin markers are attached to the subject according to the predefined marker protocol. Thereafter, while still wearing the markers, the subject is transferred to the biplanar imaging system to take the radiographs. Finally MOCAP data is recorded in the motion lab. The second panel summarizes the data processing, performed by the researcher. This includes CT segmentation which is required for subject-specific modeling; and pre-processing the MOCAP data (labeling, cropping the trial and converting for compatibility with OpenSim). In the final panel, the subject-specific model and pre-processed MOCAP data are used to perform inverse kinematics (OpenSim), obtaining continuous joint angles (and translations) for each DOF defined in the model, allowing further analysis. Items in dashed boxes are shown for completeness but will not be discussed in this section, as they have been discussed previously or are outside the scope of this work: The acquisition of the CT images (part of the clinician's medical exam), biplanar radiography and CT segmentation (both already extensively discussed in Topic 1), and pre-processing MOCAP data (a standardized process) will not be discussed (again).

This section aims to comprehensively evaluate and discuss the various steps in the developed workflow in specific view of their respective kinematic (A) accuracy and (B) reliability, finally (C) summarizing suggestions for the prioritization of future workflow improvements.

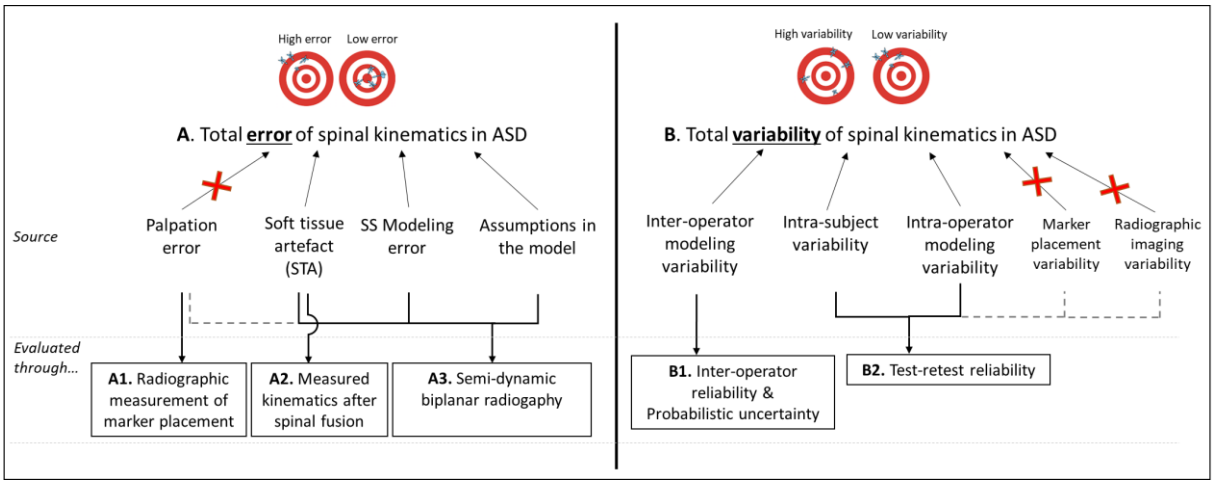

Figure 73: Schematic of the sources of error/variability contributing to the total error/variability of spinal kinematics in ASD, and the respective evaluation methods used to quantify them. Due to the specific design of the workflow certain sources such as 'palpation error', 'marker placement variability' and 'radiographic imaging variability' are not affecting the spinal kinematics (as indicated by the red cross), yet there are still shown for completeness.

The outline of this section is illustrated in Figure 73. Firstly to evaluate accuracy, the contribution to the total error of spinal kinematics (**A**) was evaluated using three methods (i.e. the radiographic measurement of marker placement, the measurement of kinematics after spinal fusion and a kinematic evaluation through semi-dynamic biplanar radiography, respectively referenced in Figure 73 as A1, A2 and A3 and detailed below), which quantified the impact of four sources of error (i.e. palpation error, soft tissue artefact, subject-specific modeling error and assumptions in the model) identified within the workflow. Secondly to evaluate uncertainty, the contribution to the total variability of spinal kinematics (**B**) was evaluated using two reliability methods (i.e. operator-reliability and test-retest evaluations, respectively referenced Figure 73 as B1 and B2 and detailed below), quantifying the impact of five sources of variability (i.e. inter- and intra-operator modeling variability, intra-subject variability, marker placement variability and radiographic imaging variability) identified within the workflow.

A. Total error on spinal kinematics in ASD

The error (or inaccuracy) of our workflow is defined as the difference between the measured and the actual IV joint motion. As indicated above and in Figure 73, we used three evaluation methods to assess four specific sources of error, each further detailed below.

A1. Palpation error evaluated through radiographic measurement of marker placement

The physiotherapist attaches the markers on the subject's skin relying on external palpation and visual inspection of the anatomical landmarks (Figure 74A). The use of biplanar imaging of subjects instrumented according to the marker protocol provides a unique ground truth to quantify associated palpation errors in ASD subjects. Therethrough, the 3D distance between the *actual* placement of skin markers and their *correct* position can be quantified; with the latter being defined as the skin position closest to the targeted bony landmark (Figure 74B).

Figure 74: (**A**) Image of a physiotherapist palpating the spinal processes through the skin before placing the markers on the subject according to the predefined marker protocol. (**B**) Illustration of the calculated palpation error. The center of the base of a skin marker is considered as the actual marker position *(C)*. The optimal marker position is identified by fitting a circle on the sagittal image. The center point of the circle is placed on the anatomical landmark which the corresponding marker aims to track, i.e. *(A)* the most posterior point of the spinal processes. The first point where the circle reaches the skin surface *(B)*, representing the shortest distance between the landmark and the skin, is considered to be the optimal marker position. The distance *(D)* between the actual and optimal position is the palpation error (Severijns and Overbergh et al., 2021).

Specifically for our marker protocol (introduced in Chapter 1), Severijns and Overbergh et al. (2021) quantified the 3D palpation error in 20 ASD subjects and 10 control subjects. The mean (maximal) 3D palpation error in ASD and control subjects measured 15.5 mm (25.4 mm) and 14.0 mm (19.4 mm), respectively. Furthermore, this palpation error resulted in an incorrect level identification for 37% of the placed markers in ASD patients. This indicates the necessity to subject-specifically correct marker placement prior to analyzing IV kinematics in ASD. Thereto, this PhD work similarly exploited the unique, simultaneous availability of ground truth anatomical landmark positions and the correspondingly defined skin-mounted marker positions in biplanar x-ray images. Indeed, as described in "*Topic 1: Biplanar radiographic imaging is key for subject-specific modeling in ASD patients*", erroneous placement of the

markers is accounted for in the model based on the relative 3D distance between both. However, a remaining limitation lies in the need for the actual marker to have been placed within reasonable proximity of the associated anatomical landmark. Although the position of the virtual marker on the MS model is defined subject-specifically to guarantee adequate marker-based actuation of the model, the further the marker is placed from the targeted anatomical landmark, the less representative its recorded trajectory will likely be for the tracked vertebra. Yet, **the subject-specific definition of virtual markers effectively eliminates the influence of palpation error on the kinematics given that the markers were placed within reasonable proximity of the anatomies aimed to track**.

A2. Soft tissue artefacts evaluated through kinematic measurements after spinal fusion

All skin-marker based motion capture systems are subject to error originating from STAs. These are caused by the relative motion of the skin to the underlying anatomical structures, due to for example muscle contraction or inertial effects (Mahallati et al., 2016; Zemp et al., 2014). To evaluate their effect on the kinematics accuracy, Chapter 4 exploited the opportunity of motion analysis following spinal fusion to evaluate the effect of STA on the IV joint angles during forward flexion, using the developed subject-specific modeling workflow and dedicated spinal marker protocol. During the maximal voluntary trunk flexion motion, on average, a change of 0.99° degrees in the fixed IV joints was measured due to the presence of STA. It should however be noted that these values may not be fully representative of STAs of subjects in their pre-operative condition, as scarring tissue, the presence of instrumentation and reduced ROM could have an additional effect. To further improve our estimations of the effect of STA on spinal kinematics in ASD, dynamic medical imaging should be used while wearing the markers. Yet, **based on the results of this work one degree can be used as an upper bound on the accuracy of marker-based spinal kinematics due to STAs when using the developed workflow.**

A3. STA, subject-specific modelling error and assumptions in the model evaluated through semi-dynamic biplanar radiography

On top of the previously discussed STAs, also the introduction of error during subject-specific modeling and assumptions in the model are limiting the accuracy of spinal kinematics (Figure 73). To validate marker-driven, model-based simulation of movement, Hicks et al. (2015) suggest to compare the simulations to independent experiments. However, regarding IV joint kinematics in ASD patients, no studies were available that report IV joint kinematics in ASD. Additionally, the unique shape and motion pattern of each ASD patient precludes validation based on group-wise comparisons. Therefore, this work has turned to medical imaging to quantify the accuracy of marker-driven MS kinematic simulations (Chapter 1). More specifically, we performed a semi-dynamic validation using biplanar radiography in a bent positon (Figure 75), in which, in addition to the unavoidable STA, the effect of errors due to subject-specific modeling and model assumptions on IV joint kinematics were quantified (Figure 73). Using the model defined in an upright posture, a kinematic simulation of the bent position was performed only based on the 3D marker positions extracted from the bent image as input. This marker-driven simulation was then compared to a newly generated ground-truth model based on the images in the bent position. Unfortunately, this semi-dynamic approach, is only partially representative for the accuracy during true dynamic motion as it only considers two static postures, i.e. the initial (upright) and final (bent) position. As such, inertial effects of markers and soft tissue were indeed not considered. However, true dynamic validation either requires dynamic medical imaging (e.g. dynamic fluoroscopy (Breen et al., 2019)) or invasive bone-pins (see *section 'Measuring spinal kinematics'* on p. 25) which was beyond the scope of this work. Therefore, to date, we present the results of our semi-dynamic validation as our most complete evaluation of the overall workflow accuracy, reporting **mean marker-based tracking accuracies between 3.1–5.0 mm and 2.9–5.3° for vertebral positions and rotations, respectively.**

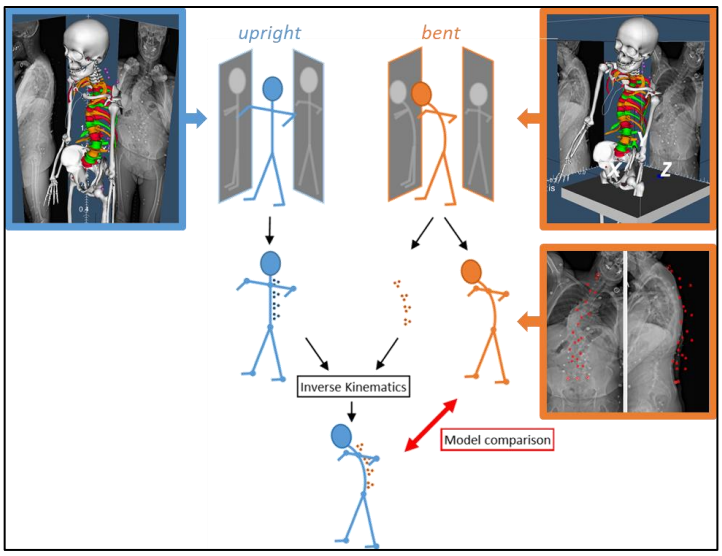

Figure 75: Evaluation of the marker-driven kinematic accuracy of MS models in ASD using semi-dynamic biplanar radiography.

As indicated in Figure 73, these error values arise from the modeling error, assumptions in the model and the previously described STAs. We further discuss the modeling error (A3.1) and assumptions in the model (A3.2) as individual sources of error below.

A3.1 Subject-specific modeling error

We quantified the accuracy of subject-specific modeling, reporting mean errors on the reconstructed vertebral positions and orientations of 0.71-1.59 mm and 1.25-2.27°, respectively (Chapter 1). These accuracy values were comparable to other clinically-used reconstruction software. However, as previously discussed (*"Topic 1: Biplanar radiographic imaging is key for subject-specific modeling in ASD patients"* of this discussion), this *in vitro* validation using a plastinated cadaver (Figure 76) was not fully representative for *in vivo* ASD subjects due to the differences in radiographic image quality and a priori knowledge of a healthy spinal alignment. More specifically, the cortical bone of the vertebral edges was easier to identify on the x-rays because the plastinated cadaver no longer had organs or a chest obscuring the view. Also, as discussed above, a healthy spinal alignment is intuitively easier to reconstruct as opposed to complex 3D malalignments in combination with vertebral deformations. In the future, this validation should therefore be repeated based on a more representative plastinated cadaver or an artificial, ASD-specific phantom ideally including deformed vertebrae, spinal malalignment as well as soft tissues. With regards to the modeling method, future improvements should also focus on reducing operator reliance, for example through automated image processing for the optimization of image registration (Aubert et al., 2019).

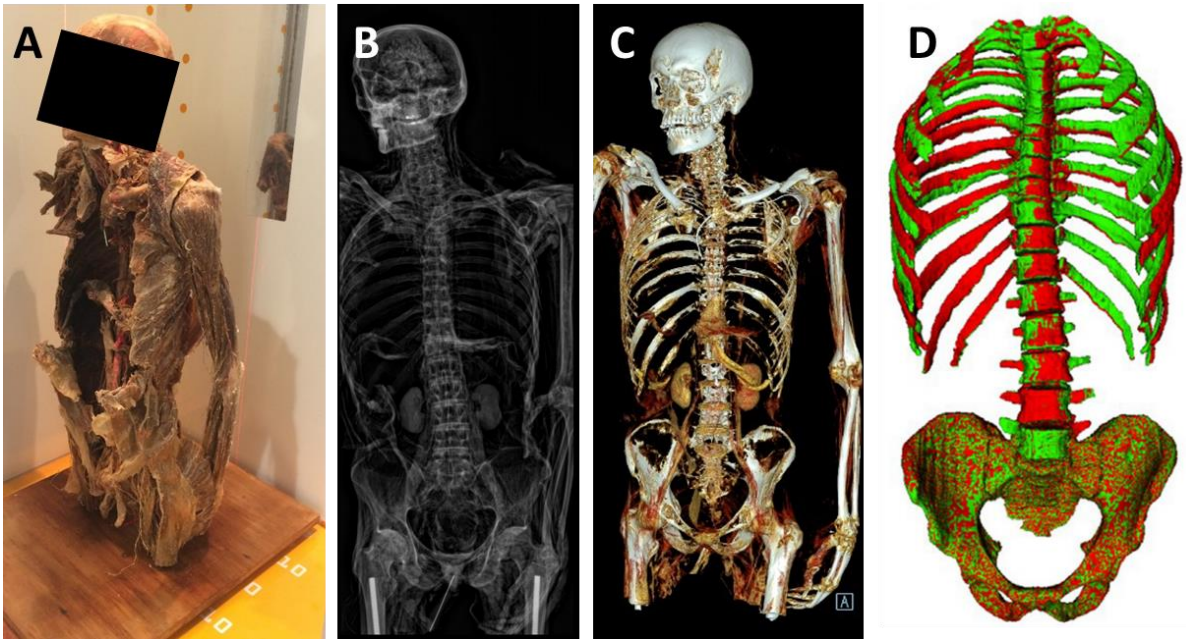

Figure 76: To create the reference data (e.g. CT or MRI) to quantify the accuracy subject-specific modeling should be taken simultaneously with the biplanar radiographic images to avoid changes in spinal alignment between acquisitions (as illustrated previously in Figure 65). As this was technically not feasible, we used a plastinated cadaver (Chapter 1), which would provide a constant/fixed spinal alignment for upright biplanar imaging and lying CT imaging. Image (**A**) shows the plastinated cadaver, devoid of organs and rigidly fixated in the spine, while being imaged upright in the biplanar radiography system, (**B**) the coronal x-ray image (sagittal image not shown here) and (**C**) a 3D rendering of the CT taken in a lying position. Finally, (**D**) shows the subject-specific model as created in the modeling method (red), superimposed on the ground truth CT segmentation (green).

A3.2 Assumptions in the model

As described previously (section *'Challenges for use of musculoskeletal models and simulation in adult spinal deformity'* on p. 34), practical limitations prevent us from placing sufficient markers on each individual vertebra. To describe individual vertebral kinematics based on a limited set of markers and prevent the system from being underdetermined during the inverse kinematics optimization, we were required to make assumptions in the model that limit the accuracy of the estimated kinematics.

Firstly, each IV joint was modeled as a three-DOF ball-and-socket joint, thereby assuming a fixed instantaneous axis of rotation (IAR). However, the true physiological FSU presents with six DOF as the IV disc is capable of 3D displacement, and thus has a mobile IAR (Bogduk and Twomey, 1997). Although this assumption thus removes 3 DOF for each vertebral joint in the model, it inherently limits the accuracy of the spinal kinematics as translation is not permitted and all intervertebral motion has to be expressed as rotations.

As a second required assumption for preventing under-determination of the system, kinematic interpolation was applied to obtain IV kinematics for joints in-between skin-marker tracked vertebrae (*'regions'* spanned by green vertebrae in Figure 77A). However, it is important to note that this interpolation was not defined on a subject-specific basis, but rather based on prior experiments in the literature on healthy subjects (Overbergh et al., 2020) as no such experimental data was available for ASD subjects. This could have negatively affected the accuracy of the IV joint kinematics. Moreover, this modeling assumption forced us to exclude *regions* of the spine that contained both fused and unfused vertebrae when determining spinal kinematics after spinal fusion surgery in Chapter 4. Similarly, in case of excessive rigidity at a specific IV level, for example due to ankylosing spondylitis (inflammation followed by new bone formation spanning the IV disc), IV motion would still be calculated although none was present in case kinematic interpolation values are not adjusted subject-specifically.

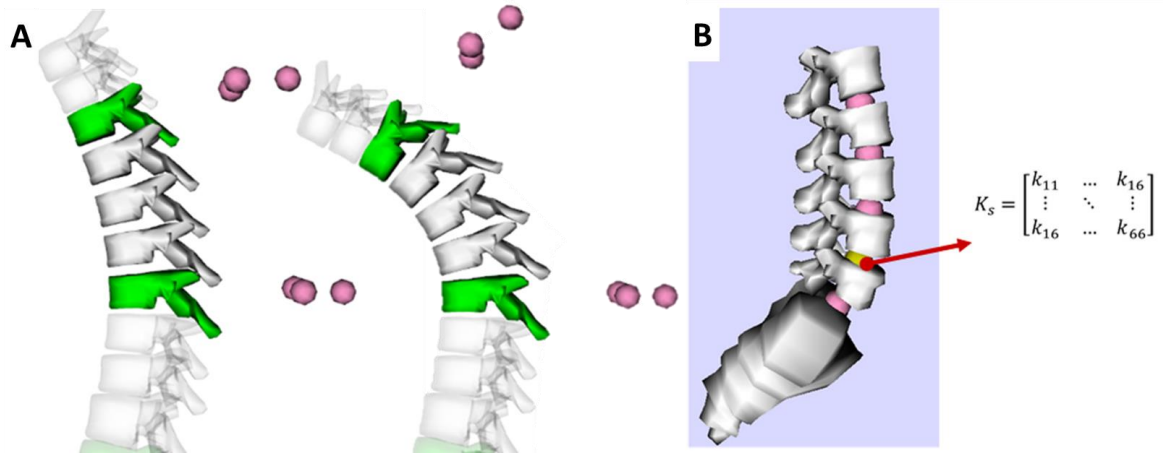

Figure 77: (**A**) Joint constraints (kinematic interpolation) implemented in the model interpolate motion over the segments within a group (defined as the set of IV joints spanned by kinematic fully determined vertebrae (green)) during the global optimization of the inverse kinematics. (**B**) In the work of Bruno et al. (2015b) IV joint stiffness matrices were defined in each of the lumbar joints.

Compared to both methods above, attempts have already been made in the literature to further increase the physiological accuracy of the IV joints in MS models of healthy subjects. A first approach integrates stiffness in the IV disc (Figure 77B) (Bruno et al., 2015b; Wang et al., 2020). Recently, through balancing the amount of DOFs in the thoracolumbar spine with joint constraints the physiological accuracy and marker error was optimized in healthy models (Alemi et al., 2021). However, degeneration of intervertebral discs, as in ASD, is known to alter its mechanical properties including its stiffness (Inoue and Orías, 2011). As a result, subject-specific stiffness values should be defined to increase subject-specificity and model accuracy. To this end, dynamic optimization approaches have been introduced in healthy subjects that solve spine kinematics through the calibration of the mechanical properties of the IV joint by requiring dynamic consistency (Wang et al., 2021). However, translating this research to the ASD population is still unexplored. Alternatively, medical imaging-based approaches could be implemented to determine subject-specific stiffness values. For example, based on MRI-based assessment of IV disc structure and degeneration (Benneker et al., 2005; Wijayathunga et al., 2019), a reduction of the interpolation value or increase of the stiffness could be implemented to reduce the contribution of degenerated and more rigid IV joints to the motion. Such information on IV stiffness could also be obtained from radiographic images of a subject in flexion/extension, lateroflexion and axial rotation (Berger et al., 2015). To conclude, such approaches have clear potential to even further increase the accuracy of IV kinematics.

B. Total variability of spinal kinematics in ASD

Human involvement in (biomechanical) measurements typically raises questions regarding the introduced variability in the process and, inversely, the reliability of the process' output. Also the workflow to measure spinal kinematics in ASD, presented in this work, is dependent on human interaction for the following steps (in reference to Figure 72): The physiotherapist placing markers on the subject, the radiology operator positioning the patient in the biplanar radiographic imaging system and the modeling operator. Lastly, also the subject being measured is a source of variability. Regarding the variability introduced by each of the human interactors, the modeling method was developed to primarily limit the influence of the physiotherapist and the radiology operator. As these have already been discussed in detail in section "*Palpation error evaluated through radiographic measurement of marker placement*" on p. 179 and section "*Unique contributions of biplanar imaging to the subject-specific modeling workflow*" on p. 165, respectively, these will not be discussed again in this section. Rather this section will further detail the reliability associated with the involvement of the modeling operator, and the subject being measured.

B1. Inter-operator variability in subject-specific modeling evaluated through inter-operator reliability testing and probabilistic uncertainty.

As mentioned in Topic 1 of this discussion, the method for reconstructing the spinal alignment relies on manual interaction of an operator (Figure 69). This introduces variability in reconstructed spinal alignment between trained operators that measure 0.552-0.739 mm and

0.96°-1.68° for the median body positions and orientations, respectively. Additionally, the variability of marker reconstruction was very small (median: 0.26 mm). Lastly, the median variability of joint definition was 0.566-1.058 mm and 1.16°-1.95°, for positions and orientations respectively. This variability in the reconstruction of spinal alignments, marker reconstructions and the joint definitions could likely be even further reduced in the future by increased operator training or eliminating variability in operator-dependent modelling steps through increased automation of the model creation procedures, as discussed above in section *"Subject-specific modeling* error*"* on p. 182.

When evaluating its effect on the kinematics in terms of spino-pelvic ROM parameters, the inter-operator agreement was excellent with ICC values ranging from 0.875 (TK) to (almost) 1 (LL, SVA, PT, T1-SPI, T9-SPI), showing a high to very high kinematic agreement amongst the three operators. However, as these sources of variability also affect the output in terms of IV kinematics, Chapter 2 further quantified the probabilistic effects of subject-specific spino-pelvic modeling uncertainty on IV kinematics in ASD patients through a Monte-Carlo probabilistic simulation. Inter-operator-dependent modeling parameters (i.e. the virtual markers, bodies and IV joint definition) were thereto sampled from their respective a-priori defined statistical distributions and combined to create a representative set of probable model variations. Using these models, we obtained **small mean 90% confidence intervals (1.04°-1.75°) for IV joint angles**. The operator dependency of the modeling workflow only has a small effect on the measurements of IV joint kinematics. This indicates the modeling method is highly reliable for kinematic analysis of spinal motion.

B2. Intra-subject variability in the execution of motion and intra-operative modeling variability evaluated through test-retest reliability.

The lack of consistency with which a subject is performing the tasks, i.e. intra-subject variability in the execution of motor tasks (Figure 73) in the motion lab, is a well-known source of intrinsic variability (Schwartz et al., 2004), and this will also impact the smallest detectable difference (as defined in Chapter 2) in spinal kinematics.

Indeed, in Chapter 2, a test-retest repeatability analysis quantified the combined intra-subject and intra-operator variability (Figure 73) of the entire workflow in spinal kinematics through repeated measurements over a two-week time interval. Our **test-retest reliability results, expressed as spino-pelvic parameters, were excellent (ICC $>$ 0.75)** and comparable to parameters previously reported in ASD (Severijns et al., 2020) and healthy (Mousavi et al., 2018) population, with the exception of the thoracic kyphosis (TK) parameter which presented with poor reliability (ICC$<$0.40).

This analysis was associated with several important limitations. Firstly, opposed to the work of Severijns et al. (2020) and Mousavi et al. (2018) (exclusively evaluating intra-subject variability), our results reflect the combined effect of the subject repeating the movement on two separate days (i.e. intra-subject variability) and the same operator re-creating the model (i.e. intra-operator variability). In the future, a repeatability analysis could be performed on a

set of trunk flexion motions performed on the same day (i.e. within the same motion analysis session) thereby isolating the intra-subject variability from the intra-operator variability as the model does not need to be recreated. This isolated trial-to-trial variability would likely be smaller compared to our reported two-week variability. Alternatively, in order to isolate the effects of intra-operator variability on the kinematics, a single operator could create several models of the same subject to measure the same motion trial. Yet, we assumed the intra-operator variability to be equal to or smaller than the inter-operator variability.

Secondly, we quantified the variability based on the ROM rather than considering variability in the individual spinal kinematics. Indeed, evaluating only the initial and final phase of the motion in terms of ROM of spino-pelvic parameters (as in Chapter 3 and Chapter 4) does not provide any insight in the dynamic motion pattern itself. For example, Figure 78 shows the test-retest results of an ASD subject as reported trough the T1-SPI angle. Based on a comparison of the ROM of the T1-SPI parameter, we would conclude that the T1-SPI ROM was repeatable. However, detailed evaluation of the kinematic pattern between both sessions based on the continuous, time-dependent T1-SPI angles revealed additional insights into the motion strategy. Indeed, as shown in Figure 78, a steeper curve of the T1-SPI angle was found during the second session compared to the first session, indicating an accelerated initial flexion phase. While these ROM evaluations of spino-pelvic parameters are common practice within spinal motion evaluation (D. Gelalis et al., 2009; Mousavi et al., 2018; O'Grady et al., 2021; Schmid et al., 2016; Severijns et al., 2020) and thus proved useful for comparison with the literature, care should be taken as such semi-dynamic evaluation disregards dynamic kinematic features that may be relevant.

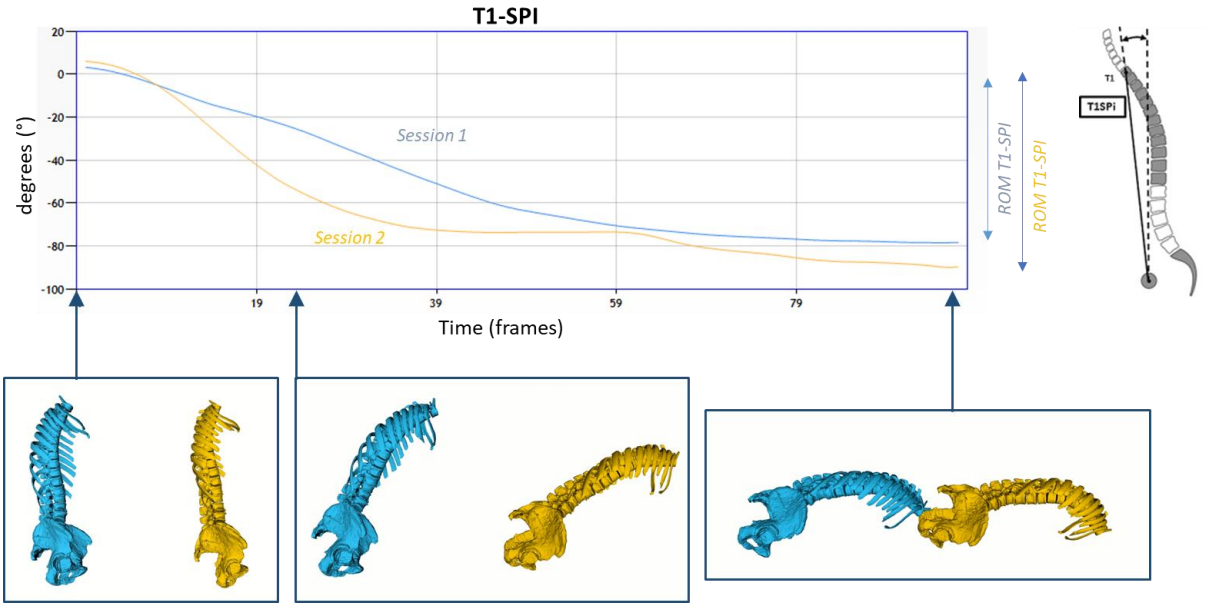

Figure 78: We quantified the reliability using the ROM of spino-pelvic parameters (T1-spino-pelvic inclination [T1-SPI] in this illustration) during the forward trunk flexion as in Severijns et al. (2020). However, this is not a true dynamic validation as only the initial and final position of the motion is considered when calculate the ROM. A fully dynamic comparison would allow evaluating the overall kinematic pattern.

Thirdly, adequate standardization of the movement instructions is of utmost importance to limit intra-subject variability of the spinal kinematics. This can be illustrated based on data of one ASD subject, suffering from a predominantly lumbar spinal deformity, who initially performed a maximal trunk flexion primarily engaging her lumbar region with limited range of motion in the thoracic region (Figure 79A). However, in the second session seven days later, her motion strategy changed, a rigid lumbar region with primarily engagement of her thoracic region (Figure 79B), despite that there were no interventions, injury or illness during this seven-day period. Although, the cause of this altered movement strategy could not objectively be determined, the subject might have interpreted the instructions differently. This highlights the importance of adequate standardization. The use of guides and reaching targets (as in Mahallati et al. (2016)), could improve the test-retest reliability. On the contrary, excessive standardization may obscure voluntary motion strategies as the motion during the flexion task may become more artificial and less representative of activities of daily living. Therefore, evaluation of tasks of daily living, here for example picking up a pen from the floor while being seated, may be a better alternative rather than providing excessively detailed instructions of an analytical motion as the forward flexion. This way the risk of 'overthinking the motion' and thereby altering the movement strategy could be limited.

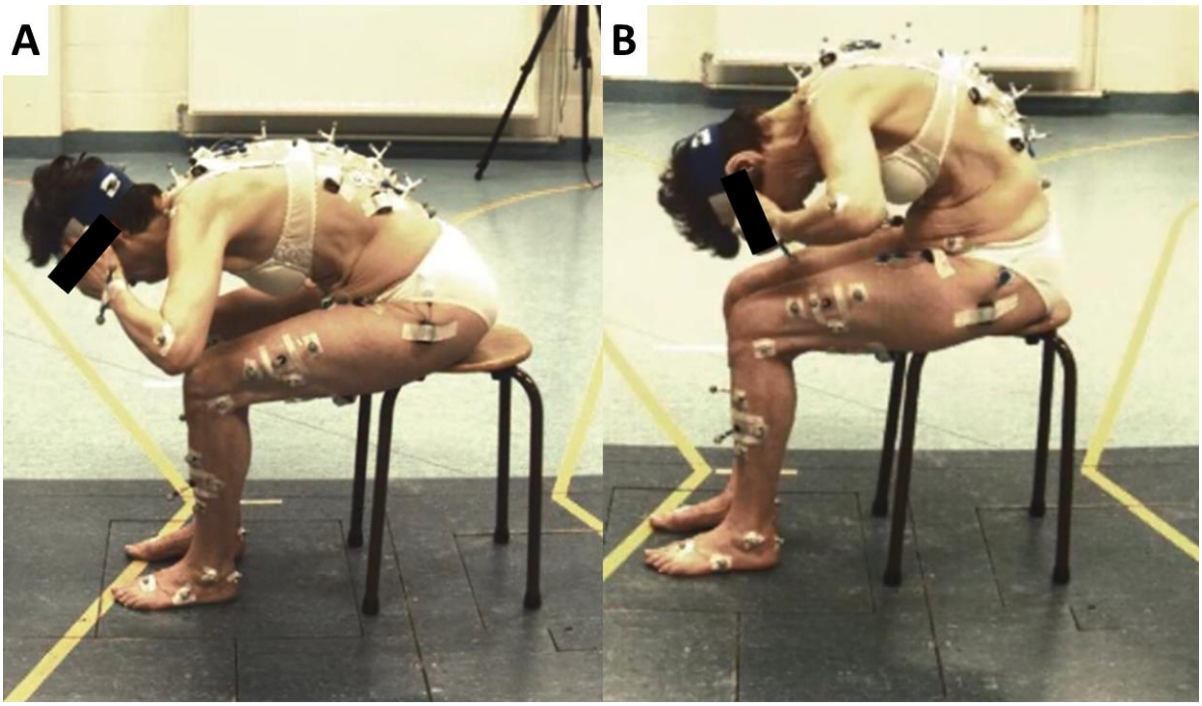

Figure 79: Both images represent the final position of a maximal voluntary trunk flexion motion of the same ASD subject during two separate motion analysis sessions, seven days apart. While in (**A**) a rigid thoracic but mobile lumbar region was used to reach the flexed position, in (**B**) the subject used a rigid lumbar but mobile thoracic region.

C. Summary of error and variability

In this last subsection, we will discuss the performance of the workflow as a whole summarizing suggestions for prioritizing future improvements to the workflow regarding the accuracy (C1) and reliability (C2) of the spinal kinematics. Because of the co-dependence of consecutive steps in the workflow and the non-linearity of the inverse kinematics algorithm, it was not possible to isolate and quantify each source of error or uncertainty.

C1. Kinematic error of the complete workflow

Firstly, we can neglect the effect of palpation error as this is largely corrected for during subject-specific definition of the virtual markers. As for the remaining sources of error, the evaluation using semi-dynamic biplanar radiography (Chapter 1) offers the most complete accuracy evaluation of the entire workflow, i.e. integrating effects from STA, modeling error and assumptions of the model. The mean spinal kinematic error was 3.05–4.97 mm and 2.92–5.31° for vertebral positions and orientations, respectively. Comparing this to the isolated effect of unavoidable STAs on the spinal kinematics (mean error 0.99°), we should prioritize the improvement of the model towards more accurate and physiologic representation of the subject's anatomy and kinematic function. Moreover, as the quantification of the reconstruction accuracy of the modeling method was comparable to clinically used alternatives, **the largest gain in accuracy is likely to be made in the optimization of the model assumptions regarding improved kinematic physiologic resemblance to the ASD subject.**

C2. Kinematic variability of the complete workflow

Regarding the variability introduced by each of the human interactors, the introduced variability by the physiotherapist and radiology operator were assumed to be negligible. As the remaining human aspects could currently not be avoided, i.e. the variability introduced by the modeling operator and the subjects being measured, they were further investigated. While the operator-dependent modeling aspects were evaluated through inter-operator variability testing and simulations of probabilistic uncertainty, a test-retest reliability analysis concluded that the largest variability currently originates from intra-subject differences in motor task execution. However, although further improvements in motor task instructions are plausible, one should be careful not to over-standardize and thereby lose the voluntary nature of the motion. In summary, **future improvements should focus on minimizing operator-dependency as a source of variability in modeling and investigate means to improve standardization of the motion while warranting its resemblance to real daily activities and voluntariness.**

While the modeling method of the workflow was designed to prevent the effect of palpation error during marker placement and patient-positioning error during imaging, the creation of a subject-specific model together with the limiting assumptions in the model appear to be the largest contributors to error in measuring spinal kinematics. Furthermore, the introduced variability due to its reliance on operators for modeling was limited compared to the slightly larger intra-subject variability in performing a motion task. In summary, although the presented workflow remains susceptible to error and uncertainty, it was demonstrated to have good accuracy and robust reliability.

Topic 3: Suggestions for clinical translation

Although the work in this dissertation mainly focused on methodological developments and the validation thereof, this section will discuss the current limitations of the workflow for extension towards larger study cohorts and provide suggestions to facilitate clinical translation. More specifically, the following prerequisites for clinical integration of the workflow with the aim of complementing the static evaluations with dynamic information on spine function are (A) a clinically feasible workflow, (B) intuitive integration of the complex spinal kinematics data and (C) a still to be demonstrated added value towards surgical outcome optimization (Clinical gap 3), each discussed below.

A. Clinical feasibility of the workflow

As methodological developments were the primary focus of this dissertation, only a limited number of ASD patients were included (n=15). In follow-up work targeting larger study populations, the feasibility in terms of time cost[6] will gain more importance. As introduced earlier in *"Topic 1: Biplanar radiographic imaging is key for subject-specific modeling in ASD patients"* of this discussion, creating the subject-specific models is currently a time-consuming and laborious process, mainly due to (1) CT image segmentation and (2) model reconstruction, as further discussed below.

First, segmenting individual vertebral segments from CT is tedious and is currently the most time-consuming step (ranging between 3 and 7 hours per subject) of the entire workflow. Although intensity-based thresholding reduces manual labor, low image quality and the presence of severe vertebral degeneration (e.g. calcifications spanning the IV space) considerably limit the efficacy of basic semi-automated procedures tools that delineate and/or separate vertebrae and only minimally reduce the need for subsequent manual interventions. Furthermore, CT imaging involves harmful ionization. Therefore, future work could evaluate MRI as a non-ionizing alternative for 3D imaging, in particular when combined with dedicated bone segmentation algorithms (which often involve the use of deformable models or neural networks) (Liu et al., 2021; Schmid and Magnenat-Thalmann, 2008). Alternatively, prior to applying the workflow on a larger scale, it could be investigated to what extent the geometrical detail can be reduced without significantly affecting the 3D alignment reconstruction and subsequent outcome parameters. If confirmed, statistical shape models (SSM) could be used as an alternative to the time consuming CT-segmented vertebrae. A SSM represents an average shape of a 3D object together with its variation in shape over the population (Illes et al., 2012). Based on the anatomical landmarks identified on the biplanar images and their 3D reconstruction, the resulting point cloud could guide the SSM to the best-matching vertebral shape instance in the SSM. Alternative to manual indication of landmarks, more recent work suggests using convolutional neural networks to automatically deform a full spine model

[6] Financial feasibility is also being investigated within our research group, but falls out of the scope of this dissertation (Neyens, 2020).

directly based on the biplanar images (Aubert et al., 2019). So far, these methodological advances have not been applied for use for constructing spine MS models in ASD.

Secondly, regarding the biplanar imaging modeling, the time cost of the different steps in the modeling platform were recorded during an inter-operator reliability study (Chapter 2) (Figure 80). As might be expected, the actual time cost to create a model depends on the subject-specific deformity (complexity of the alignment and severity of degeneration) and medical image quality (biplanar and CT imaging), as previously discussed in *"Topic 1: Biplanar radiographic imaging is key for subject-specific modeling in ASD patients"* of this discussion. Furthermore, also the operator proficiency with the modeling workflow and the associated learning curve will strongly impact the time cost. This is shown in Figure 80A, where the reduction in time cost of marker identification (which is largely independent of the complexity of the spinal deformity) is shown throughout the learning phase. Alternatively, more automated biplanar radiographic reconstructions (Galbusera et al., 2020) are evolving, which would improve clinical feasibility in terms of time cost while at the same time reducing operator-induced variability of subject-specific modeling.

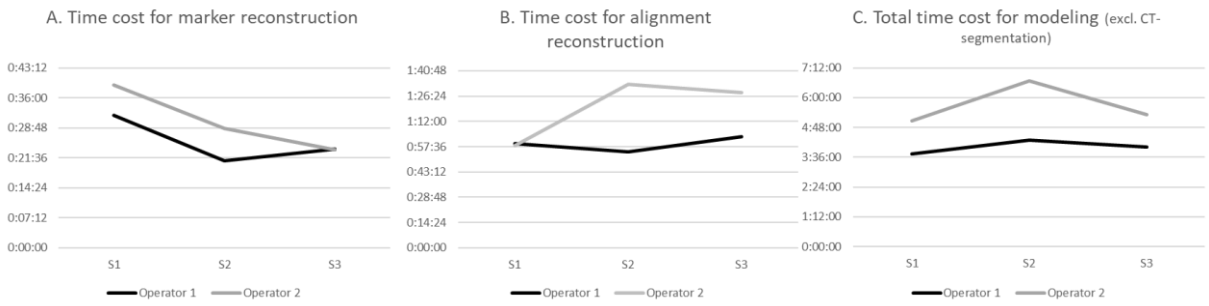

Figure 80: The time cost for modeling was registered for two of the three operators in the inter-operator variability study of Chapter 2 (the third operator developed the method and was thus already familiar with the software). The subjects (S1-S3) are numbered in reference to Figure 69 (p.173) displaying the 3D model of the deformity. (**A**) Creating subject-specific models is associated with a learning curve. Time cost for the marker reconstruction decreased as the operators modeled more subjects. (**B**) The time cost for alignment reconstruction increased, possibly related to the increased complexity of the spinal deformity (see Figure 69 on p.173). (**C**) The total time cost for modeling (including landmark identification and IV joint definition, but excluding CT segmentation) varied between 3h 43min and 6h 40min.

Lastly, the current workflow requires high fidelity input on motion from a 3D motion laboratory combined with a biplanar radiographic imaging system within walking distance from each other. Traveling long distances, for example to another facility, while wearing the markers is practically unfeasible as patients are required to limit clothing to their underwear. This close proximity is also needed to ensure preservation of the spatial relation of the skin markers to the anatomy during imaging and motion capture. Indeed, the attached skin markers are preferably not detached. As a promising alternative to the optical motion capture system, low-cost inertial measurement units (IMUs), and in extension other wearables, are recently being used in spinal research as they bypass the need of an advanced motion capture laboratory (Graham et al., 2020; Hajibozorgi and Arjmand, 2016; O'Grady et al., 2021). However, this

approach also requires accurate definition of the sensor to body orientation. At this time, the complexity of the spinal structure, the inability to isolate spinal segments and the underlying structural deformities would still advocate the use of medical imaging with the wearable sensors in place.

In summary, the current workflow is time intensive as our newly developed modeling method aimed for the highest level of detail achievable. In the future, the minimally required level of detail for answering the specific research question will need to be identified. Furthermore, integration of dedicated algorithms should be considered to (semi-) automate time-demanding parts of the workflow.

B. Suggestions for data integration

As described in **Clinical gap 3**, 2D static image-based measures are currently the primary quantitative drivers in surgical decision-making towards an optimal spinal alignment correction in ASD. However, the functional outcome which is of great concern to the patient and causally related to post-surgical complications (Ryu et al., 2021; Yoo et al., 2019), is currently only limitedly incorporated in the clinical pre- and post-operative assessment. In this work, we introduced an advanced MS modeling method to measure dynamic IV kinematics of the deformed spine, otherwise not measurable non-invasively *in vivo*.

Pathological kinematics, for example of the lower limbs during gait, are typically represented as a graph with the angle of the hip, knee and/or ankle angles throughout one or more gait cycles. In addition, a normative range is indicated, which allows evaluating if the subject's gait pattern is within acceptable ranges. For spinal kinematics in ASD, two main issues are currently limiting interpretation of curve-based data representations: (1) the excessive amount of curves to report the high number of joints and their DOF in the thoracic and lumbar region (adding up to 51 subplots) and (2) the limited relevance of separately analyzing IV joint angles as the combined analysis with the highly subject-specific spinal deformity itself may have a higher value (e.g. SDEI and SKDI).

Towards future clinical integration it thus seems crucial to investigate multiple ways of synthesizing whole spine IV joint kinematics, into intuitive and meaningful concepts. Hereto, we recommend a step-wise approach. More specific, and as will be further illustrated below, the developments in this dissertation focused on (1) the extension of already used radiography-based, 2D clinical concepts towards 3D kinematic information, thereby directly addressing Clinical gap 2 and (2) the introduction of new concepts/metrics to describe the dynamic IV characteristics in pre-operative ASD subjects. Finally, their added value was evaluated in relation to the current 2D static image-based measures

1) Extend the definition of current clinical concepts with a third dimensionality and time-component.

Conventional radiographic analysis of spinal deformity only quantifies the static skeletal body structure, which is limiting the conclusions on functional abilities in ASD subjects. However, the use of MS models allows to extend these currently used 2D, static, radiographic concepts to 3D, dynamic, parameters. In Chapter 2, the dynamic equivalent radiographic parameters were introduced as model-based spino-pelvic parameters and evaluated in terms of reliability.

Thereafter, six common spino-pelvic parameters in the sagittal plane, i.e. lumbar lordosis (LL), thoracic kyphosis (TK), sagittal vertical axis (SVA, Figure 81A), pelvic tilt (PT) and T1 and T9 spino-pelvic inclination (T1-SPI, T9-SPI) were calculated for every time frame. To this end, the measured IV joint kinematics (i.e. relative motion at the joint between two interconnected bodies) were converted to body kinematics (i.e. absolute motion of a body expressed in a fixed ground reference frame) using the API of OpenSim 3.3 (Stanford University, USA). This way, the 3D trajectory of each anatomical landmark throughout the trunk flexion motion could be determined as the location of the anatomical landmarks on the body segments (previously indicated during the mesh-based IV joint definition when creating the model (Overbergh et al., 2020) is fixed during the motion.

The acetabular cavities of pelvis were used to define the sagittal and coronal plane in which the spino-pelvic parameters are expressed. Figure 81 illustrates the definition for the sagittal vertical axis (SVA), which can also be applied to calculate the PT, SS, LL, TK and spino-pelvic inclinations (Chapter 2: Appendix 1).

As a proof of concept, eight ASD patients underwent a spinopelvic analysis using a biplanar imaging system followed by performance of a series of motion tasks in the 3D motion lab, including gait. As shown in Figure 81D, multi-body simulations were then used to estimate dynamic equivalent radiographic parameters during gait. Importantly, classic 2D radiographic analysis of the eight subjects provided an average (SD) SVA of 40.4 mm (38.4 mm) while the dynamic analysis calculated a time-averaged SVA of 69.2 mm (30.2 mm) with an average dynamic range of 20.4 mm (7.7 mm) during gait, indicating the low representativeness of static radiographic measures for dynamic spine function.

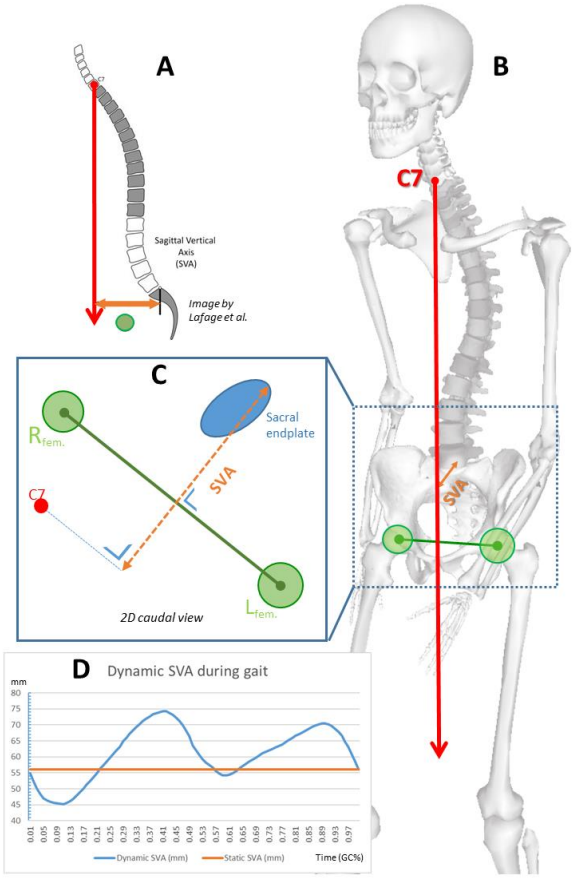

Figure 81: Illustration of the sagittal vertical axis (SVA) measurement, as: (**A**) a traditional 2D measurement and (**B**) a virtual augmentation on a skeletal model during simulated gait. (**C**) Definition of its 3D equivalent. (**D**) Static (orange) and dynamic (during a gait cycle (GC), blue)).

In summary, skeletal models of the spine, created based on load-bearing biplanar images and driven by 3D motion capture data, can be used to calculate dynamic and 3D equivalent radiographic measures. Care was taken to define these 3D equivalent parameters in agreement with their well-integrated 2D radiographic parameters, thereby facilitating intuitive, low-barrier, integration in the clinical world. In line with the need of a step-wise integration of model-derived parameters in clinical practice, this approach integrates the substantial amount of IV joint kinematic data into comprehensive curves. The clinician can then directly relate these curves to the conventional radiographic parameters, while fully exploiting the potential of the measured IV joint kinematics. Future research should further analyze the clinical added value over the current static 2D evaluation

2) New metrics for spinal kinematic analysis in ASD

Pathological spinal kinematics are difficult to interpret considering the large amount of detailed data and the unique character of each spinal deformity affecting the joint kinematics. To this end, as discussed in Chapter 3, two novel parameters were developed and applied on a pilot ASD population (n=15): The spinal kinematic deviation index (SKDI) and spinal deformity engagement index (SDEI). They reflect the relative amount of compensatory directional motion and the relative use of the IV joints weighted by their graded deformity, respectively. We investigated, for the first time, the relation between static spinal deformity and altered kinematic behavior of the affected FSUs during a maximal forward flexion motion, albeit in a

relatively small population. Our analysis indicated that the currently used static image-based parameterizations are not the sole determinants for the amount of spinal kinematic compensation (i.e. SKDI) as reflected in the low correlations between spino-pelvic parameters and vertebral body deformation (i.e. SDI). On the other hand, subjects engaging their deformed region (i.e. a high SDEI) are more likely to present a more prominent kinematic compensation strategy (i.e. high SKDI) to perform global trunk flexion as reflected by the strong correlation (0.694, p=0.004) between the SDEI and the SKDI. Indeed, subjects presenting mainly static features of ASD do not necessarily present dynamic kinematic compensation, rather, a motion strategy engaging the deformed region seems to be a prerequisite for kinematic compensation. This insight further contributes to the growing awareness in literature that static alignment is not the sole driver of dynamic, functional limitations in ASD. For example, Haddas et al. (2018) documented important differences in kinematic variables of gait in patients with spinal disorders compared to healthy subjects. They recommend the use of gait analysis as part of the clinical evaluation as it provides objective measures of function. Additionally, Kawkabani et al. (2021) suggest to account for dynamic compensation mechanisms when planning surgical correction and physiotherapy aiming to correct gait correction in subjects with ASD. Lastly, Diebo et al. (2018) suggest gait analysis to be the future in ASD research, with potential clinical application, to improve the understanding of dynamic compensatory mechanisms. In the future, insights considering a patient's specific spinal motion strategy based on the newly introduced parameters could potentially benefit clinical management and aid in the pre-surgical evaluation contributing to improved functional outcome in ASD. For example, the relative use of the deformed region pre-operatively, as quantified using the new metrics, could affect the surgeon's decision regarding the fusion length.

C. Illustration of the potential value of novel kinematic concepts towards post-operative pain and function improvement

Large discrepancies have been documented between patient expectations and observed outcomes following corrective surgery in ASD (**Clinical gap 3**). Specifically, the anticipated pain reduction and functional improvements in terms of self-reported health related quality of life (HRQoL) after fusion surgery were much higher than experienced by the patient post-operatively (Ryu et al., 2021; Yoo et al., 2019). Dynamic, pre-operative evaluations, as introduced in this dissertation could potentially aid in the better prediction of post-operative function. As an illustration, below, we explore the relation between pre-operative spinal kinematics and post-operative outcomes in terms of HRQoL in a pilot study.

In addition to the pre- and post-operative motion analysis and medical imaging of Chapter 4, five ASD subjects were asked to complete questionnaires describing their self-reported HRQoL before and six months after spinal fusion surgery: the Scoliosis Research Society questionnaire (SRS-22r) (Asher et al., 2003) and the Core Outcome Measurement Index (COMI) questionnaire (Mannion et al., 2016). The SRS-22r and COMI questionnaires each report specific categories related to self-reported HRQoL: The SRS-22r questionnaire summarizes the results into the following categories: function, pain, self-image, mental health and satisfaction with management (Asher et al., 2003). The COMI questionnaire categorizes in pain and

function (Mannion et al., 2016). For further analyses we specifically focused on the aspects that reported large pre-vs. post-operative discrepancies and therefore extracted the SRS-*function* and SRS-*pain* categories from the SRS-22r questionnaire. From the COMI questionnaire, we used the COMI-*function* and COMI-*pain* categories. Additionally, before starting the motion analysis on both measurement occasions, the patients were asked to complete a Visual Analog Scale (VAS) (Hawker et al., 2011) assessing their current pain level on a scale from 0 (no pain) to 10 (most pain). After having performed the maximal voluntary trunk flexion motion, and a series of other functional tasks not included in this work (e.g. stair walking, stepping over and lifting a box), subjects were asked to complete the VAS score again. We refer to VAS1 and VAS2 as the pain scales before and after the motion analysis, respectively. For each subject, the difference between the corresponding -*function* and -*pain* scores, pre- and post-operatively, was calculated (Table 36).

Table 36: Pre-operative SKDI and SDEI values, as well as difference between pre- and post-operative function and pain scoring. Scoring systems that inversely represent pain and function (COMI and VAS scores) were multiplied by -1 so a positive differential value indicates an improvement in function or pain compared to the pre-operative state. Differences among the HRQoL and pain scoring originate from the specific questions and the scoring system. For example, the COMI reports on the self-reported pain and function over at least one (max. four) week(s). The SRS-22r asks the patient to reflect about a minimal period of three (max. six) months. The VAS, however, reports on the level of pain about 10 min before and after performing the maximal trunk flexion motion.

	Pre-operative		Pre- to post-operative difference (positive values indicate improvement)					
Subject	SKDI	SDEI	ΔSRS-function	ΔSRS-pain	ΔCOMI-Function	ΔCOMI-pain	ΔVAS1	ΔVAS2
1	1.01	0.28	1.0	1.4	5.0	2.0	0.8	4.3
2	0.51	0.21	0.4	0.2	1.3	0.0	1.7	2.3
3	0.54	0.67	1.0	1.8	1.3	8.0	5.0	8.5
4	1.19	0.48	-1.4	0.2	-8.8	3.0	3.0	4.7
5	0.83	0.50	0.8	0.4	0.0	2.0	3.3	3.1

The pre-operative IV joint angles throughout the maximal voluntary forward trunk flexion were processed as in Chapter 3. More specifically, the amount of kinematic compensation, defined as normalized out-of-plane joint motion during a single-plane trunk flexion, was quantified by the spinal kinematic deviation index (SKDI) (Chapter 3). The relative contribution of IV joint motion involving deformed vertebral bodies to the overall spine motion was evaluated with the spinal deformity engagement index (SDEI) (Chapter 3) (Table 36). Finally, to evaluate the relation between pre-operative kinematics and post-operative improvement in HRQoL, Pearson correlation coefficients were determined between (1) the SKDI and all differential HRQoL parameters; and (2) the SDEI and all differential HRQoL parameters using SPSS 26 (IBM SPSS Statistics) (Figure 82 and Table 37).

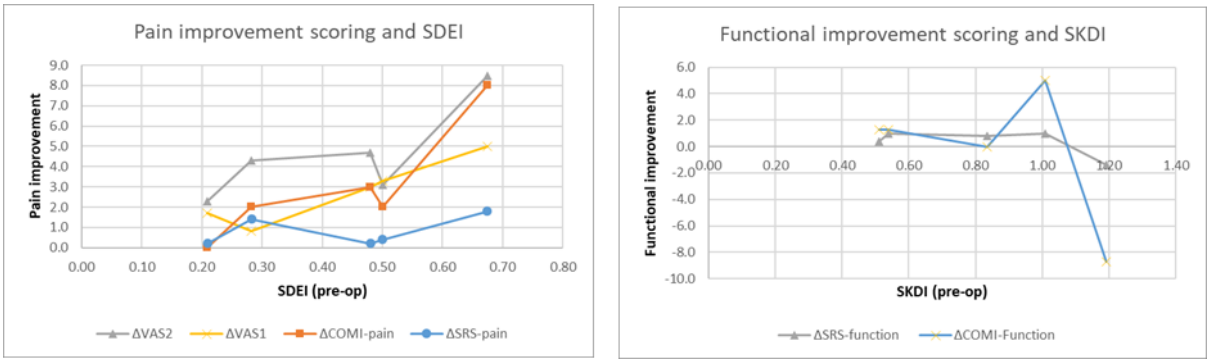

Figure 82: (left) The pre- versus post-operative pain improvement (expressed as a positive value) in relation to the pre-operatively calculated SDEI parameter. (right) The pre-vs. post-operative functional improvement (expressed as a positive value) in relation to the pre-operatively calculated SKDI parameter.

Table 37: Pearson correlation coefficients (significance) between the differential (Δ) functional and pain scoring systems; and the SKDI and SDEI. (Significance level set at 0.05)

	ΔSRS-function	ΔSRS-pain	ΔCOMI-Function	ΔCOMI-pain	ΔVAS1	ΔVAS2
SKDI	-0.601 (0.284)	-0.239 (0.698)	-0.507 (0.384)	-0.192 (0.785)	-0.301 (0.622)	-0.151 (0.809)
SDEI	-0.005 (0.994)	0.415 (0.448)	-0.302 (0.621)	0.881 (**0.048**)	0.940 (**0.018**)	0.792 (0.110)

We noticed a higher post-operative pain improvement in subjects presenting a higher SDEI pre-operatively (Figure 82-left). This finding suggests that, in our pilot population, subjects with a higher engagement of the deformed regions before surgery, presented with a larger pain reduction than subjects that limitedly engaged their deformed regions. Secondly, we observed a trend towards lower post-operative functionality improvement in subjects presenting with a higher SKDI pre-operatively (Figure 82-right). This suggests that subjects that used more kinematic compensation pre-operatively, presented less functional improvements at six months after surgery. Alternatively, subjects that only presented limited kinematic compensation strategies pre-operatively, presented a higher functionality improvement.

IV joint kinematics provide a unique quantitative biomarker of spinal motion behavior of ASD patients. However, the application of the workflow to larger cohorts will require further optimization to reduce the time-cost towards improved feasibility. Secondly, the IV joint kinematics are not easily interpretable because of the inherent large amount of detailed data, which are difficult to compare with other ASD subjects or healthy subjects due to the highly subject-specific nature of each spinal deformity affecting the IV joint definitions and consequent kinematics. Several concepts for data reduction and integration were therefore proposed. Explorations of the 3D kinematic data suggests this data to be complementary to current clinical methods. Thirdly, although requiring more subjects, our pilot evaluations relating these new dynamic concepts to functional outcome in individual patients illustrate possible avenues for future research in which kinematics evaluations could potentially aid surgical-decision making.

Topic 4: Future work and generic application of the developments

In this dissertation the methodological foundations were laid for subject-specific modeling and simulation in ASD. This section of the discussion will suggest future developments within ASD as well as in more generic applications outside the scope of this work.

A. Future work

Fifteen unique subject-specific models of ASD patients were created in this dissertation, having subject-specifically defined spino-pelvic alignment, bone geometry, marker placement and IV joint definition (Figure 83). In the future they could be used for (1) the kinematic analysis of additional motions and/or (2) performing more in depth biomechanical analyses of musculoskeletal loading.

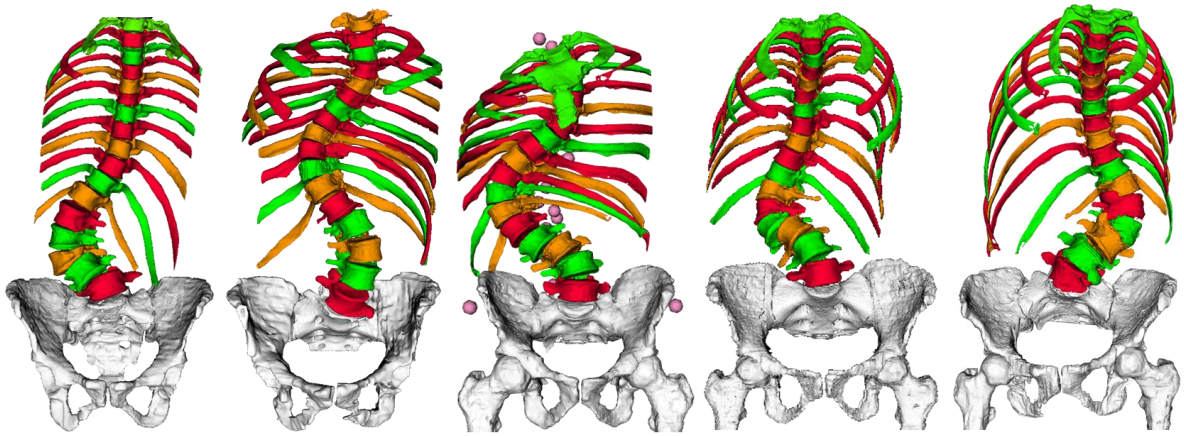

Figure 83: An illustration of five available subject-specific ASD models created in this dissertation.

1) In this dissertation, we only focused on using the modeling workflow for evaluating IV angles during a forward trunk flexion motion. However, a large amount of additional activities of daily living were recorded in the motion lab (walking, lifting objects, stair walking, reaching, sit-to-stand, stand-to-sit, stepping over a box). Future work could thus focus on more extensively documenting IV kinematics and further exploring their possible relation to ASD functionality in daily life.
2) Building further on the created ASD models, future research could extend the current simulation workflow towards, for example, the calculation of muscle forces and even joint reaction forces to document IV loading. Additional to the optical motion capture data used in this dissertation, integrated force platforms recorded ground reaction forces during motion, representing external forces and moments acting on the subject. Also, through the attachment of electromyography (EMG) sensors, the activity of superficial muscles was recorded. In the future, this data can be useful to simulate joint reaction forces (external loads) or validate simulations of muscle activation (EMG) as shown in Figure 84. Indeed, simulation-based measurements that were previously not applicable in ASD due to the lack of adequately representative models, can now be further

explored. For example, in previously published studies, spinal loads (Beaucage-Gauvreau et al., 2019; Connolly et al., 2021; Ignasiak et al., 2018b; Schmid et al., 2020b) and muscle activations (Connolly et al., 2021) were analyzed in healthy or AIS subjects and surgical outcome was predicted based on pre-operative, model-based data (Ignasiak, 2020). However, for these applications, personalization of the spinal alignment of a MS model should include personalization of the muscular anatomy. Indeed, the generic model that served as the base for our subject-specific models already includes muscles as defined by Bruno et al. (2015) (Figure 85A). However, the geometry and properties of the musculature is based on generic musculoskeletal models that can be reasonably assumed to be unrepresentative of the ASD population. First, spinal malalignment alters muscle paths with respect to the spine. Consequently the moment-arms of muscles are affected by changes in the relative position of the bones (Figure 85B-C). As a result, the capacity of a muscle to generate a given motion as well as how the associated forces transferred to the spine is altered (Diebo et al., 2015). In the future, also subject-specific muscle geometry should be integrated in the model. Thereto, the developed modeling platform can be easily extended to include an MRI-based spinal muscle modeling pipeline as e.g. in Scheys et al. (2005). Such extension allows to superimpose the model onto the MRI, manually redefining the muscle path while navigating through the 3D space of the MRI and was already pilot tested (Figure 85D).

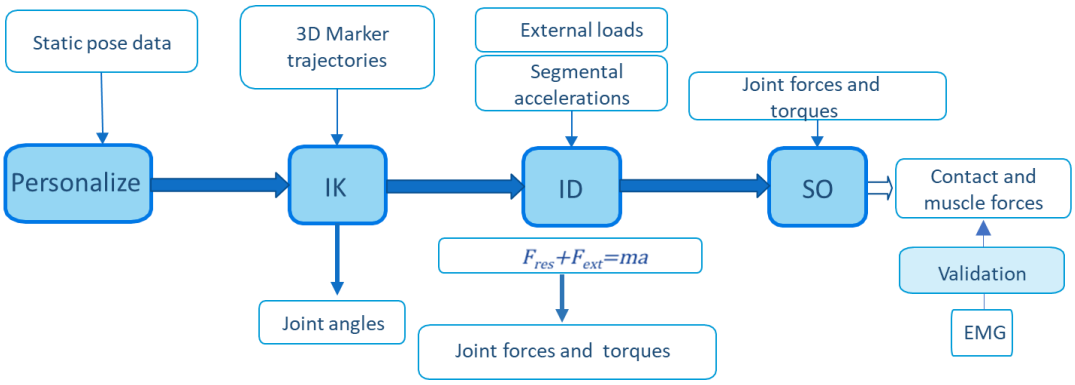

Figure 84: Illustration of the most commonly used simulation pipeline developed by OpenSim. This dissertation has focused on measuring joint angles through inverse kinematics (IK). However, opposed to using *static pose data* to personalize the model prior to performing IK, the model was personalized through medical imaging. Consecutive steps in the pipeline can calculate joint forces and torques (inverse dynamics (ID)), muscle activation and forces (static optimization, SO) and joint contact forces. These can then be validated through respectively, experimentally measured IV pressures (contact forces) and electromyography (EMG muscle forces). The presented simulation pipeline is not the only available pipeline, it rather demonstrates the analysis flow and the interdependency of the analysis steps.

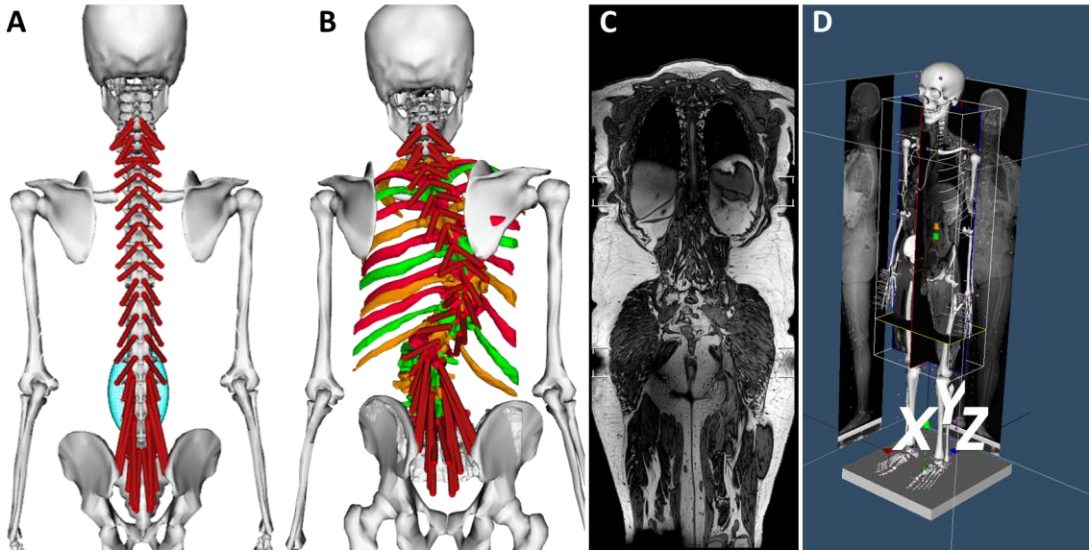

Figure 85: (**A**) a generic and (**B**) subject-specific model with visualization of the multifidus muscle. (**C**) A full body MRI of an ASD subject. (**D**) Pilot work towards the extension of the modeling platform for muscle personalization.

B. Generic application of the developments outside the scope of this dissertation

Throughout the course of this work, the methodological implementations were applied broader then what was discussed above. This section will thereto illustrate the generic character of the work through (1) ASD related and (2) non ASD-specific research.

1) Alternative application of specific developments for research in ASD

First, the biplanar imaging system was used to evaluate the relation between anatomy and balance. Today, a vertical line through the center of the C7 vertebral body (i.e. the C7-plumb line) is clinically used to estimate the position of the global center of mass (COM) of the patient with respect to the spine. However, the use of the biplanar imaging system together with the developed software platform and modifications to the imaging system itself, have allowed to directly measure this position. Thereto, a force platform that measures the location of the center of pressure (COP) was rigidly integrated in the biplanar imaging system. A vertical line through the COP, referred to as the gravity line (equivalent to the C7-plumb line) (Figure 86A), crosses the COM of the subject. This 3D gravity line can then be projected onto the radiographic image pair based on a preceding calibration procedure (Figure 86B-C). Measuring this 3D gravity line replaces the need for estimations thereof using the C7-plumb line. Importantly, this allowed to develop a new parameter, the transverse gravitational deviation index (TGDI, Figure 86), which documents the relation between anatomy and balance in ASD. For more detail the reader is referred to Moke and Overbergh et al. (2020).

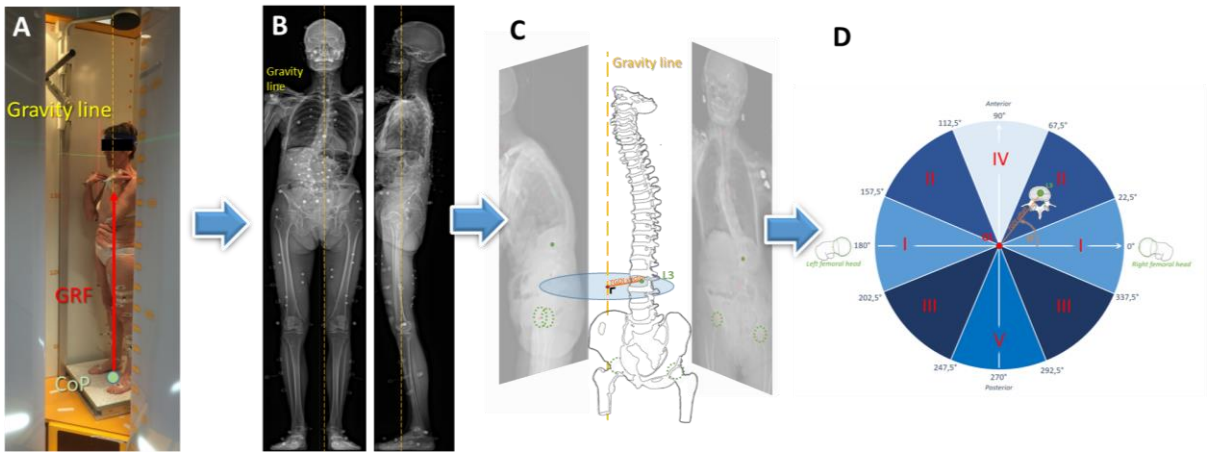

Figure 86: (**A**) The integration of a force measuring platform in the biplanar imaging system together with the developments made in Chapter 1 allowed to (**B,C**) augment the radiographic images with the gravity line of a patient (3D to 2D projection). Alternatively, the 2D to 3D reconstruction of anatomical landmarks allowed the development of the (**D**) transverse gravitational deviation index (TGDI): a novel static 3D measurement describing the position of the gravity line relative to the spinal alignment. (Images modified with permission from Moke and Overbergh et al. (2020) under open access license of Wolters Kluwer Health.)

Second, the dynamic assessment of global spinal alignment in terms of spino-pelvic parameters (such as lumbar lordosis and thoracic kyphosis) using motion capture data was recently improved based on the developments of Chapter 1. More specifically, a spline-based measurement method (Ignasiak et al., 2017) was modified for use in ASD patients by using the 2D to 3D reconstruction capabilities of the developed modeling platform that allow to virtually relate the actual skin marker positions to the center of the corresponding vertebral bodies (i.e. correction for anatomy) (Figure 87) (Severijns et al., 2020). This enabled the dynamic measurement of spinal alignment using skin markers in severely deformed spines. During a sit to stand motion in ASD patients (n=8), this polynomial method of Severijns et al. (2020) with correction for anatomy presented with a higher reliability compared to the uncorrected method using the skin marker positions.

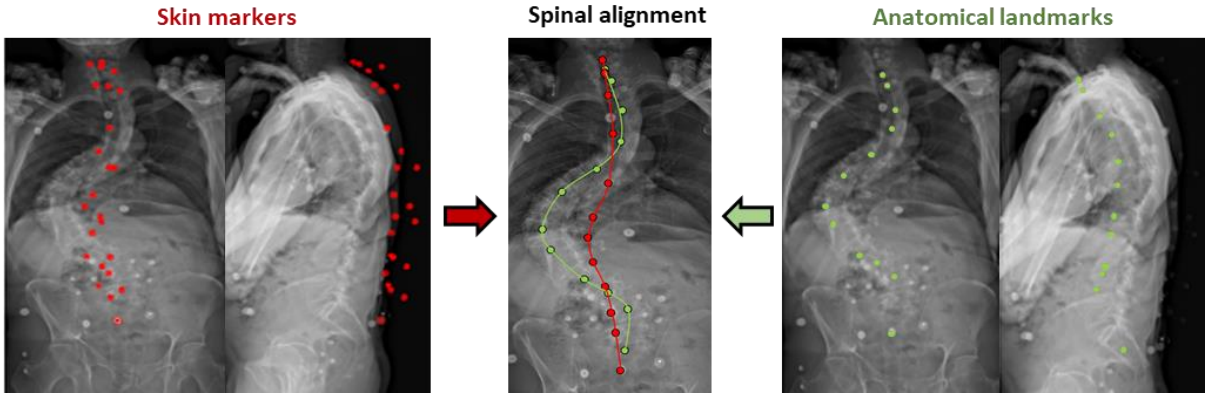

Figure 87: A spline-based method to measure global alignment was improved through 3D correction of the skin marker position to the vertebral body of the ASD patient. (Images modified from Severijns et al. (2020) with permission from Elsevier.)

2) Translation of developments to other orthopaedic research domains

First, the platform for image-based modeling has great potential for subject-specific MS modeling of other body regions than the spine. While developing the workflow and the processing tools of this dissertation, we warranted its generic nature to allow easy application to other orthopaedic research domains or extension for other purposes. Indeed, the modeling platform has been made in such a way that it is compatible for any OpenSim 3.3[7] model, for example in the lower limb (Figure 88). The modeling platform also has potential in the field of joint arthroplasty, as it can also be used to subject-specifically include implants in a MS model. For example, in shoulder arthroplasty, the implant can be integrated in the model using biplanar radiographs and combined with 3D motion capture data to accurately measure post-operative motion (Figure 89).

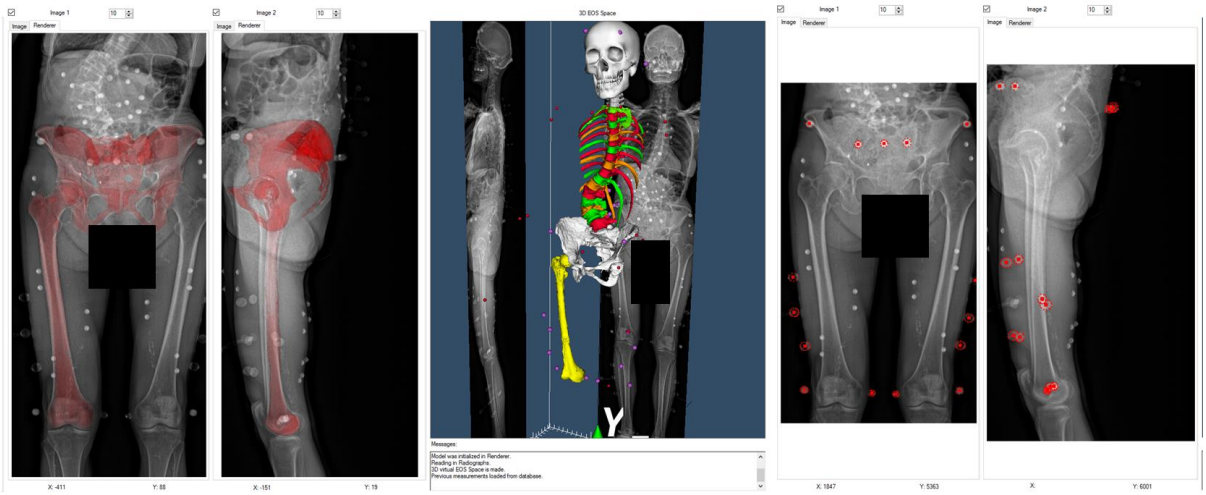

Figure 88: This figure illustrates the use of the platform to extend a spine model with subject-specific lower limb geometry. The developed modeling platform is not limited to use for spinal alignment personalization. Any skeletal anatomy that can be clearly imaged using biplanar radiographic imaging can be subject-specifically modeled.

[7] During the course of this PhD a new version of OpenSim was released (4.0) in which modifications to the model code were made. Compatibility with the new version of OpenSim cannot be assured yet.

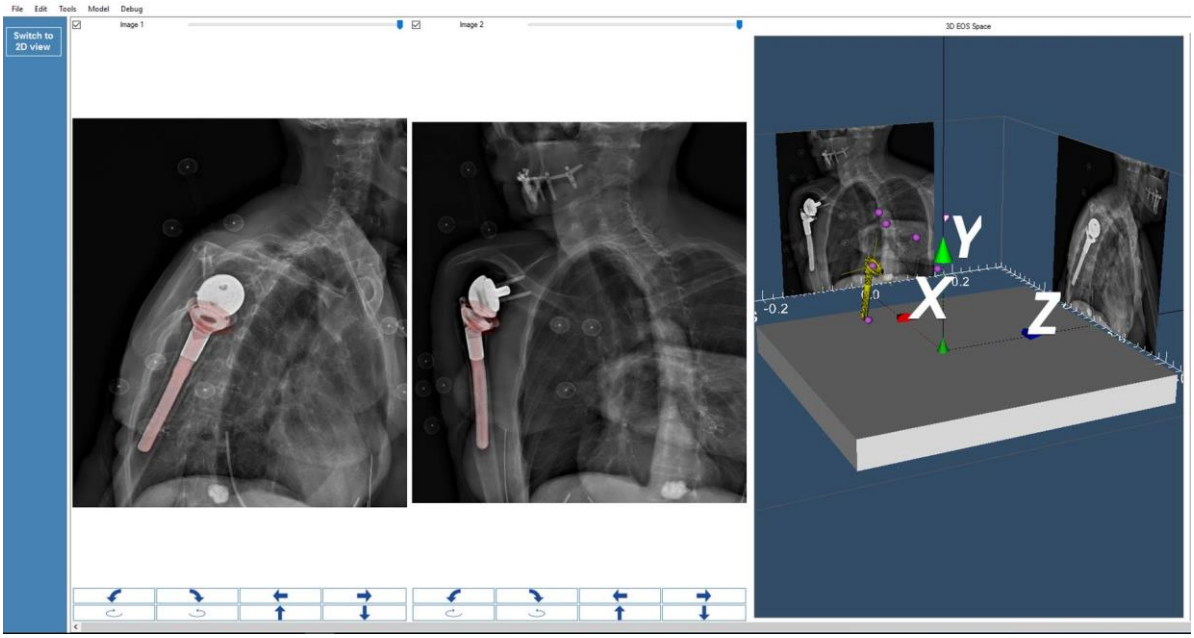

Figure 89: The modeling platform is used to register a shoulder implant.

Second, to process the large amounts of data associated with probabilistic modeling (such as the Monte-Carlo probabilistic simulations of Chapter 2), software tools were developed to process this data and minimize repetitive tasks for the researcher (Figure 90). Furthermore, once the model is created, tools have been developed to automate the simulations and extraction of the novel dynamic parameters (Chapter 3). All the tools have been developed in a generic fashion with an intuitive user interface, so they are easily applicable for similar research.

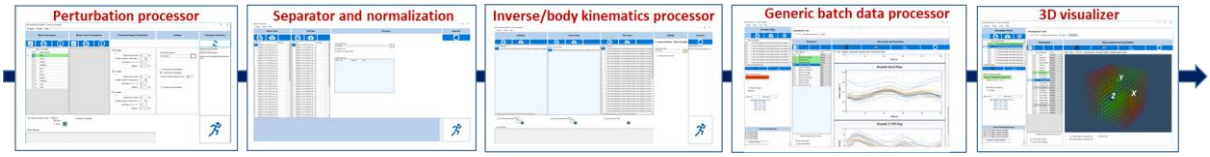

Figure 90: Illustration of generically developed tools, plugged into a pipeline, automating data processing.

A solid foundation for future modeling and kinematic measurements in ASD was laid, offering a wide range of opportunities to further investigate general functionality in ASD patients. Furthermore, the developments are not limited to ASD but can be easily applied in other orthopaedic research thanks to the generic nature of the created software. In summary, this dissertation resulted in a generic modeling platform combining different methods for model-based analyses in other orthopaedic research domains.

General conclusion

To improve assessment and surgical decision-making, this work introduced musculoskeletal computer models and multi-body simulations to advance the biomechanical insights of the ASD spine. On the long term, the developed workflow has the potential and the required accuracy to lead the way from current 2D static, towards integrated 3D, functional evaluation of spinal deformities.

Indeed, following the rapid advances in 3D modeling and computer simulation and the trend towards personalized medicine, subject-specific modeling and simulation-based analysis might become part of the (standard) clinical assessment of ASD patients. This way, a scenario may become feasible where, before the patient undergoes spinal surgery, the treating physician first requests a dynamic computer simulation to help in the clinical decision-making process and inform the patient on the post-operative functional outcome.

References

Abdel-Aziz, Y.I., Karara, H.M., 2015. Direct Linear Transformation from Comparator Coordinates into Object Space Coordinates in Close-Range Photogrammetry. Photogramm. Eng. Remote Sens. 81, 103–107.

Ackland, D.C., Lin, Y.C., Pandy, M.G., 2012. Sensitivity of model predictions of muscle function to changes in moment arms and muscle-tendon properties: A Monte-Carlo analysis. J. Biomech. 45, 1463–1471.

Actis, J.A., Honegger, J.D., Gates, D.H., Petrella, A.J., Nolasco, L.A., Silverman, A.K., 2018. Validation of lumbar spine loading from a musculoskeletal model including the lower limbs and lumbar spine. J. Biomech. 68, 107–114.

Aebi, M., 2005. The adult scoliosis. Eur. Spine J. 14, 925–948.

Ailon, T., Smith, J.S., Shaffrey, C.I., Lenke, L.G., Brodke, D., Harrop, J.S., Fehlings, M., Ames, C.P., 2015. Degenerative spinal deformity. Neurosurgery 77, S75–S91.

Alemi, M.M., Burkhart, K.A., Lynch, A.C., Allaire, B.T., Mousavi, S.J., Zhang, C., Bouxsein, M.L., Anderson, D.E., 2021. The Influence of Kinematic Constraints on Model Performance During Inverse Kinematics Analysis of the Thoracolumbar Spine. Front. Bioeng. Biotechnol. 9, 1–15.

Anderson, F.C., Pandy, M.G., 2001. Dynamic optimization of human walking. J. Biomech. Eng. 123, 381–390.

Asher, M., Lai, S.M., Burton, D., Manna, B., 2003. The reliability and concurrent validity of the Scoliosis Research Society-22 patient questionnaire for idiopathic scoliosis. Spine (Phila. Pa. 1976). 28, 63–9.

Aubert, B., Vazquez, C., Cresson, T., Parent, S., Guise, J. De, 2019. Towards automated 3D spine reconstruction from biplanar radiographs using CNN for statistical spine model fitting. IEEE Trans. Med. Imaging PP, 1.

Aubin, C.E., Labelle, H., Ciolofan, O.C., 2007. Variability of spinal instrumentation configurations in adolescent idiopathic scoliosis. Eur. Spine J. 16, 57–64.

Barba, N., Ignasiak, D., Villa, T.M.T., Galbusera, F., Bassani, T., 2021. Assessment of trunk muscle activation and intervertebral load in adolescent idiopathic scoliosis by musculoskeletal modelling approach. J. Biomech. 114, 110154.

Barrey, C., Roussouly, P., Perrin, G., Le Huec, J.C., 2011. Sagittal balance disorders in severe degenerative spine. Can we identify the compensatory mechanisms? Eur. Spine J. 1–8.

Bassani, T., Casaroli, G., Galbusera, F., 2019. Dependence of lumbar loads on spinopelvic sagittal alignment : An evaluation based on musculoskeletal modeling. PLoS One 14, 1–19.

Bassani, T., Ottardi, C., Costa, F., Brayda-Bruno, M., Wilke, H.-J., Galbusera, F., 2017a. Semiautomated 3D Spine Reconstruction from Biplanar Radiographic Images: Prediction of Intervertebral Loading in Scoliotic Subjects. Front. Bioeng. Biotechnol. 5, 1–11.

Bassani, T., Stucovitz, E., Qian, Z., Briguglio, M., Galbusera, F., 2017b. Validation of the AnyBody full body musculoskeletal model in computing lumbar spine loads at L4L5 level. J. Biomech. 58, 89–96.

Bastian, L., Lange, U., Knop, C., Tusch, G., Blauth, M., 2001. Evaluation of the mobility of adjacent segments after posterior thoracolumbar fixation: A biomechanical study. Eur. Spine J. 10, 295–300.

Beaucage-Gauvreau, E., Robertson, W.S.P., Brandon, S.C.E., Fraser, R., Freeman, B.J.C., Graham, R.B., Thewlis, D., Jones, C.F., Robertson, W.S.P., Brandon, S.C.E., Fraser, R., Freeman, B.J.C., Graham, R.B., Thewlis, D., Jones, C.F., 2019. Validation of an OpenSim full-body model with detailed lumbar spine for estimating lower lumbar spine loads during symmetric and asymmetric lifting tasks. Comput. Methods Biomech. Biomed. Engin. 22, 451–464.

Benneker, L.M., Heini, P.F., Anderson, S.E., Alini, M., Ito, K., 2005. Correlation of radiographic and MRI parameters to morphological and biochemical assessment of intervertebral disc degeneration. Eur. Spine J. 14, 27–35.

Berger, S., Marcello, O., Schuman, S., Schneider, J., Studer, D., Hasler, C., Zheng, G., Büchler, P., 2015. Patient-

specific spinal stiffness in AIS: a preoperative and noninvasive method. Eur. Spine J. 24, 249–255.

Bess, S., Schwab, F., Lafage, V., Shaffrey, C.I., Ames, C.P., 2013. Classifications for Adult Spinal Deformity and Use of the Scoliosis Research Society-Schwab Adult Spinal Deformity Classification. Neurosurg. Clin. NA 24, 185–193.

Blondel, B., Wickman, A.M., Apazidis, A., Lafage, V.C., Schwab, F.J., Bendo, J.A., 2013. Selection of fusion levels in adults with spinal deformity: An update. Spine J. 13, 464–474.

Bogduk, N., Twomey, L.T., 1997. Clinical anatomy of the lumbar spine and sacrum, 3rd ed. ed. Churchill Livingstone, New York (N.Y.).

Boos, N., Aebi, M., 2008. Spinal Disorders, Fundamentals of Diagnosis and Treatment. Springer.

Borbély, B.J., Szolgay, P., 2017. Real-time inverse kinematics for the upper limb: A model-based algorithm using segment orientations. Biomed. Eng. Online 16, 1–29.

Breen, Alexander, Claerbout, E., Hemming, R., Ayer, R., Breen, Alan, 2019. Comparison of intra subject repeatability of quantitative fluoroscopy and static radiography in the measurement of lumbar intervertebral flexion translation. Sci. Rep. 9, 1–9.

Briggs, A.M., Diee, J.H. Van, Wrigley, T. V, Greig, A.M., Phillips, B., Lo, S.K., Bennell, K.L., 2007. and Trunk Muscle Force. Phys. Ther. 87, 595–607.

Briggs, A.M., Wrigley, T. V., Van Die??n, J.H., Phillips, B., Lo, S.K., Greig, A.M., Bennell, K.L., 2006. The effect of osteoporotic vertebral fracture on predicted spinal loads in vivo. Eur. Spine J. 15, 1785–1795.

Brink, R.C., Colo, D., Schlösser, T.P.C., Vincken, K.L., Stralen, M. Van, Hui, S.C.N., Shi, L., Chu, W.C.W., Cheng, J.C.Y., Castelein, R.M., 2017. Upright, prone, and supine spinal morphology and alignment in adolescent idiopathic scoliosis. Scoliosis Spinal Disord. 12, 1–9.

Bruno, A.G., Bouxsein, M.L., Anderson, D.E., 2015a. Development and validation of a musculoskeletal model of the fully articulated thoracolumbar spine and rib cage. J. Biomech. Eng. 137, 1–10.

Bruno, A.G., Burkhart, K., Allaire, B., Anderson, D.E., Bouxsein, M.L., 2017. Spinal Loading Patterns From Biomechanical Modeling Explain the High Incidence of Vertebral Fractures in the Thoracolumbar Region. J. Bone Miner. Res. 32, 1282–1290.

Bruno, A.G., Cheng, B., Wang, W., Bouxsein, M.L., Anderson, D.E., 2015b. Incorporating Six Degree-of- Freedom Intervertebral Joint Stiffness in a Lumbar Spine Musculoskeletal Model — Method and Performance in Flexed Postures. J. Biomech. Eng. 137, 1–9.

Buckland, A.J., Vira, S., Oren, J.H., Lafage, R., Harris, B.Y., Spiegel, M.A., Diebo, B.G., Liabaud, B., Protopsaltis, T.S., Schwab, F.J., Lafage, V., Errico, T.J., Bendo, J.A., 2016. When is compensation for lumbar spinal stenosis a clinical sagittal plane deformity? Spine J. 16, 971–981.

Burkhart, K., Grindle, D., Bouxsein, M.L., Anderson, D.E., 2020. Between-session reliability of subject-specific musculoskeletal models of the spine derived from optoelectronic motion capture data. J. Biomech. 112.

Burkhart, K.A., Bruno, A.G., Bouxsein, M.L., Bean, J.F., Anderson, D.E., 2017. Estimating apparent maximum muscle stress of trunk extensor muscles in older adults using subject-specific musculoskeletal models. J. Orthop. Res. 498–505.

Cazzola, D., Holsgrove, T.P., Preatoni, E., Gill, H.S., Trewartha, G., 2017. Cervical Spine Injuries : A Whole-Body Musculoskeletal Model for the Analysis of Spinal Loading 1–25.

Cho, K.J., Kim, Y.T., Shin, S.H., Suk, S. Il, 2014. Surgical treatment of adult degenerative scoliosis. Asian Spine J. 8, 371–381.

Chow, D.H.K., Keith, D.K., Evans, J.H., Leong, J.C.Y., 1996. Effects of short anterior lumbar interbody fusion on biomechanics of neighboring unfused segments. Spine (Phila. Pa. 1976). 21, 549–555.

Christophy, M., Senan, N.A.F., Lotz, J.C., O'Reilly, O.M., 2012. A Musculoskeletal model for the lumbar spine. Biomech. Model. Mechanobiol. 11, 19–34.

Cignoni, P., Callieri, M., Corsini, M., Dellepiane, M., Ganovelli, F., Ranzuglia, G., 2008. MeshLab : an Open-Source Mesh Processing Tool. Sixth Eurographics Ital. Chapter Conf. 129–136.

Connolly, L.E.P., Schmid, S., Moschini, G., Meier, M.L., Senteler, M., 2021. Motion Capture-driven Musculoskeletal

Spine Modeling: An OpenSim-based Inverse Kinematics Approach 1–14.

Cook, C., 2003. Coupling Behavior of the Lumbar Spine: A Literature Review. J. Man. Manip. Ther. 11, 137–145.

Cook, D.J., Gladowski, D.A., Acuff, H.N., Yeager, M.S., Cheng, B.C., 2012. Variability of manual lumbar spine segmentation. Int. J. Spine Surg. 6, 167–173.

Corr, D.T., Hart, D.A., 2013. Biomechanics of Scar Tissue and Uninjured Skin. Adv. Wound Care 2, 37–43.

Crans, G.G., Genant, H.K., Krege, J.H., 2005. Prognostic utility of a semiquantitative spinal deformity index. Bone 37, 175–179.

D. Gelalis, I., E. DeFrate, L., S. Stafilas, K., E. Pakos, E., D. Kang, J., G. Gilbertson, L., 2009. Three-dimensional analysis of cervical spine motion : reliability of a computer assisted magnetic tracking device compared to inclinometer. Eur. Spine J. 18, 276–281.

Damsgaard, M., Rasmussen, J., Christensen, S.T., Surma, E., de Zee, M., 2006. Analysis of musculoskeletal systems in the AnyBody Modeling System. Simul. Model. Pract. Theory 14, 1100–1111.

de Zee, M., Hansen, L., Wong, C., Rasmussen, J., Simonsen, E.B., 2007. A generic detailed rigid-body lumbar spine model. J. Biomech. 40, 1219–1227.

Degenhardt, B.F., Starks, Z., Bhatia, S., 2020. Reliability of the DIERS Formetric 4D Spine Shape Parameters in Adults without Postural Deformities. Biomed Res. Int. 2020.

Delp, S.L., Anderson, F.C., Arnold, A.S., Loan, P., Habib, A., John, C.T., Guendelman, E., Thelen, D.G., 2007. OpenSim: open-source software to create and analyze dynamic simulations of movement. IEEE Trans. Biomed. Eng. 54, 1940–1950.

Delp, S.L., Loan, J.P., Hoy, M.G., Zajac, F.E., Topp, E.L., Rosen, J.M., 1990. An interactive graphics-based model of the lower extremity to study orthopaedic surgical procedures. IEEE Trans. Biomed. Eng. 37, 757–767.

Delp, S.L.S., Anderson, F.C.F., Arnold, A.S.A., Loan, P., Habib, A., John, C.T.C., Guendelman, E., Thelen, D.G.D., 2007. OpenSim: Open source to create and analyze dynamic simulations of movement. IEEE Trans. Biomed. Eng. 54, 1940–1950.

Dickey, J.P., Pierrynowski, M.R., Bednar, D.A., Yang, S.X., 2002. Relationship between pain and vertebral motion in chronic low-back pain subjects. Clin. Biomech. 17, 345–352.

Diebo, B., Liu, S., Lafage, V., Schwab, F., 2014. Osteotomies in the treatment of spinal deformities: Indications, classification, and surgical planning. Eur. J. Orthop. Surg. Traumatol. https://doi.org/10.1007/s00590-014-1471-7

Diebo, B.G., Ferrero, E., Lafage, R., Challier, V., Liabaud, B., Liu, S., Vital, J.-M., Errico, T.J., Schwab, F.J., Lafage, V., 2015. Recruitment of compensatory mechanisms in sagittal spinal malalignment is age and regional deformity dependent: a full-standing axis analysis of key radiographical parameters. Spine (Phila. Pa. 1976). 40, 642–9.

Diebo, B.G., Shah, N. V., Boachie-Adjei, O., Zhu, F., Rothenfluh, D.A., Paulino, C.B., Schwab, F.J., Lafage, V., 2019. Adult spinal deformity. Lancet 394, 160–172.

Diebo, B.G., Shah, N. V., Pivec, R., Naziri, Q., Patel, A., Post, N.H., Assi, A., Godwin, E.M., Lafage, V., Schwab, F.J., Paulino, C.B., 2018. From static spinal alignment to dynamic body balance: Utilizing motion analysis in spinal deformity surgery. JBJS Rev. 6, e3.

Fagan, M.J., Julian, S., Mohsen, A.M., 2002. Finite element analysis in spine research. Proc. Inst. Mech. Eng. Part H J. Eng. Med. 216, 281–298.

Fairbank, J.C., Pynsent, P.B., 2000. The Oswestry Disability Index. Spine (Phila. Pa. 1976). 25, 2940–52; discussion 2952.

Faraj, S.S.A., van Hooff, M.L., Holewijn, R.M., Polly, D.W., Haanstra, T.M., de Kleuver, M., 2017. Measuring outcomes in adult spinal deformity surgery: a systematic review to identify current strengths, weaknesses and gaps in patient-reported outcome measures. Eur. Spine J. 26, 2084–2093.

Favier, C.D., Finnegan, M.E., Quest, R.A., Honeyfield, L., McGregor, A.H., Phillips, A.T.M., 2021. An open-source musculoskeletal model of the lumbar spine and lower limbs: a validation for movements of the lumbar spine: Additional data. Comput. Methods Biomech. Biomed. Engin.

Fon, G.T., Pritt, M.J., A. Cole Thies, J., 1980. Normal Kyphosis: Range in Normal Subjects. Am. Roentgen Ray Soc. 134, 979–983.

Fujii, R., Sakaura, Æ.H., Mukai, Æ.Y., Hosono, N., Ishii, Æ.T., Iwasaki, Æ.M., Yoshikawa, H., Sugamoto, Æ.K., 2007. Kinematics of the lumbar spine in trunk rotation : in vivo three-dimensional analysis using magnetic resonance imaging. Spine J 16, 1867–1874.

Galbusera, F., Niemeyer, F., Bassani, T., Sconfienza, L.M., Wilke, H.J., 2020. Estimating the three-dimensional vertebral orientation from a planar radiograph: Is it feasible? J. Biomech. 102, 109328.

Genant, H.K., Wu, C.Y., van Kuijk, C., Nevitt, M.C., 1993. Vertebral fracture assessment using a semiquantitative technique. J. Bone Miner. Res. 8, 1137–1148.

Ghezelbash, F., Eskandari, A.H., Shirazi-Adl, A., Arjmand, N., El-Ouaaid, Z., Plamondon, A., 2017. Effects of motion segment simulation and joint positioning on spinal loads in trunk musculoskeletal models. J. Biomech. 70, 149–156.

Ghezelbash, F., Shirazi-adl, A., Arjmand, N., El-Ouaaid, Z., Plamondon, A., 2016. Subject-specific biomechanics of trunk: musculoskeletal scaling , internal loads and intradiscal pressure estimation. Biomech. Model. Mechanobiol. 15, 1699–1712.

Glaser, D. a., Doan, J., Newton, P.O., 2012. Comparison of 3-Dimensional Spinal Reconstruction Accuracy. Spine (Phila. Pa. 1976). 37, 1391–1397.

Gonnella, C., Paris, S. V, Kutner, M., 1982. Reliability in Evaluating Passive Intervertebral Motion. Phys. Ther. 62, 436–444.

Gottipati, P., Fatone, S., Koski, T., Sugrue, P.A., Ganju, A., 2014. Crouch gait in persons with positive sagittal spine alignment resolves with surgery. Gait Posture 39, 372–377.

Gracovetsky, S., Newman, N., Pawlowsky, M., Lanzo, V., Davey, B., Robinson, L., 1995. A database for estimating normal spinal motion derived from noninvasive measurements. Spine (Phila. Pa. 1976).

Graham, R.B., Dupeyron, A., van Dieën, J.H., 2020. Between-day reliability of IMU-derived spine control metrics in patients with low back pain. J. Biomech. 113, 110080.

Guvenc, Y., Akyoldas, G., Senturk, S., Erbulut, D., Yaman, O., Ozer, A.F., 2019. How to reduce stress on the pedicle screws in thoracic spine? Importance of screw trajectory: A finite element analysis. Turk. Neurosurg. 29, 20–25.

Ha, Y., Maruo, K., Racine, L., Schairer, W.W., Hu, S.S., Deviren, V., Burch, S., Tay, B., Chou, D., Mummaneni, P. V, Ames, C.P., Berven, S.H., 2013. Proximal junctional kyphosis and clinical outcomes in adult spinal deformity surgery with fusion from the thoracic spine to the sacrum: a comparison of proximal and distal upper instrumented vertebrae. J. Neurosurg. Spine 19, 360–369.

Haddas, R., Ju, K.L., Belanger, T., Lieberman, I.H., 2018. The use of gait analysis in the assessment of patients afflicted with spinal disorders. Eur. Spine J. 27, 1712–1723.

Hajibozorgi, M., Arjmand, N., 2016. Sagittal range of motion of the thoracic spine using inertial tracking device and effect of measurement errors on model predictions. J. Biomech. 49, 913–918.

Han, K.S., Zander, T., Taylor, W.R., Rohlmann, A., 2012. An enhanced and validated generic thoraco-lumbar spine model for prediction of muscle forces. Med. Eng. Phys. 34, 709–716.

Hannah, I., Montefiori, E., Modenese, L., Prinold, J., Viceconti, M., Mazzà, C., 2017. Sensitivity of a juvenile subject-specific musculoskeletal model of the ankle joint to the variability of operator-dependent input. Proc. Inst. Mech. Eng. Part H J. Eng. Med. 231, 415–422.

Harrison, D.E., Colloca, C.J., Harrison, D.D., Janik, T.J., Haas, J.W., Keller, T.S., 2005. Anterior thoracic posture increases thoracolumbar disc loading. Eur. Spine J. 14, 234–242.

Hassanzadeh, H., Jain, A., El Dafrawy, M.H., Ain, M.C., Mesfin, A., Skolasky, R.L., Kebaish, K.M., 2012. Three-Column Osteotomies in the Treatment of Spinal Deformity in Adult Patients 60 Years Old and Older: Outcome and Complications. Spine (Phila. Pa. 1976). 38, 726–731.

Hawker, G.A., Mian, S., Kendzerska, T., French, M., 2011. Measures of adult pain: Visual Analog Scale for Pain (VAS Pain), Numeric Rating Scale for Pain (NRS Pain), McGill Pain Questionnaire (MPQ), Short-Form McGill Pain Questionnaire (SF-MPQ), Chronic Pain Grade Scale (CPGS), Short Form-36 Bodily Pain Scale

(SF. Arthritis Care Res. 63, 240–252.

Hemming, R., Sheeran, L., van Deursen, R., Sparkes, V., 2018. Non-specific chronic low back pain: differences in spinal kinematics in subgroups during functional tasks. Eur. Spine J. 27, 163–170.

Heneghan, N.R., Balanos, G.M., 2010. Soft tissue artefact in the thoracic spine during axial rotation and arm elevation using ultrasound imaging: A descriptive study. Man. Ther. 15, 599–602.

Hicks, J.L., Uchida, T.K., Seth, A., Rajagopal, A., Delp, S.L., 2015. Is My Model Good Enough? Best Practices for Verification and Validation of Musculoskeletal Models and Simulations of Movement. J. Biomech. Eng. 137, 020905.

Holzbaur, K.R.S., Murray, W.M., Delp, S.L., 2005. A model of the upper extremity for simulating musculoskeletal surgery and analyzing neuromuscular control. Ann. Biomed. Eng. 33, 829–840.

Horton, W.C., Brown, C.W., Bridwell, K.H., Glassman, S.D., Suk, S. Il, Cha, C.W., 2005. Is there an optimal patient stance for obtaining a lateral 36″ radiograph?: A critical comparison of three techniques. Spine (Phila. Pa. 1976). 30, 427–433.

Hui, S.C.N., Pialasse, J.P., Wong, J.Y.H., Lam, T. ping, Ng, B.K.W., Cheng, J.C.Y., Chu, W.C.W., 2016. Radiation dose of digital radiography (DR) versus micro-dose x-ray (EOS) on patients with adolescent idiopathic scoliosis: 2016 SOSORT- IRSSD "John Sevastic Award" Winner in Imaging Research. Scoliosis Spinal Disord. 11, 1–8.

Ignasiak, D., 2020. A novel method for prediction of postoperative global sagittal alignment based on full-body musculoskeletal modeling and posture optimization. J. Biomech. 102, 109324.

Ignasiak, D., Dendorfer, S., Ferguson, S.J., 2016. Thoracolumbar spine model with articulated ribcage for the prediction of dynamic spinal loading. J. Biomech. 49, 959–966.

Ignasiak, D., Peteler, T., Fekete, T.F., Haschtmann, D., Ferguson, S.J., 2018a. The influence of spinal fusion length on proximal junction biomechanics: a parametric computational study. Eur. Spine J. 27, 2262–2271.

Ignasiak, D., Rüeger, A., Ferguson, S.J., 2017. Multi-segmental thoracic spine kinematics measured dynamically in the young and elderly during flexion. Hum. Mov. Sci. 54, 230–239.

Ignasiak, D., Rüeger, A., Sperr, R., Ferguson, S.J., 2018b. Thoracolumbar spine loading associated with kinematics of the young and the elderly during activities of daily living. J. Biomech. 70, 175–184.

Ilharreborde, B., Even, J., Lefevre, Y., Fitoussi, F., Presedo, A., Souchet, P., Penneçot, G.F., Mazda, K., 2008. How to determine the upper level of instrumentation in Lenke types 1 and 2 adolescent idiopathic scoliosis: A prospective study of 132 patients. J. Pediatr. Orthop. 28, 733–739.

Illes, T., Somoskeoy, S., Illés, T., Somoskeöy, S., 2012. The EOS ™ imaging system and its uses in daily orthopaedic practice. Int. Orthop. 36, 1325–1331.

Inoue, N., Orías, A.A.E., 2011. Biomechanic of disc degeneraion. Orthop. Clin. North Am. 42, 487–499.

Iorio, J.A., Jakoi, A.M., Singla, A., 2016. Biomechanics of degenerative spinal disorders. Asian Spine J. 10, 377–384.

Izzo, R., Guarnieri, G., Guglielmi, G., Muto, M., 2013. Biomechanics of the spine . Part I : Spinal stability. Eur. J. Radiol. 82, 118–126.

Jalalian, A., Gibson, I., Tay, E.H., 2013. Computational biomechanical modeling of scoliotic spine: Challenges and opportunities. Spine Deform. 1, 401–411.

Jalalian, A., Tay, F.E.H., Arastehfar, S., Liu, G., 2016. A patient-specific multibody kinematic model for representation of the scoliotic spine movement in frontal plane of the human body. Multibody Syst. Dyn. 1–24.

Kadoury, S., Cheriet, F., Laporte, C., Labelle, H., 2007. A versatile 3D reconstruction system of the spine and pelvis for clinical assessment of spinal deformities. Med. Biol. Eng. Comput. 45, 591–602.

Kainz, H., Modenese, L., Lloyd, D.G., Maine, S., Walsh, H.P.J., Carty, C.P., 2016. Joint kinematic calculation based on clinical direct kinematic versus inverse kinematic gait models. J. Biomech. 49, 1658–1669.

Kawkabani, G., Saliby, R.M., Mekhael, M., Rachkidi, R., Massaad, A., Ghanem, I., Kharrat, K., Kreichati, G., Saad, E., Lafage, V., Lafage, R., Skalli, W., Assi, A., 2021. Gait kinematic alterations in subjects with adult spinal deformity and their radiological determinants. Gait Posture 88, 203–209.

Kim, H.K., Zhang, Y., 2017. Estimation of lumbar spinal loading and trunk muscle forces during asymmetric lifting tasks: application of whole-body musculoskeletal modelling in OpenSim. Ergonomics 60, 563–576.

Kim, Y.J., Hyun, S.J., Cheh, G., Cho, S.K., Rhim, S.C., 2016. Decision making algorithm for adult spinal deformity surgery. J. Korean Neurosurg. Soc. 59, 327–333.

King, H.A., Moe, J.H., Bradford, D.S., Winter, R.B., 1983. The selection of fusion levels in thoracic idiopathic scoliosis. J. Bone Jt. Surg. - Ser. A 65, 1302–1313.

Konieczny, M.R., Senyurt, H., Krauspe, R., 2013. Epidemiology of adolescent idiopathic scoliosis. J. Child. Orthop. 7, 3–9.

Konz, R.J., Fatone, S., Stine, R.L., Ganju, A., Gard, S.A., Ondra, S.L., 2006. A kinematic model to assess spinal motion during walking. Spine (Phila. Pa. 1976). 31, 898–906.

Kotwal, S., Pumberger, M., Hughes, A., Girardi, F., 2011. Degenerative Scoliosis: A Review. HSS J. 7, 257–264.

Kretzer, R.M., 2017. Adult Degenerative Spinal Deformity: Overview and Open Approaches for Treatment. Spine (Phila. Pa. 1976). 42, S16.

Kuai, S., Guan, X., Liu, W., Ji, R., Xiong, J., Wang, D., Zhou, W., 2019. Prediction of the Spinal Musculoskeletal Loadings during Level Walking and Stair Climbing after Two Types of Simulated Interventions in Patients with Lumbar Disc Herniation. J. Healthc. Eng. 2019.

Kushchayev, S. V., Glushko, T., Jarraya, M., Schuleri, K.H., Preul, M.C., Brooks, M.L., Teytelboym, O.M., 2018. ABCs of the degenerative spine. Insights Imaging 9, 253–274.

Lafage, V., Schwab, F., Skalli, W., Hawkinson, N., Gagey, P., Ondra, S., Farcy, J., 2008. Standing balance and sagittal plane spinal deformity: analysis of spinopelvic and gravity line parameters. Spine (Phila. Pa. 1976). 33, 1572–1578.

Le Huec, J.C., Faundez, A., Dominguez, D., Hoffmeyer, P., Aunoble, S., 2014. Evidence showing the relationship between sagittal balance and clinical outcomes in surgical treatment of degenerative spinal diseases: a literature review. Int. Orthop. 39, 87–95.

Leardini, A., Chiari, L., Della Croce, U., Cappozzo, A., 2005. Human movement analysis using stereophotogrammetry. Part 3. Soft tissue artifact assessment and compensation. Gait Posture 21, 212–25.

Lenke, Lawrence G., Betz, R.R., Haher, T.R., Lapp, M.A., Merola, A.A., Harms, J., Shufflebarger, H.L., 2001. Multisurgeon assessment of surgical decision-making in adolescent idiopathic scoliosis curve classification, operative approach, and fusion levels. Spine (Phila. Pa. 1976). 26, 2347–2353.

Lenke, L G, Engsberg, J.R., Ross, S. a, Reitenbach, A., Blanke, K., Bridwell, K.H., 2001. Prospective dynamic functional evaluation of gait and spinal balance following spinal fusion in adolescent idiopathic scoliosis. Spine (Phila. Pa. 1976). 26, E330–E337.

Leroux, M. a, Zabjek, K., Simard, G., Badeaux, J., Coillard, C., Rivard, C.H., 2000. A noninvasive anthropometric technique for measuring kyphosis and lordosis: an application for idiopathic scoliosis. Spine (Phila. Pa. 1976). 25, 1689–1694.

Li, Guoan, Wang, S., Passias, P., Xia, Q., Li, Gang, Wood, K., 2009. Segmental in vivo vertebral motion during functional human lumbar spine activities. Eur. Spine J. 18, 1013–1021.

List, R., Gülay, T., Stoop, M., Lorenzetti, S., List Renate, 2013. Kinematics of the Trunk and the Lower Extremities During Restricted and Unrestricted Squats. J. Strength Cond. Res. 27, 1529–1538.

Liu, X., Han, C., Wang, H., Wu, J., Cui, Y., Zhang, X., Wang, X., 2021. Fully automated pelvic bone segmentation in multiparameteric MRI using a 3D convolutional neural network. Insights Imaging 12.

Lu, T.W., O'Connor, J.J., 1999. Bone position estimation from skin marker co-ordinates using global optimisation with joint constraints. J. Biomech. 32, 129–134.

Luo, T.D., Stans, A.A., Schueler, B.A., Larson, A.N., 2015. Cumulative Radiation Exposure With EOS Imaging Compared With Standard Spine Radiographs. Spine Deform. 3, 144–150.

MacWilliams, B.A., Rozumalski, A., Swanson, A.N., Wervey, R.A., Dykes, D.C., Novacheck, T.F., Schwartz, M.H., 2013. Assessment of three-dimensional lumbar spine vertebral motion during gait with use of indwelling bone pins. J. Bone Jt. Surg. - Ser. A 95, 1–9.

Mahallati, S., Rouhani, H., Preuss, R., Masani, K., Popovic, M.R., 2016. Multisegment Kinematics of the Spinal Column : Soft Tissue Artifacts Assessment. J. Biomech. Eng. 138, 1–8.

Majdouline, Y., Aubin, C.-E., Robitaille, M., Sarwark, J.F., Labelle, H., 2007. Scoliosis Correction Objectives in Adolescent Idiopathic Scoliosis. J. Pediatr. Orthop. 27, 775–781.

Mannion, A.F., Knecht, K., Balaban, G., Dvorak, J., Grob, D., 2004. A new skin-surface device for measuring the curvature and global and segmental ranges of motion of the spine: Reliability of measurements and comparison with data reviewed from the literature. Eur. Spine J. 13, 122–136.

Mannion, A.F., Vila-Casademunt, A., Domingo-Sàbat, M., Wunderlin, S., Pellisé, F., Bago, J., Acaroglu, E., Alanay, A., Pérez-Grueso, F.S., Obeid, I., Kleinstück, F.S., European Spine Study Group (Essg), 2016. The Core Outcome Measures Index (COMI) is a responsive instrument for assessing the outcome of treatment for adult spinal deformity. Eur. Spine J. 2638–48.

Martelli, S., Valente, G., Viceconti, M., Taddei, F., 2015. Sensitivity of a subject-specific musculoskeletal model to the uncertainties on the joint axes location. Comput. Methods Biomech. Biomed. Engin. https://doi.org/10.1080/10255842.2014.930134

Mayer, T.G., Tencer, A.F., Kristoferson, S., Mooney, V., 1984. Use of noninvasive techniques for quantification of spinal range-of-motion in normal subjects and chronic low-back dysfunction patients. Spine (Phila. Pa. 1976). https://doi.org/10.1097/00007632-198409000-00009

Mc Donnell, P., Mc Hugh, P.E., O'Mahoney, D., 2007. Vertebral osteoporosis and trabecular bone quality. Ann. Biomed. Eng. 35, 170–189.

McAviney, J., Roberts, C., Sullivan, B., Alevras, A.J., Graham, P.L., Brown, B.T., 2020. The prevalence of adult de novo scoliosis: A systematic review and meta-analysis. Eur. Spine J. https://doi.org/10.1007/s00586-020-06453-0

McDonnell, M., Shah, K.N., Paller, D.J., Thakur, N.A., Koruprolu, S., Palumbo, M.A., Daniels, A.H., 2016. Biomechanical Analysis of Pedicle Screw Fixation for Thoracolumbar Burst Fractures. Orthopedics 1–5.

Melhem, E., Assi, A., El Rachkidi, R., Ghanem, I., 2016. EOS® biplanar X-ray imaging: concept, developments, benefits, and limitations. J. Child. Orthop. 10, 1–14.

Moke, L., 2018. Determinants of health-related quality of life in patients with adult spinal deformity: Additional value of dynamic biomechanical measures. KU Leuven.

Moke, L., Overbergh, T., Severijns, P., Schelfaut, S., Moens, P., Van De Loock, K., Hermans, L., Molenaers, G., Jonkers, I., Scheys, L., 2020. The Transverse Gravitational Deviation Index, a Novel Gravity Line-Related Spinal Parameter, Relates to Balance Control and Health-Related Quality of Life in Adults with Spinal Deformity. Spine (Phila. Pa. 1976). 45, E25–E36.

Mor, V., Laliberte, L., JN, M., Wiemann, M., 1984. The Karnofsky Performance Status Scale: An examination of its reliability and validity in a research setting. Cancer 53, 2002–2007.

Mörl, F., Blickhan, R., 2006. Three-dimensional relation of skin markers to lumbar vertebrae of healthy subjects in different postures measured by open MRI. Eur. Spine J. 15, 742–751.

Mousavi, S.J., Tromp, R., Swann, M.C., White, A.P., Anderson, D.E., 2018. Between-session reliability of opto-electronic motion capture in measuring sagittal posture and 3-D ranges of motion of the thoracolumbar spine. J. Biomech. 79, 248–252.

Myers, C.A., Laz, P.J., Shelburne, K.B., Davidson, B.S., 2015. A Probabilistic Approach to Quantify the Impact of Uncertainty Propagation in Musculoskeletal Simulations. Ann. Biomed. Eng. 43, 1098–1111.

Navacchia, A., Myers, C.A., Rullkoetter, P.J., 2016. Prediction of In Vivo Knee Joint Loads Using a Global Probabilistic Analysis. J. Biomech. Eng. 138, 4032379.

Needham, R., Naemi, R., Healy, A., 2016. Multi-segment kinematic model to assess three-dimensional movement of the spine and back during gait. Prosthet. Orthot. Int. 40, 624–635.

Neyens, C., 2020. Cost Calculation of a Balance and Motion Analysis for Adult Spinal Deformity Patients. KU Leuven.

O'Grady, M., O'Dwyer, T., Connolly, J., Condell, J., Muñoz Esquivel, K., D. O'Shea, F., Gardiner, P., Wilson, F., 2021. Measuring spinal mobility using an inertial measurement unit system: A validation study in axial

spondyloarthritis. Diagnostics 11, 1–17.

Oda, I., Abumi, K., Cunningham, B.W., Kaneda, K., McAfee, P.C., 2002. An in vitro human cadaveric study investigating the biomechanical properties of the thoracic spine. Spine (Phila. Pa. 1976). 27, 64–70.

Orina, J.N., Berven, S.H., 2017. Principles of deformity correction, in: Essentials of Spinal Stabilization. Springer International Publishing, pp. 487–504.

Overbergh, T., Severijns, P., Beaucage-gauvreau, E., Ackermans, T., Moke, L., Jonkers, I., Scheys, L., 2021. Subject-Specific Spino-Pelvic Models Reliably Measure Spinal Kinematics During Seated Forward Bending in Adult Spinal Deformity. Front. Bioeng. Biotechnol. 9, 1–11.

Overbergh, T., Severijns, P., Beaucage-Gauvreau, E., Jonkers, I., Moke, L., Scheys, L., 2020. Development and validation of a modeling workflow for the generation of image-based, subject-specific thoracolumbar models of spinal deformity. J. Biomech. 110, 109946.

Panjabi, M., Yamamoto, I., Oxland, T., Crisco, J., 1989. How does posture affect coupling in the lumbar spine? Spine (Phila. Pa. 1976). https://doi.org/10.1097/00007632-198909000-00015

Panjabi, M.M., Brand, R.A., White, A.A., 1976. Three-dimensional flexibility and stiffness properties of the human thoracic spine. J. Biomech. 9, 185–192.

Panjabi, M.M., Tech, D., Oxland, T.R., Yamamoto, I., Crisco, J.J., 1994. Mechanical properties of the human cervical spine as shown by three-dimensional load-displacement curves. J. Bone Jt. Surg. 76-A, 413–424.

Papi, E., Bull, A.M.J., McGregor, A.H., 2019. Spinal segments do not move together predictably during daily activities. Gait Posture 67, 277–283.

Pasha, S., Cahill, P.J., Dormans, J.P., Flynn, J.M., 2016. Characterizing the differences between the 2D and 3D measurements of spine in adolescent idiopathic scoliosis. Eur. Spine J. 25, 3137–3145.

Pasha, S., Flynn, J., 2018. Data-driven Classification of the 3D Spinal Curve in Adolescent Idiopathic Scoliosis with an Applications in Surgical Outcome Prediction. Sci. Rep. 8, 2–11.

Paul, J.C., Petrizzo, A., Rizzo, J.R., Bianco, K., Maier, S., Errico, T.J., Lafage, V., 2015. Feasibility of a Cost-Effective, Video Analysis Software-Based Mobility Protocol for Objective Spine Kinematics and Gait Metrics: A Proof of Concept Study. PM R 7, 336–339.

Pearcy, M.J., Bogduk, N., 1988. Instantaneous Axes of Rotation of the Lumbar Intervertebral Joints. Spine (Phila. Pa. 1976). 13, 1033–1041.

Pellisé, F., Vila-Casademunt, A., Ferrer, M., Domingo-Sàbat, M., Bagó, J., Pérez-Grueso, F.J.S., Alanay, A., Mannion, A.F., Acaroglu, E., 2014. Impact on health related quality of life of adult spinal deformity (ASD) compared with other chronic conditions. Eur. Spine J. 24, 3–11.

Pichelmann, M. a, Lenke, L.G., Bridwell, K.H., Good, C.R., O'Leary, P.T., Sides, B. a, 2010. Revision rates following primary adult spinal deformity surgery: six hundred forty-three consecutive patients followed-up to twenty-two years postoperative. Spine (Phila. Pa. 1976). 35, 219–226.

Pillet, H., Sangeux, M., Hausselle, J., El Rachkidi, R., Skalli, W., Rachkidi, R. El, Skalli, W., 2014. A reference method for the evaluation of femoral head joint center location technique based on external markers. Gait Posture 39, 655–658.

Pratali, R.R., Nasreddine, M.A., Diebo, I.B., Carlos, I.I., Oliveira, E.A.S., Iii, I.V.L., 2018. Normal values for sagittal spinal alignment : a study of Brazilian subjects. Clinics 1–8.

Preuss, R.A., Popovic, M.R., 2010. Three-dimensional spine kinematics during multidirectional, target-directed trunk movement in sitting. J. Electromyogr. Kinesiol. 20, 823–832.

Quint, U., Wilke, H.J., 2008. Grading of degenerative disk disease and functional impairment: Imaging versus patho-anatomical findings. Eur. Spine J. 17, 1705–1713.

Raabe, M.E., Chaudhari, A.M.W., 2016. An investigation of jogging biomechanics using the full-body lumbar spine model: Model development and validation. J. Biomech. 49, 1238–1243.

Rast, F.M., Graf, E.S., Meichtry, A., Kool, J., Bauer, C.M., 2016. Between-day reliability of three-dimensional motion analysis of the trunk: A comparison of marker based protocols. J. Biomech. 49, 807–811.

Reeves, P.N., Narendra, K.S., Cholewicki, J., 2007. Spinal stability: the six blind men and the elephant. Clin.

Biomech. 22, 266–274.

Robitaille, M., Aubin, C.E., Labelle, H., 2007. Intra and interobserver variability of preoperative planning for surgical instrumentation in adolescent idiopathic scoliosis. Eur. Spine J. 16, 1604–1614.

Rosenlund, S., Holsgaard-Larsen, A., Overgaard, S., Jensen, C., 2016. The Gait Deviation Index is associated with hip muscle strength and patient-reported outcome in patients with severe hip osteoarthritis - A cross-sectional study. PLoS One 11, 1–14.

Roth, A.K., Beheshtiha, A.S., van der Meer, R., Willems, P.C., Arts, J.J., Ito, K., van Rietbergen, B., 2021. Validation of a finite element model of the thoracolumbar spine to study instrumentation level variations in early onset scoliosis correction. J. Mech. Behav. Biomed. Mater. 117, 104360.

Rupp, T.K., Ehlers, W., Karajan, N., Günther, M., Schmitt, S., 2015. A forward dynamics simulation of human lumbar spine flexion predicting the load sharing of intervertebral discs, ligaments, and muscles. Biomech. Model. Mechanobiol. 14, 1081–1105.

Ryu, W.H.A., Platt, A., O'Toole, J.E., Fontes, R., Fessler, R.G., 2021. Patient Expectations of Adult Spinal Deformity Correction Surgery. World Neurosurg. 146, e931–e939.

Salem, W., Coomans, Y., Dugailly, P., 2015. Sagittal Thoracic and Lumbar Spine Profiles in Upright Standing and Lying Prone Positions Among Healthy Subjects 40.

Sanchez-Mariscal, F., Gomez-Rice, A., Izquierdo, E., Pizones, J., Zuniga, L., Alvarez-Gonzalez, P., 2014. Survivorship analysis after primary fusion for adult scoliosis. Prognostic factors for reoperation. Spine J. 14, 1629–1634.

Scheer, J.K.I., Tang, J. a, Smith, J.S., Klineberg, E., Hart, R.A., Mundis, G.M., Burton, D.C., Hostin, R., O'Brien, M.F., Bess, S., Kebaish, K.M., Deviren, V., Lafage, V., Schwab, F.J., Shaffrey, C.I., Ames, C.P., 2013. Reoperation rates and impact on outcome in a large, prospective, multicenter, adult spinal deformity database: clinical article. J. Neurosurg. Spine 19, 464–470.

Scheys, L., Campenhout, A. Van, Spaepen, A., Suetens, P., Jonkers, I., 2008. Personalized MR-based musculoskeletal models compared to rescaled generic models in the presence of increased femoral anteversion : Effect on hip moment arm lengths 28, 358–365.

Scheys, L., Desloovere, K., Spaepen, A., Suetens, P., Jonkers, I., 2011a. Calculating gait kinematics using MR-based kinematic models. Gait Posture 33, 158–164.

Scheys, L., Desloovere, K., Suetens, P., Jonkers, I., 2011b. Level of subject-specific detail in musculoskeletal models affects hip moment arm length calculation during gait in pediatric subjects with increased femoral anteversion. J. Biomech. 44, 1346–1353.

Scheys, L., Jonkers, I., Schutyser, F., Pans, S., Spaepen, A., Suetens, P., 2005. Image based methods to generate subject-specific musculoskeletal models for gait analysis 1281, 62–67.

Schmid, J., Magnenat-Thalmann, N., 2008. MRI Bone Segmentation Using Deformable Models and Shape Priors, in: Metaxas, D., Axel, L., Fichtinger, G., Székely, G. (Eds.), Medical Image Computing and Computer-Assisted Intervention -- MICCAI 2008. Springer Berlin Heidelberg, Berlin, Heidelberg, pp. 119–126.

Schmid, S., Burkhart, K.A., Allaire, B.T., Grindle, D., Anderson, D.E., 2020a. Musculoskeletal full-body models including a detailed thoracolumbar spine for children and adolescents aged 6–18 years. J. Biomech. 102, 109305.

Schmid, S., Burkhart, K.A., Allaire, B.T., Grindle, D., Bassani, T., Galbusera, F., Anderson, D.E., 2020b. Spinal Compressive Forces in Adolescent Idiopathic Scoliosis With and Without Carrying Loads: A Musculoskeletal Modeling Study. Front. Bioeng. Biotechnol. 8, 1–12.

Schmid, S., Studer, D., Hasler, C.C., Romkes, J., Taylor, W.R., Brunner, R., Lorenzetti, S., 2015. Using skin markers for spinal curvature quantification in main thoracic adolescent idiopathic scoliosis: An explorative radiographic study. PLoS One 10.

Schmid, S., Studer, D., Hasler, C.C., Romkes, J., Taylor, W.R., Lorenzetti, S., Brunner, R., 2016. Quantifying spinal gait kinematics using an enhanced optical motion capture approach in adolescent idiopathic scoliosis. Gait Posture 44, 231–237.

Schroeder, J., Reer, R., Braumann, K.M., 2015. Video raster stereography back shape reconstruction: a reliability study for sagittal, frontal, and transversal plane parameters. Eur. Spine J. 24, 262–269.

Schwab, F., Lafage, V., Boyce, R., Skalli, W., Farcy, J., 2006. Gravity Line Analysis in Adult Volunteers Age-Related Correlation With Spinal Parameters , Pelvic Parameters , and Foot Position 31, 959–967.

Schwab, F., Ungar, B., Blondel, B., Buchowski, J., Coe, J., Deinlein, D., DeWald, C., Mehdian, H., Shaffrey, C., Tribus, C., Lafage, V., 2012. Scoliosis Research Society-Schwab adult spinal deformity classification: a validation study. Spine (Phila. Pa. 1976). 37, 1077–82.

Schwab, F.J., Blondel, B., Bess, S., Hostin, R., Shaffrey, C.I., Smith, J.S., Boachie-Adjei, O., Burton, D.C., Akbarnia, B.A., Mundis, G.M., Ames, C.P., Kebaish, K., Hart, R.A., Farcy, J.-P., Lafage, V., 2013. Radiographical Spinopelvic Parameters and Disability in the Setting of Adult Spinal Deformity. Spine (Phila. Pa. 1976). 38, E803–E812.

Schwartz, M.H., Trost, J.P., Wervey, R.A., 2004. Measurement and management of errors in quantitative gait data. Gait Posture 20, 196–203.

Senteler, M., Weisse, B., Rothenfluh, D.A., Snedeker, J.G., 2015. Intervertebral reaction force prediction using an enhanced assembly of OpenSim models. Comput. Methods Biomech. Biomed. Engin. 5842, 1–11.

Severijns, P., Moke, L., Overbergh, T., Van de Loock, K., Desloovere, K., Scheys, L., 2017. Are static sagittal compensation strategies preserved during walking in adult spinal deformity? Gait Posture 57, 188–189.

Severijns, P., Overbergh, T., Schmid, S., Moke, L., 2021. Spinal Palpation Error and Its Impact on Skin Marker-Based Spinal Alignment Measurement in Adult Spinal Deformity. Front. Bioeng. Biotechnol. 9, 1–9.

Severijns, P., Overbergh, T., Thauvoye, A., Baudewijns, J., Monari, D., Moke, L., Desloovere, K., Scheys, L., 2020. A subject-specific method to measure dynamic spinal alignment in adult spinal deformity. Spine J. 20, 934–946.

Shayestehpour, H., Rasmussen, J., Galibarov, P., Wong, C., 2021. An articulated spine and ribcage kinematic model for simulation of scoliosis deformities. Multibody Syst. Dyn.

Shrout, P.E., Fleiss, J.L., 1979. Intraclass correlations: Uses in assessing rater reliability. Psychol. Bull. 86, 420–428.

Simon, A.L., Ferrero, E., Larson, A.N., Kaufman, K.R., 2018. Stereoradiography imaging motion artifact: does it affect radiographic measures after spinal instrumentation? Eur. Spine J. 27, 1105–1111.

Smith, J.S., Klineberg, E., Lafage, V., Shaffrey, C.I., Schwab, F., Lafage, R., Hostin, R., Jr, G.M.M., Errico, T.J., Kim, H.J., Protopsaltis, T.S., Hamilton, D.K., Scheer, J.K., Soroceanu, A., Kelly, M.P., Line, B., Gupta, M., Deviren, V., Hart, R., Burton, D.C., Bess, S., 2016. Prospective multicenter assessment of perioperative and minimum 2-year postoperative complication rates associated Associated With Adult Spinal Deformity Surgery 25, 1–14.

Smith, J.S., Klineberg, E., Schwab, F., Shaffrey, C.I., Moal, B., Ames, C.P., Hostin, R., Fu, K.-M.G., Burton, D., Akbarnia, B., Gupta, M., Hart, R., Bess, S., Lafage, V., 2013a. Change in Classification Grade by the SRS-Schwab Adult Spinal Deformity Classification Predicts Impact on Health-Related Quality of Life Measures: Prospective Analysis of Operative and Non-operative Treatment. Spine (Phila. Pa. 1976). 38, 1663–1671.

Smith, J.S., Shaffrey, C.I., Berven, S., Glassman, S., Hamill, C., Horton, W., Ondra, S., Schwab, F., Shainline, M., Fu, K.-M.G., Bridwell, K., 2009a. Operative versus nonoperative treatment of leg pain in adults with scoliosis: a retrospective review of a prospective multicenter database with two-year follow-up. Spine (Phila. Pa. 1976). 34, 1693–1698.

Smith, J.S., Shaffrey, C.I., Berven, S., Glassman, S., Hamill, C., Horton, W., Ondra, S., Schwab, F., Shainline, M., Fu, K.M., Bridwell, K., 2009b. Improvement of back pain with operative and nonoperative treatment in adults with scoliosis. Neurosurgery 65, 86–93.

Smith, J.S., Shaffrey, C.I., Bess, S., Shamji, M.F., Brodke, D., Lenke, L.G., Fehlings, M.G., Lafage, V., Schwab, F., Vaccaro, A.R., Ames, C.P., 2017. Recent and Emerging Advances in Spinal Deformity. Neurosurgery 80, S70–S85.

Smith, J.S., Shaffrey, C.I., Fu, K.-M.G., Scheer, J.K., Bess, S., Lafage, V., Schwab, F., Ames, C.P., 2013b. Clinical and radiographic evaluation of the adult spinal deformity patient. Neurosurg. Clin. N. Am. 24, 143–56.

Soroceanu, A., Diebo, B.G., Burton, D., Smith, J.S., Deviren, V., Shaffrey, C., Kim, H.J., Mundis, G., Ames, C., Errico, T., Bess, S., Hostin, R., Hart, R., Schwab, F., Lafage, V., 2015. Radiographical and Implant-Related Complications in Adult Spinal Deformity Surgery. Spine (Phila. Pa. 1976). 40, 1414–1421.

Souza, R. dos S., Alves, A.S. de, 2014. 3D-To-2D Registration for the EOS Biplanar Radiographic Imaging System,

Igarss 2014. owa City, IA, USA.

Steffen, T., Rubin, R., Baramki, H., Antoniou, J., Marchesi, D., Aebi, M., 1997. A new technique for measuring lumbar segmental motion in vivo. Spine (Phila. Pa. 1976). 22, 156–166.

Štern, D., Njagulj, V., Likar, B., Pernuš, F., Vrtovec, T., 2013. Quantitative vertebral morphometry based on parametric modeling of vertebral bodies in 3D. Osteoporos. Int. 24, 1357–1368.

Taneichi, H., Inami, S., Moridaira, H., Takeuchi, D., Sorimachi, T., Ueda, H., Aoki, H., Iimura, T., 2020. Can we stop the long fusion at L5 for selected adult spinal deformity patients with less severe disability and less complex deformity? Clin. Neurol. Neurosurg. 194, 105917.

Terran, J., Schwab, F., Shaffrey, C.I., Smith, J.S., Devos, P., Ames, C.P., Fu, K.M.G., Burton, D., Hostin, R., Klineberg, E., Gupta, M., Deviren, V., Mundis, G., Hart, R., Bess, S., Lafage, V., 2013. The SRS-schwab adult spinal deformity classification: Assessment and clinical correlations based on a prospective operative and nonoperative cohort. Neurosurgery 73, 559–568.

Turner, J.D., Akbarnia, B.A., Eastlack, R.K., Bagheri, R., Nguyen, S., Pimenta, L., Marco, R., Deviren, V., Uribe, J., Mundis, G.M., 2015. Radiographic outcomes of anterior column realignment for adult sagittal plane deformity: a multicenter analysis. Eur. Spine J. 24, 427–432.

Valente, G., Crimi, G., Vanella, N., Schileo, E., Taddei, F., 2017. NMSBUILDER: Freeware to create subject-specific musculoskeletal models for OpenSim. Comput. Methods Programs Biomed. 152, 85–92.

Valente, G., Pitto, L., Testi, D., Seth, A., Delp, S.L., Stagni, R., Viceconti, M., Taddei, F., 2014. Are subject-specific musculoskeletal models robust to the uncertainties in parameter identification? PLoS One 9.

Valente, G., Taddei, F., Jonkers, I., 2013. Influence of weak hip abductor muscles on joint contact forces during normal walking: Probabilistic modeling analysis. J. Biomech. 46, 2186–2193.

Valero-Cuevas, F.J., Johanson, M.E., Towles, J.D., 2003. Towards a realistic biomechanical model of the thumb: The choice of kinematic description may be more critical than the solution method or the variability/uncertainty of musculoskeletal parameters. J. Biomech. 36, 1019–1030.

Vasavada, A.N., Hughes, E., Nevins, D.D., Monda, S.M., Lin, D.C., 2018. Effect of Subject-Specific Vertebral Position and Head and Neck Size on Calculation of Spine Musculoskeletal Moments. Ann. Biomed. Eng. 46, 1844–1856.

Vasavada, A.N., Li, S., Delp, S.L., 1998. Influence of muscle morphometry and moment arms on the moment-generating capacity of human neck muscles. Spine (Phila. Pa. 1976). 23, 412–422.

Verheyden, G., Nieuwboer, A., Van de Winckel, A., De Weerdt, W., 2007. Clinical tools to measure trunk performance after stroke: a systematic review of the literature. Clin. Rehabil. 21, 387–394.

Wada, O., Tateuchi, H., Ichihashi, N., 2014. The correlation between movement of the center of mass and the kinematics of the spine, pelvis, and hip joints during body rotation. Gait Posture 39, 60–64.

Wang, M.Y., Lu, Y., Anderson, D.G., Mummaneni, P. V, 2014. Minimally Invasive Spinal Deformity Surgery.

Wang, W., Baran, G.R., Betz, R.R., Samdani, A.F., Pahys, J.M., Cahill, P.J., 2014. The Use of finite element models to assist understanding and treatment for scoliosis: A review paper. Spine Deform. 2, 10–27.

Wang, W., Wang, D., De Groote, F., Scheys, L., Jonkers, I., 2020. Implementation of physiological functional spinal units in a rigid-body model of the thoracolumbar spine. J. Biomech. 98, 109437.

Wang, W., Wang, D., Falisse, A., Severijns, P., Overbergh, T., Moke, L., Scheys, L., De Groote, F., Jonkers, I., 2021. A Dynamic Optimization Approach for Solving Spine Kinematics While Calibrating Subject-Specific Mechanical Properties. Ann. Biomed. Eng. Under review with minor revisions.

Wesseling, M., De Groote, F., Meyer, C., Corten, K., Simon, J.-P., Desloovere, K., Jonkers, I., 2016. Subject-specific musculoskeletal modelling in patients before and after total hip arthroplasty. Comput. Methods Biomech. Biomed. Engin. 19, 1683–1691.

Widmer, J., Fornaciari, P., Senteler, M., Roth, T., Snedeker, J.G., Farshad, M., 2019. Kinematics of the Spine Under Healthy and Degenerative Conditions : A Systematic Review. Ann. Biomed. Eng. 47, 1491–1522.

Wijayathunga, V.N., Tanner, S.F., Ridgway, J.P., Wilcox, R.K., 2019. An in Vitro Study of the Intervertebral Disc Structure Using 3T Magnetic Resonance Imaging. Spine (Phila. Pa. 1976). 44, 793–800.

Wilke, H.J., Herkommer, A., Werner, K., Liebsch, C., 2017. In vitro analysis of the segmental flexibility of the thoracic spine. PLoS One 12, 1–17.

Wong, K.W.N., Luk, K.D.K., Leong, J.C.Y., Wong, S.F., Wong, K.K.Y., 2006. Continuous dynamic spinal motion analysis. Spine (Phila. Pa. 1976). 31, 414–419.

Wren, T.A.L., Otsuka, N.Y., Bowen, R.E., Scaduto, A.A., Chan, L.S., Sheng, M., Hara, R., Kay, R.M., 2011. Influence of gait analysis on decision-making for lower extremity orthopaedic surgery: Baseline data from a randomized controlled trial. Gait Posture 34, 364–9.

Wu, G., 2002. Letter to the editor: ISB recommendation on definitions of joint coordinate system of various joints for the reporting of human joint motion—part I: ankle, hip, and spine. J. Biomech. 35, 543–548.

Wu, M., Wang, S., Driscoll, S.J., Cha, T.D., Wood, K.B., Li, G., 2014. Dynamic Motion Characteristics of the Lower Lumbar Spine: Implication to Lumbar Pathology and Surgical Treatment. Eur. Spine J. 23, 2350–2358.

Wui, S.H., Hyun, S.J., Kang, B., Kim, K.J., Jahng, T.A., Kim, H.J., 2020. Bicortical screw purchase at upper instrumented vertebra (UIV) can cause uiv fracture after adult spindeformity surgery: A finite element analysis study. Neurospine 17, 377–383.

Xia, Q., Wang, S., Kozanek, M., Passias, P., Wood, K., Li, G., 2010. In-vivo motion characteristics of lumbar vertebrae in sagittal and transverse planes. J. Biomech. 43, 1905–1909.

Xu, M., Yang, J., Lieberman, I., Haddas, R., 2017. Finite element method-based study for effect of adult degenerative scoliosis on the spinal vibration characteristics. Comput. Biol. Med. 84, 53–58.

Yagi, M., Ohne, H., Konomi, T., Fujiyoshi, K., Kaneko, S., Takemitsu, M., Machida, M., Yato, Y., Asazuma, T., 2017. Walking balance and compensatory gait mechanisms in surgically treated patients with adult spinal deformity. Spine J. 17, 409–417.

Yao, Y.C., Kim, H.J., Bannwarth, M., Smith, J., Bess, S., Klineberg, E., Ames, C.P., Shaffrey, C.I., Burton, D., Gupta, M., Mundis, G.M., Hostin, R., Schwab, F., Lafage, V., 2021. Lowest Instrumented Vertebra Selection to S1 or Ilium Versus L4 or L5 in Adult Spinal Deformity: Factors for Consideration in 349 Patients With a Mean 46-Month Follow-Up. Glob. Spine J.

Yoo, J.S., Patel, D. V., Mayo, B.C., Massel, D.H., Karmarkar, S.S., Lamoutte, E.H., Singh, K., 2019. Postoperative satisfaction following lumbar spinal fusion surgery: Patient expectation versus actuality. J. Neurosurg. Spine 31, 676–682.

Youssef, J. a, Orndorff, D.O., Patty, C. a, Scott, M. a, Price, H.L., Hamlin, L.F., Williams, T.L., Uribe, J.S., Deviren, V., 2013. Current status of adult spinal deformity. Glob. spine J. 3, 51–62.

Zander, T., Dreischarf, M., Schmidt, H., 2016. Sensitivity analysis of the position of the intervertebral centres of reaction in upright standing - a musculoskeletal model investigation of the lumbar spine. Med. Eng. Phys. 38, 297–301.

Zanjani-Pour, S., Meakin, J.R., Breen, Alex, Breen, Alan, 2018. Estimation of in vivo inter-vertebral loading during motion using fluoroscopic and magnetic resonance image informed finite element models. J. Biomech. 70, 134–139.

Zemp, R., List, R., Gulay, T., Elsig, J.P., Naxera, J., Taylor, W.R., Lorenzetti, S., 2014. Soft tissue artefacts of the human back: Comparison of the sagittal curvature of the spine measured using skin markers and an open upright MRI. PLoS One 9.

Zhang, X., Aiyangar, A., Zheng, L., Tashman, S., Anderst, W., 2013. Capturing Three-dimensional In Vivo Lumbar Intervertebral Joint Kinematics Using Dynamic Stereo-X-ray Imaging. J. Biomech. Eng. 136, 1–9.

Zhang, X., Chan, F.K., Parthasarathy, T., Gazzola, M., 2019. Modeling and simulation of complex dynamic musculoskeletal architectures. Nat. Commun. 10, 1–12.

Zhang, X., Xiong, J., 2003. Model-guided derivation of lumbar vertebral kinematics in vivo reveals the difference between external marker-defined and internal segmental rotations. J. Biomech. 36, 9–17.

Appendices

About the author

In 2014, Thomas received a Bachelor's degree in Engineering Science at the KU Leuven (Belgium). In his following Master's education he developed an interest for orthopaedics, for the first time acquainting with Prof. Lennart Scheys – who was, together with Prof. Lieven Moke, at that time founding a spinal deformity research unit within the Institute for Orthopaedic Research and Training (IORT) of the University Hospitals of Leuven (UZ Leuven, Belgium). A successful master thesis, guided by Prof. Lennart Scheys, Prof. Ilse Jonkers and Prof. Lieven Moke, marked the end of his magna cum laude degree in Biomedical Engineering (2016, KU Leuven, Belgium) and served as a precursor for this dissertation. In October 2016 Thomas started his PhD training as a researcher within the IORT, where he worked as part of the spinal deformity research group. During this time he received the outstanding researcher award twice (2017 and 2018) from the OpenSim team at Stanford, and recently he received the best abstract and presentation award on the virtual symposium on 'Motion Analysis and Musculoskeletal Modeling in Treatment of Spinal Disorders' (2021). Thomas also seats in the Council of the Department Development and Regeneration (KU Leuven) as elected AAP/BAP representative.

Curriculum vitae

Articles in international peer reviewed journals

First or joined first author

Overbergh, T., Severijns, P., Beaucage-Gauvreau, E., Ackermans, T., Moke, L., Jonkers, I., Scheys, L., 2021. Subject-Specific Spino-Pelvic Models Reliably Measure Spinal Kinematics During Seated Forward Bending in Adult Spinal Deformity. Front. Bioeng. Biotechnol. 9, 1–11.

Severijns P. & Overbergh T., Schmid S., Scheys L, Moke L. (2021) Spinal palpation error and its impact on skin marker-based spinal alignment measurement in adult spinal deformity. Frontiers in Bioengineering and Biotechnology, 9, 1–9.

Overbergh T., Severijns P., Beaucage-Gauvreau E., Jonkers I., Moke L., Scheys L. (2020) Development and validation of a modeling workflow for the generation of image-based, subject-specific thoracolumbar models of spinal deformity. J Biomech., 110:109946.

Moke L. & Overbergh T., Severijns P., Schelfaut S., Moens P., Van de Loock K., Hermans L., Molenaers G., Jonkers I., Scheys L. (2020) The Transverse Gravitational Deviation Index, a Novel Gravity Line-Related Spinal Parameter, Relates to Balance Control and Health-

Related Quality of Life in Adults With Spinal Deformity. Spine (Phila Pa 1976)., 45(1):E25-E36.

Co-author

Severijns, P., Overbergh, T., Desloovere, K., Moke, L., Scheys, L. (2022) Spinopelvic movement strategies during sit-to-stand and stand-to-sit in adult spinal deformity. Gait and Posture, 92 :15-23

Severijns P., Overbergh T., Ackermans T., Beaucage-Gauvreau E., Brumagne S., Desloovere K., Scheys L, Moke L. (2021) The Function Assessment scale for Spinal Deformity (FASD): validity and reliability of a new clinical scale. Spine (Phila Pa 1976) *(Ahead of print)*

Severijns P., Moke L., Overbergh T., Beaucage-Gauvreau E., Ackermans T., Desloovere K., Scheys L. (2021) Dynamic sagittal alignment and compensation strategies in adult spinal deformity during walking. Spine J., 20:S1529-9430(21)00088-7. 1059–1071.

Wang, W., Wang, D., Falisse, A., Severijns, P., Overbergh, T., Moke, L., Scheys, L., De Groote, F., Jonkers, I., (2021). A Dynamic Optimization Approach for Solving Spine Kinematics While Calibrating Subject-Specific Mechanical Properties. Annals of Biomedical Engineering. Eng., 10.1007/s10439-021-02774-3

Severijns, P., Overbergh, T., Thauvoye, A., Baudewijns, J., Monari, D., Moke, L., Desloovere, K., Scheys, L. (2020). A subject-specific method to measure dynamic spinal alignment in adult spinal deformity. Spine J., 20 (6), 934-946.

Severijns, P., Overbergh, T., Scheys, L., Moke, L., Desloovere, K. (2019). Reliability of the balance evaluation systems test and trunk control measurement scale in adult spinal deformity. PLOS ONE, 14 (8), Art.No. ARTN e0221489.

Abstracts presented at national and international conferences

First or presenting author

Overbergh T., Severijns P., Beaucage-Gauvreau E., Ackermans T., Moke L., Jonkers I., Scheys L. (2021) Subject-specific spino-pelvic models reliably measure spinal kinematics during forward bending in adult spinal deformity. Presented at the Virtual Symposium on "Motion Analysis and Musculoskeletal Modeling in Treatment of Spinal Disorders ". – Oral presentation

Overbergh, T., Severijns, P., Moke, L., Jonkers, I., Scheys, L. (2019). Radiographic spinopelvic parameters in ASD: A dynamic evaluation. Presented at the Eurospine 2019, Helsinki, Finland.

Overbergh, T., Severijns, P., Moke, L., Jonkers, I., Scheys, L. (2019). Differences in vertebral motion between an adult spinal deformity patient and a healthy subject: A case study. Presented at the Eurospine 2019, Helsinki, Finland.

Overbergh, T., Severijns, P., Moke, L., Jonkers, I., Scheys, L. (2019). Simulation-based vertebral kinematics using an image-based modelling platform. Presented at the EORS (European Orthopaedic Research Society), Maastricht, the Netherlands.

Overbergh, T., Severijns, P., Wesseling, M., Moke, L., Jonkers, I., Scheys, L. (2018). The next step in routine creation of subject-specific models: A hybrid radiograph-based musculoskeletal model. In: World Congress of Biomechanics, (2018), (Abstract No. P1198). Presented at the World Congress of Biomechanics, Dublin, Ireland.

Severijns, P. & Overbergh, T., Scheys, L. (contributor) (2018). A dynamic evaluation and modelling platform for Adult Spinal Deformities. Presented at the Orthopaedica Belgica Fall Course 2018, Brussels, Belgium.

Overbergh, T., Severijns, P., Wesseling, M., Moke, L., Vanpeteghem, A., Van de loock, K., Jonkers, I., Scheys, L. (2018). Quantification of kinematic error in multi-body simulations of spinal deformity subjects. Presented at the Orthopaedic Research Society (ORS) Annual Meeting, New Orleans, USA.

Overbergh, T., Wesseling, M., Severijns, P., Moke, L., Jonkers, I., Scheys, L. (2016). Personalized musculoskeletal modeling of spinal deformities based on stereoradiographic images for biomechanical analysis of motion. Presented at the Belgian National Day on Biomedical Engineering, Royal Academy Palace, Brussels, Belgium.

Co-author

Severijns P., Overbergh T., Ackermans T., Beaucage-Gauvreau E., Brumagne S., Desloovere K., Scheys L, Moke L. (2021) The Function Assessment scale for Spinal Deformity (FASD): validity and reliability of a new clinical scale. Presented at the EUROSPINE annual meeting 2021, Vienna, Austria. – Oral presentation

Severijns, P., Overbergh, T., Desloovere, K., Moke, L., Scheys, L. (2021) Spinopelvic movement strategies during sit-to-stand in adult spinal deformity. Presented at the EUROSPINE annual meeting 2021, Vienna, Austria. – Poster presentation

Severijns P., Overbergh T., Schmid S., Scheys L., Moke L. (2021) Spinal Palpation Error and Its Impact on Skin Marker-Based Spinal Alignment Measurement in Adult Spinal Deformity. Presented at the XXVIII Congress of the International Society of Biomechanics, Stockholm, Sweden. – Oral presentation

Severijns P., Overbergh T., Schmid S., Scheys L., Moke L. (2021) Spinal Palpation Error and Its Impact on Skin Marker-Based Spinal Alignment Measurement in Adult Spinal Deformity. Presented at the Virtual Symposium on "Motion Analysis and Musculoskeletal Modeling in Treatment of Spinal Disorders". – Oral presentation

Severijns, P., Overbergh, T., Van de loock, K., Desloovere, K., Moke, L., Scheys, L. (2020). Spinal fusion surgery affects sagittal vertical axis during walking in adult spinal deformity. Presented at the EUROSPINE 2020, Virtual meeting.

Severijns, P., Overbergh, T., Desloovere, K., Scheys, L., Moke, L. (2019). From static to dynamic: sagittal alignment and compensation strategies during walking in Adult Spinal Deformity. Presented at the EUROSPINE annual meeting 2019, Helsinki, Finland.

Severijns, P., Overbergh, T., Desloovere, K., Moke, L., Scheys, L. (2019). Spinal alignment during motion and its relation to balance control in Adult Spinal Deformity. Presented at the EUROSPINE annual meeting 2019, Helsinki, Finland.

Severijns, P., Overbergh, T., Desloovere, K., Moke, L., Scheys, L. (2019). Assessment of dynamic spinal alignment through instrumented motion analysis. Presented at the EORS 2019 (European Orthopaedic Research Society), Maastricht, the Netherlands.

Severijns, P., Overbergh, T., Desloovere, K., Moke, L., Scheys, L. (2019). Sagittal alignment and compensation from static to dynamic in Adult Spinal Deformity. Presented at the ESBiomech Conference 2019 (European Society of Biomechanics), Vienna, Austria.

Severijns, P., Overbergh, T., Desloovere, K., Moke, L., Scheys, L. (2019). Assessment of dynamic spinal alignment through instrumented motion analysis. Presented at the ESBiomech Conference 2019 (European Society of Biomechanics), Vienna, Austria.

Wang, W., Overbergh, T., Severijns, P., Wesseling, M., Moke, L., De Groote, F., Scheys, L., Jonkers, I. (2018). Estimating spine loading using an advanced full-body musculoskeletal model. Presented at the 8th World Congress of Biomechanics, Dublin, Ireland.

Moke, L., Severijns, P., Overbergh, T., Bartholomeeussen, S., Van de loock, K., Hermans, L., Scheys, L. (2018). Diagnostic performance of the Balance Evaluation Systems Test for sagittal malalignment in Adult Spinal Deformity. Presented at the American Academy of Orthopaedic Surgeons Annual Meeting 2018, New Orleans, USA.

Severijns, P., Overbergh, T., Moke, L., Van de loock, K., Desloovere, K., Scheys, L. (2018). Dynamic parameters relate to radiographic parameters and balance performance in Adult Spinal Deformity. In: ORS annual meeting 2018. Presented at the ORS annual meeting 2018, New Orleans, USA.

Severijns, P., Overbergh, T., Moke, L., Van de loock, K., Desloovere, K., Scheys, L. (2018). Does the dynamic sagittal profile of Adult Spinal Deformity patients change after 10 minutes walking? Presented at the ORS annual meeting 2018, New Orleans, USA.

Severijns, P., Moke, L., Overbergh, T., Van de loock, K., Desloovere, K., Scheys, L. (2017). Are static sagittal compensation strategies preserved during walking in adult spinal deformity? In: Gait & Posture: vol. 57, (188-189). Presented at the Annual Meeting of the European Society for Movement Analysis in Adults and Children (ESMAC), Trondheim, Norway.

Organizations

Council of the Department Development and Regeneration (KU Leuven)
Elected AAP/BAP representative
October 2020 – present

Educational Committee for Biomedical Engineering (KU Leuven)
Student Representative
October 2015 – July 2016

Advisory Board of the Engineering Mechanics Department (KU Leuven)
Student Representative
October 2015 – July 2016

Honors and Awards

- **Best abstract and presentation award** on the virtual symposium on 'Motion Analysis and Musculoskeletal Modeling in Treatment of Spinal Disorders' (2021)
- The **2017 and 2018 Stanford Outstanding Researcher Award** for my PhD project on 'An image-based musculoskeletal modeling platform for simulation-based analysis of dynamic motor function in adult spinal deformity', awarded by NIH National Center for Simulation in Rehabilitation Research (NCSRR), Stanford University, USA. NCSRR awards seed grants for innovative, well-designed pilot projects to accelerate the development of advanced simulation techniques and the use of simulations in rehabilitation research.
- **Master Thesis Award 2016** (Materialise NV.)
  Master Thesis: "Personalized musculoskeletal modeling of spinal deformities based on stereoradiographic images: use for biomechanical analysis of posture and motion." Thesis supervisors: Prof. dr. Ir. Lennart Scheys & Prof. dr. Ilse Jonkers

Training and Certifications

- Foundations Of Business Development (Strategy, Marketing, Finance, Business Modelling and Ecosystems, Entrepreneurship), Flanders Business School, November 2020
- ICH Good Clinical Practice (GCP-E6 (R2)) obtained October 2020
- Introduction to leadership obtained June 2020

Scientific acknowledgements, personal contributions and conflict of interest statement

Scientific acknowledgements

I kindly acknowledge all co-authors for their valuable contributions to the different studies within this doctoral thesis: Prof. Lennart Scheys, Prof. Ilse Jonkers, Prof. Lieven Moke, Dr. Pieter Severijns, Dr. Erica Beaucage-Gauvreau and Dr. Thijs Ackermans. I would also like to thank Rowie De Buysschere, Charline Dilen, Kristel Van de Loock, Lore Hermans and Inès Decostere for their participation in patient recruitment and data management in all studies. Additonally, I acknowledge Lieven Moke, Sebastiaan Schelfaut and Pierre Moens for their contribution in patient recruitment. Lastly, I would like to thank Dr. Mariska Wesseling for her help in conceptualizing this work in its early stages. Regarding Chapter 1, we acknowledge Dr. Thijs Ackermans for his thorough review. We would also like to thank Prof. Friedl De Groote, Dr. Christopher Dembia and the OpenSim team for their technical expertise during the revision of this chapter. Regarding Chapter 3, we thank students Ines De Ceuster, Pauline Bataillie, Marnicq van Es and Mircea Presura for their assistance in CT-segmentation. Lastly, we would like to thank all subjects participating in this study.

All work was funded by internal KU Leuven C2 funds (ASESP-P), Medtronic, internal UZ Leuven Academic research funding (KOOR) and Research Foundation – Flanders (FWO-SB/1S56017N)

Personal contribution

Conceptualization of the different investigations within this doctoral thesis was performed with the assistance of the promotor team (Prof. Lennart Scheys, Prof. Ilse Jonkers, Prof. Lieven Moke). Together with Dr. Pieter Severijns the author, Thomas Overbergh, collected the motion capture data and biplanar radiography data of all subjects presented in this dissertation. CT-segmentation, a part of the modeling procedure, was performed by the author, with the exception of six subjects whose CT was segmented by students Ines De Ceuster, Pauline Bataillie, Marnicq van Es and Mircea Presura. All subjects were modeled by the author, with the exception of the three alternative versions created by the two other operators (Dr. Erica Beaucage-Gauvreau and Dr. Thijs Ackermans) each, in the inter-operator variability study of Chapter 2. Furthermore, in Chapter 3 the subjects underwent radiographic parameterization which was performed by the treating physician, Prof. Lieven Moke. The author processed and analyzed all data, performed all statistical analyses and drafted all four manuscripts included in this doctoral thesis. All steps of the project were supervised by the promotor and co-promotors.

Conflict of interest statement

Thomas Overbergh: No conflict of interest to be disclosed relevant to this work.

Prof. Lennart Scheys, is co-holder of KU Leuven C2 project "Advanced Spinal Evaluation and Surgical Planning Platform (ASESP-P), an advanced platform for the evaluation and surgical planning of spine problems 2017-2021", co-holder of FWO "An integrated dynamic evaluation platform to support clinical decision-making in adult spinal deformity", co-holder of FWO "Multimodal biomechanical analysis of spinal deformity with sagittal plane misalignment" and co-holder of UZ Leuven project "The development of an orthopaedic evaluation platform 2014-2018".

Prof. Ilse Jonkers: No conflict of interest to be disclosed relevant to this work.

Prof. Lieven Moke, is holder of a clinical doctoral grant of the Research Foundation - Flanders (FWO) 2015-2017 (FWO File Number 1573 - FWO Application Number 1702316N), co-holder of research grant from Clinical Research and Education Board UZ Leuven 2016 (Klinische Onderzoeks- en Onderwijsraad (KOOR)), co-holder of KU Leuven Medtronic educational chair for spinal deformity research 2013-2017, collaborator of KU Leuven C2 project Advanced Spinal Evaluation and Surgical Planning Platform (ASESP-P), an advanced platform for the evaluation and surgical planning of spine problems 2017-2021.

Pieter Severijns: holder of doctoral grant strategic basic research of the Research Foundation - Flanders (FWO) (1S56017N).

Erica Beaucage-Gauvreau: No conflict of interest to be disclosed relevant to this work.

Thijs Ackermans: No conflict of interest to be disclosed relevant to this work.